T H E U N I V E R S I T Y O F T U L S A

THE GRADUATE SCHOOL

WELL-PLACEMENT OPTIMIZATION

by

Fahim Forouzanfar

A dissertation submitted in partial fulfillment of

the requirements for the degree of Doctor of Philosophy

in the Discipline of Petroleum Engineering

The Graduate School

The University of Tulsa

2012

T H E U N I V E R S I T Y O F T U L S A

THE GRADUATE SCHOOL

WELL-PLACEMENT OPTIMIZATION

by
Fahim Forouzanfar

A DISSERTATION

APPROVED FOR THE DISCIPLINE OF

PETROLEUM ENGINEERING

By Dissertation Committee

_____, Chairperson
Albert C. Reynolds

_____
Gaoming Li

_____
Richard Redner

_____
Ovadia Shoham

ABSTRACT

Fahim Forouzanfar (Doctor of Philosophy in Petroleum Engineering)

Well-Placement Optimization

Directed by Albert C. Reynolds

208 pp., Chapter 6: Conclusions

(508 words)

A gradient-based well-placement algorithm for optimizing the number of wells, their locations and well controls is developed. Furthermore, a derivative-free well-placement algorithm for more general well trajectory wells such as horizontal, vertical and directional wells is presented in this work.

In the first part of this work, a gradient-based optimization algorithm with the gradients calculated by the adjoint method is developed to solve the general well-placement problem which simultaneously optimizes the number of wells, the well locations and the rates of rate-controlled vertical injection and production wells. Fixing the well controls and the expected reservoir life a priori during the well-placement optimization results in a sub-optimal solution. To overcome this problem and to mitigate the effects of an ad hoc specification of both operating well rates and operational reservoir life, an initialization step is proposed to determine an appropriate total reservoir water injection rate and/or total reservoir production rate for the specified operational life of the reservoir. Also, a practical method is proposed for imposing nonlinear bound constraints on the bottomhole pressure of each well; this procedure does not require the calculation of the gradients of the bottomhole pressure constraints.

In the second part of this work, a new methodology for the efficient estimation of the location, length and trajectory of 3D vertical, horizontal and directional wells is developed that maximizes the life-cycle net-present-value (NPV) of production from a given reservoir. With this methodology, the well controls and the expected reservoir life are specified a priori for the well-placement problem. Although it is more natural to specify the operating bottomhole pressure of wells, the procedure also works if well controls correspond to specified rates. For vertical or horizontal wells, the well-placement problem is formulated in terms of four continuous variables, the x_{w}, y_{w} and z_{w} coordinates of the center point of the well and the length, l_{w}, of the well. For a directional well, the well trajectory parameters are the x_{w}, y_{w} and z_{w} coordinates of the center point of the well, the length of the well, l_{w}, and θ_{w} and φ_{w} which are the orientation angles of the well in the horizontal and vertical directions, respectively. A NPV functional is defined by distributing the rate of the well among "gridblock perforations" which are "close" to the trajectory of the well. The NPV functional by our model is based on the life-cycle NPV of production from the reservoir and it is a function of these continuous well trajectory parameters. Conceptually, this NPV functional can be maximized using any algorithm but since commercial simulators do not provide all derivatives needed for a gradient-based optimization algorithm, we apply a derivative-free optimization (DFO) algorithm, BOBYQA. For the straightforward formulation of the optimal well-placement problem, BOBYQA performs relatively poorly. A cogent way for the transformation of the control variables is proposed in order to improve the performance of BOBYQA for the well-placement optimization problem. Because a DFO algorithm is applied, the technology developed here can be easily applied using any reservoir simulator.

ACKNOWLEDGEMENTS

I would like to express my utmost gratitude to my advisor Dr. Albert C. Reynolds for his continuous excellent support, guidance, insights, encouragement and patience over the course of this research. It has been an honor working with Dr. Reynolds as he is an example of an outstanding researcher. He is not only a great advisor, but an excellent professor passing his infinite knowledge onto his students who look upon him as an inspirational mentor.

I would also like to express my appreciation to Dr. Gaoming Li, Dr. Richard Redner and Dr. Ovadia Shoham for agreeing to serve in my committee and review my work. Special thanks goes to Dr. Gaoming Li for his valuable suggestions and comments. I would like to extend my gratitude and appreciation to all the other faculty members of the McDougall School of Petroleum Engineering at The University of Tulsa for their support and contributions to my academic achievements.

I am grateful to all my colleagues and friends at The University of Tulsa, my fellow graduate students in The University of Tulsa's Petroleum Reservoir Exploitation Projects (TUPREP) research group, and, Mrs. Judy Teal, Mrs. Loreta Watkins and Mrs. Lori Watts for their support and help during my study in this university.

I would like to thank the companies supporting TUPREP research group for their financial contribution and interest in my research. This support is greatly appreciated. I would also like to acknowledge the financial, academic and technical support of The University of Tulsa, and its staff. I particularly appreciate the Bellwether fellowship provided partial financial support for this research.

This work is dedicated to my family, especially my parents, for their unconditional love, support, and encouragement.

TABLE OF CONTENTS

LIST OF TABLES

LIST OF FIGURES

CHAPTER 1

INTRODUCTION

Determining the optimal number of the production and injection wells as well as determining good locations and completions of the production and injection wells are critical steps in preparing the development plan for a reservoir when the objective is to optimally develop and produce a reservoir. The distance of a production well from the aquifer, gas cap or injection wells, the reservoir layers to be penetrated and the length of the perforated or open section of a well greatly influence the well performance. Therefore, the use of a well-placement optimization algorithm is required.

Solution of the general well-placement optimization problem would require simultaneous estimation of the optimal number of wells, well type, well locations and trajectories and operating conditions for the life of the reservoir by maximizing a measure of the field net-present-value. Although dozens of papers have been written on the individual components of the problem, the general problem is far from solved. Well-placement optimization is a challenging optimization problem due to the high dimension and the complexity of the optimization search space and also the computational costs associated with the function evaluations. The number of wells, the location and trajectory of the wells and their controls results in a high dimensional and complex optimization search space. Also the optimization is computationally very demanding as every objective function evaluation requires one reservoir simulation run. Therefore, an efficient robust well-placement optimization algorithm is desirable.

1.1 Well-Placement Optimization Algorithms

As mentioned previously, the general well-placement optimization problem which considers simultaneously optimizing the number of wells, well type, well locations and trajectories and well operating conditions for life cycle of the reservoir is far from solved. Many researchers have focused on solving individual components of the problem. Virtually all papers on optimal well-placement assume the number of wells are fixed and the well operating conditions, wellbore pressures or rates, and the reservoir life are specified and fixed when optimizing well locations and trajectories (completions). Perhaps, we should mention, however, that in the optimization procedures used by Handels et al. [16] and Emerick et al. [13] the optimal number of wells may change by a very small number during the optimization process. Also, in the optimization procedures proposed by Yeten et al. [44] and Onwunalu and Durlofsky [26], the number of laterals of a multi-lateral well is optimized during the optimization process. Additionally, in the optimization method developed by Yeten et al. [44], the well controls (wellbore pressures or rates) are also optimized and Beckner and Song [3] proposed an algorithm to optimize the schedule of the wells (the time to bring the wells online).

The perforations of a well are introduced into the simulation model as the indices of the perforated gridblocks. For a 3D vertical, horizontal or directional well, it is most common to define the indices of the endpoint gridblocks of each well as the optimization variables. Thus, finding the optimum location of a well is most naturally formulated as a discrete optimization problem where the perforation gridblock indices of the endpoints of the wells are the optimization variables, even though the actual physical problem of determining optimal well locations is a continuous problem. In the Beckner and Song [3] and Bittencourt and Horne [4] well-placement optimization methods, a vector of integer numbers containing the indices of the active gridblocks determine the possible locations for the wells. Centilmen et al. [9], Bangerth et al.

[2] and Ozdogan and Horne [27] considered the optimization of 2D vertical wells where the ("i", "j") gridblock indices are the optimization variables. In the well-placement optimization method of Emerick et al. [13], a directional well is a straight line and the gridblock indices of the two endpoints of the well are the optimization variables. Lee et al. [20] proposed a node-based configuration for well trajectories. Based on their representation, a well trajectory is defined as one or several nodes, called "kick-off" points. The path connecting the nodes gives the well trajectory. In their representation, the maximum number of the nodes is predefined. In the Yeten et al. [44] well-placement method, a nonconventional (multi-lateral) well contains a mainbore and a number of laterals which are to be optimized. The mainbore and each lateral of the well are represented by independent straight lines in 3D. The mainbore is represented by a straight line which is defined by the three coordinate locations of the heel (h_x, h_y, h_z), the projected length of the mainbore on the $x-y$ plane (l_{xy}), the orientation angle in the $x-y$ plane (θ) and the depth to the trajectory endpoint (t_z). Each lateral of the well is also a straight line that is parameterized in terms of its junction point on the mainbore (j) and the three parameters (l_{xy}, θ, t_z) of the lateral. The maximum number of laterals is pre-specified. Yeten et al. [44] represented the real space (x, y, z) coordinate location of the points on a simulation grid by using their corresponding ("i", "j", "k") gridblock indices.

To solve the discrete optimal well-placement problem, most researchers have focused on using non-gradient-based optimization algorithms, i.e., the genetic algorithm (Bittencourt and Horne [4], Yeten et al. [44], Ozdogan and Horne [27] and Lee et al. [20], Emerick et al. [13]), neural networks (Centilmen et al. [9] and Yeten et al. [44]), simulated annealing (Beckner and Song [3] and Norrena and Deutsch [25]). The genetic algorithm appears to be the most widely used derivative-free algorithm for solving the discrete well-placement optimization problem. Yeten et al. [44] used the genetic algorithm method to optimize the type, well control, location and tra-

jectory of non-conventional wells. To improve the computational efficiency of the optimization run, Yeten et al. [44] implemented artificial neural networks and hill climbing algorithms in their well-placement method. Lee et al. [20] implemented the genetic algorithm to optimize the location and trajectory of wells in a 2D reservoir by optimizing the configuration of the well trajectory nodes ("kick off" points). Emerick et al. [13] also applied the genetic algorithm method to optimize the location, completion and the type (injection or production) of wells. They applied their method to a field case, where the "best" locations and trajectories of injection and production wells were tentatively selected by experienced reservoir engineers. These best locations and trajectories were used in the initial population for the genetic algorithm. Generally speaking, discrete derivative-free optimization algorithms are slow and require a very large number of reservoir simulation runs to obtain convergence and thus require significant computer time.

Some researchers have investigated gradient-based optimization algorithms for the optimal well-placement problem to improve the computational cost of the optimization. Bangerth et al. [2] introduced integer simultaneous perturbation stochastic approximation (SPSA) and integer finite difference (FD) algorithms to solve the discrete optimal well-placement problem for vertical wells. The proposed well-placement algorithms are gradient-based methods where the gradients are computed by SPSA or finite difference methods. In their integer SPSA and integer finite difference optimization algorithms, the perturbation and step size values are integer numbers. Note, Bangerth et al. [2] assumed that the derivatives of the objective function (NPV) can be well approximated by finite differences on the integer lattice of the simulation model. This may not be a good assumption if the simulation model has a course simulation grid and/or the permeability field of the reservoir is very heterogeneous. Also, the computation of the gradients with the finite difference is not computationally efficient when the number of wells and hence the number of parameters is

large. A successful application of a gradient-based optimization procedure requires a method for efficient computation of the gradient of the objective function with respect to the vector of the optimization parameters. This requires the definition of continuous optimization parameters so that the objective function (usually NPV) is a differentiable function of these parameters. Also, it requires a reservoir simulator with the appropriate adjoint code, but adjoint code for computing these gradients is not commonly provided in commercial reservoir simulators. Handels et al. [16], Zandvliet [45], Sarma and Chen [36], Wang et al. [41] and Zhang et al. [47] reformulated the optimal well-placement problem for vertical wells so that it can be treated as an optimization problem on continuous variables and solved the optimal well-placement problem with efficient gradient-based methods.

The method of Handels et al. [16] and Zandvliet [45] are the first attempts to use a gradient-based optimization algorithm for optimal well placement where optimal well locations are defined as those that maximize NPV over a specific total production time specified a priori. Although this method still seeks to find the discrete ("i", "j") indices of optimal well location, wells are moved from simulator gridblock to simulator gridblock based on a gradient calculation. Specifically, eight "pseudo-wells" with very small injection or production rates are placed around each actual well. Although the pseudo-wells have a negligible impact on the NPV, the gradient of the NPV with respect to all the pseudo-well rates can be obtained with one backward adjoint run. Based on this gradient calculation, a well is moved to the location of the pseudo-well that has the largest positive gradient regardless of whether this movement actually increases or decreases NPV. Thus, NPV may oscillate (increase and then decrease) from iteration to iteration of the optimization algorithm and it is not possible to use a standard convergence criterion. In our application of this method, we terminate iteration when a well configuration repeats from a previous iteration. We choose the well locations corresponding to the iter-

ation with the highest NPV value as the optimal well locations. The well controls are predetermined and fixed for the specified reservoir production life; hence, the final well locations depend on the specified well controls (Zandvliet [45]). Handels et al. [16] and Zandvliet [45] considered only vertical wells and in their procedure; the location of a well is effectively at the center of a gridblock. Sarma and Chen [36] extended the Handels et al. [16] method in a way that approximately accounts for the actual location, $(x_{\mathrm{w}}, y_{\mathrm{w}})$, of a vertical well in a gridblock, i.e., they treated the well location $(x_{\mathrm{w}}, y_{\mathrm{w}})$ as continuous variables. Sarma and Chen [36] also introduced a method to find the "best" direction for moving the wells to increase the NPV. In their method, a well is surrounded by pseudo-wells at the neighboring gridblocks but unlike the Handels et al. [16] procedure, the rate of a well is distributed among the well and its pseudo-wells as a function of the well location, $(x_{\mathrm{w}}, y_{\mathrm{w}})$. The optimization parameters are the actual locations of wells. Sarma and Chen [36] applied their method to find the locations of bottomhole pressure-controlled vertical wells for 2D flow problems. Their method requires the derivative of the objective function with respect to the productivity index (PI) multipliers of the pseudo-wells and the original well. In their implementation, the gradients are computed by the adjoint method.

Vlemmix et al. [40] developed an adjoint-based well trajectory optimization method which is effectively an extension of the Handels et al. [16] idea to three dimensions. In the Vlemmix et al. [40] method, the well trajectory is determined by connecting the estimated trajectory points. The optimization algorithm moves the trajectory points to find the optimum trajectory of the well. In order to find the proper direction of the move for a well's trajectory points, the initial trajectory points are surrounded by "pseudo side tracks" at all adjacent gridblocks in each direction. Typically, there are pseudo side tracks to the four adjacent gridblocks of each trajectory point. The side tracks are given a very small perforation length so that their influence on the overall flow is negligible. The sensitivity of the objective

function to the inflow area in the side track is determined by the adjoint method for each pseudo side track. Using these sensitivities (derivatives), a set of "attractor" points is constructed, one for each trajectory point. The attractor points are used to move trajectory points in an improving direction at each iteration.

Wang et al. [41] and Zhang et al. [47] proposed a method for the optimization of the location of injection rate-controlled wells. In their procedure, a large number of injection wells are initially placed in the reservoir and the total injection rate is uniformly distributed among those injectors. A modified net-present-value functional, which also accounts for the drilling cost of a well, is defined as the objective function to be maximized. A derivative-based optimization method is used to optimize the modified NPV functional with respect to the rates of the wells. Some well rates go to zero during an optimization iteration and the corresponding wells are therefore eliminated. The injection wells that remain when the algorithm converges provide an estimate of the optimal well locations. This method is applicable for the rate-controlled wells only.

Recently Onwunalu and Durlofsky [26] and Bouzarkouna et al. [5] defined the well-placement optimization using continuous real variables as the optimization parameters. They used iterative population-based stochastic optimization algorithms because of the non-smooth shape of the objective function. Onwunalu and Durlofsky [26] implemented particle swarm optimization (PSO) for determining the location and type (injector or producer) of directional and lateral wells. The parametrization of a nonconventional (multi-lateral) well in Onwunalu and Durlofsky [26] is similar to the one used by Yeten et al. [44], however, the optimization variables are continuous real variables. They also compared the performance of PSO with a binary implementation of the genetic algorithm (bGA) for the optimization of a vertical production well, and in this example PSO outperformed bGA. Bouzarkouna et al. [5] used "the covariance matrix adaptation evolution strategy" (CMA-ES) for

the optimal placement of nonconventional (multi-lateral) wells. CMA-ES is also an iterative population-based stochastic optimization algorithm. In the Bouzarkouna et al. [5] well-placement optimization method, the trajectory of the mainbore of a multi-lateral well is defined by a sequence of points which determine the segments of the wells. The heel of the mainbore is defined in the Cartesian coordinate system, (x, y, z), and the intermediate points and the endpoint of the mainbore are defined in their corresponding spherical coordinate system, (r, θ, φ), with respect to their bases (the previous point on the mainbore segment). For the laterals of the well, the starting point of a lateral is located on a segments of the mainbore and it is defined by its distance from the heel of the well. The endpoint of a lateral is defined in the spherical coordinate system corresponding to its starting point. Note, the number of segments of a well and the number of laterals are pre-specified. Spherical coordinates are used as they allow for straightforward control of the well lengths of the segments and laterals of the well by imposing a box constraint. Bouzarkouna et al. [5] compared the performance of CMA-ES with a continuous implementation of the genetic algorithm for optimizing the locations of an injector and a producer in the PUNQ reservoir, and found that CMA-ES outperformed GA. They also introduced an implementation of local meta-models (local quadratic approximation model) with CMA-ES which can improve the computational efficiency of the CMA-EA method.

1.2 Research Contributions and Dissertation Outline

1.2.1 Research Contributions

The development of practical and efficient techniques for well-placement optimization is a research problem of great interest. The first contribution of this research is to propose a derivative-based optimization algorithm for the optimal placement of vertical production and injection wells with the appropriate gradients computed from the adjoint method. The algorithm determines the optimum number of wells

to be placed in the reservoir, the optimum location of each well and the optimal well controls (rates) of each well subject to nonlinear well bottomhole pressure constraints. In the proposed method, bound constraints are put on wellbore pressures because, in reality, a water injection well is always constrained by a maximum bottomhole pressure and a producing well always has a minimum bottomhole pressure constraint. As upper and lower bottomhole pressure constraints represent nonlinear constraints when the optimization parameters or well controls are flow rates, adding bound constraints on bottomhole pressures adds a significant complication to the optimization problem. As derivatives of the bottomhole pressure constraints with respect to the control variables (rates) are not available with the commercial simulator used, a novel method is devised to ensure the satisfaction of these nonlinear bottomhole pressure constraints for rate-controlled wells. The method does not require the gradient of these nonlinear constraints on pressure. Also an initialization stage is proposed where the optimal total injection/production rates for the expected life of the reservoir are determined. In most of the optimal well-placement algorithms presented in the literature, the well controls and the expected reservoir life are both specified a priori and fixed during optimization, which may result in a very sub-optimal solution. To overcome this problem, an initialization step is proposed to find appropriate total reservoir injection/production rates for a specified reservoir life. Then, in the second stage, these total rate constraints are used as equality constraints when applying a gradient projection method to reduce the wells to an optimal number at optimal locations as well as optimizing the well controls of the remaining wells.

The second contribution of this work is to define a relatively smooth continuous NPV objective function for the placement of vertical, horizontal and directional wells. Here, an efficient derivative-free optimization algorithm is applied to solve the well-placement optimization problem because the gradients needed are not available.

A vertical or horizontal well is considered as a column or a row of perforated gridblocks and the proposed well-placement algorithm estimates the optimal location of the center point, $(x_{\mathrm{w}}, y_{\mathrm{w}}, z_{\mathrm{w}})$, and length, l_{w}, of each well. The directional well is represented by a straight line in spherical coordinate system, where $(x_{\mathrm{w}}, y_{\mathrm{w}}, z_{\mathrm{w}})$ determines the well center point, l_{w} is the length of the well and θ_{w} and φ_{w} are the directional angles. In order to define the NPV functional with our model, the rate of the well is distributed not only among the gridblocks penetrated by the well, but also among the gridblocks "close" to the well. A derivative-free optimization (DFO) algorithm, Bound Optimization BY Quadratic Approximation (BOBYQA), is used to solve the optimization problem; BOBYQA uses the simulator as a "black box" and there is no need to compute gradients. BOBYQA which was developed by Powell [34], tries to find the optimum solution of an optimization problem by minimizing a sequence of quadratic approximations of the objective function subject to predefined bounds on the optimization variables. To improve the performance of BOBYQA, a cogent way is proposed to re-scale the optimization variables for the well-placement optimization problem.

1.2.2 Dissertation Outline

There are six chapters and one appendix in this dissertation. In Chapter 2, we introduce the NPV functional that we use as the objective function to be maximized in the well-placement optimization problem. A brief description of the gradient projection and BOBYQA optimization algorithms we use for solving the defined optimization problems are also presented in Chapter 2. Chapter 3 presents details of the proposed derivative-based two-stage optimization algorithm for optimizing the number of the wells to be placed in the reservoir, their locations and controls. The computational results for both single-stage and two-stage optimization algorithms and a comparison with the Handels et al. [16] method are included in this chapter. Chapter 4 covers the proposed algorithm for optimizing the well

locations and lengths of vertical and horizontal production and injection wells using a DFO algorithm. The results for the optimization of well locations and completions in homogeneous and heterogeneous synthetic 3D reservoirs are also given in Chapter 4. Chapter 5 considers the optimization of well locations and trajectories of general directional wells using a DFO algorithm, BOBYQA. The computational results for the optimization of directional wells in homogeneous and heterogeneous synthetic 3D reservoir are also presented in Chapter 5. Chapter 6 presents the conclusions and a brief discussion and summary of the research contribution of this dissertation. In Appendix A, the detailed formulations for two well models for representing directional wells in commercial simulators are given.

CHAPTER 2

OBJECTIVE FUNCTION AND OPTIMIZATION ALGORITHMS FOR WELL-PLACEMENT OPTIMIZATION

The cumulative oil production from a reservoir or the net-present-value (NPV) of production from a reservoir are the two most common objective functions chosen for maximization in the well-placement optimization problem. In this dissertation, we choose the NPV of production from a reservoir as the objective function to be maximized in the well-placement optimization problem. The detailed form of the specific well-placement optimization problems defined for optimizing 2D vertical rate-controlled wells, 3D horizontal and vertical wells and 3D directional wells are given at the beginning of Chapters 3, 4 and 5, respectively.

In this chapter, we first introduce net-present-value functional as the objective function of the well-placement optimization problem. Then we briefly explain two optimization algorithms we use in this work which are: (1) Gradient projection method, which is a gradient-based algorithm for solving the optimization problems subject to the linear constraints, and (2) Bound Optimization BY Quadratic Approximation, BOBYQA, method which is a derivative-free optimization method to solve the optimization problems subject to predefined bounds on the optimization variables.

2.1 Net-Present-Value Definition

In the optimal well-placement problems discussed in this dissertation, the objective function is defined based on the net-present-value (NPV) of production from the reservoir. For a three-phase reservoir under water flooding, the NPV is

defined by

$$\text{NPV} = \sum_{n=1}^{N_t} \left[\sum_{j=1}^{N_{\text{prd}}} \left(r_o q_{o,j}^n - r_w q_{w,j}^n + r_g q_{g,j}^n \right) - \sum_{i=1}^{N_{\text{inj}}} \left(r_{w,\text{inj}} q_{\text{winj},i}^n \right) \right] \frac{\Delta t^n}{(1+b)^{t^n/365}}, \quad (2.1)$$

where N_t is the number of reservoir simulation time steps; N_{inj} and N_{prd}, respectively, denote the number of water injection and oil production wells, respectively; Δt^n represents the size of the nth simulation timestep in days; t^n represents the total simulation time in days at the end of the nth timestep; $q_{o,j}^n$, $q_{w,j}^n$ in STB/D and $q_{g,j}^n$ in MSCF/D, respectively, represent the average oil, water and gas production rates of the jth producer over the nth simulation timestep; $q_{\text{winj},i}^n$ in STB/D is the average water injection rate of the ith water injection well over the nth simulation timestep; r_o in \$/STB is the oil revenue per unit volume; r_g in \$/MSCF is the gas revenue per unit volume; r_w in \$/STB is the disposal cost per unit volume of produced water; $r_{w,\text{inj}}$ in \$/STB is the water injection cost per unit volume and b is the annual discount rate. Note that in Eq. 2.1, we have assumed constant economical parameters for the whole production life of the reservoir.

2.2 Gradient Projection Method

The detailed formulation and procedure of the gradient projection method is given in Nocedal and Wright [23, 24], Chen [10]. However, the gradient projection method we use in this research is adopted for the well-placement problem which does not exactly follow the procedure. The detailed algorithm of our gradient projection method for the well-placement optimization including the procedures for determining the active constraints and the step length at each optimization iteration are given in Chapter 3 of this dissertation. Here we explain the formulations of computing the search direction with projecting the gradient of the objective function onto the hyperplane of the active constraints. For the purpose of illustration, consider the

maximization of the objective function $J[u]$ subject to the linear equality constraints,

$$\max_{u} J[u], \tag{2.2}$$

subject to

$$e_i(u) = 0 \qquad i = 1, 2, \ldots, n_e. \tag{2.3}$$

where u is a n-dimensional column vector of the optimization variables and e_i denotes the ith equality constraint which can be an active bound constraint or any defined linear equality constraint for the optimization problem. The linear equality constraints in Eq. 2.3 can be written in the matrix form of

$$Au = b, \tag{2.4}$$

where A is a $n_e \times n$ matrix and b is a n_e-dimensional column vector. In the gradient projection optimization algorithm for the well-placement problem, the vector of control variables at maximization iteration $\ell + 1$ is updated by

$$u^{\ell+1} = u^{\ell} + \alpha^{\ell+1} d^{\ell+1}, \tag{2.5}$$

where $\alpha^{\ell+1}$ and $d^{\ell+1}$ are the step length and the search direction at iteration $\ell + 1$, respectively. As it is mentioned above, the procedure for determining the active constraints (matrix A) and the step length, $\alpha^{\ell+1}$, are given in Chapter 3. Here we only discuss the computation of the search direction, $d^{\ell+1}$.

At iteration ℓ, all the optimization constraints are satisfied and therefore,

$$Au^{\ell} = b, \tag{2.6}$$

The search direction $d^{\ell+1}$ should be an uphill direction ($(g^{\ell})^T d^{\ell+1} \geq 0$) which the

linear constraints in Eq. 2.4 are satisfied along this direction, therefore,

$$Au^{\ell+1} = Au^{\ell} + \alpha^{\ell+1} Ad^{\ell+1} = b, \tag{2.7}$$

Comparing Eqs. 2.6 and 2.7, it follows that

$$Ad^{\ell+1} = 0, \tag{2.8}$$

Therefore, the search direction $d^{\ell+1}$ needs to be an uphill direction which satisfies Eq. 2.8. Such a $d^{\ell+1}$ is found by projecting the gradient g^{ℓ} onto the hyperplane of the linear constraints. To compute $d^{\ell+1}$, we solve the following constrained minimization problem,

$$\min ||g^{\ell} - d^{\ell+1}||^2, \tag{2.9}$$

subject to the constraints given in Eq. 2.8. To solve the minimization problem, we define the Lagrangian function,

$$L(d^{\ell+1}, \lambda) = (g^{\ell} - d^{\ell+1})^T (g^{\ell} - d^{\ell+1}) + (Ad^{\ell+1})^T \lambda, \tag{2.10}$$

where λ is the vector of Lagrangian multipliers. To solve for $d^{\ell+1}$, we set,

$$\nabla_{d^{\ell+1}} L = 2d^{\ell+1} - 2g^{\ell} + A^T \lambda = 0. \tag{2.11}$$

If A is full rank, then sing Eq. 2.10 in Eq. 2.11 and solving for λ from Eq. 2.11 yields,

$$\lambda = 2(AA^T)^{-1} Ag^{\ell}. \tag{2.12}$$

Substituting the value of λ from Eq. 2.12 in Eq. 2.11 and solving for $d^{\ell+1}$ yields,

$$d^{\ell+1} = (I - A^T (AA^T)^{-1} A) g^{\ell}. \tag{2.13}$$

or

$$d^{\ell+1} = Pg^{\ell}. \tag{2.14}$$

where $P = (I - A^T(AA^T)^{-1}A)$ is the projection matrix.

The search direction given in Eq. 2.13 should satisfy two required conditions, i.e., it should be an uphill direction and the linear constraints should be satisfied along this direction. Here we verify these two conditions for the search direction given in Eq. 2.13. Pre-multiplication of Eq. 2.13 by A gives,

$$Ad^{\ell+1} = (A - AA^T(AA^T)^{-1}A)g^{\ell} = 0. \tag{2.15}$$

So any point along the search direction satisfies the constraints.

Next we show that the search direction $d^{\ell+1}$ is an uphill direction.

$$(g^{\ell})^T d^{\ell+1} = (g^{\ell} - d^{\ell+1} + d^{\ell+1})^T d^{\ell+1} = (g^{\ell} - d^{\ell+1})^T d^{\ell+1} + (d^{\ell+1})^T d^{\ell+1} \tag{2.16}$$

From Eq. 2.11, we note that

$$(g^{\ell} - d^{\ell+1})^T d^{\ell+1} = 0.5\lambda^T A d^{\ell+1} = 0. \tag{2.17}$$

Therefore, Eq. 2.16 becomes,

$$(g^{\ell})^T d^{\ell+1} = (d^{\ell+1})^T d^{\ell+1} = ||d^{\ell+1}||^2 \geq 0. \tag{2.18}$$

Equality in Eq. 2.18 holds only if $d^{\ell+1}$=0 or the gradient is orthogonal to the hyperplane of the linear constraints. Except this, the search direction given by Eq. 2.13 is an uphill direction.

2.3 Bound Optimization BY Quadratic Approximation (BOBYQA)

Bound Optimization BY Quadratic Approximation, BOBYQA, is a derivative-free iterative algorithm based on the quadratic approximation of the objective function (Powell [31], Powell [32], Powell [33] and Powell [34]). The subroutine seeks the minimum of an objective function, $J[u]$, subject to the bound constraints,

$$\min J[u] \qquad \text{such that} \qquad u^{\text{low}} \leq u \leq u^{\text{up}}, \tag{2.19}$$

where u is an n-dimensional vector containing all optimization variables. At the ℓth iteration, BOBYQA constructs a quadratic approximation $Q^\ell[u]$ of $J[u]$ such that

$$Q^\ell[\hat{\mathrm{u}}_j^\ell] = J[\hat{\mathrm{u}}_j^\ell], \qquad j = 1, 2, \ldots, m, \tag{2.20}$$

where $\hat{\mathrm{u}}_j^\ell$ are interpolation points which change from iteration to iteration and $n+2 \leq m \leq [(n+1)(n+2)]/2$. The quadratic $Q^\ell[u]$ can be written as

$$Q^\ell[u] = c^\ell + (u - u_0^\ell)^T g^\ell + \frac{1}{2}(u - u_0^\ell)^T G^\ell (u - u_0^\ell), \tag{2.21}$$

where u_0^ℓ is the initial approximation to the optimal u. The point u_0^ℓ, and accordingly c^ℓ, is changed at certain iterations (see Powell [34]). If Eq. 2.21 were the first three terms of the Taylor series approximation of $J[u]$ about u_0^ℓ, then G^ℓ would be the Hessian of Q^ℓ and g^ℓ would be equal to $\nabla J[u_0^\ell]$; thus, here, we simply refer to G^ℓ as the Hessian. G^ℓ is always required to be a real symmetric $n \times n$ matrix. To determine $Q^\ell[u]$, we must find the scalar c^ℓ, the n-linear coefficients, i.e., the n-dimensional column vector g^ℓ and all entries of $n \times n$ matrix G^ℓ which represent the quadratic coefficients. Because G^ℓ is required to be symmetric, only the $n(n+1)/2$ upper diagonal estimate of G^ℓ, the scaler c^ℓ and the n entries of g^ℓ need to be determined. Thus, in total, there are $n_t = [(n+1)(n+2)]/2$ coefficients that must be found

to define $Q^\ell[u]$. Determination of $Q^\ell[u]$ could be done using $m = n_t$ interpolation points (see Eq. 2.20), but to construct the quadratic at the first iteration, $Q^1[u]$, $m = n_t$ evaluations of $J[\hat{\mathrm{u}}_j^1]$, $j = 1, 2, \ldots, m$ are required. (In our approximation, evaluation of $J[u]$ at a $\hat{\mathrm{u}}_j^1$ requires one reservoir simulation run.) Thus, if the number of controls, n, is large, it is not computationally efficient to run the simulator n times to simply construct the first quadratic approximation of J. The algorithm of Powell [34] requires $m \geq n+2$ where $n+1$ interpolation conditions can be used to evaluate c^ℓ and g^ℓ and the remaining $m-(n+1)$ interpolation conditions can be used to determine some of the entries of G^ℓ. However, if $m < [(n+1)(n+2)]/2$, there are not enough interpolation conditions to determine all the entries of G^ℓ. Thus, similar to quasi-Newton methods, the algorithm at the ℓth iteration minimizes the Frobenius norm of the change in the Hessian

$$\delta G^\ell = G^\ell - G^{\ell-1}, \tag{2.22}$$

where at the first interaction ($\ell = 1$), G^0 is the $n \times n$ null matrix. Thus, the problem of determining Q^ℓ is defined by minimizing $\|\delta G^\ell\|_F^2$, subject to the interpolation conditions of Eq. 2.20 with $(n+2) \leq m < [(n+1)(n+2)]/2$. Powell [34] suggests using $m = n+6$ or $m = 2n+1$. The choice of $m = 2n+1$ is motivated by the fact that $2n+1$ interpolation conditions would be sufficient to determine c^ℓ, g^ℓ and the diagonal entries of G^ℓ. For the results presented in this dissertation, we use $m = 2n+1$ when the number of wells, and hence the number of optimization variables, is small. However, in the cases where n is fairly large, we use $m = n+2$ or $m = n+6$. In BOBYQA, the initial interpolation points are generated by making m perturbations about the initial point, $u_0^1 = u_{\text{init}}$, in the n coordinate directions. Such perturbations effectively provide information for approximating derivatives of $J[u]$ by finite difference methods, Powell [34]. At each subsequent iteration, only one interpolation point is changed so that at each subsequent iteration only one new

evaluation of $J[u]$ is required.

BOBYQA implements a truncated conjugate gradient trust-region method (Conn et al. [11], Powell [33] and Powell [34]). The optimization algorithm terminates when the trust-region radius becomes smaller than the minimum trust-region radius. Once $Q^\ell[u]$ has been determined, it is minimized subject to the bound constraints of Eq. 2.19 by an active set version of the truncated conjugate gradient (Powell [34]) to find u^ℓ, the new approximation to the parameter vector which minimizes $J[u]$. Note G^ℓ is not generally positive definite so Q^ℓ is not generally convex. In the next iteration, the set of interpolation points is updated by replacing one old interpolation point with u^ℓ so that the number of interpolation points is constant throughout the iterative process.

BOBYQA utilizes two trust-region radii; Δ_ℓ which is the trust-region radius at iteration ℓ and ρ_ℓ which is a lower bound on Δ_ℓ. At iteration ℓ, BOBYQA finds a step d_ℓ which minimizes $Q^\ell[u^\ell + d^\ell]$ subject to the condition

$$\frac{1}{2}\rho_\ell \leq ||d_\ell|| \leq \Delta_\ell, \tag{2.23}$$

and such that $u^{\ell+1} = u^\ell + d^\ell$ satisfies the bound constraints of Eq. 2.19. The purpose of the bound

$$\Delta_\ell \geq \rho_\ell, \qquad \ell = 1, 2, \ldots. \tag{2.24}$$

is to postpone the use of short steps (small values of $||d_\ell||$) until late in the calculation (Powell [34]). The user of BOBYQA has to supply the initial value of ρ_ℓ, which is denoted by ρ_{beg}, and the minimum value of ρ_ℓ, which is denoted by ρ_{end}. The optimization algorithm terminates at the iteration at which $\rho_\ell = \rho_{end}$ but the algorithm indicates that a reduction in ρ_ℓ is required at the next iteration (Powell [34]). BOBYQA sets the initial trust-region radius to $\Delta_1 = \rho_1 = \rho_{beg}$. The value of the outer trust region radius at the next iteration, $\Delta_{\ell+1}$, depends on the ratio of $r_{\ell+1}$

defined by

$$r_{\ell+1} = \frac{J[u^\ell] - J[u^\ell + d^\ell]}{Q[u^\ell] - Q[u^\ell + d^\ell]} = \frac{Q[u^\ell] - J[u^\ell + d^\ell]}{Q[u^\ell] - Q[u^\ell + d^\ell]}. \tag{2.25}$$

BOBYQA computes $\Delta_{\ell+1}$ by

$$\Delta_{\ell+1} = \begin{cases} \min[\frac{1}{2}\Delta_\ell, ||d_\ell||] & \text{if} \quad r_{\ell+1} \leq 0.1, \\ \max[\frac{1}{2}\Delta_\ell, ||d_\ell||] & \text{if} \quad 0.1 < r_{\ell+1} \leq 0.7, \\ \max[\frac{1}{2}\Delta_\ell, 2||d_\ell||] & \text{if} \quad r_{\ell+1} > 0.7, \end{cases} \tag{2.26}$$

except that $\Delta_{\ell+1}$ is set to ρ_ℓ if $\Delta_{\ell+1}$ computed from Eq. 2.26 satisfies $\Delta_{\ell+1} \leq 1.5\rho_\ell$. The inner radius ρ_ℓ is monotonically decreasing but at most iterations, $\rho_{\ell+1} = \rho_\ell$ (see Powell [34]). When a reduction in ρ_ℓ is required, BOBYQA applies the formula,

$$\rho_{\ell+1} = \begin{cases} \rho_{end} & \text{if} \quad \rho_\ell \leq 16\rho_{end}, \\ (\rho_\ell \rho_{end})^{\frac{1}{2}} & \text{if} \quad 16\rho_{end} < \rho_\ell \leq 250\rho_{end}, \\ 0.1\rho_{end} & \text{if} \quad \rho_\ell > 250\rho_{end}. \end{cases} \tag{2.27}$$

As we will discuss in later chapters of this dissertation, the objective function in the well-placement problem is noisy, i.e., exhibit discrete jumps as part of the well crosses a gridblock boundary and these jumps can conceivably introduce very localized local minima. Recall that, $\rho_\ell/2$ is the lower bound on the "trust-region" step, $||d_\ell||$, see Eq. 2.23. In order to decrease the chance of fast convergence to a local minimum with a high value of the objective function by rapidly reducing the size of ρ_ℓ, in our implementation of BOBYQA, we modify Eq. 2.27 to

$$\rho_{\ell+1} = \begin{cases} \rho_{end} & \text{if} \quad \rho_\ell \leq 2\rho_{end}, \\ (\rho_\ell \rho_{end})^{\frac{1}{2}} & \text{if} \quad \rho_\ell > 2\rho_{end}. \end{cases} \tag{2.28}$$

Eq. 2.28 will generally result in a smaller decrease in ρ_ℓ than Eq. 2.27 because in

Eq. 2.27, $\rho_{\ell+1}$ is set equal to ρ_{end} when $\rho_\ell \leq 16\rho_{end}$; however, in Eq. 2.28, $\rho_{\ell+1}$ is not set equal to ρ_{end} until $\rho_\ell \leq 2\rho_{end}$. According to Powell [34], a decrease in ρ_ℓ happens when "the work with current ρ_ℓ is found to be finished," i.e., the trust-region method could not find a new point which decreases the objective function. Therefore, Eq. 2.28 not only postpones taking smaller steps to later optimization iterations but also, the optimization domain $[\frac{1}{2}\rho_\ell, \Delta_\ell]$ is investigated with more iterations before shrinking the investigation radius by decreasing the lower bound on the trust-region radius. For the purpose of an intuitive illustration, suppose the current iterate is very close to a weak local minimum introduced by a noisy objective function and the work with the current inner trust-region radius is finished. If the inner trust-region radius is radically reduced, the optimization algorithm may converge to this local minimum which is not desirable. By using Eq. 2.28, we hope that the optimization algorithm will skip over local minima (at least those arising from a noisy objective function) and converge to a local optimum solution with smaller value of the objective function. Based on our observations, Eq. 2.28 reduces the chance of fast convergence to a local minimum which represents an unacceptably high value of the objective function, but may increase the number of optimization iterations required to obtain convergence. As we explain in the following chapters, the values of ρ_{beg} and ρ_{end} are usually close in our implementation of BOBYQA for the well-placement optimization problem and therefore, using Eq. 2.28 instead of Eq. 2.27 does not increase the computational cost of the method significantly.

CHAPTER 3

TWO-STAGE WELL PLACEMENT OPTIMIZATION METHOD BASED ON ADJOINT GRADIENT

Wang et al. [41] introduced a gradient-based procedure to optimize locations of water injection wells. Their main idea was to initialize the optimization procedure by placing an injection well in every gridblock not containing a producing well. In addition, they added a term to the conventional NPV function to account for the cost of drilling each well. Then well rates are adjusted to maximize NPV over a specified reservoir lifetime. If the rate of one of the initial wells becomes zero, the well is eliminated from the system and the cost of drilling that well is removed from the modified NPV function. As the problem requires the rates of some wells go to zero, Wang et al. [41] applied the steepest ascent algorithm with limited step size so that at most one well is eliminated at each iteration which is computationally inefficient when the initial number of wells is large. Zhang et al. [47] significantly improved the computational efficiency of the optimization procedure using a gradient-projection method. With the projected gradient, at early iterations, it is often possible to remove several wells during a single iteration.

In this chapter we improve the basic methodology introduced in Wang et al. [41] and Zhang et al. [47] so that it can be applied to more realistic problems, i.e., three-dimensional three-phase flow problems where the objective is to optimize not simply the location of water injection wells, but the location of both producers and injectors. In addition, unlike the work of Wang et al. [41] and Zhang et al. [47], we put bound constraints on wellbore pressures because, in reality, a water injection well always has a maximum bottomhole pressure constraint and producing

wells always have a minimum bottomhole pressure constraint. As upper and lower bottomhole pressure constraints represent nonlinear constraints when our parameters (well controls) are flow rates, adding bound constraints on bottomhole pressures adds a significant complication to the optimization problem. As the commercial simulator used (Eclipse 300) does not provide the gradient of these nonlinear constraints on pressure, we have devised a novel method to ensure the satisfaction of these nonlinear bottomhole pressure constraints for rate-controlled wells.

We also present a methodology which attempts to mitigate the effects of an ad hoc specification of both operating well rates and operational reservoir life as well as the number of wells by using an initialization step. Most of the well-placement algorithms specify a priori both the number of wells to be drilled and the operating rates (or pressures) for the specified operational life of the reservoir. Therefore, the final optimal well locations may not be optimal when different well rates (or pressures) and/or reservoir production life are specified. The initialization step is proposed to determine an appropriate total reservoir water injection rate and/or total reservoir production rate for the specified operational life. During the initialization stage, a large number of wells are placed in the reservoir and few if any are eliminated. After the initialization stage, a second stage is performed in which we estimate (i) the optimal number of water injection wells and/or producing wells; (ii) the optimal location of these wells and (iii) the optimal rates at these wells. Both stages use a gradient-based optimization algorithm with the relevant gradient computed by a combination of the adjoint method and analytical methods for linear constraints which are imposed using a gradient-projection method.

3.1 Well-Placement Problem Definition

Following the basic ideas of Wang et al. [41] and Zhang et al. [47], the problem of determining the optimal location of new wells (injectors and producers) is equivalent to the problem of maximizing a modified net-present-value (NPV) functional,

$J[u]$, where u denotes the vector of well controls (flow rates) and $J[u]$ is defined by

$$J(u) = \text{NPV} - \sum_{i=1}^{N_{\text{inj}}} \left[f_{\text{inj},i}\,(u)\, C_{\text{inj}} \right] - \sum_{j=1}^{N_{\text{prd}}} \left[f_{\text{prd},j}\,(u)\, C_{\text{prd}} \right], \tag{3.1}$$

where NPV denotes the standard net-present-value function defined in Eq. 2.1, C_{inj} represents the cost of drilling one injection well and C_{prd} represents the cost of drilling one producing well. N_{inj} and N_{prd}, respectively, denote the initial number of injection wells and the initial number of production wells that are placed in the reservoir at the initial step of the optimization procedure developed in here. In this optimization algorithm, we use large values of N_{inj} and N_{prd} but at convergence, the optimal number of injectors and optimal number of producers, respectively, are typically far smaller than N_{inj} and N_{prd}. In order to economically justify drilling each well, the resulting increase in the NPV function must be greater than the cost of drilling that well. Note that the two sums on the right side of Eq. 3.1 represent the costs of drilling wells. If the optimum value of the kth injection well's rate is zero, then $f_{\text{inj},k}\,(u) = 0$, the corresponding kth cost term in the first sum of Eq. 3.1 will be zero and the kth injection well will not be drilled. On the other hand, if the optimal solution includes drilling well k, we wish to have $f_{\text{inj},k}\,(u)$ to be equal to, or very close to 1 so that the cost of drilling this well will be fully accounted for in the modified NPV function, $J[u]$.

At each potential injection well, the injection rate is the control whereas at the jth producing well, the total liquid rate, $q_{\text{prd},j}$, is the control. Thus, the vector of all controls is given by

$$u = [q_{\text{inj},1}, q_{\text{inj},2}, \cdots, q_{\text{inj},N_{\text{inj}}}, q_{\text{prd},1}, q_{\text{prd},2}, \cdots, q_{\text{prd},N_{\text{prd}}}]^T. \tag{3.2}$$

NPV in Eq. 3.1, represents the standard net-present-value including the oil and gas revenues and the injection and production water cost and is defined in Eq. 2.1.

The functional $J[u]$ is maximized subject to constraints on the controls (well rates) using a gradient-projection method. Following Eq. 3.1, the derivative of the objective function, $(J(u))$, is

$$\nabla_u J(u) = \left[\frac{\partial J(u)}{\partial u_k}\right], \tag{3.3}$$

where

$$\frac{\partial J(u)}{\partial u_k} = \frac{\partial \text{NPV}}{\partial u_k} - \sum_{i=1}^{N_{\text{inj}}} \left[\frac{\partial f_{\text{inj},i}(u)}{\partial u_k} C_{\text{inj}}\right] - \sum_{j=1}^{N_{\text{prd}}} \left[\frac{\partial f_{\text{prd},j}(u)}{\partial u_k} C_{\text{prd}}\right]. \tag{3.4}$$

The gradient of NPV with respect to the control vector u is computed with the adjoint method for multiphase flow (Wu et al. [42], Li et al. [22], Brouwer and Jansen [6], Sarma et al. [35] and Kraaijevanger et al. [19]) with the gradient terms in the summations of Eq. 3.4 computed analytically. In this work, we use the "Eclipse Reservoir Optimization" option in Eclipse 300 for the gradient calculation. This option gives the derivative of NPV with respect to each control variable at each control step, i.e., $\frac{\partial \text{NPV}}{\partial u_k^n}$, where u_k^n is the kth control variable at the nth control step. For the well-placement problem, however, we specify each well control (the total rate at each well) as constant throughout the reservoir life, i.e., $u_k^n = u_k$ for all n. The gradient of NPV for the whole reservoir life with respect to u_k can be computed as

$$\frac{\partial \text{NPV}}{\partial u_k} = \sum_{n=1}^{N_c} \left(\frac{\partial \text{NPV}}{\partial u_k^n} \frac{\partial u_k^n}{\partial u_k}\right) = \sum_{n=1}^{N_c} \frac{\partial \text{NPV}}{\partial u_k^n}. \tag{3.5}$$

where N_c is the number of control steps.

As noted previously, we want the term $f_{\text{inj},i}(u)C_{\text{inj}}$ in Eq. 3.1 to represent an accurate approximation of the cost of drilling injection well i. If $f_{\text{inj},i}(u) = 0$ the well is deleted from the system, i.e., is not drilled and the associated drilling cost does not contribute to the total cost of drilling injection wells, which is given by the first sum on the right side of Eq. 3.1; whereas if the well is actually drilled we want $f_{\text{inj},j}(u) = 1$. While these two limiting values of 0 and 1 are desirable, at the

same time, we need to define $f_{\text{inj},i}(u)$ so that it is continuously differentiable and its derivatives take on values during optimization that are non-negligible compared to the corresponding values of the derivatives of NPV. It is not possible to satisfy these conditions on the gradient of $f_{\text{inj},i}(u)$ and also have $f_{\text{inj},i}(u) = 1$ for $q_{\text{inj},i} \neq 0$ and $f_{\text{inj},i}(u) = 0$ for $q_{\text{inj},i} = 0$. Similar comments apply to the $f_{\text{prd},j}(u)$ terms which account for the cost of drilling producing wells. Thus, we make some compromise on the choice of $f_{\text{inj},i}(u)$ and $f_{\text{prd},j}(u)$ to obtain a feasible and efficient algorithm.

We would also like the gradient of the drilling cost function for an individual well to be a decreasing function of the well's control (injection or production rate), i.e., the gradient of the drilling cost function for a well with a lower rate should have a larger value comparing to the gradient of the drilling cost function for a well with higher rate. Since in the computation of the derivative of the objective function $J[u]$, (Eq. 3.4), the gradient of NPV is reduced by the gradient of the cost term, this property helps eliminating the wells with low rates.

We propose the following functions for the drilling cost terms at the ℓth iteration of the optimization algorithm:

$$f^{\ell}_{\text{inj},i}\left(q^{\ell}_{\text{inj},i}\right) = \left(\frac{q^{\ell}_{\text{inj},i}}{q^{\ell-1}_{\text{inj},i}}\right)^{\beta}, \tag{3.6}$$

for $i = 1, 2, \cdots N_{\text{inj}}$ and

$$f^{\ell}_{\text{prd},j}\left(q^{\ell}_{\text{prd},j}\right) = \left(\frac{q^{\ell}_{\text{prd},j}}{q^{\ell-1}_{\text{prd},j}}\right)^{\beta}, \tag{3.7}$$

for $j = 1, 2, \cdots N_{\text{prd}}$. Note that $q^{\ell}_{\text{inj},i}$ and $q^{\ell-1}_{\text{inj},i}$, respectively, represent the injection rate of well i at the current (ℓth) and previous (($\ell-1$)st) iterations of the optimization algorithm. A similar comment applies to $q^{\ell}_{\text{prd},j}$ and $q^{\ell-1}_{\text{prd},j}$. The term β is a constant and takes a positive value less than or equal 1.0. In the computational results section presented at the end of this chapter, a sensitivity analysis on the value of β is provided, where for the other examples in the results section we use $\beta = 0.25$.

Differentiating Eq. 3.6 with respect to the well control ($q^{\ell}_{\mathrm{inj},i}$) gives

$$\frac{\partial f^{\ell}\left(q^{\ell}_{\mathrm{inj},i}\right)}{\partial q^{\ell}_{\mathrm{inj},i}} = \frac{\beta}{\left(q^{\ell-1}_{\mathrm{inj},i}\right)^{\beta}\left(q^{\ell}_{\mathrm{inj},i}\right)^{1-\beta}}, \tag{3.8}$$

which is strongly dependent on $q^{\ell}_{\mathrm{inj},i}$ particularly for small values of $q^{\ell}_{\mathrm{inj},i}$, a characteristic which is useful for driving rates to zero (eliminating wells) during the optimization process. $q^{\ell}_{\mathrm{inj},i}$ can be written as $q^{\ell}_{\mathrm{inj},i} = \gamma q^{\ell-1}_{\mathrm{inj},i}$, where γ is a positive number and can be less than or greater than 1. Therefore, Eq. 3.8 is rewritten as

$$\frac{\partial f^{\ell}\left(q^{\ell}_{\mathrm{inj},i}\right)}{\partial q^{\ell}_{\mathrm{inj},i}} = \frac{\beta}{\left(q^{\ell-1}_{\mathrm{inj},i}\right)^{\beta}\left(\gamma q^{\ell-1}_{\mathrm{inj},i}\right)^{1-\beta}} = \frac{\beta}{\left(q^{\ell-1}_{\mathrm{inj},i}\right)\left(\gamma\right)^{1-\beta}} \tag{3.9}$$

In Fig. 3.1, the value of $\frac{\partial f^{\ell}\left(q^{\ell}_{\mathrm{inj},i}\right)}{\partial q^{\ell}_{\mathrm{inj},i}}$ is plotted with respect to $q^{\ell}_{\mathrm{inj},i}$ for three different values of $q^{\ell-1}_{\mathrm{inj},i}$. Note that in this plot the value of β is assumed $\beta = 0.25$. As it is shown in this figure, larger $q^{\ell}_{\mathrm{inj},i}$ results a smaller value for the derivative of the drilling cost function. Also, a larger value of the rate of a well at the previous iteration, results in a smaller value of the gradient of the cost function. These two properties of the derivative are both favorable since they help to eliminate the wells with smaller and decreasing rates. The problem with the proposed drilling cost function is in evaluating the objective function. As the well rate can decrease or increase significantly from iteration to iteration, the function in Eq. 3.6 can take values significantly different than 1.0 for $q^{\ell}_{\mathrm{inj},i} \neq 0$. (Using the βth root for $\beta < 1$ in Eqs. 3.6 and 3.7 moderates this deviation from unity.) However, to avoid this potential difficulty, we simply use the definitions of Eqs. 3.6 and 3.7 when computing gradients but when evaluating $J[u]$, we set $f_{\mathrm{inj},i} = 1.0$ if $q_{\mathrm{inj},i} > 0$ and set $f_{\mathrm{prd},j} = 1.0$ whenever $q_{\mathrm{prd},j} > 0$. The examples presented here were all done with this procedure.

For well-placement optimization, we wish to maximize the modified NPV functional $J[u]$ subject to bound constraints and possibly equality and inequality

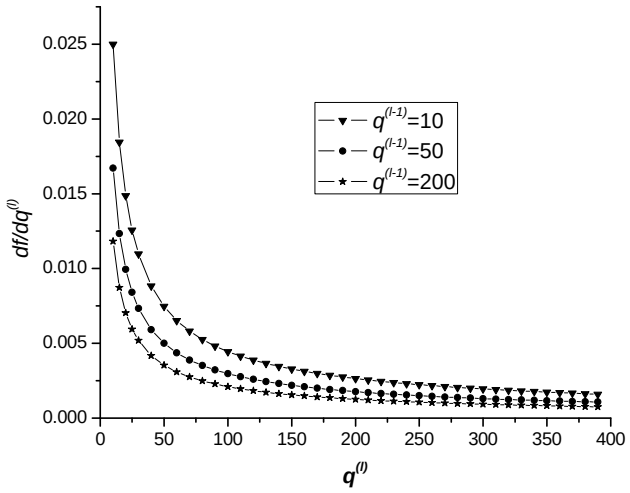

Figure 3.1: Derivative of the cost function versus rate of the well.

constraints. Bound constraints would naturally include minimum and maximum values of flowing bottomhole pressures and well flow rates. As we have defined the controls as well rates, a constraint on bottomhole pressure is a nonlinear function of the control vector and the calculation of its gradient could not be done analytically. In the well-placement optimization procedures presented here, a method is introduced to avoid violation of bounds on wellbore pressure by adjusting the upper bound on the rate so the well can always operate under a specified rate control and does not switch to bottomhole pressure control during an iteration of the optimization algorithm. This obviates the need to compute gradients of nonlinear constraints and bound constraints are explicitly imposed only on the components of the rate control vector during an iteration of the optimization algorithm.

In addition, equality constraints are imposed on the total injection rate and the total production rate. This is done not because it is required for the definition of the well optimization problem but because it improves the robustness and efficiency of the algorithm we use here which starts with a large number of potential wells and tries to eliminate a large number of them during iterations of the optimization algorithm. By using an equality constraint on the total injection rate and

the total production rate, if $J[u]$ is increased by increasing the rates at some wells, the rates at some other wells must be decreased. As the only way to eliminate a well is to decrease its rate to zero, the equality constraints on total rates tend to promote our objective of eliminating some wells. On the other hand, specifying the total injection (or production) rate a priori is difficult as if it is too large, we may not be able to reset a well's rate to avoid violation of specified bounds on flowing bottomhole pressure. More importantly, the final optimum location of the wells are dependent on the specified total rates. To avoid this potential problem, a two-stage optimization procedure is introduced where in the first initialization stage, we try to find appropriate values to use for the total injection rate and total production rate when specifying the equality constraints.

3.2 Gradient Projection for Linear Constraints

In the optimization algorithm, we maximize the functional $J(u)$, subject to the following constraints,

$$\sum_{i=1}^{N_{\text{inj}}} q_{\text{inj},i} = q_{\text{t,inj}}, \tag{3.10}$$

$$\sum_{j=1}^{N_{\text{prd}}} q_{\text{prd},j} = q_{\text{t,prd}}, \tag{3.11}$$

$$0 \le q_{\text{inj},i} \le q_{\text{inj},i}^{\text{up}}, \qquad 1 \le i \le N_{\text{inj}}, \tag{3.12}$$

$$0 \le q_{\text{prd},j} \le q_{\text{prd},j}^{\text{up}}, \qquad 1 \le j \le N_{\text{prd}}. \tag{3.13}$$

In the initialization stage where we determine approximate total rates, we use only the bound constraints. The upper bound, $q_{\text{inj},i}^{\text{up}}$ is initially set equal to $q_{\text{t,inj}}$ for all i and $q_{\text{prd},j}^{\text{up}}$ is initially set equal to $q_{\text{t,prd}}$ for all j. However, the upper bound for the rate of a well can decrease during optimization. More detail is given in the following paragraphs where we also explain the procedure for satisfying the bottomhole pressure constraints of the wells.

The total rate constraints (Eqs. 3.10 and 3.11) and all active bound constraints at iteration ℓ are linear and can be written in the matrix form,

$$A^{\ell}u^{\ell} = b^{\ell}, \tag{3.14}$$

where A^{ℓ} is an $M \times (N_{\text{inj}} + N_{\text{prd}})$ matrix, b^{ℓ} is an M-dimensional column vector; M is the number of active constraints at iteration ℓ which in the optimization algorithm includes the linear total rate constraints and the active bound constraints. For example, in the case where there are two active bound constraints (the rates of the first injector and the second producer are at their lower and upper bounds, respectively), A and b, respectively, are given by,

$$A^{\ell} = \begin{bmatrix} 1 & 1 & \cdots 1 & 0 & 0 & \cdots & 0 \\ 0 & 0 & \cdots 0 & 1 & 1 & \cdots & 1 \\ 1 & 0 & \cdots 0 & 0 & 0 & \cdots & 0 \\ 0 & 0 & \cdots 0 & 0 & 1 & \cdots & 0 \end{bmatrix}, \tag{3.15}$$

and

$$b^{\ell} = \begin{bmatrix} q_{t,\text{inj}} \\ q_{t,\text{prd}} \\ 0 \\ q^{\text{up}}_{\text{prd},i} \end{bmatrix}. \tag{3.16}$$

During maximization, the control vector is updated as

$$u^{\ell+1} = u^{\ell} + \alpha^{\ell+1} d^{\ell+1}, \tag{3.17}$$

where ℓ is the iteration index, $d^{\ell+1}$ is the search direction obtained by projecting the

gradient $g^\ell = \nabla_u J[u^\ell]$ onto the hyperplane of the active constraints, i.e.,

$$d^{\ell+1} = \left[I - (A^\ell)^T (A^\ell (A^\ell)^T)^{-1} A^\ell\right] g^\ell. \tag{3.18}$$

As it is shown in Chapter 2, the projected gradient $d^{\ell+1}$ is uphill ($(g^\ell)^T d^{\ell+1} > 0$) where $d^{\ell+1} \neq 0$, and the active constraints are satisfied at the $(\ell+1)$st iteration as long as they are satisfied at the ℓth iteration, i.e., $A^\ell d^{\ell+1} = 0$.

3.3 Well-Placement Optimization Algorithm

In this section, we discuss the well-placement optimization algorithm. In the following, first, we introduce the method for considering the bottomhole pressure constraints in the well-placement problem. Then the procedure for determining the active bound constraints is described and at the end, the well-placement algorithm is presented. In the following discussions of this chapter, we use general notation and let u_i^{low} and u_i^{up}, respectively, represent the lower and upper bound for the ith control variable, u_i.

3.3.1 Bottomhole Pressure Nonlinear Constraints

With the definition of the optimal well location problem described in here, the well controls are the total liquid production rate at producers and the water injection rate at injectors, which are held constant for the whole reservoir life. However, for application to real fields, we would wish impose some lower limit on the bottomhole pressure at a producing well and an upper limit on the wellbore pressure at each injection well, for example to keep the pressure below parting pressure to avoid fracturing the formation. These pressure constraints for injection well and producing wells, respectively are written as

$$p_{\text{wf,inj},i} < p_{\text{wf,max}}, \tag{3.19}$$

for $i = 1, 2, \cdots N_{\text{inj}}$ and

$$p_{\text{wf,prd},j} > p_{\text{wf,min}}, \tag{3.20}$$

for $j = 1, 2, \cdots N_{\text{prd}}$. As each bottomhole pressure is a nonlinear function of the well rates, the constraints in Eqs. 3.19 and 3.20 are nonlinear state-control constraints and if these pressure constraints are added to the constrained optimization problem, the gradients of these constraints with respect to the controls (well rates) must be calculated during each iteration of the optimization algorithm. Although this gradient calculation can be done with the adjoint method, our objective is to couple our well-placement algorithms with commercial simulators. Since Eclipse 300, which is used in the examples presented here, and other commercial simulators do not provide the adjoint gradient of bottomhole pressure with respect to well controls where the well controls are well rates, we impose a practical way to ensure that these bottomhole pressure constraints are satisfied during well-placement optimization without explicitly adding the constraints to the optimization problem definition. The proposed method for changing the rate of a well to fix the bottomhole pressure constraint violation is shown in Fig. 3.2.

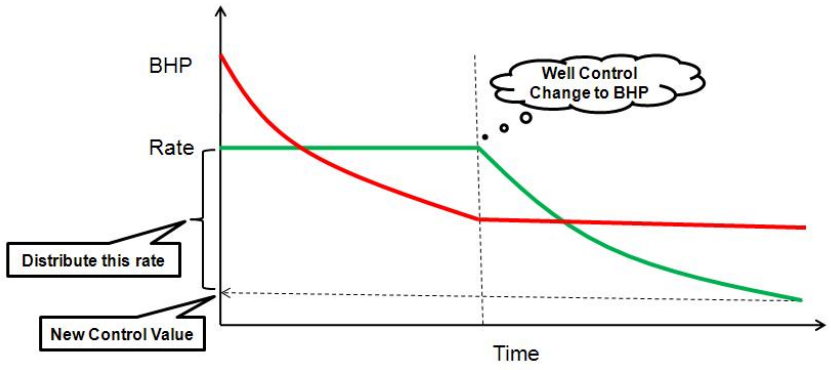

Figure 3.2: Schematic of the production rate and BHP changes of a production well in time.

In the proposed method, we explicitly include the bottomhole pressure constraints in the input file of the reservoir simulator during each iteration of the well-

placement optimization. Note that the well controls for the producers and injectors, respectively are the constant total liquid production and water injection rates which are estimated by the optimization algorithm at each iteration. If a well cannot meet the constant rate target specified in the current control vector without violating the bottomhole pressure constraint, we will cut the rate before doing the optimization step in a way that ensures the well can produce (or inject) at the specified rate without violating its pressure constraint. Because the total production rate and the total injection rate are fixed by the two equality constraints, if the producing (or injection) rate is cut at one well, the rate at one or more other wells must be increased to satisfy the relevant equality constraint on total rate. We propose the following method to make these rate changes.

Recall that the first N_{inj} components of the control vector u correspond to controls (water injection rates) at the N_{inj} potential injection wells and the last N_{prd} entries of u correspond to controls (total liquid production rates) at the N_{prd} potential producing wells. $u^{\ell+1}$ is the vector of controls estimated by the optimization algorithm at iteration $\ell + 1$. If the jth producer is switched from the rate control $q^{\text{opt}}_{\text{prd},j} \equiv u^{\ell+1}_{j+N_{\text{inj}}}$ to production at the minimum bottomhole pressure during the simulation run using the controls specified by $u^{\ell+1}$, then we simply set $u^{\ell+1}_{j+N_{\text{inj}}}$ equal to the minimum producing rate obtained at any time step of the reservoir simulation run:

$$u^{\ell+1}_{j+N_{\text{inj}}} = q_{\text{prd, min},j} \tag{3.21}$$

Also, in order to prevent a violation of the bottomhole pressure constraint at future iterations of the optimization algorithm, we modify the upper bound on $u_{j+N_{\text{inj}}}$ as

$$u^{\text{up}}_{j+N_{\text{inj}}} = q_{\text{prd, min},j} \tag{3.22}$$

We apply the preceding rate control modification at each producing well where

the well producing condition was switched to minimum bottomhole pressure control during the reservoir simulation run. Because some well flow rates are decreased by this modification, the sum of the producing rates is no longer equal to the total production rate, $q_{t,\text{prd}}$ specified in the equality constraint of Eq. 3.11. To satisfy this equality constraint, we must increase the production rates at some wells where the bottomhole pressure constraint was not violated. Assuming that the components of $u^{\ell+1}$ that were set equal to the corresponding minimum rate by this procedure are given by $u^{\ell+1}_{k_j}$, $j = 1, 2, \cdots m_p$, the sum of the last N_{prd} components of $u^{\ell+1}$ is equal to the $q_{t,\text{prd}} - q_{\text{prd,redis}}$ where

$$q_{\text{prd,redis}} = \sum_{j=1}^{m_p} \left(q^{\text{opt}}_{\text{prd},k_j} - q_{\text{prd,min},k_j} \right). \tag{3.23}$$

To satisfy the equality constraint of Eq. 3.11, we must increase the rates at some wells where the bottomhole pressure constraint was not violated and the sum of these rates increases must sum to $q_{\text{prd,redis}}$. Although there are many ways to distribute this total rate $q_{\text{prd,redis}}$, we want to do so in a way that does not tend to introduce new violations of the minimum bottomhole pressure constraint. The best procedure we have found to minimize the number of new violations of the minimum bottomhole pressure constraint is to distribute $q_{\text{prd,redis}}$ inversely proportional to the well rates. Specifically, if $u^{\ell+1}_{N_{\text{inj}}+n_i} = q^{\text{opt}}_{\text{prd},n_i}$, $i = 1, 2, \cdots m_q$, denotes the set of producing liquid rate controls that were honored throughout the reservoir simulation run, the rate controls at these wells are changed to

$$u^{\ell+1}_{N_{\text{inj}}+n_i} = \frac{1}{q^{\text{opt}}_{\text{prd,inv}}} \frac{1}{q^{\text{opt}}_{\text{prd},n_i}} q_{\text{prd,redis}} + q^{\text{opt}}_{\text{prd},n_i}, \tag{3.24}$$

where $q^{\text{opt}}_{\text{prd,inv}}$ is defined by

$$q^{\text{opt}}_{\text{prd,inv}} = \sum_{i=1}^{m_q} \frac{1}{q^{\text{opt}}_{\text{prd},n_i}}. \tag{3.25}$$

This procedure distributes $q_{\text{prd, redis}}$ to lower rate wells so that wells that are already producing at high rate will not be increased to a rate that can not be achieved without violating the minimum bottomhole pressure restriction. Exactly the same procedure is used to modify rate controls at injection wells if the upper bound on the injection pressure cannot be honored with the injection rate specified by the injection rate components of $u^{\ell+1}$.

3.3.2 Identifying Active Bound Constraints

In the gradient projection method, we need to determine which wells have active lower or upper bound constraint to form the matrix A (matrix of constraints). The lower bound constraint of a well is active if the rate of the well is zero. Once this happens, the well is eliminated and the lower bound constraint will remain active for the rest of the iterations. The upper bound constraints on rate for injectors and producers are initially set at the total injection and production rates, respectively. Therefore, in this situation the upper bound of a well would be active only if the rate of this well is equal to the total rate constraint which implies that this is the only producer or injector that remains. However, as we previously explained (Eq. 3.22), the upper bound constraint value of the rate of a well can decrease within the optimization process for honoring the bottomhole pressure constraints set in the reservoir simulator. When such a modification occurs, it is possible to have several wells with rates equal to their upper bound values. For the gradient projection method, we need to determine the wells that have active upper and lower bound constraints to construct matrix A (Eq. 3.14) for the calculation of the projected gradient using Eq. 3.18.

The task of identifying active bound constraints is more difficult than it appears to be. The change in upper bound values to satisfy the bottomhole pressure constraints discussed above further complicates the situation. As an example, consider the case where the rate control for injector i was changed to $u_i^{\ell+1} = q_{\text{inj, min},i}$

and the upper bound constraint was changed to $u_i \leq u_i^{\text{up}} \equiv q_{\text{inj, min},i}$ in a previous iteration. If the component of the next computed search direction corresponding to the rate control for injection well i is positive, a step in the search direction would increase u_i to a value greater than $u_i^{\text{up}} = q_{\text{inj, min},i}$ which would be likely to result in a violation of the maximum bottomhole pressure constraint. To avoid this possibility, one should make $u_i = q_{\text{inj, min},i}$ an active constraint and recompute the projected gradient with this active constraint. If the component of the search direction corresponding to the rate control for injection well i is negative, a step in the search direction would decrease u_i to a value smaller than u_i^{up} which would not cause a violation of the maximum bottomhole pressure constraint so the constraint $u_i \leq q_{\text{inj,min},i}$ should remain inactive. In order to consider this situation, an algorithm is proposed to rigorously determine the wells with the active upper bound constraints. The upper (lower) bound constraint of a well is active if the two following conditions are both satisfied: (i) the rate of the well is at its upper (lower) bound value, (ii) the search direction of the next optimization iteration tends to increase (decrease) the value of the control. Therefore, the state of a bound constraint for a control in an iteration depends on both the value of the control and the vector of the gradient of the objective function with respect to all controls at that iteration. The proposed procedure for identifying the active bound constraints is based on a successive application of the gradient projection formula (Eq. 3.18). In this procedure, first, we assume that all the wells have inactive bound constraints. Then, wells with active bound constraint are identified one by one. At the end of this procedure, all the wells with active bound constraints are identified. Once all the active constraints are identified, the matrix of active constraints (matrix A in Eq. 3.18) is constructed accordingly. This matrix is needed for gradient projection at each iteration of the optimization algorithm. For simplicity, here we only consider the case of identifying the active upper bounds. However, the approach can be easily extended to identify inactive lower

bounds which allows an eliminated well to reopen in a future optimization iteration. The successive gradient projection procedure follows:

Procedure for Identifying Active Upper Bound Constraints:

a) Assume that all the wells with zero rate have active lower bound constraint. Assume that the upper bound constraint for all wells are inactive. Therefore the only present constraints are active lower bound constraints (and the total rate constraints if they are present). Consider all the active constraints in addition to the constant total rate constraints (if they are present) and construct matrix A.

b) Project the gradient, g, to the current active constraints, matrix A, by applying Eq. 3.18 to compute the search direction d. Note that a step in the direction of d is uphill and honors all the active constraints present in matrix A.

c) Consider the computed components of the search direction, d, (projected gradient), for all the wells which (i) have their rates at their upper bound value and (ii) have inactive upper bound constraints. If there is none which satisfies both (i) and (ii) then goto step (e).

d) If the search direction component corresponding to all the wells which satisfy both (i) and (ii) are negative, then go to step (e). Otherwise, choose the one which satisfies (i) and has the largest positive search direction component. Set the upper bound constraint for this well active. Update the matrix A accordingly and go to step (b).

e) If we arrive at this step, all the wells with their rates at their upper bounds and with positive search direction components are set to active. Therefore, all the active lower and upper bound constraints are identified and matrix A is constructed.

3.3.3 Optimization Algorithm

In the following, we present the well-placement optimization algorithm. In order to achieve the goal of eliminating more than one well per iteration by setting its rate to zero, we attempt to project the gradient onto L bounds at the same time where L is a positive integer which represents the maximum number of wells we try to force to their upper or lower bound at one iteration of the optimization algorithm. Note that putting the rate of a well at its lower bound is equivalent to eliminating that well. Given the control variables at ℓth iteration, u^ℓ and the search direction $d^{\ell+1}$, at least one component of u^ℓ would reach either its lower or upper bound if the step size $\alpha^{\ell+1}$ were set equal to $\alpha^{\ell+1}_{\max}$ defined as

$$\alpha^{\ell+1}_{\max} = \min\left(\alpha^{\ell+1}_{\max,i}\right), \tag{3.26}$$

where

$$\alpha^{\ell+1}_{\max,i} = \begin{cases} \frac{u_i^{\text{low}} - u_i^\ell}{d_i^{\ell+1}} & \text{if } d_i^{\ell+1} < 0, \\ \\ \frac{u_i^{\text{up}} - u_i^\ell}{d_i^{\ell+1}} & \text{if } d_i^{\ell+1} > 0. \end{cases} \tag{3.27}$$

The step size $\alpha^{\ell+1} = \alpha^{\ell+1}_{\max}$ puts the rate of at least one well to its lower (zero) or upper bound. If the step size results in $u_k = q_{\text{inj},k}$ equal to its lower bound, then the kth injection well is eliminated from the system. A similar comment applies to the case where the rate at a producing well is equal to its lower bound, the step size defined by Eq. 3.26 is used.

One additional comment is needed before discussing the optimization algorithm. If the step size defined by Eq. 3.26 does not give $J[u^{\ell+1}] > J[u^\ell]$, then we need to cut the step size until we obtain an increase in the objective function. Here, we simply cut the step size by a factor of 1/2. Steps of the well-placement optimization algorithm follow:

Well-Placement Optimization Algorithm:

1. Specify L, the number of wells we attempt to put at their lower/upper bound at each iteration. This is equivalent to the maximum number of wells that we try to eliminate at one iteration. Set the iteration index to $\ell = 1$.

2. Check for the stopping criteria: all the wells are at active constraint. If the criteria are met, terminate the algorithm. Otherwise, compute the gradient $g^\ell = \nabla_u J[u^\ell]$ and proceed to the next iteration.

3. Set $k = 1$ and $u^{0,\ell+1} = u^\ell$. If $[(N_{inj} + N_{prd}) - M] \leq L$, set $L = 1$, where M is the number of active constraints in the previous iteration, $\ell - 1$.

4. Identify the active constraints, which include the upper/lower bound constraints and the total rate constraints. Form the matrix of constraints (matrix A^ℓ) by implementing the procedure from the previous section. Apply Eq. 3.18 to project the gradient to the active constraints to obtain the search direction $d^{\ell+1}$ (Eq. 3.18), which is now denoted by $d^{k,\ell+1}$.

5. Set $\alpha^{k,\ell+1} = \alpha_{\max}$ where $\alpha_{\max}$ is computed from Eqs. 3.26 and 3.27. Set $u^{k,\ell+1} = u^{k-1,\ell+1} + \alpha^{k,\ell+1} d^{k,\ell+1}$. From our previous discussion the number of components (well rates) of $u^{k,\ell+1}$ that are equal to their lower or upper bound values is strictly greater than the number of components of $u^{k-1,\ell+1}$ that are equal to their lower or upper bound. Thus, this step will increase the number of active constraints by at least one. (Note that in steps 4 and 5, no reservoir simulation runs are required.)

6. Repeat steps 4 and 5 for $k = 2, 3, \cdots L$, to obtain $u^{k,\ell+1}$. From the discussion at step 5, setting $u^{\ell+1} = u^{L,\ell+1}$ puts at least L well rates equal to the one of their bound values (eliminates them from the system or puts them equal to their upper bound values). Note, at this point $k = L$, and we must check to see if by eliminating k wells, $k = L, L-1, \cdots, 1$, we increase $J[u]$.

7. In the current step, we run the simulator with the controls specified by $u^{k,\ell+1}$ and calculate $J[u^{k,\ell+1}]$.

8. If (a) $k \geq 1$, (b) $J[u^{k,\ell+1}] > J[u^{\ell}]$, and (c) no bottomhole pressure constraints are violated, set $u^{\ell+1} = u^{k,\ell+1}$. Increase the iteration index ℓ by one, set $L = k$, and go to step 2. Otherwise, go to step 9.

9. If $k > 1$, decrease k by one and go to step 7. Otherwise, we must have $k = 1$ and we go to step 10.

10. If we arrive at this step, there are only two possibilities. (a) If $J[u^{1,\ell+1}] > J[u^{\ell}]$ and a bottomhole pressure constraint is violated at one or more wells, then we redistribute rates and modify the upper bound constraint values as in Eq. 3.22. We repeat the rate redistribution if other well bottomhole pressure constraint violation occurs. $u_{rd}^{\ell+1}$ is the modified rates after performing the rate redistribution procedure. If $J[u_{rd}^{\ell+1}] > J[u^{\ell}]$, then set the $u^{\ell+1} = u_{rd}^{\ell+1}$, increase the iteration index ℓ by one, set $L = 1$ and go to step 2. Otherwise, the rate redistribution procedure resulted in a smaller $J[u]$ value and we then go to situation (b). (b) If $J[u^{1,\ell+1}] \leq J[u^{\ell}]$, then set $\alpha^{\ell+1} = 0.5\alpha^{1,\ell+1}$ and set $u_c^{\ell+1} = u^{\ell} + \alpha^{\ell+1} d^{1,\ell+1}$. If $J[u_c^{\ell+1}] > J[u^{\ell}]$, we check for the bottomhole pressure constraint violations. If no bottomhole pressure constraint is violated, set $u^{\ell+1} = u_c^{\ell+1}$, increase the iteration index ℓ by one, set $L = 1$ and go to step 2. Otherwise if $J[u_c^{\ell+1}] \leq J[u^{\ell}]$, we decrease the current step size $\alpha^{\ell+1}$ by a factor of 2 again and repeat the process. Cutting the step size by a factor of two is repeated at most five times. If the modified NPV function, $J[u]$ did not improve after 5 times of cutting the step length, we go to step 11. Note if we reach the point where we cut the step size in half, then no well rates are set to one of its bounds during the iteration, we are simply changing some of the rates to attempt to increase the modified NPV function, $J[u]$. Once $J[u_c^{\ell+1}] > J[u^{\ell}]$,

we check the bottomhole pressure constraint violation for $u = u_c^{\ell+1}$. If no bottomhole pressure constraints are violated, set $u^{\ell+1} = u_c^{\ell+1}$, increase the iteration index ℓ by one, set $L = 1$ and go to step 2. Otherwise, the rate redistribution procedure resulted a lower $J[u]$, therefore go to step 11.

11. If we arrive at this step, the modified NPV functional, $J[u]$, did not improve by cutting the step length for five times or the rate redistribution (for satisfying the bottomhole pressure constraints) performed after cutting the step length, resulted in a lower $J[u]$. Here, we set $\alpha^{\ell+1} = \alpha^{1,\ell+1}$, $u^{1,\ell+1} = u^{\ell} + \alpha^{1,\ell+1} d^{1,\ell+1}$. As discussed below, continuing to iterate by this process can allow the algorithm to escape from a strong local minimum as is illustrated by later examples. Now, check the bottomhole pressure constraint violation for $u = u^{1,\ell+1}$. If no bottomhole pressure constraints are violated, set $u^{\ell+1} = u^{1,\ell+1}$, increase the iteration index ℓ by one, set $L = 1$ and go to step 2. If a pressure constraint is violated at one or more wells, then similarly we redistribute rates and modify the upper bound constraint values as in Eq. 3.22. We repeat the rate redistribution if other well bottomhole pressure constraint violation occurs. When all the bottomhole pressure constraints are satisfied, set $u^{\ell+1} = u_{rd}^{\ell+1}$, which $u_{rd}^{\ell+1}$ are the modified rates after performing the rate redistribution procedure. Set $L = 1$ and go to step 2.

The procedure described above is for the general case of optimizing both producers and injectors simultaneously. A similar procedure can be applied for finding the optimal locations of only injection wells or only producing wells. Note that the value of L, the number of wells which we try to force to their bound, is modified during the optimization iterations.

Because we seek to identify more than one local maximizer, step 2 does not employ a standard convergence test. If in step 10, we are not able to find a $u^{\ell+1}$ with $J[u^{\ell+1}] > J[u^{\ell}]$, it may be because we are at a local maximum of $J[u]$. In this

case, in step 11, we take a step of length $\alpha^{\ell+1} = \alpha^{1,\ell+1}$ and $u^{\ell+1} = u^{\ell} + \alpha^{\ell+1} d^{1,\ell+1}$. In many cases, this step will result in the elimination of exactly one well, but at a minimum we have projected the gradient onto one additional bound so we can return to step 2 and try again to obtain a larger value of $J[u]$. This simple procedure allows us to escape from a local maximum. With this process, the optimization algorithm may do several steps where at each step, we eliminate exactly one well or at least increase the number of active constraints by one, but do not increase the NPV functional $J[u]$, i.e., we have $J[u^{\ell+1}] \leq J[u^{\ell}]$. However, after several such steps, we again start to increase $J[u]$ from iteration to iteration until we encounter another local maximum. By continuing this process we often find a few local maximum, then we simply pick the optimal solution, (u^*), the local maximum which gives the largest value of $J[u]$. We always continue gradient projection iterations until we reach the point in step 2 where no degrees of freedom remain for the control variables for the next gradient projection iteration. For the stopping criteria, we check for the number of active constraints (number of wells with active lower or upper bound constraints plus the total rate constraints). The stopping criterion is when the number of active constraints is equal to the number of control variables. In this situation, there are no degrees of freedom remaining and we terminate the algorithm. Note that in the most general case where we place both the injection and production wells at the same time, this convergence criterion is met when either of the two following conditions are satisfied: (i) the number of injection wells with active lower or upper bound constraint plus one is equal to the number of injection wells. (ii) the number of production wells with active lower or upper bound constraint plus one is equal to the number of production wells. Once the stopping criterion is met, we terminate the algorithm. The u^{ℓ} corresponding to the highest value of $J[u]$ will be returned as the optimal solution of the well-placement problem.

3.4 Initialization Step for the Well-Placement Algorithm

The "optimal well locations" determined by methods presented in the literature depend on the specified well rates (or pressures) and the specified operational life of the reservoir. For example, suppose we wish to drill a single additional water injection well in a reservoir that is under production but currently has a single producing well. If a small water injection rate and a short reservoir life time are specified, an optimal location of the injector will be closer to the producer than for the case where a high water injection rate and a much longer reservoir life time are specified. The well-placement optimization algorithm we developed has the advantage that only the total reservoir injection or production rates need to be specified and optimal rates for individual wells are determined simultaneously with location during the optimization process. Nevertheless, our method is still sensitive to the total rates specified and the operational time specified. By invoking the initialization algorithm described in this section to determine the total injection or production rates to be used in the equality constraints of Eq. 3.10 (or Eq. 3.11), we have found that the robustness and efficiency of our well-placement algorithm is improved. Note that the initialization can be performed when placing the injection or the production wells only while the other group of wells are considered to operate on their specified well control.

Here, we explain the initialization procedure for placing the injection wells. For this purpose, we assume the production wells are already placed and have their specified well control. In this initialization stage, we determine the appropriate total injection rate by maximizing the conventional NPV functional of Eq. 2.1. Then we use the total injection rate obtained from this step in the equality constraint of Eq. 3.10 and apply the well-placement optimization algorithm defined in the previous section to maximize the functional J defined in Eq. 3.1 subject to the total injection rate constraint and the bound constraints. In the initialization stage where appropri-

ate total rate is determined for a specified reservoir life time, no equality constraints are imposed; however, an upper bound for each well rate is specified and this bound may decrease for a well in order to satisfy the bottomhole pressure constraint of the well. We still attempt to drive the rate control for some wells to a lower bound (zero) or an upper bound by taking a step size as defined by Eq. 3.26, i.e., we still use a projection gradient type algorithm. We stop the optimization procedure when both of the following criteria are satisfied: (A) the algorithm takes a step smaller than the step size of Eq. 3.26 (which means that we could not take a step large enough to reach the next bound constraint) and (B) the change in the total rate between two successive iterations is less than one percent of the estimated total rate.

The specific steps of the total rate initialization algorithm for the injection well locations follows:

Total Rate Initialization Algorithm:

1. Distribute a large number of injectors in the reservoir. Specify an arbitrary total injection rate and specify the upper bound values for the injection rate of the wells, $q_{\mathrm{inj},i}^{\mathrm{up}}$. A reasonable choice for the initial total injection rate is a fraction of pore volume of the reservoir. This total rate is distributed uniformly among the injection wells.

2. Next we apply the well-placement optimization algorithm derived earlier to maximize the standard NPV by modifying injection rates but with two changes: (a) no equality constraint on total injection rate is used; and (b) at the $(\ell+1)$st iteration of the optimization algorithm, we redefine the upper bound on the injection rate of injection well i as

$$u_i^{\mathrm{up},\ell+1} = q_{\mathrm{inj},i}^{\mathrm{up},\ell+1} = \min\left\{q_{\mathrm{inj},i}^{\mathrm{up}}, 2q_{\mathrm{inj},i}^{\ell}, q_{\mathrm{inj},i}^{\mathrm{up,BHP}}\right\}, \tag{3.28}$$

where $q_{\mathrm{inj},i}^{\mathrm{up}}$ is the initially specified upper bound for the rate of injection well i

and $q_{\text{inj},i}^{\text{up,BHP}}$ is the approximation of the maximum rate that can be used without violating the upper bound on the injection well pressure. The value of $q_{\text{inj},i}^{\text{up,BHP}}$ would be explicitly determined only if injection well i was unable to inject at the optimal rate determined without violating the bottomhole pressure constraint. If this modification did not occur, we would set $q_{\text{inj},i}^{\text{up,BHP}} = q_{\text{inj},i}^{\text{up}}$. Eq. 3.28 limits the maximum change in a well's rate in order to avoid sudden huge changes in the total injection rate. Note that, during an optimization step, we will typically eliminate some injectors by taking their injection rates to the lower bound of zero.

3. The initialization step is continued until meeting the convergence criteria, which are defined by

$$\frac{|q_{\text{inj,t}}^{\ell+1} - q_{\text{inj,t}}^{\ell}|}{\max\left\{q_{\text{inj,t}}^{\ell}, 1\right\}} < 0.01 \quad \text{and} \quad \alpha^{\ell+1} < \alpha_{\max}^{\ell+1}, \tag{3.29}$$

where

$$q_{\text{inj,t}}^{\ell+1} = \sum_{i=1}^{N_{\text{inj}}} q_{\text{inj},i}^{\ell+1}. \tag{3.30}$$

$q_{\text{inj,t}}^{\ell+1}$ and $q_{\text{inj,t}}^{\ell}$ are the estimated total injection rates at iterations $(\ell+1)$ and ℓ, respectively.

A similar procedure is applied for the initialization step when placing the producers. We still apply the gradient projection method without any total rate constraint to optimize NPV while we modify the upper bound constraints in the same way as in the preceding initialization algorithm.

3.5 Computational Results

3.5.1 Example 1: 2D Heterogenous Reservoir

Example 1 is a 2D, two phase (oil-water), heterogeneous reservoir. The reservoir size is 3000×2000 ft with a 15×10 grid system. Porosity is constant and equal to 0.25 throughout the reservoir. The log-permeability field of the reservoir is shown in Fig. 3.3. The total and hydrocarbon pore volumes of this reservoir are 13.6 and 10.6 MMRB, respectively. The reservoir has two fixed production wells at gridblocks $(6, 6)$ and $(13, 4)$. The bottomhole pressure at producers is fixed and equal to $1,000$ psi. Initially 40 injection wells are placed in the reservoir. The initial well locations are shown in Fig. 3.3. The oil price is 80 \$/STB and water injection and water production costs are 10 \$/STB and 30 \$/STB, respectively and the annual discount rate is $b = 0$. The drilling cost of each injection well is $\$1,000,000$. The maximum bottomhole pressure constraint for injection wells is $9,000$ psi. Through this simple example, the importance and effectiveness of the proposed initialization step is discussed.

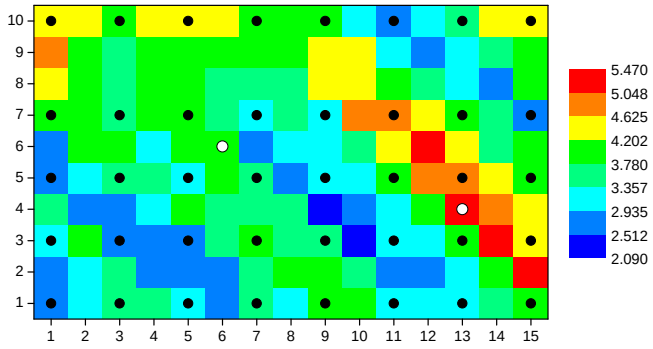

Figure 3.3: Initial injection well locations, Example 1.

Two cases are considered in this example. The first case is the well-placement optimization without the initialization step. In this case, the total injection rate for the reservoir is specified. In the second case, first we apply the initialization step

to find the optimum total injection rate for the reservoir. Then, the well-placement optimization is performed with the computed total injection rate.

Case 1: Optimization of the Injection Well Locations Under Total Injection Rate Constraint: In this case, the well-placement optimization is performed with two different total injection rate constraints of $q_{\mathrm{t,inj}} = 400$ and $q_{\mathrm{t,inj}} = 4,000$ STB/D. In both cases, the total injection rates are initially distributed uniformly between all injectors and the maximum bottomhole pressure for injectors is $9,000$ psi. The producing reservoir life is set equal to 4 years. The final well locations are shown in Figs. 3.4(a) and 3.4(b) for the total injection rates of $q_{\mathrm{t,inj}} = 400$ and $4,000$ STB/D, respectively. In these two figures, the well locations are plotted in the NPV map of the production from the reservoir with the total injection rates of $q_{\mathrm{t,inj}} = 400$ and $4,000$ STB/D, respectively. The NPV maps are generated numerically by putting a single injection well injecting at the specified injection rate and computing the modified NPV function which includes the cost of drilling the injection well. By moving the single injector from gridblock to gridblock we generate the NPV map.

In Figs. 3.4(a) and 3.4(b), it can be observed that, the rate of the well directly influences the NPV map which indicates that the optimum location of a well with a specified rate is dependent to the injection rate of the well. For a lower injection rate, the NPV map shows that gridblocks closer to the producers are more favorable for the water injection but the injection well still has to be far enough away so that water production is negligible. For the larger injection rate the preferable location for the injection well should be far away from the producers in gridblock $(1, 1)$ according to Fig. 3.4(b), to minimize water production. The optimum NPV for the total injection rate constraints of $q_{\mathrm{t,inj}} = 400$ STB/D and $4,000$ STB/D, respectively, are $\$5.11 \times 10^7$ and $\$9.12 \times 10^7$. Note that both these NPVs are higher than the NPV of the production from the reservoir with a single injection well, which according to the NPV maps are $\$5.10 \times 10^7$ for $q_{\mathrm{t,inj}} = 400$ STB/D and $\$5.80 \times 10^7$ for $q_{\mathrm{t,inj}} =$

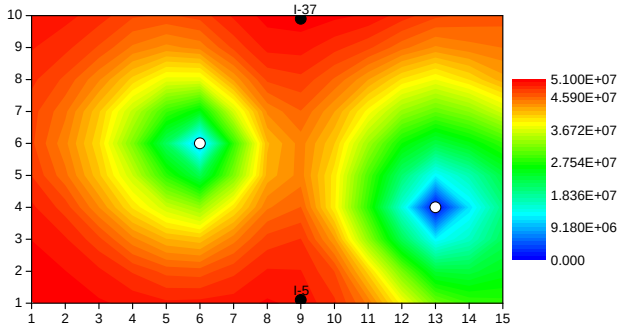

(a) $q_{\mathrm{t,inj}} = 400$

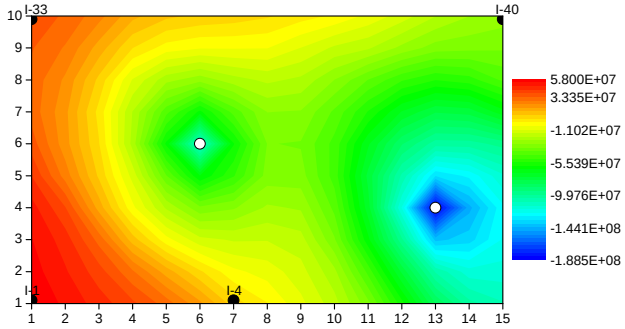

(b) $q_{\mathrm{t,inj}} = 4,000$

Figure 3.4: Final injection well locations with no initialization used to determine the total injection rate constraint, Example 1, Case 1.

Table 3.1: Optimal injection rate allocation with $q_{\mathrm{t,inj}} = 400$, Example 1, Case 1.

I-5	I-35	J (\$)
182.2	217.8	5.11×10^7

4,000 STB/D, respectively. The optimum rates of the wells for the two cases are summarized in Tables 3.1 and 3.2.

Note that for $q_{\mathrm{t,inj}} = 4,000$ STB/D we have four injection wells at the estimated optimal locations where as in the low injection rate case, $q_{\mathrm{t,inj}} = 400$ STB/D, all but two injection wells are eliminated by our optimization algorithm. This is the expected result because if the specified total injection rate is increased, then more wells are required to inject that amount of water. Also, a larger injection rate increases the chance of a maximum bottomhole pressure constraint violation which in our algorithm will cause a redistribution of the residual injection rate among wells.

Table 3.2: Optimal injection rate allocation with $q_{\mathrm{t,inj}} = 4000$, Example 1, Case 1.

I-1	I-4	I-33	I-40	J (\$)
915.6	1240.8	1312.3	531.3	9.12×10^7

The initialization step tries to find an appropriate value for the total injection rate; therefore the optimum well locations are less influenced by the specified controls of the wells. Case 2 presents the injection well-placement optimization when the total rate constraint is determined by the initialization step.

Case 2: Optimization of the Injection Well Locations with Initialization of Total Injection Rate: In this case, we apply the initialization method to find the appropriate total injection rate to use in the equality constraints of Eq. 3.10 before applying the well-placement algorithm to find the optimal well locations of the injectors. To test the reliability of the procedure, we tried two different initial injection rates in the initialization process, namely $4,000$ STB/D and 400 STB/D. Recall that when doing the initialization step, no equality constraint is used on the total rate so the total rate may change from iteration to iteration of the initialization algorithm. As in Case 1, we start with 40 injectors and the initial total injection rate is uniformly distributed among the wells. With an initial total injection rate of $q_{\mathrm{t,inj}} = 400$ STB/D and $4,000$ STB/D, respectively, the initialization process gave an estimated optimal total injection rate of 2027.5 STB/D and 2042.9 STB/D, respectively. These final optimal total injection rates determined in the initialization stage are also listed in Tables 3.3 and 3.4. Figs. 3.5(a) and 3.5(b) show the final optimum injection well locations obtained for the initial total injection rates of 400 and $4,000$ STB/D, respectively. These locations are shown in the NPV map for a single injector with $q_{\mathrm{t,inj}} = 2,000$ STB/D.

The complete algorithm converged with 122 simulation runs for the high initial total injection rate case and with 126 simulation runs for the low initial total injection

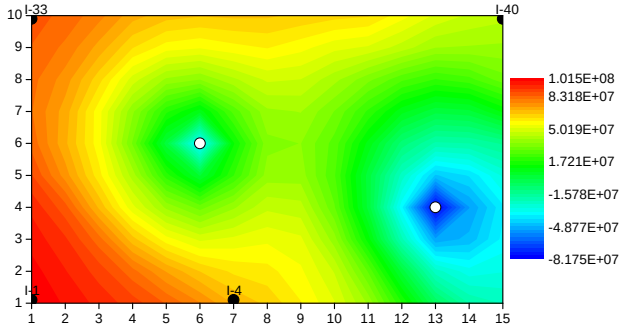

(a) with initial $q_{\text{t,inj}} = 400$

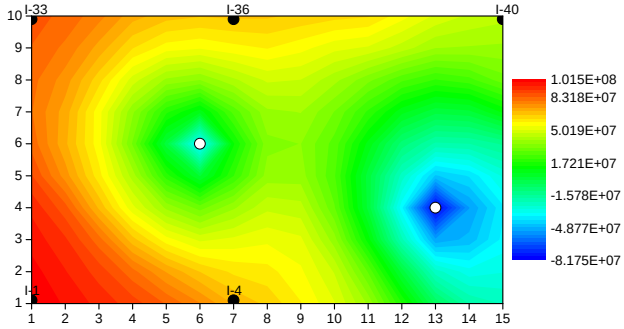

(b) with initial $q_{\text{t,inj}} = 4,000$

Figure 3.5: Final injection well locations with total injection rate determined from the initialization algorithm, Example 1, Case 2.

Table 3.3: Optimal injection rate allocation and estimated total injection rate with initial $q_{\text{t,inj}} = 400$, Example 1, Case 2.

I-1	I-4	I-33	I-40	$q_{\text{t,inj}}$	J (\$)
564.7	1147.5	118.2	197.1	2027.5	1.33×10^8

rate case. The final well locations are similar in Figs. 3.5(a) and 3.5(b), but in Fig. 3.5(b) we are left with an additional injector at I-36. The estimated optimal values of modified NPV (J) are essentially identical. Compared to Case 1, applying the initialization process to estimate the total injection rates yields a much higher value of J: $\$1.33 \times 10^8$ for Case 2 as opposed to $\$5.11 \times 10^7$ and $\$9.12 \times 10^7$ for Case 1. The two-stage well-placement, which incorporates the initialization step, resulted in a more reasonable total injection rate, also the injection well locations are not severely influenced by the specified total injection rate.

Table 3.4: Optimal injection rate allocation and estimated total injection rate with initial $q_{\mathrm{t,inj}} = 4000$, Example 1, Case 2.

I-1	I-4	I-33	I-36	I-40	$q_{\mathrm{t,inj}}$	J (\$)
463.4	553.3	373.1	373.2	279.8	2042.9	1.33×10^8

3.5.2 Example 2: 3D, 3-Phase PUNQ Reservoir

PUNQ is a three-phase, three-dimensional reservoir simulation model. The reservoir has five simulation layers and it is bounded to the east and south by a fault. A small gas cap is located in the center of the dome shaped structure. The reservoir is in communication with a fairly strong aquifer to the north and west. The aquifer is a numerical aquifer which is introduced by converting some of the inactive cells in the original model to active cells containing only water and adding a row of gridblocks with high pore volume along the north and south edges and one column of gridblocks of high pore volume along the west edge. The porosity of aquifer gridblocks is 0.95. For the case where we consider an inactive aquifer, the porosity of the aquifer gridblocks are changed to 0.0001. The drilling cost of a well, for both injectors or producers, is $\$10,000,000$. The oil price is set at 80 \$/STB, water injection costs at 10 \$/STB, water production costs at 30 \$/STB and b at 0.0. We do not consider any revenue or cost for the produced gas from the reservoir. The maximum bottomhole pressure constraint for injectors is $6,000$ psi and the minimum bottomhole pressure constraint for producers is $1,500$ psi. The initial datum pressure at a depth of 7726.38 feet is $3,400$ psi. The production life of the reservoir is 25 years. The porosity, horizontal permeability, vertical permeability distributions and initial fluid distribution are shown in Figs. 3.6 to 3.9, respectively. For the well-placement problems considered here, the wells are perforated in all 5 layers. For three cases considered, the optimal well locations are shown in the plots of layer-1 horizontal log-permeability field, see, for example Fig. 3.10(a).

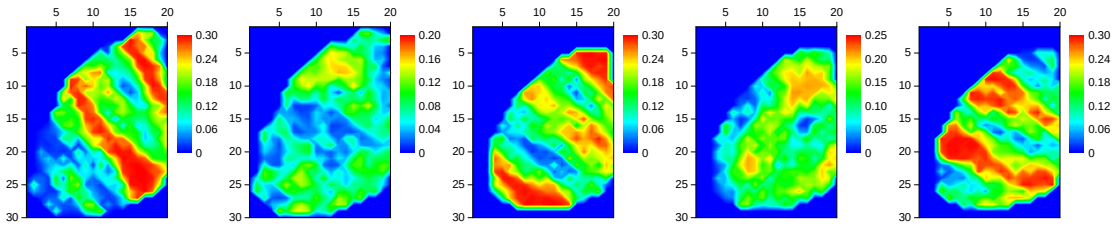

Figure 3.6: The porosity field of the PUNQ reservoir.

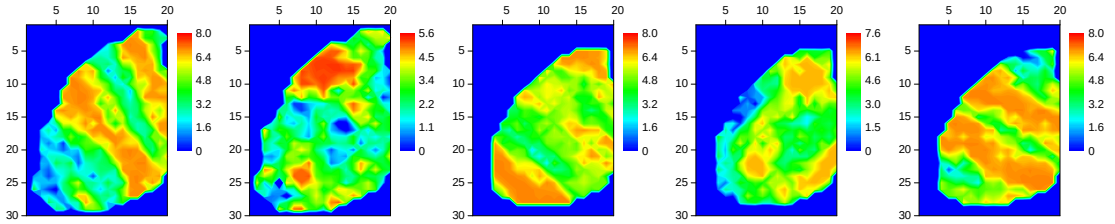

Figure 3.7: The horizontal log-permeability field of the PUNQ reservoir.

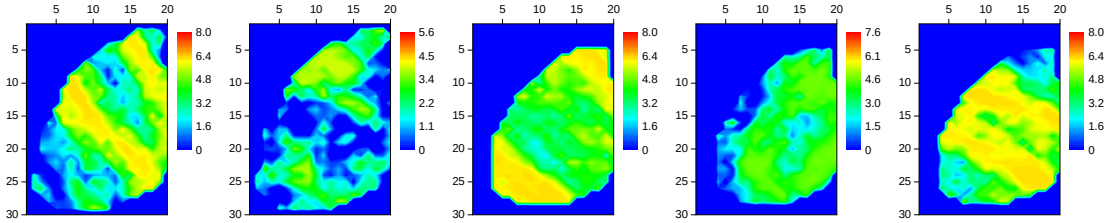

Figure 3.8: The vertical log-permeability field of the PUNQ reservoir.

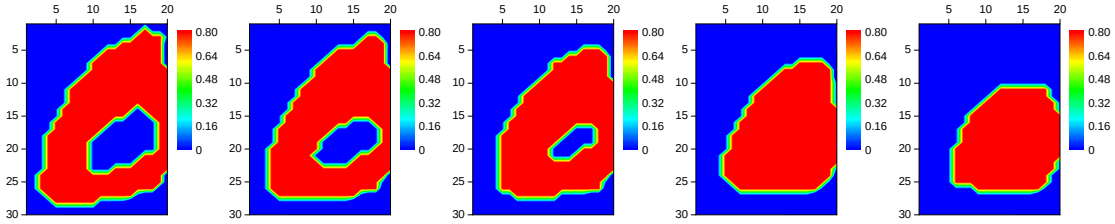

Figure 3.9: The initial oil saturation distribution of the PUNQ reservoir.

Case 1: Optimal Placement of Injection Wells for the PUNQ Reservoir without Aquifer: In this case, we consider the optimization of the injection well locations. We use the original PUNQ production well locations for the six producers in the reser-

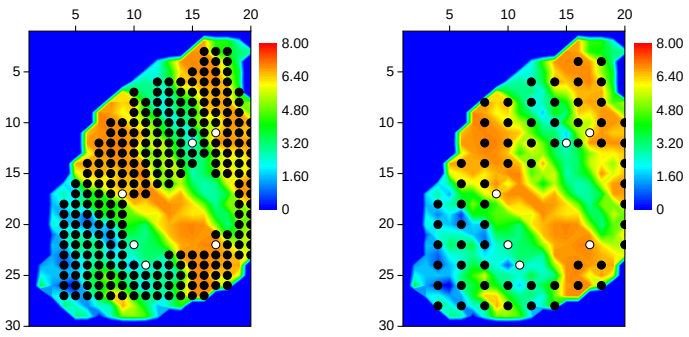

(a) 258 initial injectors (b) 65 initial injectors

Figure 3.10: The initial injection well locations, PUNQ reservoir without aquifer, Example 2, Case 1.

voir. The numerical aquifer is inactive. Note that all the producers and injectors are perforated in all reservoir layers. The initial total water injection rate is set to $5,600$ STB/D.

To check the robustness of our algorithm, we start with two initial sets of injectors, Case (1a) has 258 injectors where each of them is assigned a rate of 21.705 STB/D, so the total injection rate is $5,600$ STB/D. In Case (1b), each of 65 initial water injection wells is assigned a rate of 86.15 STB/D. The initial well locations are shown in Figs. 3.10(a) and 3.10(b).

Figs. 3.11(a) and 3.11(b) show the final optimal injection well locations obtained using well-placement optimization algorithm without the initialization step with the constant total water injection rate specified as $q_{\mathrm{t,inj}} = 5,600$ STB/D. In Case (1a), 8 injectors remained whereas in Case (1b), 7 injectors remained. The optimization algorithm required 232 and 202 reservoir simulation runs to terminate for Case (1a) and (1b), respectively.

Figs. 3.12(a) and 3.12(b) show the final optimal injection well locations obtained using the initialization procedure to determine an appropriate total water injection rate to use in the equality constraint of Eq. 3.19. With initialization, one less injection well remains at the estimated optimum for both Case (1a) and Case (1b). When using the two-stage procedure, which incorporates the initialization step,

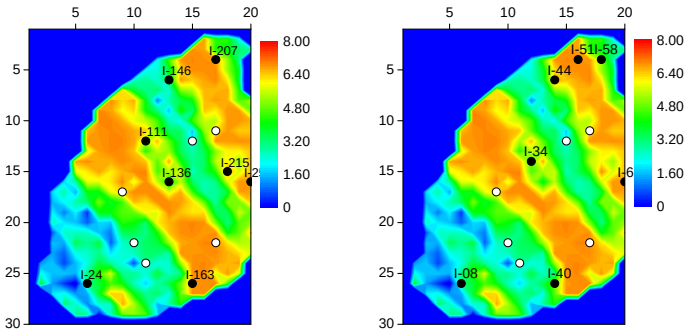

(a) 258 initial injectors (b) 65 initial injectors

Figure 3.11: Final injection well locations with no initialization used to determine the total injection rate constraint, PUNQ reservoir without aquifer, Example 2, Case 1.

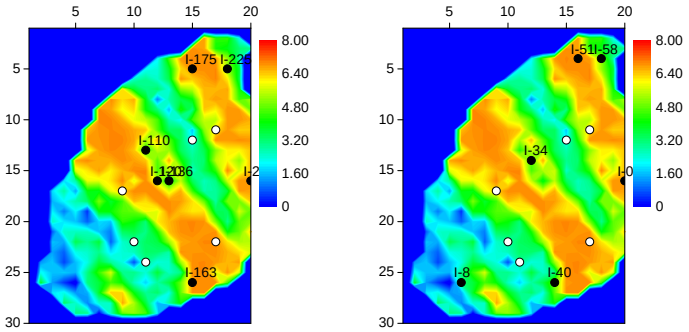

(a) 258 initial injectors (b) 65 initial injectors

Figure 3.12: Final injection well locations with total injection rate determined from the initialization algorithm, PUNQ reservoir without aquifer, Example 2, Case 1.

248 and 126 simulation runs were required to terminate the optimization for Case (1a) and Case (1b), respectively.

The plot of $J[u]$ versus optimization iteration number are shown in Figs. 3.13(a) and 3.13(b) for both single-stage and two-stage optimizations with 258 and 65 initial injection wells, respectively. Note that in Fig. 3.13(a), there is a break in ordinate axis. Recall that the objective function in the initialization stage is the NPV without considering the drilling costs of the wells. Therefore, the objective functions at the end of the initialization stage of the two-stage algorithm is larger than the value of the objective function at corresponding iterations of the single-stage optimization. When the initialization stage terminates and the well-placement optimization goes to

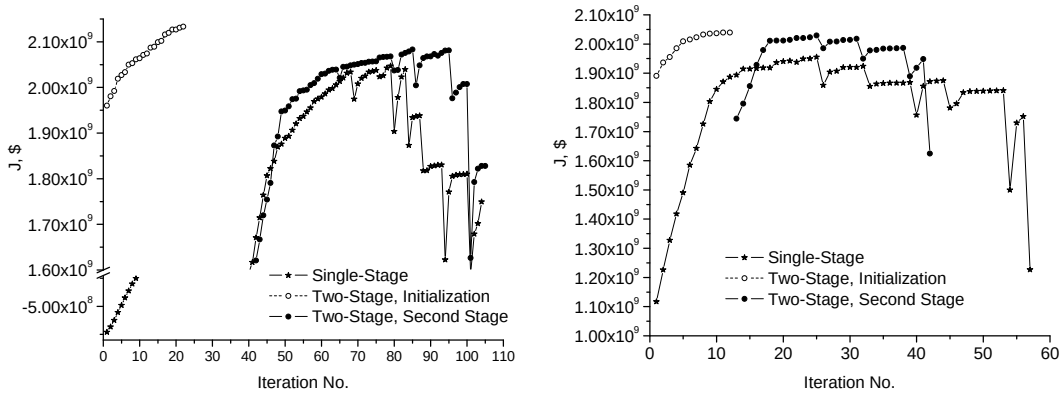

(a) 258 initial injectors (b) 65 initial injectors

Figure 3.13: Plot of objective function versus optimization iteration number for placement of injection wells in the PUNQ reservoir without aquifer, Example 2, Case 1.

the second stage, there is a sharp decrease in the objective function, which is due to consideration of the drilling costs of the remaining wells in the modified NPV function, $J[u]$. That is possible for the well-placement optimization to become trapped in a strong local maximum. In the two-stage case of Fig. 3.13(a), after iteration 40, we are in the second stage of the algorithm. At any point thereafter, a decrease in the $J[u]$ corresponds to an iteration where the algorithm is continued after converging to a local maximum. These local maxima occur at iterations 64, 79, 85, 91, 95 and 100. Note, however, the overall maximum of $J = \$2.08 \times 10^9$ occurs the local maximum at iteration 85 after the algorithm has successfully escaped the local maximum encountered at iterations 64 and 79. A similar situation is happened for the single-stage procedure. The local maxima occur at iterations 68, 79, 87, 93 and 100; however, the overall maximum of $J = \$2.03 \times 10^9$ occurs at iteration 79.

Optimum injection rate allocation and the estimate of the maximum J value are summarized in Tables 3.5 and 3.6 for the two different optimization procedures. In the total rate initialization step, the initial total injection rate is $5,600$ STB/D and after optimization the optimum injection rates are $3,502$ and $3,428$ STB/D, respectively, for the initial well locations of Case (1a) and Case (1b), respectively. The

Table 3.5: Optimal injection rate allocation and J value without total rate initialization, Example 2, Case 1.

	I-24	I-111	I-136	I-146	I-163	I-207	I-215	I-252	J (\$)
258 wells	345.8	640.7	1219.3	661.0	609.3	984.8	641.7	497.5	2.05×10^9

	I-8	I-34	I-40	I-44	I-51	I-58	I-62	J (\$)
65 wells	595.4	649.3	601.3	696.2	419.7	673.5	1964.7	1.95×10^9

Table 3.6: Optimal injection rate allocation and J value, Total injection rate determined from the initialization algorithm, Example 2, Case 1.

	I-110	I-120	I-136	I-163	I-175	I-225	I-252	$q_{\mathrm{t,inj}}$	J (\$)
258 wells	339.5	149.9	519.3	592.5	664.7	395.1	841.3	3502.3	2.08×10^9

	I-8	I-34	I-40	I-51	I-58	I-62	$q_{\mathrm{t,inj}}$	J (\$)
65 wells	489.6	412.2	548.2	839.9	230.2	907.7	3427.8	2.03×10^9

optimum J values for the cases with total injection rate initialization are $\$2.08 \times 10^9$ and $\$2.03 \times 10^9$, respectively, for the cases with 258 and 65 initial injection wells, respectively. However, the optimum modified NPV function value for the cases of without the initialization step are $\$2.05 \times 10^9$ and $\$1.95 \times 10^9$, respectively for 258 and 65 initial injection wells, respectively. Note, the initialization step decreased total water injection rate from $5,600$ STB/D to roughly $3,500$ STB/D.

We applied the Handels et al. [16] method starting with the final injection well locations and rates obtained both with and without total injection rate initialization for both Case (1a) (258 initial injectors) and Case (1b) (65 initial injection wells). The J values in three cases decreases as a function of iteration as shown in Fig. 3.14 which indicates that the Handels et al. [16] method failed to improve our results in those three cases. For the case of no initialization for the rates and starting with 258 initial injectors, Handels et al. [16] method improved NPV from 2.04×10^9 to 2.11×10^9. The final well locations for this case obtained by the procedure of Handels et al. [16] is shown in Fig. 3.15. Note that the final well locations from Handels et al. [16] method (Fig. 3.15) is very similar to the starting locations which are obtained

by our algorithm (Fig. 3.11(a)). Indeed, in the final Handels et al. [16] method locations, injection wells I-111, I-138 and I-215 are moved only one gridblock from the final locations that were calculated with our algorithm.

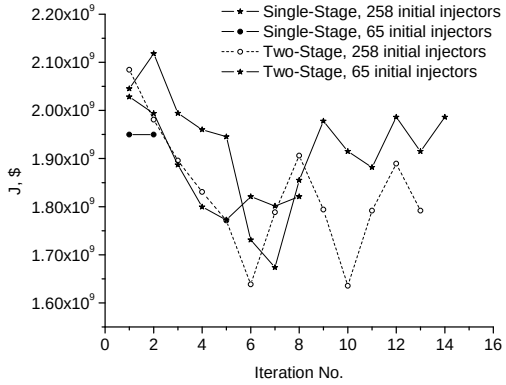

Figure 3.14: Plot of J versus iteration from Handels et al. [16] method starting with final injector locations and rates from our algorithm, PUNQ reservoir without aquifer.

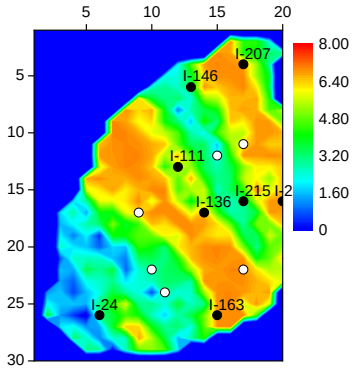

Figure 3.15: The final injection well locations with Handels et al. [16] method for the case with no initialization used to determine the total injection rate constraint and starting with 258 injectors, PUNQ reservoir with aquifer, Example 2, Case 1.

Case 2: Optimal Placement of Production Wells for the PUNQ Reservoir with Aquifer: In this case, we consider the optimization of production well locations in PUNQ reservoir with the numerical aquifer. There are no injection wells in the reservoir. We consider the initial total liquid production rate to be $5,600$ STB/D, which

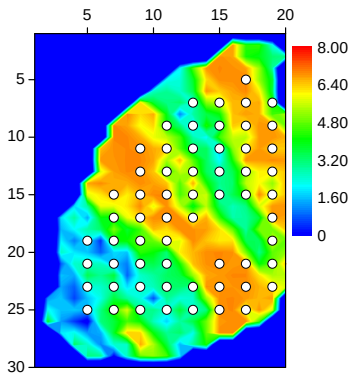

Figure 3.16: The initial production well locations, PUNQ reservoir with aquifer, Example 2, Case 2.

will result in total production approximately equal to 40% of the initial reservoir oil in place within the 25 years of production life if the oil rate is equal to the total liquid rate. We start with 61 producers where each producer has an initial liquid rate of 91.80 STB/D. The initial production well locations are shown in Fig. 3.16.

Fig. 3.17 shows the final optimal production well locations (5 producers remained) obtained using the well-placement optimization algorithm with the constant total liquid production rate specified as $q_{\mathrm{t,prd}} = 5,600$ STB/D without using the initialization algorithm to determine an appropriate total liquid production rate. The optimization algorithm required 92 reservoir simulation runs to terminate. Fig. 3.18 shows the final optimal production well locations (8 producers remained) obtained using the initialization procedure to determine an appropriate production rate to use in the equality constraint of Eq. 3.11. When using the two-stage procedure, 119 simulation runs were required to terminate the optimization. Optimum production rate allocation and estimate of the maximum J value are summarized in Tables 3.7 and 3.8 for the two different optimization procedures. In the total rate initialization step, the initial total liquid production rate is $5,600$ STB/D and after optimization is $8,459.5$ STB/D. The optimum J values for the cases with and without the total production rate initialization are $\$3.05 \times 10^9$ and $\$3.27 \times 10^9$, respectively. Note

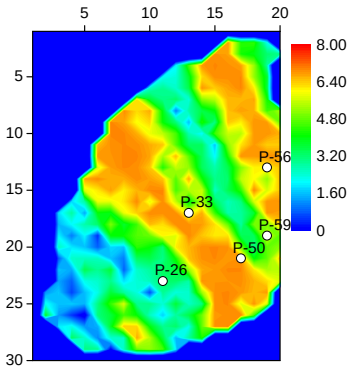

Figure 3.17: Final production well locations with no initialization used to determine the total production rate constraint, PUNQ reservoir with aquifer, Example 2, Case 2.

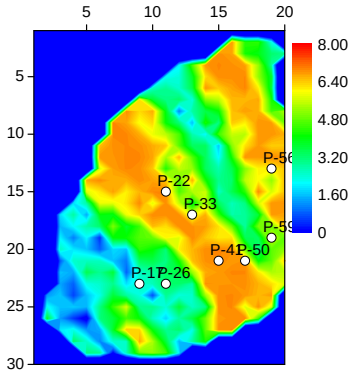

Figure 3.18: Final production well locations with total production rate determined from the initialization algorithm, PUNQ reservoir with aquifer, Example 2, Case 2.

Table 3.7: Optimal production rate allocation and J value without total rate initialization, Example 2, Case 2.

P-26	P-33	P-50	P-56	P-59	J ($)
714.6	1085.2	1125.5	1753.7	921.0	3.05×10^9

that, in the well-placement optimization with the initialization stage, the total production rate from the reservoir is increased and a larger number of producers remain. However, the optimal well locations by the single-stage and two-stage well-placement optimizations are similar.

The plot of the objective function for single-stage and two-stage optimization procedure are shown in Fig. 3.19. Again a sharp decrease in the objective function happens at the first iteration of the second stage as the drilling cost of the remaining wells are added to the objective function.

Table 3.8: Optimal production rate allocation and J value, Total production rate determined from the initialization algorithm, Example 2, Case 2.

P-17	P-22	P-26	P-33	P-41	P-50	P-56	P-59	$q_{\mathrm{t,prd}}$	J ($)
314.2	335.6	246.2	835.3	1727.6	1828.3	2160.6	1078.9	8526.7	3.27×10^9

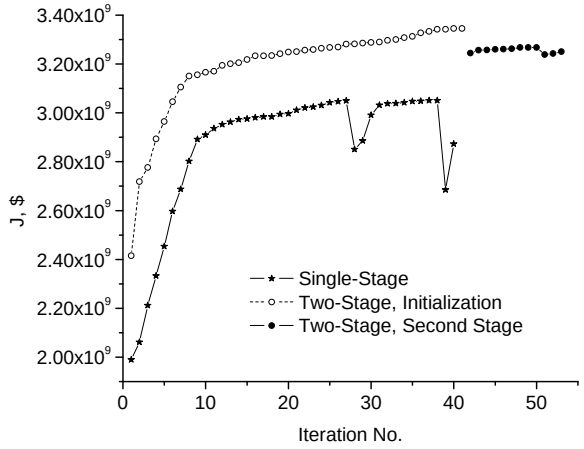

Figure 3.19: Objective function versus iteration number for placement of production wells in the PUNQ reservoir with aquifer, Example 2, Case 2.

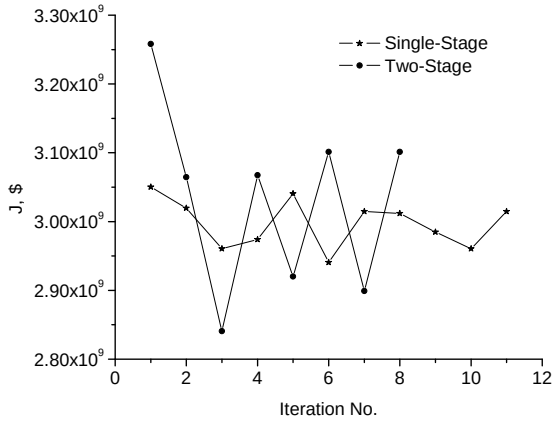

Figure 3.20: Plot of J versus iteration from Handels et al. [16] method starting with our final producer's locations and rates, PUNQ reservoir with aquifer.

We applied the Handels et al. [16] method starting with the final production well locations and rates obtained both with and without total production rate initialization. The J values in both cases decreases as a function of iteration as shown in Fig. 3.20 which indicates that the Handels et al. [16] method failed to improve our results. In our final results, all the wells satisfy the BHP constraint. However, when Handels et al. [16] method moves the wells, some BHP controls cannot be honored with the specified production rates.

The original PUNQ reservoir has 6 production wells. In the following, we

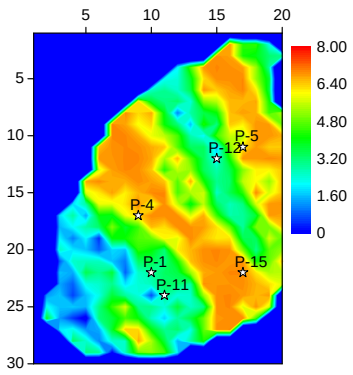

Figure 3.21: Original production well locations, PUNQ reservoir with aquifer.

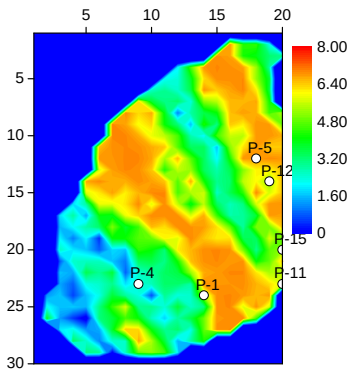

Figure 3.22: Optimal production well locations by Handels et al. [16] method.

apply the Handels et al. [16] method starting with 6 production wells with a total liquid production rate of 5,600 STB/D. This total production rate is uniformly distributed among the 6 producers. The initial well locations are the ones from the original PUNQ reservoir example shown in Fig. 3.21. The final optimum well locations obtained with Handels et al. [16] method are shown in Fig. 3.22. The initial J value is $\$2.10 \times 10^9$ considering the drilling cost of each well of $\$10,000,000$ and the final optimum J value increased to $\$2.80 \times 10^9$, which is significantly lower than the optimum values of J obtained by our method with (Table 3.8) and without (Table 3.7) total production rate initialization. Note that the Handels et al. [16] method assumes a uniform production rate from all wells and a well may be converted to BHP control when the BHP constraint is violated.

Case 3: Optimal Placement of Injection and Production Wells for the PUNQ Reservoir without Aquifer: The porosity of the aquifer gridblocks is reduced from 0.95 to 0.0001 to make the effect of the aquifer negligible. We start with 65 injectors and 61 producers. We consider two initial configurations for the initial injection and production well locations. For this case, we set the total injection and liquid production rate constraints to 5,600 STB/D with these total rates uniformly distributed

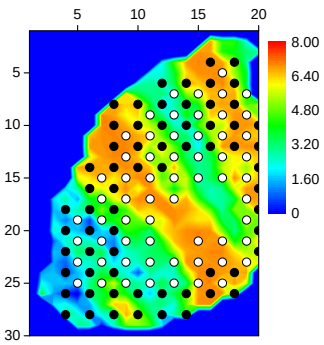

(a) Initial well locations, Configuration 1.

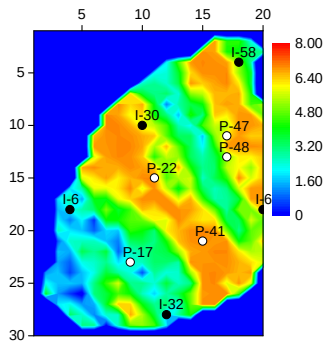

(b) Final well locations, Configuration 1.

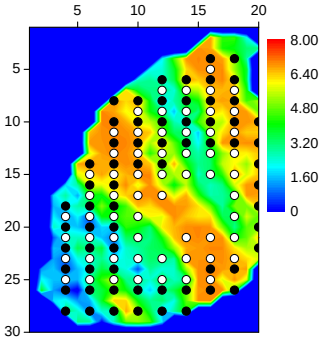

(c) Initial well locations, Configuration 2.

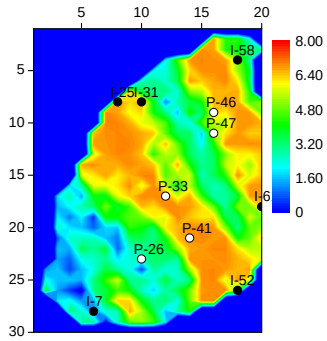

(d) Final well locations, Configuration 2.

Figure 3.23: The initial and optimum well locations for simultaneous injector and producer optimization, PUNQ reservoir without aquifer, Example 2, Case 3.

among injection and production wells. The initial configuration of the injection and production well locations as well as the final optimized well locations for both initial well configurations are shown in Fig. 3.23. The injectors are shown as solid black circles and the producers are shown as solid white circles.

The final number of injectors and producers are respectively 5 and 5 for the first initial configuration and 6 and 5 for the second one. The final J value for configurations 1 and 2, respectively, are $\$2.42 \times 10^9$ and $\$2.58 \times 10^9$. To obtain these results required 253 and 257 reservoir simulation runs, for configurations 1 and 2, respectively.

The plot of the objective function versus the number of optimization iterations is shown in Fig. 3.24. Similar to previous cases, a decrease in the objective

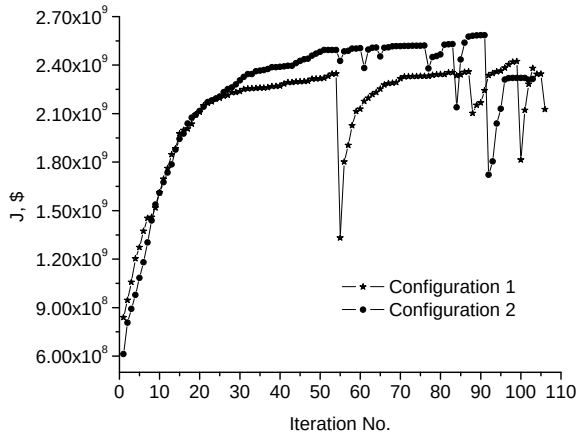

Figure 3.24: Objective function versus iteration number for simultaneous placement of injectors and producers, PUNQ reservoir without aquifer, Example 2, Case 3.

Table 3.9: Optimal production and injection rate allocation with total rate constraints and no initialization step, Initial well configuration 1, Example 2, Case 3.

Producers	Rate	Injectors	Rate
P-17	1025.9	I-6	1406.0
P-22	1064.2	I-30	786.5
P-41	1517.5	I-32	837.7
P-47	1543.0	I-58	877.8
P-48	449.3	I-61	1692.1

function is observed when the algorithm is forced out of a strong local optimum, e.g., iterations 54, 83, 87, 99 and 103 of the optimization with initial configuration 1 and iterations 54, 60, 64, 76 and 91 of the optimization with initial well configuration 2. The overall maximum occur at iterations 99 and 91 for the configuration 1 and 2, respectively. Optimum production and injection rate allocation values are summarized in Tables 3.9 and 3.10 for the two initial well configurations.

We applied the Handels et al. [16] method starting with the final injection and production well locations and rates obtained for the both configurations. The J value for both cases as a function of iteration is shown in Fig. 3.25. The Handels et al. [16] method improved our J values slightly, from $\$2.42 \times 10^9$ to $\$2.47 \times 10^9$ for configuration one and from $\$2.58 \times 10^9$ to $\$2.60 \times 10^9$ for the second initial

Table 3.10: Optimal production and injection rate allocation with total rate constraints and no initialization step, Initial well configuration 2, Example 2, Case 3.

Producers	Rate	Injectors	Rate
P-26	1653.8	I-7	96.0
P-33	1491.5	I-25	657.4
P-41	844.9	I-31	1003.6
P-46	371.0	I-52	551.9
P-47	1238.8	I-58	829.7
-	-	I-61	2461.4

configuration. The final well locations are shown in Fig. 3.26. Comparing Fig. 3.26(a) with Fig. 3.23(b), we see that the Handels et al. [16] algorithm only slightly changed the well locations. The location of well P-48 is changed significantly, however the other well locations are very similar. However, for the initial configuration 2 case, the Handels et al. [16] algorithm made a more significant change in some well locations, compare Fig. 3.26(b) with Fig. 3.23(d). In particular P-41 is moved outside the channel and injectors I-25 and I-31 were collapsed into a single injector. Thus, this example suggests that we should at least try to improve results using the Handels et al. [16] method to move wells after we have estimated the optimal number, rates and location of both production and injection wells from our algorithm.

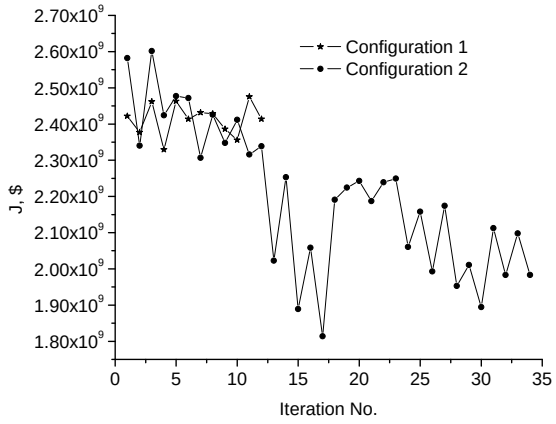

Figure 3.25: Plot of J versus iteration from Handels et al. [16] method starting with our final well locations and rates for both initial well location configurations, PUNQ reservoir without aquifer.

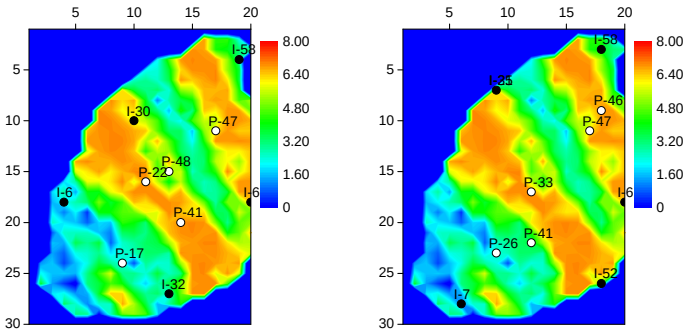

(a) Configuration 1. (b) Configuration 2.

Figure 3.26: The final well locations from Handels et al. [16] method starting with our final well locations, PUNQ reservoir without aquifer, Example 2, Case 3.

3.5.3 Sensitivity Analysis on the Value of β

We previously suggested using $\beta = 0.25$ in the drilling cost functions of wells introduced in Eqs. 3.6 and 3.7. Here, we present the results of a sensitivity analysis on β. For illustration we consider, optimization of injection well locations in PUNQ reservoir without aquifer, Example 2, Case (1b) and Example 2, Case 2, optimizing the production well locations in the PUNQ reservoir with an aquifer, for the sensitivity analysis. Note that, in the results presented in Cases 1 and 2 in the previous sections the value $\beta = 0.25$ is used.

In this sensitivity analysis, we run the same cases with $\beta = 0.1$, 0.5 and 1.0. For injection well location optimization, we chose the case with 65 initial injection wells with the initial locations shown in Fig. 3.10(b). The initial production well locations for optimization are shown in Fig. 3.16. The summary of runs for the injection well-placement and production well-placement are shown in Tables. 3.11 and 3.12. The final optimum well locations for the optimization of the injectors and producers, respectively, with different values for β are respectively shown in Figs. 3.27 and 3.28, respectively.

Optimum value of the modified NPV functional J are very close for all the values of β. All cases have some well locations in common, however, more wells

remained than the others. This suggests that the convergence of the method to an optimum solution is not sensitive to the value of β. However, the number of wells and number of required simulation runs might be different with different values of β.

Table 3.11: Summary of sensitivity runs for β for placement of injection wells.

	Sim. Runs	Wells remained	NPV
$\beta = 0.1$	112	6	$\$1.96 \times 10^9$
$\beta = 0.25$	202	7	$\$1.95 \times 10^9$
$\beta = 0.5$	147	7	$\$1.95 \times 10^9$
$\beta = 1.0$	124	7	$\$1.95 \times 10^9$

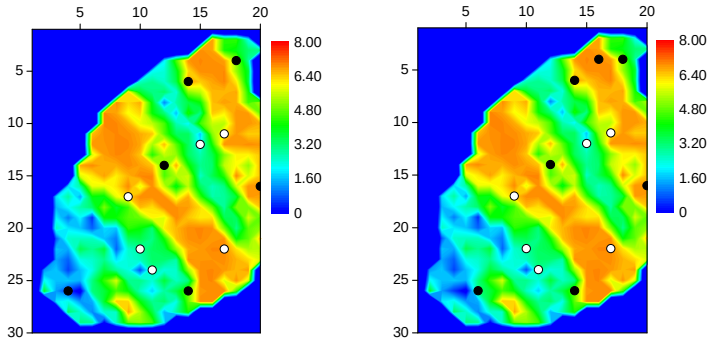

(a) $\beta = 0.1$.

(b) $\beta = 0.25$.

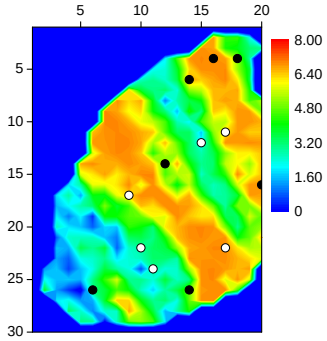

(c) $\beta = 0.5$.

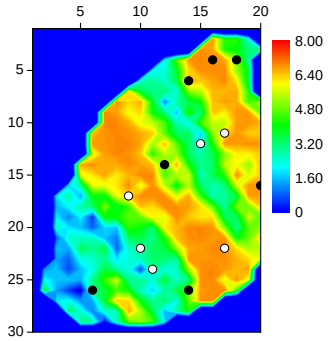

(d) $\beta = 1.0$.

Figure 3.27: The optimum final injection well locations with optimization runs with different β, PUNQ reservoir without aquifer.

Table 3.12: Summary of sensitivity runs for β for placement of production wells.

	Sim. Runs	Wells remained	NPV
$\beta = 0.1$	141	9	$\$3.05 \times 10^9$
$\beta = 0.25$	92	5	$\$3.05 \times 10^9$
$\beta = 0.5$	86	8	$\$3.05 \times 10^9$
$\beta = 1.0$	81	5	$\$3.05 \times 10^9$

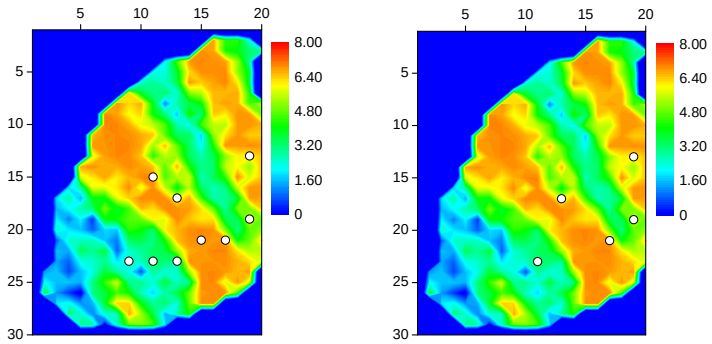

(a) $\beta = 0.1$.

(b) $\beta = 0.25$.

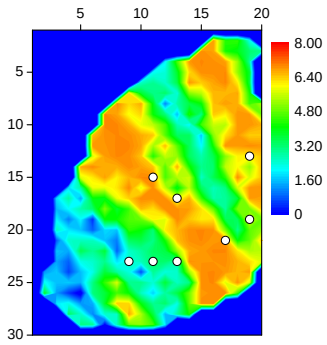

(c) $\beta = 0.5$.

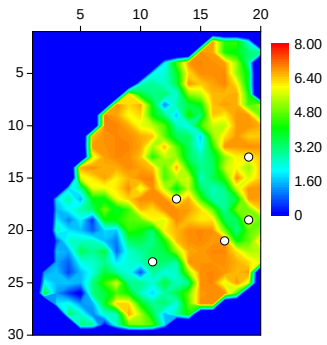

(d) $\beta = 1.0$.

Figure 3.28: The optimum final production well locations with optimization runs with different β, PUNQ reservoir with aquifer.

CHAPTER 4

OPTIMIZATION OF THE WELL LOCATIONS AND COMPLETIONS FOR VERTICAL AND HORIZONTAL WELLS

In this chapter, a new methodology for estimation of the location and completions of 3D horizontal and vertical wells that maximize the life-cycle net-present-value (NPV) of production from a given reservoir is presented. Here, the well can be either a rate-controlled or a bottomhole pressure-controlled injection or production well, however, the well control values and the production life of the reservoir are fixed. A vertical well is a column of perforated gridblocks in the "k" (or z) direction. A horizontal well is considered as a perforated row of gridblocks in the "i" (or x) or "j" (or y) direction. Because of the way wells are commonly modeled in reservoir simulators, the optimal well-placement is usually formulated as a discrete optimization problem, where the center point of the well is moved from the center of one gridblock to the center of another gridblock at each iteration of whatever optimization algorithm is used. However, in reality, the optimal well-placement is a continuous optimization problem as the center point of the well can be located at any point within the reservoir and it does not have to be at the center of a gridblock. Here, the well-placement problem is formulated in terms of four continuous variables, the x_{w}, y_{w} and z_{w} coordinates of the center point of the well and the length, l_{w}, of the well. A procedure is developed to modify well-productivity indices in the reservoir simulator to account for the location of the centerline of a well within gridblocks and to define the life-cycle NPV of production as a function of these four continuous well parameters, $(x_{\mathrm{w}}, y_{\mathrm{w}}, z_{\mathrm{w}}, l_{\mathrm{w}})$. This NPV functional is maximized using BOBYQA which uses the simulator as a "black box" and there is no need to compute gradients.

For a derivative-free optimization (DFO) algorithm, BOBYQA is reasonably efficient and it was recently applied for production optimization, Shuai et al. [39]. However, to improve the performance of BOBYQA, we provide a cogent way to re-scale the optimization variables. Similar to gradient-based optimization methods, BOBYQA may converge to a local optimum. Thus, in general, it may be a good idea to apply the algorithm for a set of different initial guesses. For field applications, convergence to a local maximum may actually be less of a problem because field engineers would always have a rough idea of what well locations are optimal. In this chapter, we first explain the method for converting the discrete optimization problem of placing horizontal and vertical wells into a problem with continuous optimization variables. Then the application of the derivative-free optimization technique is explained. Finally, some results for the optimization of horizontal and vertical well locations and completions in homogeneous and heterogeneous synthetic 3D reservoirs are presented.

4.1 Well-Placement Problem Definition

In the optimal well-placement problem, the objective function is the net-present-value (NPV) of production from the reservoir defined in Eq. 2.1. In a conventional commercial reservoir simulator, a well is typically modeled by specifying the gridblocks penetrated by the well and then specifying an effective well index for each penetrated gridblock. For simplicity in presentation of the theoretical ideas, we assume that all gridblocks penetrated by a horizontal well can be represented by a row of gridblocks in either the "i" (or x) direction or "j" (or y) direction and that each vertical well penetrates only a column of gridblocks in the "k" (or z) direction; see Fig. 4.1.

As each gridblock is uniquely associated with some set of gridblock indices, ("i", "j", "k"), we could estimate a set of ("i", "j", "k") indices penetrated by each of a specified number of wells which maximize the value of NPV. If the optimization

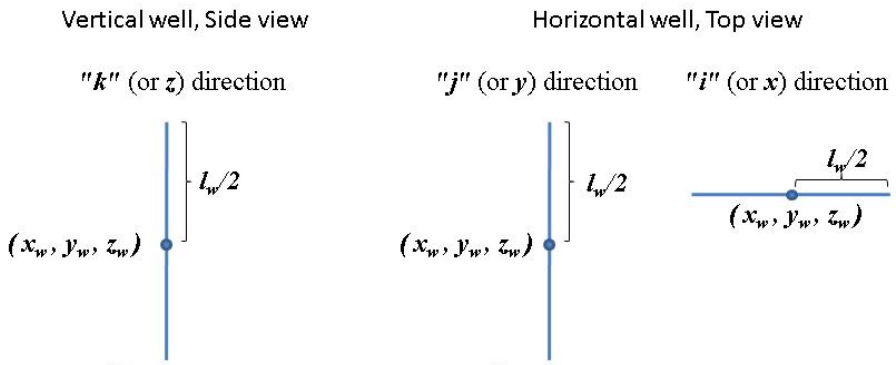

Figure 4.1: Schematic view of a vertical and a horizontal well.

problem were defined this way, it would be a discrete optimization problem. Instead, we extend the idea of Sarma and Chen [36] to write our well-placement problem in terms of continuous variables so that more efficient optimization methods (gradient-based optimization methods or methods that use an approximate gradient, Li and Reynolds [21] and Zhao et al. [48]) can be applied. In our case, we use the derivative-free optimization algorithm BOBYQA (Powell [34]) which is discussed in Chapter 2.

In our approach, a 3D horizontal or vertical well is defined by four continuous variables. These variables are: $(x_{\mathrm{w}}, y_{\mathrm{w}}, z_{\mathrm{w}})$, which are the spatial coordinates of the well center point, and l_{w}, which is the length of the well; see Fig. 4.1. As the optimization code that we use is based on minimizing an objective function, we consider minimizing $J[u]$ where $J[u] = -\mathrm{NPV}$ and u is the vector of variables which represent well locations. The continuous optimization problem is then defined by

$$\min_{u} J[u], \tag{4.1}$$

subject to

$$u^{\mathrm{low}} \leq u \leq u^{\mathrm{up}}, \tag{4.2}$$

where $u = [x_{\mathrm{w},1}, y_{\mathrm{w},1}, z_{\mathrm{w},1}, l_{\mathrm{w},1}, \ldots, x_{\mathrm{w},N_{\mathrm{well}}}, y_{\mathrm{w},N_{\mathrm{well}}}, z_{\mathrm{w},N_{\mathrm{well}}}, l_{\mathrm{w},N_{\mathrm{well}}}]^T$ is the vector of

optimization variables. N_{well} is the number of wells, and $(x_{\text{w},j}, y_{\text{w},j}, z_{\text{w},j})$ and $l_{\text{w},j}$, respectively, define the location of the center point and the length of well j. Note we assume the direction of the centerline of each well is predefined so that by specifying $(x_{\text{w},j}, y_{\text{w},j}, z_{\text{w},j}, l_{\text{w},j})$, we uniquely define the location of well j. Eq. 4.2 defines simple bound constraints for every optimization variable. The bound constraints for the optimization variables $x_{\text{w},j}$, $y_{\text{w},j}$ and $z_{\text{w},j}$ are defined according to the reservoir boundaries because the center point of each well is required to be inside the reservoir. The upper bound for $l_{\text{w},j}$ is defined by simply setting a maximum length of the well.

4.2 Continuous Approximation of the Discrete Optimization Problem

As noted above, the trajectory of well j, and hence, the gridblocks that are penetrated by well j are completely determined by the four-dimensional vector of parameters, $[x_{\text{w},j}, y_{\text{w},j}, z_{\text{w},j}, l_{\text{w},j}]^T$. Also, we assume that the "i", "j" and "k" directions are oriented in x, y and z coordinate directions, respectively.

Production and injection wells are represented by sink and source terms in the flow equation. Here, we consider a 3D vertical or horizontal well as a line source/sink term. In reservoir simulation models, the well source/sink terms are incorporated into the model with so-called "well models." Well models are used to model the flow between the gridblock and the wellbore by relating the wellbore and well gridblock pressures. Peaceman [28, 29, 30] introduced the most famous well model which is widely used directly or in some modified form in commercial reservoir simulators. Well models typically assume radial flow toward the well inside a gridblock and relate the flowing wellbore pressure, p_w, and the gridblock pressure, p_o, by the following type of equation:

$$p_w - p_o = \frac{q\mu}{2\pi\alpha kh} \ln \frac{r_w}{r_o}. \tag{4.3}$$

Here, α is a unit conversion factor with $\alpha = 1.127 \times 10^{-3}$ for field units which are used here; q is the flow rate at reservoir conditions in RB/day; μ is the viscosity of

the fluid in cp; k in md is the "effective" permeability of the gridblock in the "radial direction"; h in ft is the net length of the perforation interval; r_w is the wellbore radius in ft and r_o in ft is an "equivalent radius," which makes Eq. 4.3 correct when p_o is the gridblock pressure. Eq. 4.3 assumes that the skin factor is zero. Eq. 4.3 is for single-phase flow, but the multi-phase flow well model equation is similar. In Eclipse 100, the well model equation applies the following well inflow performance equation of phase p for each perforation (connection) of the well, (Schlumberger [38]),

$$q^n_{\mathrm{p},\ell} = T_{w,\ell} M^n_{\mathrm{p},\ell}(p^n_\ell - p^n_w - H^n_{w,\ell}), \tag{4.4}$$

where $q^n_{\mathrm{p},\ell}$ is the volumetric flow rate of phase p in perforation (connection) ℓ at time t^n. $T_{w,\ell}$ is the perforation transmissibility factor and $M^n_{\mathrm{p},\ell} = \frac{k_{r_{\mathrm{p},\ell}}}{\mu_{\mathrm{p},\ell}}$ is the phase mobility at the perforation which is evaluated based on the properties of the gridblock corresponding to the perforation at time t^n; where $k_{r_{\mathrm{p},\ell}}$ and μ_{p} are the phase "p" relative permeability and viscosity of fluid at perforation ℓ, respectively. Throughout we denote the term $T_{w,\ell}M^n_{\mathrm{p},\ell}$ as the productivity index of the perforation. The pressures p^n_ℓ and p^n_w, respectively, are the gridblock pressure and the bottomhole pressure in psi at time t^n, and $H^n_{w,\ell}$ is the wellbore pressure head between the perforation and the well's bottomhole pressure datum depth at time t^n. The perforation transmissibility factor, $T_{w,\ell}$, is computed with the following relationship for Cartesian grids (Schlumberger [38]):

$$T_{w,\ell} = \frac{\alpha\theta_\ell k_\ell h_\ell}{\ln(r_{o,\ell}/r_w) + s_\ell}, \tag{4.5}$$

where, α is the unit conversion factor, and θ_ℓ is the angle of the corresponding perforation with the well in radians. In a Cartesian grid, $\theta_\ell = 2\pi$, because the connection is assumed to be in the center of the grid block. For a well located on an edge (or a corner) of a Cartesian grid block, $\theta_\ell = 0.5 \times 2\pi$ (or $\theta_\ell = 0.25 \times 2\pi$) (Schlumberger [38]). In Eq. 4.5, $k_\ell h_\ell$ is the product of the effective permeability

in the radial direction and the net thickness of the perforation (completed interval) within the gridblock, and s_ℓ is the skin factor of the perforation. The equivalent radius, $r_{o,\ell}$, by Peaceman's formula for a gridblock which is fully penetrated by a vertical well at the center is given by

$$r_{o,\ell} = 0.28 \left(\frac{\left[\left(\frac{k_{y,\ell}}{k_{x,\ell}} \right)^{1/2} \Delta x_\ell^2 + \left(\frac{k_{x,\ell}}{k_{y,\ell}} \right)^{1/2} \Delta y_\ell^2 \right]^{1/2}}{\left[\left(\frac{k_{y,\ell}}{k_{x,\ell}} \right)^{1/4} + \left(\frac{k_{x,\ell}}{k_{y,\ell}} \right)^{1/4} \right]} \right). \tag{4.6}$$

where Δx_ℓ and Δy_ℓ are the dimensions of the gridblock in the x and y directions, respectively. In Eq. 4.6, $k_{x,\ell}$ and $k_{y,\ell}$, respectively, are the gridblock permeabilities in the x and y directions. Similar relations but modified for the gridblock properties in the appropriate directions are used for computing $r_{o,\ell}$ for perforations of a horizontal wells in the x and y directions.

Here, we refer to kh as the "perforation connectivity," which is determined in the simulator by multiplication of the effective permeability of the gridblock in the direction of radial flow towards (or away from) the well and the net length of the perforation inside the gridblock in the direction of the well axis. For example, the connectivity of a perforation of a vertical well which penetrates the whole thickness of a rectangular gridblock is $kh = \sqrt{k_x k_y}\Delta z$, where k_x and k_y are the gridblock permeabilities in the x and y directions, respectively. For a fully-penetrated gridblock, the perforation length (h) is equal to the gridblock thickness, Δz. For a gridblock partially-penetrated by a vertical well, the perforation connectivity is defined by

$$(kh) = \sqrt{(k_x k_y)}\Delta l = \gamma \sqrt{(k_x k_y)}\Delta z, \tag{4.7}$$

where Δl is the penetrated length of the gridblock. For the horizontal and vertical well orientations considered here, we can define a productivity index (PI) multiplier which multiplies the connectivity (kh) for any gridblock perforation which is partially

penetrated by the well as

$$\gamma = \frac{\Delta l}{\Delta L}, \tag{4.8}$$

where Δl and ΔL, respectively, are the penetrated length and the dimension of the gridblock in the direction of the axis of the well.

Mathematically, a well can be incorporated into the equations describing fluid flow in porous media using a series of point sinks (or sources) defined in terms of Dirac delta functions (Gunduz and Aral [14]). In an attempt to make the well-location variables continuous and make the NPV a continuous function of the well locations, Sarma and Chen [36] distributed each well source (or sink) term among the original well and pseudo-wells introduced in neighboring gridblocks. As discussed below, we will use a fairly similar approach here, but we extend the methodology to 3D problems so we can consider both horizontal and vertical wells and can optimize not only well locations but well completions. Unlike Sarma and Chen [36], we develop methodology which can be applied regardless of whether the user wishes to specify pressure-controlled or rate-controlled wells. Also, in our methodology, we replace the connectivity of the perforations of the pseudo-wells corresponding to a well with an average perforation connectivity; when we use this average instead of the perforation connectivities, the NPV changes are smoother as function of the well-location parameters. Throughout we refer to this NPV functional as the continuous NPV functional since the NPV varies continuously when the well location changes within a gridblock; however, the defined continuous NPV is not differentiable as there is a jump discontinuity in the NPV functional when the well location moves across a gridblock boundary.

We give the details of our algorithm only for a vertical well, but exactly the same procedure is applied for a horizontal well. Consider a well with given trajectory parameters $(x_{\mathrm{w}}, y_{\mathrm{w}}, z_{\mathrm{w}}, l_{\mathrm{w}})$. For simplicity, assume that the well is vertical and that the well penetrates only one gridblock. The location of the actual well at a

particular iteration of the optimization algorithm is at a point $(x_{\rm w}, y_{\rm w}, z_{\rm w})$ which is in gridblock $(i_{\rm w}, j_{\rm w}, k_{\rm w})$. Denote the spatial location of the center point of gridblock $(i_{\rm w}, j_{\rm w}, k_{\rm w})$ by $(\bar{x}_{(i_{\rm w},j_{\rm w},k_{\rm w})}, \bar{y}_{(i_{\rm w},j_{\rm w},k_{\rm w})}, \bar{z}_{(i_{\rm w},j_{\rm w},k_{\rm w})})$. The location of the actual well is not necessarily at the center of the gridblock. To account for the actual location of the well inside a gridblock, we replace the actual well with 9 pseudo-wells where the axis of all pseudo-wells are in the same direction as the axis (centerline) of the actual well. One pseudo-well is located in gridblock $(i_{\rm w}, j_{\rm w}, k_{\rm w})$, and the 8 other pseudo-wells are located at the neighboring gridblocks in the plane perpendicular to the well's centerline (axis), e.g., for a vertical well, the pseudo-wells are located in gridblock $(i_{\rm w}, j_{\rm w}, k_{\rm w})$ and in the neighboring gridblocks in $x-y$ plane with gridblock indices $(i_{\rm w}+\bar{i}, j_{\rm w}+\bar{j}, k_{\rm w})$ where $\bar{i}, \bar{j} = -1, 0, 1$. All pseudo-wells are always located exactly at the center of their corresponding gridblocks. Therefore, the (x, y) spatial location of every pseudo-well is equivalent to the spatial location of the center of its corresponding gridblock. For a vertical well, the schematic of the actual well location and its corresponding pseudo-wells in the $x-y$ plane are shown in Fig. 4.2, where, $(x_{\rm w}, y_{\rm w}, z_{\rm w})$ shows the actual well location and pw-1 to pw-9 are the pseudo-wells. Note that like the actual well, all the pseudo-wells are vertical. Similar comments apply if the actual well is horizontal and its axis is in the "i" (or "j") direction. If the actual well axis is in the "i" (or "j") direction, the axis of all pseudo-wells is also in the "i" (or "j") direction and the pseudo-wells are perpendicular to $y-z$ (or $x-z$) plane.

We distribute the rate of the actual well among the pseudo-wells so that the pseudo-wells closer to the actual well location get a larger portion of the rate of the actual well. The equations discussed below are applied to distribute the rate of the actual well (source/sink term) among the pseudo-wells. Throughout, β_m denotes the contribution of the mth pseudo-well to the total source/sink term of a well, i.e., the portion of the rate of the original well assigned to pseudo-well m. Generally

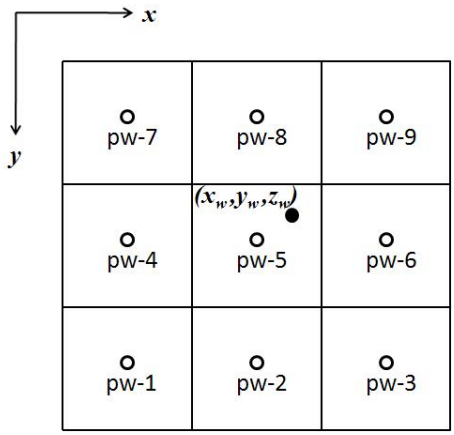

Figure 4.2: Schematic of the actual well and its corresponding pseudo-wells for a vertical well.

speaking, the axis (centerline) of the actual well is perpendicular to the $u-v$ plane. For a vertical well, $u = x$ and $v = y$. For a horizontal well with its axis in the y (or "j") direction, $u = x$ and $v = z$. For a horizontal well with its axis in the x (or "i") direction, $u = y$ and $v = z$. For a well with its axis perpendicular to the $u-v$ plane, β_m for pseudo-well m is defined by

$$\beta_m(u_{\rm w}, v_{\rm w}) = \frac{\exp\left(-\frac{(u_{{\rm pw},m}-u_{\rm w})^2}{\sigma_{\rm u}^2}\right) \times \exp\left(-\frac{(v_{{\rm pw},m}-v_{\rm w})^2}{\sigma_{\rm v}^2}\right)}{\sum_{n=1}^{9}\left(\exp\left(-\frac{(u_{{\rm pw},n}-u_{\rm w})^2}{\sigma_{\rm u}^2}\right) \times \exp\left(-\frac{(v_{{\rm pw},n}-v_{\rm w})^2}{\sigma_{\rm v}^2}\right)\right)}, \qquad m = 1, 2, \ldots, 9. \tag{4.9}$$

where $(u_{\rm w}, v_{\rm w})$ is the coordinate of the actual well in the $u-v$ plane, and $(u_{{\rm pw},m}, v_{{\rm pw},m})$ is the coordinate of the pseudo-well m in the $u-v$ plane which is located at the center of its corresponding gridblock. The summation of the β_m's is required to equal 1 so that the total rate of production (or injection) from all pseudo-wells is equal to the production rate (or injection rate) of the actual well. However, as discussed later, for pressure-controlled wells, this is actually true only if the perforation connectivity (kh) and the gridblock pressure are the same in all nine gridblocks containing pseudo wells. The parameters σ_u and σ_v must be specified by the user; larger σ values result in a larger portion of the total rate assigned to the neighboring pseudo-wells. A

larger value of σ makes the representation of the original well with pseudo-wells more approximate. On the other hand, for smaller σ values, a larger portion of the total rate will be assigned to the center pseudo-well. For pressure-controlled wells, small values of σ result in a bigger jump discontinuity when a well location crosses a gridblock boundary as the gridblock pressure at neighboring pseudo-well perforations may be very different from the one for the center pseudo-well. Based on experimentations, we recommend choosing σ_u and σ_v, respectively, to be the dimensions of the gridblock which contains $(x_{\rm w}, y_{\rm w}, z_{\rm w})$ in the u and v directions, respectively.

Two cases of rate-controlled and bottomhole pressure-controlled wells are considered. When optimizing the location of a rate-controlled well, the rate of the well is distributed between 9 pseudo-wells by

$$q_m = q \times \beta_m, \qquad m = 1, 2, \ldots, 9. \tag{4.10}$$

where q is the specified rate at the actual well and q_m is the rate of pseudo-well m.

If the well operates on constant bottomhole pressure, all the pseudo-wells are assigned the same bottomhole pressure as the actual well, however, every pseudo-well is assigned a "well index multiplier." The well index multiplier of a well, modifies the transmissibility factor of all the perforations of a well ($T_{w,\ell}$'s in Eqs. 4.4 and 4.5). The WI multipliers of pseudo-wells should sum to 1 so the sum of the rates of all the pseudo-wells is equal to the rate of the actual well. For bottomhole pressure-controlled wells, theoretically, the sum of the rates of the pseudo-wells is equal to the rate of the actual well, if (i) all the pseudo-wells have the same transmissibility factors as the original well, but weighted with a WI multiplier, and (ii) all pseudo-wells also have the same potential difference between the reservoir and the wellbore (drawdown pressure for producers and build up pressure for injection wells) (see Eq. 4.4). The

well index multiplier of every pseudo-well is given by

$$WI_m = \beta_m, \qquad m = 1, 2, \ldots, 9. \tag{4.11}$$

WI_m is the well index multiplier for pseudo-well m. However, every gridblock containing a pseudo-well may have a different gridblock size and permeability and hence a different transmissibility factor. Therefore, the sum of the rates of the pseudo-wells is not the same as the rate of the original well. In order to eliminate this inconsistency, we average the perforation connectivities (effective kh) of all nine pseudo-wells and replace the perforation connectivity of all pseudo-wells with this averaged value. If the wells penetrate more than one plane of gridblocks, then this averaging is done for each plane of gridblocks separately, as discussed later. Note, this fix will force the aforementioned condition (i) to hold but condition (ii) on pressure differentials still will not generally hold.

The transmissibility factor of a perforation is a function of the perforation gridblock size as well as the perforation gridblock effective permeability and the perforation length. In Eq. 4.5, r_o is a function of gridblock size and effective permeability according to Peaceman's equation (Eq. 4.6). For simplicity, we assume that all the pseudo-well gridblocks relevant to a perforation (simulation layer) have the same dimensions in the x, y and z directions. Moreover, if the skin is nonzero, each perforation of each pseudo-well is assigned the skin factor of the corresponding perforation of the actual well. Therefore, the variation from pseudo-well to pseudo-well in the transmissibility factor for a perforation is entirely due to the variation in kh where k is the effective "radial permeability" of the gridblock and h is the net thickness of the perforation. We average kh over all the gridblocks containing pseudo-wells. Note that k in kh does not denote horizontal permeability, but denotes the effective permeability in the plane parallel to a well; see for example Eq. 4.7. We tried three common averaging methods for averaging kh of perforation ℓ over pseudo-wells

$m = 1, 2, \ldots 9,$

a geometric average given by

$$(\overline{kh})_\ell = \left(\prod_{m=1}^{9} (kh)_{m,\ell} \right)^{1/9} = \sqrt[9]{(kh)_{1,\ell}(kh)_{2,\ell} \ldots (kh)_{9,\ell}}, \tag{4.12}$$

a weighted arithmetic average given by

$$(\overline{kh})_\ell = \sum_{m=1}^{9} \beta_m (kh)_{m,\ell}, \tag{4.13}$$

and a weighted geometric average given by

$$(\overline{kh})_\ell = \prod_{m=1}^{9} \left[(kh)_{m,\ell} \right]^{\beta_m}, \tag{4.14}$$

In the weighted averages, the weight factors β_m are given by Eq. 4.9; therefore, the average connectivity $(\overline{kh})$ is a stronger function of the permeabilities corresponding to the perforated gridblocks of the pseudo-wells that are closer to the actual well location. Replacing the connectivity of the perforations of the pseudo-wells with the average connectivity $(\overline{kh})$, smoothes the discontinuity in the NPV functional that occurs when a well moves across a gridblock boundary. A discussion on the results for different averaging methods is given in Example 1. Based on the results presented in Example 1 and other results not shown here, the weighted geometric average method gives a smoother continuous NPV as a function of spatial well locations. Therefore, we show only the results for this averaging method for the other examples.

In three dimensions, a well may penetrate several gridblocks so the line source/sink is present in several gridblocks. In this case, the actual well is again replaced by nine pseudo-wells where each pseudo-well has its axis in the same direction as the axis of the actual well and each pseudo-well penetrates the same number of gridblocks that are penetrated by the actual well. For concreteness in presenta-

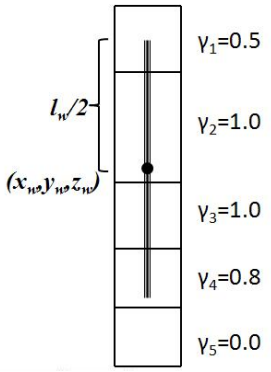

Figure 4.3: Schematic of perforations of a vertical well in multiple layers.

tion, assume a vertical well with its center point at $(x_{\rm w}, y_{\rm w}, z_{\rm w})$ which penetrates gridblocks $(i_{\rm w}, j_{\rm w}, k_{{\rm w},\ell})$, $\ell = 1, 2, \ldots, N_{\rm com}$ where $N_{\rm com} > 1$. Then the nine pseudo-wells also have perforations in simulation layers $k_{{\rm w},\ell}$, $\ell = 1, 2, \ldots, N_{\rm com}$ and the completions of the eight surrounding pseudo-wells are in gridblocks $(i_{\rm w} \pm 1, j_{\rm w}, k_{{\rm w},\ell})$, $(i_{\rm w}, j_{\rm w} \pm 1, k_{{\rm w},\ell})$, $(i_{\rm w} \pm 1, j_{\rm w} \pm 1, k_{{\rm w},\ell})$, $\ell = 1, 2, \ldots, N_{\rm com}$, i.e., the pseudo-wells are configured as in Fig. 4.2 and each pseudo-well penetrates $N_{\rm com}$ simulation layers in the z-direction. Similar to our previous discussion on partially-penetrated gridblocks, every perforation ℓ of a pseudo-well is assigned with a productivity index multiplier γ_ℓ,

$$\gamma_\ell = \frac{\Delta l_\ell}{\Delta L_\ell}, \qquad \ell = 1, \ldots, N_{\rm com}. \tag{4.15}$$

where Δl_ℓ and ΔL_ℓ, respectively, are the penetrated length of and the size of the gridblock $(i_{\rm w}, j_{\rm w}, k_{{\rm w},\ell})$ for perforation ℓ in the direction of well axis. The schematic of the perforations of a vertical well is given in Fig 4.3. Note that for a given perforation ℓ, γ_ℓ is the same for all pseudo-wells. When a well is perforated in a row or column of gridblocks, for every perforation ℓ, $(\overline{kh})_\ell$ is set equal to the average of the effective kh's of the gridblocks containing the pseudo-wells and $(\overline{kh})_\ell$ is assigned to the perforation ℓ in all pseudo-wells. For example, $(\overline{kh})_\ell$ computed with the weighted geometric average given in Eq. 4.14.

In this work, we use Eclipse 100 simulator to run the simulation model and

evaluate the NPV. At the initial stage of the optimization, all the simulation gridblock information, including geometrical information and the rock properties, are imported into the code. For given well parameters, first, the perforation gridblock indices of the center pseudo-well is determined from the values of the well parameters (the center point and length of the well) and the direction of the well. The productivity index (PI) multiplier for each perforation is computed by Eq. 4.15 using the well parameters and the geometrical grid information. The surrounding pseudo-well completions are determined based on the perforations of the center pseudo-well. For every perforation ℓ, $(\overline{kh})_\ell$ is computed based on the average of the effective kh's of the gridblocks containing perforation ℓ in pseudo-wells $m = 1, 2, \ldots, 9$, Eq. 4.14. This $(\overline{kh})_\ell$ is assigned as the effective kh for perforation ℓ of every pseudo-well. Perforation ℓ of each pseudo-well is also assigned the productivity index (PI) multipliers (γ_ℓ) computed from Eq. 4.15. Then, the contribution of each pseudo-well to the rate of the original well (β_m) is computed by Eq. 4.9. For a rate-controlled original well, all the pseudo-wells are rate-controlled wells with the rate of each pseudo-well given by Eq. 4.10. If an actual well is pressure-controlled, all the pseudo-wells are bottomhole pressure-controlled wells with the same bottomhole pressure as the original well; however, each pseudo-well is assigned a well index (WI) multiplier computed from Eq. 4.11.

Moving the actual well in a plane changes the NPV because moving the location of the well redistributes the proportions of the rate assigned to each pseudo-well. If the change in location moves the actual well across a gridblock boundary, so the gridblocks containing the actual well are modified, then the gridblocks containing the pseudo-wells are also modified. Thus as each gridblock has its own effective kh, moving the actual well across a gridblock boundary can cause discontinuity in NPV. However, because the effective $(\overline{kh})_\ell$ of perforation ℓ of all pseudo-wells is the same, the jump in NPV is reasonably small. Moreover, we use a derivative-free

optimization algorithm and such algorithms are less affected by discontinuities in derivatives than are gradient-based algorithms. Moving the well in the direction of its axis, and/or changing the length of the well, changes both the perforated gridblocks and the PI multipliers assigned to the perforations of the pseudo-wells, and hence, changes the NPV. Thus, NPV is sensitive to the vector of parameters $[x_{\rm w}, y_{\rm w}, z_{\rm w}, l_{\rm w}]^T$ which describes the well location and completions, and therefore we can estimate the optimal location and completions of a given number of production and injection wells by maximizing the NPV functional of Eq. 2.1. The algorithm that we have developed can also be applied to optimize subsets of $(x_{\rm w}, y_{\rm w}, z_{\rm w}, l_{\rm w})$. For example, when optimizing only the location of a fully-penetrating vertical well, the optimization parameters are reduced to the $(x_{\rm w}, y_{\rm w})$ coordinates of the wells. When optimizing the completions of a vertical well at a fixed location, $(z_{\rm w}, l_{\rm w})$ would be the optimization parameters. In this last case, no pseudo-wells are needed since the $(x_{\rm w}, y_{\rm w})$ coordinates of the well are considered to be fixed. However, every perforation of the well will be assigned a PI multiplier which is a function of $(z_{\rm w}, l_{\rm w})$ parameters of the well.

4.3 BOBYQA for Derivative-Free Optimization

The optimal values of the set of parameters $(x_{{\rm w},m}, y_{{\rm w},m}, z_{{\rm w},m}, l_{{\rm w},m})$, $m = 1, 2, \ldots, N_{\rm well}$ are obtained by minimizing $J = -$NPV using Bound Optimization BY Quadratic Approximation, BOBYQA. BOBYQA optimization algorithm is briefly explained in Chapter 2. Here, we present a method for normalizing the optimization variables to improve the performance of BOBYQA.

BOBYQA uses the reservoir simulator as a "black box." The optimization parameters are $u = [x_{{\rm w},1}, y_{{\rm w},1}, z_{{\rm w},1}, l_{{\rm w},1}, \ldots, x_{{\rm w},N_{\rm well}}, y_{{\rm w},N_{\rm well}}, z_{{\rm w},N_{\rm well}}, l_{{\rm w},N_{\rm well}}]^T$. The total number of the optimization variables is $n = 4 \times N_{\rm well}$. The bound values on $x_{{\rm w},m}$ and $y_{{\rm w},m}$ parameters are determined by the outer reservoir boundaries. The bounds on each $z_{{\rm w},m}$ is the depth of the top and bottom of the reservoir at $(x_{{\rm w},m}, y_{{\rm w},m})$. The

maximum and minimum values for the length of the well, $l_{\mathrm{w},m}$, are specified by the user. In BOBYQA, the same trust-region radius is applied for all the optimization parameters, therefore, in our implementation, we normalize every optimization variable and transform the original bounds to bounds on the normalized components of u. BOBYQA is then applied to the normalized variables, and hence, the parameters used in BOBYQA are all specified in the normalized domain, i.e., the values of the initial and minimum trust-region radii, ρ_{beg} and ρ_{end}, the initial point and the bound constraints are all specified in the normalized domain. The normalized components $\tilde{u}_i$, $i = 1, 2, \ldots, n$ of the normalized vector of parameters $\tilde{u}$ are defined by

$$\tilde{u}_i = \frac{(u_i - u_i^{\mathrm{low}})\rho_{end}}{D_i \epsilon_i}, \tag{4.16}$$

where D_i and ϵ_i are defined below; ρ_{end} is the minimum trust-region radius in BOBYQA which is specified by the user and u_i^{low} is the lower bound for u_i predefined in Eq. 4.2. Note when $u_i = u_i^{\mathrm{low}}$, $\tilde{u}_i = 0$ and when u_i is equal to its upper bound u_i^{up}, the corresponding upper bound for $\tilde{u}_i$ is

$$\tilde{u}_i^{\mathrm{up}} = \frac{u_i^{\mathrm{up}} - u_i^{\mathrm{low}}}{D_i} \times \rho_{end} \times \frac{1}{\epsilon_i}. \tag{4.17}$$

Thus in the transformed domain, the bound constraints are

$$\tilde{u}_i^{\mathrm{low}} \leq \tilde{u}_i \leq \tilde{u}_i^{\mathrm{up}}, \qquad 1 \leq i \leq n, \tag{4.18}$$

where $\tilde{u}_i^{\mathrm{low}} = 0$. In Eq. 4.16, D_i is the average over the optimization domain of the reservoir gridblock size in a particular coordinate direction (x, y or z) appropriate for the variable u_i. D_i, for x_{w}, y_{w} and z_{w} is respectively the average reservoir gridblock size in the x, y and z direction, respectively. The average is taken over the gridblocks inside the part of the reservoir that we consider for well-placement. The value

of D_i for the length parameter (l_{w}) of the trajectory of the well depends on the well direction. Its value for a well with its axes in the x, y and z directions, respectively, is the average gridblock size in the x, y and z directions, respectively. The term $(u_i^{\mathrm{up}} - u_i^{\mathrm{low}})/D_i$ for optimization variable i is an estimate of the number of simulation gridblocks in the original domain corresponding to variable u_i. For example, if optimization variable u_i is the x_{w} coordinate of a well center point, then $(u_i^{\mathrm{up}} - u_i^{\mathrm{low}})/D_i$ gives the approximate number of simulation gridblocks in the x direction. Note that Eq. 4.16 implies that

$$\Delta\tilde{u}_i = \frac{\Delta u_i \rho_{end}}{D_i \epsilon_i}. \tag{4.19}$$

For the optimization parameter u_i, ϵ_i is the fraction of D_i which corresponds to ρ_{end} in the normalized domain, i.e., $\Delta u_i = \epsilon_i D_i$ corresponds to $\Delta\tilde{u}_i = \rho_{end}$. For example, $\epsilon_i = 0.1$ for the optimization parameter x_{w} (or y_{w}) implies that the value of $\Delta\tilde{u}_i = \rho_{end}$ is equivalent to 0.1 of the average gridblock size in the x (or y) direction. A similar comment applies for the ϵ_i corresponding to optimization parameters z_{w} and l_{w}. From numerical experiments with BOBYQA, Powell [34] observed that the distance from the final $\tilde{u}^{\ell}$ to a local minimum of $J[\tilde{u}]$ is less than $10\rho_{end}$. Based on this observation, we choose $\epsilon_i = 0.1$ so that, for optimization variable $\tilde{u}_i$, $10\rho_{end}$ is equivalent to one average gridblock size, D_i, in the original domain. Therefore, the final well location resulting from BOBYQA and the local optimum well location would tend to be in the same gridblock, or at worst, in two adjacent gridblocks assuming that the aforementioned observation of Powell [34] is generally valid.

In applying Eq. 4.17, the upper bound values in the normalized domain are computed first for all the optimization variables. Then, the optimization variables are normalized using Eq. 4.16, which is equivalent to

$$\tilde{u}_i = \frac{u_i - u_i^{\mathrm{low}}}{u_i^{\mathrm{up}} - u_i^{\mathrm{low}}} \tilde{u}_i{}^{\mathrm{up}}, \qquad i = 1, 2, \ldots, n. \tag{4.20}$$

Note that the optimization is performed in the normalized domain; therefore for evaluating the objective function at each optimization iteration, the well parameters, u_i's are determined from

$$u_i = u_i^{\text{low}} + \frac{\tilde{u_i}}{\tilde{u_i}^{\text{up}}}(u_i^{\text{up}} - u_i^{\text{low}}), \qquad i = 1, 2, \ldots, n. \tag{4.21}$$

As we previously mentioned, BOBYQA utilizes the same trust-region radius for all optimization variables. In our work, after specifying ρ_{end}, we define the initial trust-region radius, ρ_{beg}, by

$$\rho_{beg} = \min\left(10\rho_{end}, 0.2 \min_{i=1,2,\ldots,n}(\tilde{u_i}^{\text{up}})\right). \tag{4.22}$$

As we previously discussed, we choose $\epsilon_i = 0.1$ for all the optimization variables based on the Powell's observation. Choosing $\epsilon_i = 0.1$ means that $\Delta\tilde{u}_i = 10\rho_{end}$ is equal to the length of a gridblock in one direction in the original domain. BOBYQA constructs the initial interpolation set by making ρ_{beg}-sized perturbations (in the normalized domain) in the coordinate directions; therefore, if we set $\rho_{\text{beg}} = 10\rho_{\text{end}}$, the perturbation points for constructing the initial interpolation set are about one gridblock away from the initial well locations. On the other hand, for BOBYQA, the conditions

$$\tilde{u}_i^{\text{up}} - \tilde{u}_i^{\text{low}} = \tilde{u}_i^{\text{up}} \geq 2.0\rho_{beg}, \qquad i = 1, 2, \ldots, n, \tag{4.23}$$

should hold so that it is likely that the initial interpolation points obtained by perturbations around the initial point, $\tilde{u}_{\text{init}}$, in the normalized domain are all contained within the reservoir simulation grid. If the inequality condition in Eq. 4.23 holds for the component i, but $\tilde{u}_{\text{init},i}$ is very close to one of the lower or upper bound values ($\tilde{u}_{\text{init},i} - \tilde{u}_i^{\text{low}} < \rho_{beg}$ or $\tilde{u}_i^{\text{up}} - \tilde{u}_{\text{init},i} < \rho_{beg}$), then BOBYQA may automatically change $\tilde{u}_{\text{init},i}$ away from the bound value in order to make enough room for the perturbation (see Powell [34]). Based on these considerations, Eq. 4.22 was proposed to use

a fraction (0.2) of the shortest normalized domain length among all the variables, $0.2 \min_{i=1,2,\ldots,n}(\tilde{u}_i^{\text{up}} - \tilde{u}_i^{\text{low}} = \tilde{u}_i^{\text{up}})$, for an estimate of ρ_{beg}. However, Eq. 4.22 avoids taking a large initial trust-region radius by putting an upper bound of $10\rho_{end}$ on the value of ρ_{beg}.

There is one problem that can occur when applying our implementation of BOBYQA described above. This problem arises when denormalizing the value of $\tilde{z}_{\text{w},m}^{\ell+1}$ for well m in a new well location. Since the initial lower and upper bound values for the $z_{\text{w},m}$'s ($z_{\text{w},m}^{\text{up}}$ and $z_{\text{w},m}^{\text{low}}$) are defined based on the initial well locations, when denormalizing $\tilde{z}_{\text{w},m}^{\ell+1}$ at a different location, the top and bottom surfaces of the reservoir might be different in the new location so that is possible to obtain a value of $z_{\text{w},m}^{\ell+1}$ which is outside the reservoir. To avoid this problem, we redefine the bound constraints for $z_{\text{w},m}^{\ell+1}$ at iteration $\ell+1$ based on the top and bottom depth of the reservoir at the current well location, $(x_{\text{w},m}^{\ell+1}, y_{\text{w},m}^{\ell+1})$. Therefore, the denormalized $z_{\text{w},m}^{\ell+1}$ obtained from $\tilde{z}_{\text{w},m}^{\ell+1}$ using Eq. 4.21 at the new well location is always within the top and bottom surfaces of the reservoir. Even with this modification, depending on the well length and the location of the well center point, part of a well can be located outside the reservoir; in this event, the length of the well is truncated by the reservoir boundary and only the part of the well which is located inside the reservoir is considered. Therefore, the location of the completed part of a well is always inside the reservoir, and its location is defined relative to the depth of the top and bottom surfaces of the reservoir at the well location. The following procedure explains the steps followed in iteration $\ell+1$ for the denormalization of $(\tilde{x}_{\text{w},m}^{\ell+1}, \tilde{y}_{\text{w},m}^{\ell+1}, \tilde{z}_{\text{w},m}^{\ell+1}, \tilde{l}_{\text{w},m}^{\ell+1})$ to obtain the well parameters, $(x_{\text{w},m}^{\ell+1}, y_{\text{w},m}^{\ell+1}, z_{\text{w},m}^{\ell+1}, l_{\text{w},m}^{\ell+1})$.

- Denormalize $(\tilde{x}_{\text{w},m}^{\ell+1}, \tilde{y}_{\text{w},m}^{\ell+1})$ to find the new well location $(x_{\text{w},m}^{\ell+1}, y_{\text{w},m}^{\ell+1})$ by applying Eq. 4.21,

$$x_{\text{w},m}^{\ell+1} = x_{\text{w},m}^{\text{low}} + \frac{\tilde{x}_{\text{w},m}^{\ell+1}}{\tilde{x}_{\text{w},m}^{\text{up}}}(x_{\text{w},m}^{\text{up}} - x_{\text{w},m}^{\text{low}}). \tag{4.24}$$

and

$$y_{\mathrm{w},m}^{\ell+1} = y_{\mathrm{w},m}^{\mathrm{low}} + \frac{\tilde{y}_{\mathrm{w},m}^{\ell+1}}{\tilde{y}_{\mathrm{w},m}^{\mathrm{up}}}(y_{\mathrm{w},m}^{\mathrm{up}} - y_{\mathrm{w},m}^{\mathrm{low}}). \tag{4.25}$$

Note that $x_{\mathrm{w},m}^{\mathrm{low}}$, $x_{\mathrm{w},m}^{\mathrm{up}}$, $y_{\mathrm{w},m}^{\mathrm{low}}$ and $y_{\mathrm{w},m}^{\mathrm{up}}$ are fixed and defined according to the reservoir boundaries.

- Determine $z_{\mathrm{w},m}^{\mathrm{low},\ell+1}$ and $z_{\mathrm{w},m}^{\mathrm{up},\ell+1}$ which are the depths of the bottom and top surfaces, respectively, of the reservoir at the new well location $(x_{\mathrm{w},m}^{\ell+1}, y_{\mathrm{w},m}^{\ell+1})$.

- Denormalize $\tilde{z}_{\mathrm{w},m}^{\ell+1}$ to find the depth of the well, $z_{\mathrm{w},m}^{\ell+1}$, by

$$z_{\mathrm{w},m}^{\ell+1} = z_{\mathrm{w},m}^{\mathrm{low},\ell+1} + \frac{\tilde{z}_{\mathrm{w},m}^{\ell+1}}{\tilde{z}_{\mathrm{w},m}^{\mathrm{up},\ell+1}}(z_{\mathrm{w},m}^{\mathrm{up},\ell+1} - z_{\mathrm{w},m}^{\mathrm{low},\ell+1}). \tag{4.26}$$

  Note that $z_{\mathrm{w},m}^{\mathrm{low},\ell+1}$ and $z_{\mathrm{w},m}^{\mathrm{up},\ell+1}$ are the bottom and top depths of the reservoir at the new well location $(x_{\mathrm{w},m}^{\ell+1}, y_{\mathrm{w},m}^{\ell+1})$.

- Denormalize $\tilde{l}_{\mathrm{w},m}^{\ell+1}$ to find the length of the well, $l_{\mathrm{w},m}^{\ell+1}$, by

$$l_{\mathrm{w},m}^{\ell+1} = l_{\mathrm{w},m}^{\mathrm{low}} + \frac{\tilde{l}_{\mathrm{w},m}^{\ell+1}}{\tilde{l}_{\mathrm{w},m}^{\mathrm{up}}}(l_{\mathrm{w},m}^{\mathrm{up}} - l_{\mathrm{w},m}^{\mathrm{low}}). \tag{4.27}$$

The well parameters, $(x_{\mathrm{w},m}^{\ell+1}, y_{\mathrm{w},m}^{\ell+1}, z_{\mathrm{w},m}^{\ell+1}, l_{\mathrm{w},m}^{\ell+1})$, give the location and completion interval.

BOBYQA satisfies the specified bound constraints, but for the well-placement problem considered here, the reservoir boundaries in the x and y directions cannot always be represented as simple bound constraints on $x_{\mathrm{w},m}$ and $y_{\mathrm{w},m}$. For the purpose of illustration, assume the reservoir grid in the one shown in Fig. 4.4. The dark area determines the active gridblocks. The rest of the reservoir gridblocks are inactive and are not considered as part of the feasible region for well-placement. We set the upper and lower bounds on the $(x_{\mathrm{w},m}, y_{\mathrm{w},m})$'s as the boundary of the gridded area which contains the reservoir active gridblocks. However, this region may also contain

inactive gridblocks. During the optimization procedure a well center point can move into an inactive gridblock. Therefore, the whole length of the well or some part of the well can be in the inactive region of the reservoir. If the whole length of a well is in inactive gridblocks, then the well is effectively eliminated. At every iteration of the optimization algorithm, the objective function needs to be evaluated by running the reservoir simulation.

We may consider two approaches for evaluating NPV when a well center point is moved to an inactive gridblock. The first approach is to keep the well in its location where the well center point is in an inactive gridblock. Note that in this case, it is possible that some length of the well is still in active gridblocks. However, if the whole length of the well is in inactive gridblocks, then the well will automatically be eliminated when running the simulator to evaluate the NPV functional. If the elimination of this well or part of it (by moving the well center point to an inactive gridblock) results in a lower value of NPV, this optimization iteration automatically will be rejected as the optimal solution. The main concern with this approach is that elimination of the well may result in a much larger (or smaller) NPV value, which may damage the quality of the quadratic interpolation model. The second approach is to move the location of the well center point back into an active gridblock. We have found via computational experiment (presented at the end of this chapter) that the second approach results in a more robust algorithm. To move a well center point from an inactive gridblock to an active gridblock, we move the well center point along a path which connects the current location of the well in an inactive gridblock, $(x^{\ell}_{\mathrm{w},m}, y^{\ell}_{\mathrm{w},m}, z^{\ell}_{\mathrm{w},m})$, and the location of the well with the highest NPV (lowest value of J obtained at previous iterations), $(x^{\mathrm{opt},\ell}_{\mathrm{w},m}, y^{\mathrm{opt},\ell}_{\mathrm{w},m}, z^{\mathrm{opt},\ell}_{\mathrm{w},m})$. The well center point is moved along this path until the corrected position of the well center point is located in an active gridblock. Then with this location of the well, the simulation is run to evaluate $J[u^{\ell+1}]$. This process is shown in Fig. 4.4.

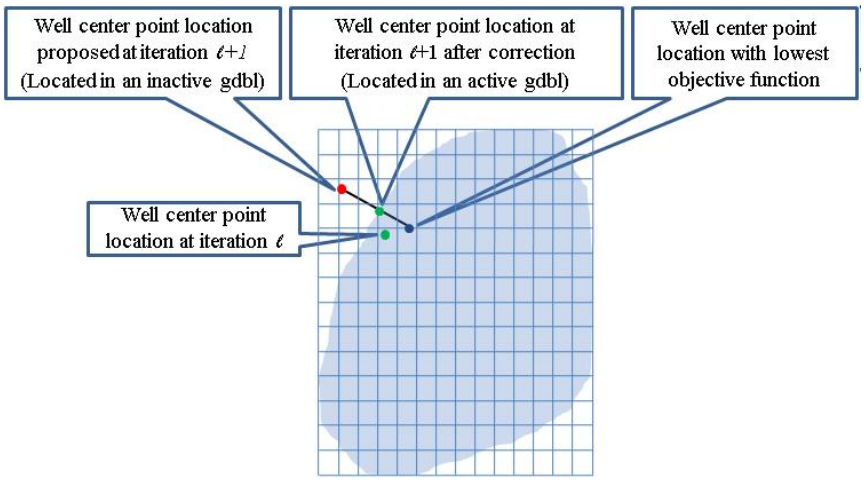

Figure 4.4: Correction of the well location to an active gridblock.

The concern about this approach is that the changes in the location of the well (well parameters $(x^{\ell}_{\mathrm{w},m}, y^{\ell}_{\mathrm{w},m}, z^{\ell}_{\mathrm{w},m})$) are applied for evaluating the objective function only; the values of the corresponding optimization variables in BOBYQA algorithm remain unchanged. (BOBYQA uses the value of the optimization variables in the process of updating the quadratic model for the next iteration.) The method of modifying the center point of the well is similar to the truncation method for honoring the bound constraints in the optimization literature. However, we do not change the values of the well parameters in BOBYQA because modifying the interpolation set of points in BOBYQA algorithm is done to ensure that the interpolation set is well poised, (Powell [34]). Changing the value of the control variables while disregarding the BOBYQA considerations can damage the well-poisedness of the interpolation set and the accuracy of the algorithm.

4.4 Computational Results

In this section, we first discuss the continuity of NPV (given in Eq. 2.1) as a function of well position parameters. Making NPV reasonably smooth is a key feature of our well-placement method. Also, the DFO optimization algorithm that we implement in our well-placement method approximates the objective function

with a smooth and continuous quadratic model. This makes BOBYQA a very good choice for optimizing the noisy objective function of the well-placement problem. One laudatory feature of our methodology is that it results in a reasonably smoother NPV. Then we provide example results generated from our algorithm for both vertical and horizontal wells in synthetic homogeneous and heterogenous reservoirs. In Example 4, we specifically investigate the two approaches for evaluating the NPV functional when the well is moved to an inactive gridblock. In all examples, the objective is to maximize the NPV by optimizing the location and length of the well in a two-phase, oil-water reservoir with water injection. In all examples, the oil price is fixed at 70 \$/STB. The water injection and disposal costs are 10 and 5 \$/STB, respectively, and the annual discount rate is $b = 0$. In Example 4, we do not consider any revenue or cost for the produced gas from the PUNQ reservoir.

4.4.1 Example 1. NPV as a Function of Well Spatial Coordinates

In this example, we consider a two-dimensional heterogeneous reservoir. The reservoir is a $2500 \times 2500 \times 50$ ft ($25 \times 25 \times 1$ gridblocks) simulation model. The reservoir has 4 producers operating at a constant bottomhole pressure equal to $3,000$ psi. The initial reservoir pressure is $3,500$ psi. The porosity and horizontal log-permeability fields of the reservoir are shown in Figs. 4.5(a) and 4.5(b). The production well locations are shown with white circles in Figs. 4.5(a) and 4.5(b).

Our objective is simply to find the best location for a single water injection well in this reservoir. We consider two cases. In the first case, the injection well operates at constant bottomhole pressure of $4,000$ psi and the reservoir life is 3 years. In the second case, the well injects at a constant injection rate of $1,000$ STB/D for 8 years. This simple example was chosen so that it is relatively easy to generate the NPV maps of the production from the reservoir, which are shown in Figs. 4.6(a) and 4.6(b) for the two cases. The NPV maps are generated numerically by putting a single injection well at each reservoir gridblock and computing the NPV

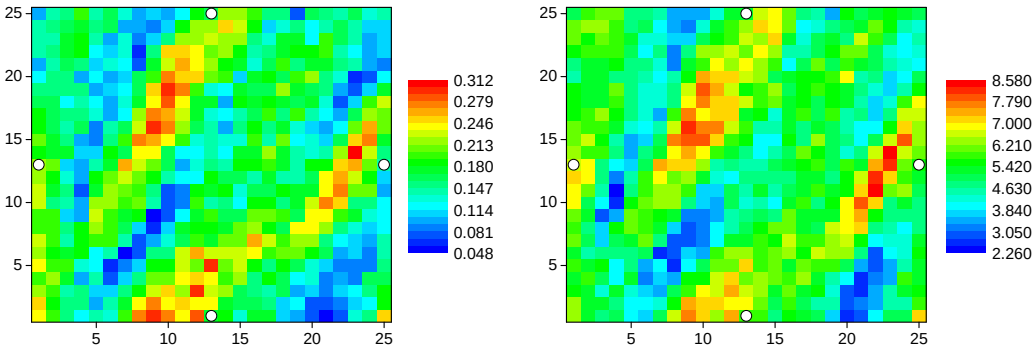

(a) Porosity (b) Log-permeability

Figure 4.5: The porosity and log-permeability fields of the heterogeneous reservoir, Example 1.

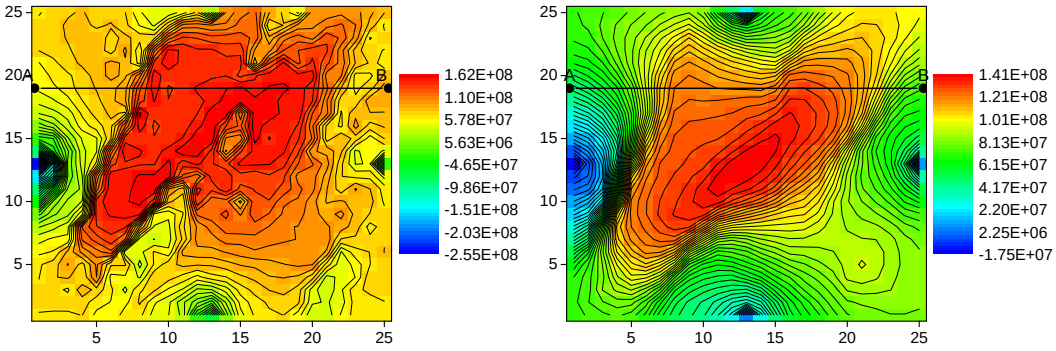

(a) Injector operating with constant BHP (b) Injector operating with constant rate

Figure 4.6: NPV maps, Example 1.

of production from the reservoir. By moving the single injector from gridblock to gridblock, we generate the NPV map. Note that the NPV map for the case of the injection well with constant injection rate is much smoother than the map for the case where the injection well operates on constant bottomhole pressure. As discussed previously, for an injector operating at a specified wellbore pressure, the injection rate of the well may change significantly as the well is moved from one gridblock to another gridblock because gridblock permeabilities vary significantly. This change in the injection rate causes a jump in NPV.

The NPV map is a discrete map, i.e., no matter where the injection well is

located within a given gridblock, we obtain the same value of NPV. To illustrate the increase in smoothness in the NPV obtained by using the permeability averaging procedure (Eqs. 4.12, 4.13 or 4.14), we consider the behavior of the NPV as the location of a single water injection well moves from point "A" to point "B" in Figs. 4.6(a) and 4.6(b). Note that there are 25 discrete values for NPV, one for each gridblock on the line from "A" to "B." In our well-placement algorithm, the gridblock indices are replaced with the spatial location of the well. To generate results, the $\tilde{x}_{\mathrm{w}}$ (the x coordinate of the injection well in the normalized domain) is moved from 0.0 to $\tilde{x}_{\mathrm{w}}^{\mathrm{up}} = 0.5$ with $\tilde{y}_{\mathrm{w}}$ fixed, which corresponds to moving the well location from point "A" to point "B." The resulting NPV values versus $\tilde{x}_{\mathrm{w}}$ are plotted in Figs. 4.7(a) to 4.7(d) for the case where the injection well is operating at a constant bottomhole pressure. Fig. 4.7(a) corresponds to the case where the perforation of each pseudo-well is assigned the kh value corresponding to its gridblock properties. Figs. 4.7(b) to 4.7(d) correspond to different methods of averaging kh over the pseudo-wells perforation gridblocks, Eqs. 4.12-4.14. In all figures, the NPV is based on the total injection rate into the nine pseudo-wells. Fig. 4.7(b) corresponds to averaging the kh with Eq. 4.12 where Figs. 4.7(c) and 4.7(d) correspond to averaging the kh with Eqs. 4.13 and 4.14, respectively. Recall that this average $\overline{kh}$ is specified as the kh for each of the nine gridblocks containing the pseudo-wells. In these plots, the discrete NPV values are shown with stars while the continuous NPV is plotted with a curve through computed values shown as small circles. Note that since there is only one water injection well, if we made similar plots for the injection rate, the smoothness of the injection rate and its agreement with the discrete injection rate would display the same characteristics exhibited in Figs. 4.7(a)-4.7(d). Similar plots for the case of the injection well operating at a constant specified injection rate are shown in Figs. 4.8(a) to 4.8(d).

The results of Figs. 4.6(a) to 4.8(d) illustrate two important points. First, the

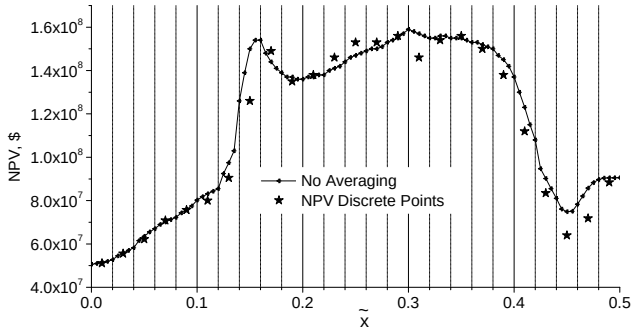

(a) No averaging

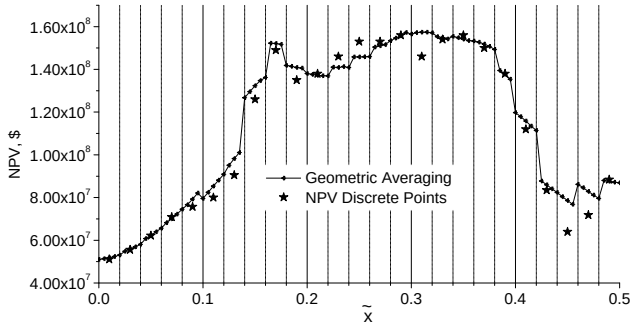

(b) Geometric average

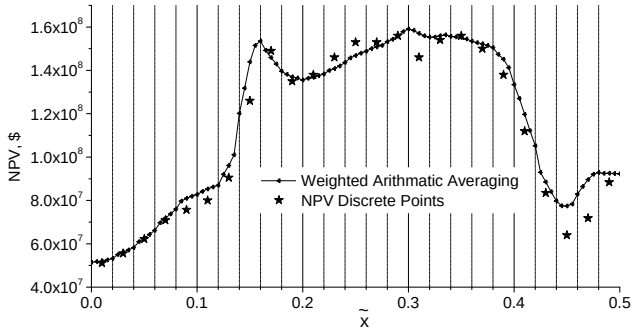

(c) Weighted arithmetic average

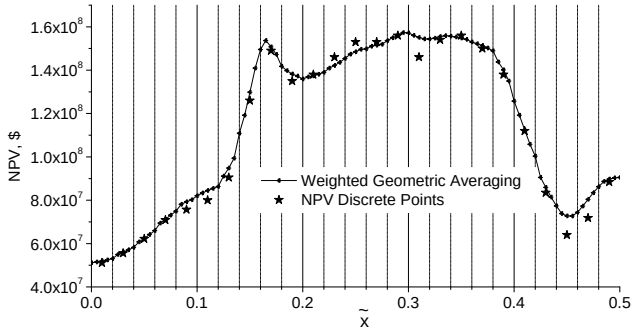

(d) Weighted geometric average

Figure 4.7: NPV as a function of $\tilde{x}_{\mathrm{w}}$, Injection well operating on constant bottomhole pressure, Example 1.

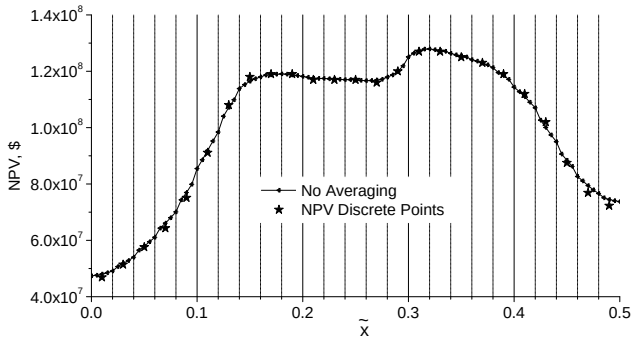

(a) No averaging

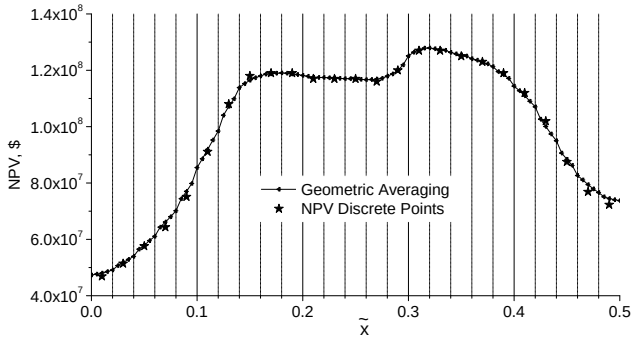

(b) Geometric average

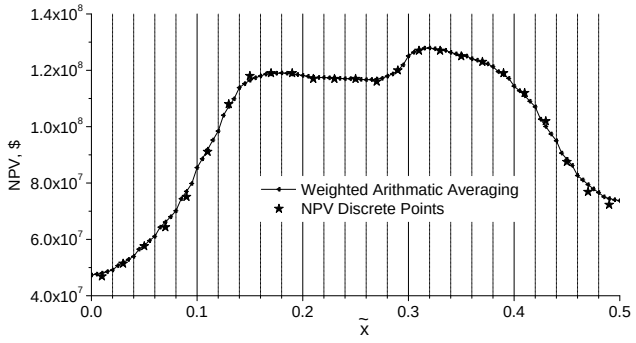

(c) Weighted arithmetic average

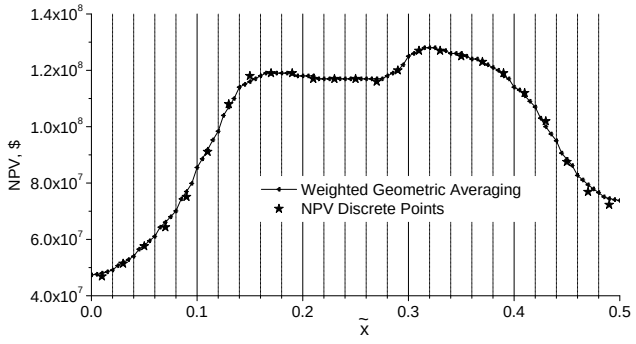

(d) Weighted geometric average

Figure 4.8: NPV as a function of $\tilde{x}_{\mathrm{w}}$, Injection well operating on constant rate, Example 1.

NPV plot for a bottomhole pressure-controlled injection well is much noisier than the NPV plot for the rate-controlled injection well case. Also, the continuous NPV function gives a less accurate approximation of the discrete NPV for bottomhole pressure-controlled wells than for rate-controlled wells (The results corresponding to Fig. 4.7 for the rate-controlled case are shown in Figs. 4.8(a)-4.8(d)). The second point is that the weighted geometric average gives a smoother continuous NPV function than the geometric and weighted arithmetic averaging methods when the injection well operates at a specified bottomhole pressure. Also, comparing to the no averaging case, the weighted geometric average gives a closer NPV approximate to the discrete NPV values. A smooth NPV functional is usually a desirable feature when any optimization method is used although it is generally much less critical when a derivative-free optimization algorithm instead of a gradient-based algorithm is used. Note, the NPV map of Fig. 4.6(a) displays several local maxima. While these local maxima might not cause any significant convergence problems for a global search method, they have the potential to cause problems for a gradient-based algorithm or even BOBYQA, which in some sense approximates a quasi-Newton method. Since the injection rate is constant for the rate-controlled wells (see our discussion of Eq. 4.10), the averaging methods are not critical for rate-controlled wells. Based on the results of Figs. 4.7 and 4.8, we use the weighted geometric average $\overline{kh}$ for all the examples. For reporting the optimum NPV and the corresponding well locations at the end of the optimization, we remove all the pseudo-wells except the center pseudo-well and set $\beta_\ell = 1.0$ for this pseudo-well, i.e., for each set of pseudo-wells, we keep only the pseudo-well in the gridblock corresponding to $(x_{\rm w}, y_{\rm w})$. Then we run the simulator with these final well locations to evaluate the NPV. This reported NPV might be slightly different than the optimum NPV estimated from the optimization.

Next, we consider the optimization of the location of a vertical injection well in the reservoir for Example 1. As the reservoir has one layer, we only optimize

Table 4.1: Initial and final well locations and the final NPV for different initial injection well locations, BHP controlled injector, Example 1.

Initial guess	Initial well loc.	Final Well loc, with kh ave.	NPV ($), with kh ave.	Final Well loc, no kh ave.	NPV ($), no kh ave.
1	$(2, 2)$	$(10, 12)$	1.58×10^8	$(6, 13)$	1.32×10^8
2	$(24, 2)$	$(25, 7)$	0.75×10^8	$(25, 4)$	0.70×10^8
3	$(2, 24)$	$(12, 14)$	1.58×10^8	$(8, 18)$	1.32×10^8
4	$(24, 24)$	$(13, 16)$	1.59×10^8	$(17, 17)$	1.61×10^8

the $(x_{\mathrm{w}}, y_{\mathrm{w}})$ coordinates of the location of the injection well. The initial and final well location of the rate-controlled and bottomhole pressure-controlled injection well are shown in Figs. 4.9 and 4.10, respectively, for the optimization algorithm without kh averaging and the optimization algorithm with kh averaging, respectively. The background plots of the figures are the NPV maps of Fig. 4.6. We applied our optimization algorithm with four different initial locations of the single injection well, namely, at gridblocks $(2, 2)$, $(24, 2)$, $(2, 24)$ and $(24, 24)$. In Figs. 4.9(a) to 4.10(b), all the initial and final locations are shown in one plot. As discussed earlier, once the optimization converges, all the pseudo-wells except the center pseudo-well are removed. The center pseudo-well, which is located at the center of the gridblock corresponding to the final well location, represents the optimum location of the injector. In these figures, the initial injection well locations are shown with a solid black star, and the four fixed producers are shown with solid white circles. The optimum injection well location is shown with solid black circles. Note the cases corresponding to the four initial locations are numbered 1 to 4 in Figs. 4.9 and 4.10. All the initial and final well locations and also the final NPV for different initial injection well locations are summarized in Tables 4.1 and 4.2, respectively, for the bottomhole pressure-controlled and rate-controlled injection well, respectively.

For the case of bottomhole pressure-controlled injection well, the optimization algorithm with kh averaging moved the injector respectively to gridblocks $(10, 12)$,

Table 4.2: Initial and final well locations and the final NPV for different initial injection well locations, Rate-controlled injector, Example 1.

Initial guess	Initial well loc.	Final Well loc, with kh ave.	NPV ($), with kh ave.	Final Well loc, no kh ave.	NPV ($), no kh ave.
1	$(2, 2)$	$(12, 12)$	1.40×10^8	$(13, 13)$	1.40×10^8
2	$(24, 2)$	$(12, 12)$	1.40×10^8	$(12, 12)$	1.40×10^8
3	$(2, 24)$	$(13, 14)$	1.38×10^8	$(13, 14)$	1.38×10^8
4	$(24, 24)$	$(14, 14)$	1.40×10^8	$(14, 14)$	1.40×10^8

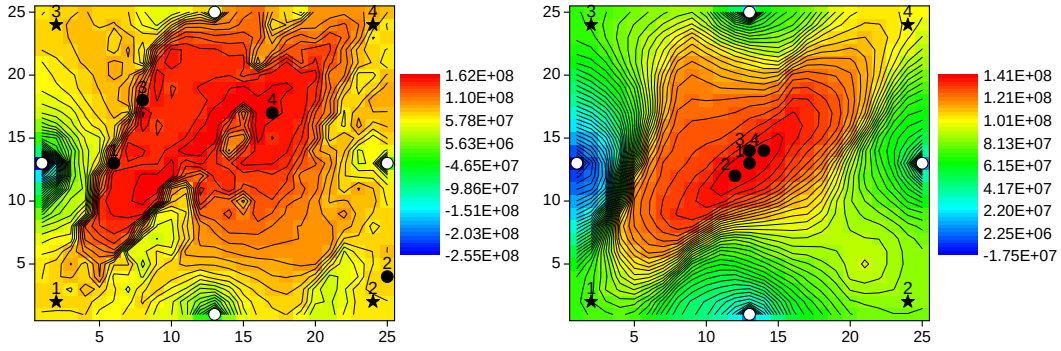

(a) Injector operating with constant BHP (b) Injector operating with constant rate

Figure 4.9: Initial and final well location of the injector, No kh averaging, Example 1. Fixed production well locations are shown with white circles. Black stars and black circles, respectively, show the initial and final locations of the injection well.

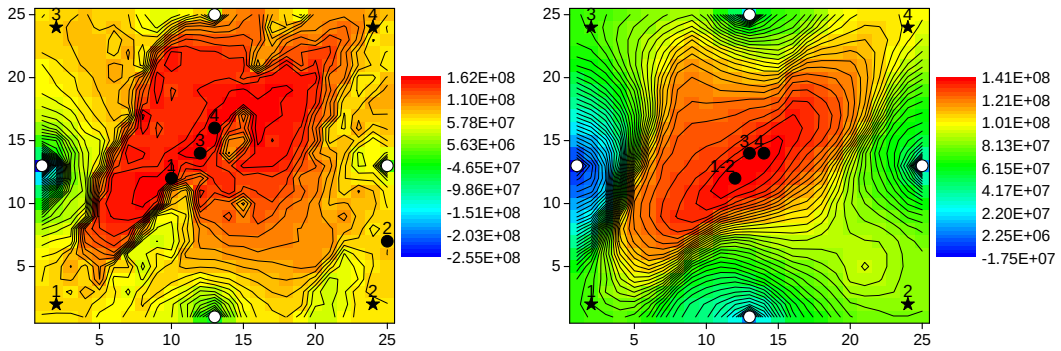

(a) Injector operating with constant BHP (b) Injector operating with constant rate

Figure 4.10: Initial and final well location of the injector, with kh averaging, Example 1. Fixed production well locations are shown with white circles. Black stars and black circles, respectively, show the initial and final locations of the injection well.

$(12, 14)$ and $(13, 16)$ in three cases of initial injection well locations at gridblocks $(2, 2)$, $(2, 24)$ and $(24, 24)$. The optimum NPV in all three of these cases is close to $\$1.58 \times 10^8$ which is fairly close to the global optimum NPV, which is equal to $\$1.61 \times 10^8$. In the case where the well was initially located at gridblock $(24, 2)$, the well is moved to gridblock $(25, 7)$, which is a local maximum next to the starting point. The optimum NPV for this case is $\$0.75 \times 10^8$. This shows that, similar to the gradient-based optimization methods, BOBYQA may converge to a local optimum point close to the initial guess.

The most important observation that can be made from the results of Figs. 4.9(a) and 4.10(a) and Table 4.1 is that the permeability averaging usually results in higher NPV values and allows the algorithm to determine a good approximation of a local maximum. From Fig. 4.10(a) we see that initial locations of 1, 3 and 4 resulted in similar estimations of the optimal well location and a virtually identical NPV value, $\$1.58 \times 10^8$ which is fairly close to the global optimum NPV value of $\$1.61 \times 10^8$. When permeability averaging is not used for bottomhole pressure-controlled wells, initial locations of 1,3 and 4 result in a distinctly different estimation of the optimal well location (Fig. 4.9(a)) and NPV values. Although with the choice of $(24, 24)$ as the initial location we actually obtained the optimal NPV of $\$1.61 \times 10^8$, overally we see, however, that using permeability averaging is more likely to result in a better NPV value.

For the case of rate-controlled injection well, the NPV map (Fig. 4.6(b)) is much smoother and appears to have only one global maximum, although the NPV values based on well locations at gridblocks near the center of the reservoir are all extremely close. In this case, the optimization algorithm with permeability averaging moved the injector to gridblock $(12, 12)$ for initial injection well locations $(2, 2)$ and $(24, 2)$ to obtain estimated NPV equal $\$1.40 \times 10^8$. In the cases where the well was initially located at gridblocks $(2, 24)$ and $(24, 24)$, respectively, the well is moved

to gridblocks $(13, 14)$ and $(14, 14)$ and the optimum NPV values are $\$1.38 \times 10^8$ and $\$1.40 \times 10^8$, respectively. The difference between the NPV for these three well locations is very small which shows that the optimization converged to very similar optimal solutions. As shown in Figs. 4.9(b) and 4.10(b) and Table 4.2, the effect of permeability averaging is negligible for a rate-controlled well.

4.4.2 Example 2. Synthetic Homogeneous 3D Reservoir

In Example 2, we apply our well-placement method to optimize the locations of vertical and horizontal wells in a homogenous reservoir for two different cases. We choose a homogeneous reservoir in this example because the optimal solutions are obvious. The reservoir is a $5,000 \times 5,000 \times 100$ ft with a $25 \times 25 \times 5$ grid simulation model. The reservoir porosity, horizontal permeability and vertical permeability are, respectively, 0.15, 100 md and 10 md. The depth of the reservoir top surface is $1,000$ ft. Gridblock sizes are 200 ft and 20 ft in the two horizontal and vertical directions, respectively. The initial reservoir pressure is $5,000$ psi. The production life of the reservoir is 30 years.

Case 1-Optimization of Vertical Producer Locations and Completions: We assume a fixed water injection well at the center of the reservoir (gridblock $(13, 13)$) which is completed in the bottom layer of the reservoir (layer 5). The injection well control is constant bottomhole pressure equal to $6,000$ psi. We optimize the locations and completions of 4 vertical producers. All the producers are operating with a constant liquid production rate of 625 STB/D, but there is a minimum bottomhole pressure constraint of $1,000$ psi. There are 16 optimization variables $(x_{\mathrm{w},m}, y_{\mathrm{w},m}, z_{\mathrm{w},m}, l_{\mathrm{w},m})$, $m = 1, 2, \ldots, 4$, i.e., 4 optimization variables for each producing well. The initial locations of producers P-1 through P-4 are at the center of gridblocks $(5, 9)$, $(18, 5)$, $(21, 18)$ and $(9, 21)$. As an initial guess, all the producers are completed in simulation layers 2, 3 and 4, i.e., $z_{\mathrm{w},m} = 1,050$ ft and $l_{\mathrm{w},m} = 60$ ft,

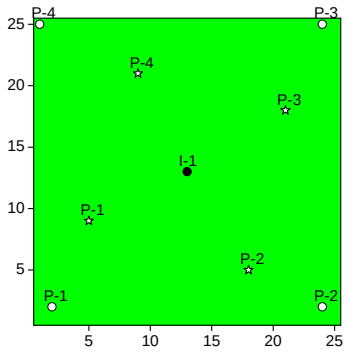

Figure 4.11: The initial and optimum locations of the vertical producers in synthetic homogenous reservoir, Example 2, Case 1. Black circle shows the location of the fixed injector. White stars and circles, respectively, show the initial and final locations of the production wells.

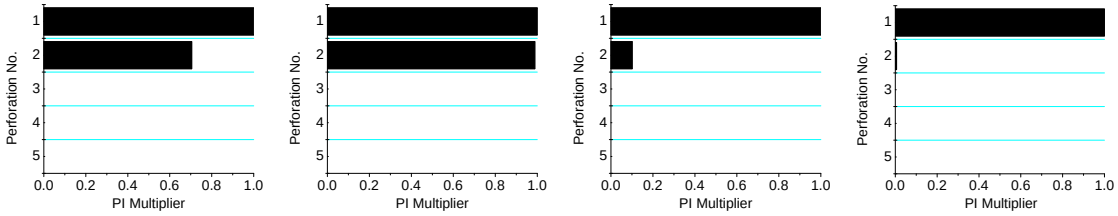

(a) well P-1 (b) well P-2 (c) well P-3 (d) well P-4

Figure 4.12: PI multipliers for perforations, Optimizing both locations and perforations simultaneously, Synthetic homogeneous reservoir, Example 2, Case 1.

$m = 1, 2, \ldots, 4$. The optimization algorithm with kh averaging converged after 147 simulation runs and NPV increased from $\$1.08 \times 10^9$ to $\$1.73 \times 10^9$. Fig. 4.11 shows the initial and optimum areal location of the producers. Note the four producers are moved toward the corners of the reservoir by the optimization algorithm with the estimated optimal locations forming an inverted 5-spot pattern. In Fig. 4.12, the estimated optimal open fraction of each perforation layer is shown for each producer. Note also that in all the producers, the top layer is fully open, while the second simulation layer is partially open to flow. This is reasonable because the injector is perforated at the bottom layer of the reservoir.

Since the reservoir is homogenous and the injection well is at the center of the reservoir, we expect an optimum solution which has symmetric well locations and

perforations, but our optimization algorithm did not achieve this. In Table 4.3, the NPV for 8 possible trial solutions with symmetric well locations and completions are listed. For a better comparison, the NPV values in Table 4.3 are reported with 4 digit precision. Note that the final NPV obtained from our optimization algorithm is $\$1.7335 \times 10^9$.

Table 4.3: Comparison of our optimum NPV with the NPV for some symmetric well locations and completions, Example 2, Case 1.

Solution	Well locations: P-1 through P-4	PI multipliers of perforations	NPV, \$
1	(1,1), (25,1), (25,25), (1,25)	$\gamma_1 = 0.5$, $\gamma_2 = \gamma_3 = \gamma_4 = 0$	1.7396×10^9
2	(1,1), (25,1), (25,25), (1,25)	$\gamma_1 = 1.0$, $\gamma_2 = \gamma_3 = \gamma_4 = 0$	1.7426×10^9
3	(1,1), (25,1), (25,25), (1,25)	$\gamma_1 = 1.0$, $\gamma_2 = 0.5$, $\gamma_3 = \gamma_4 = 0$	1.7401×10^9
4	(1,1), (25,1), (25,25), (1,25)	$\gamma_1 = \gamma_2 = 1.0$, $\gamma_3 = \gamma_4 = 0$	1.7401×10^9
5	(2,2), (24,2), (24,24), (2,24)	$\gamma_1 = 0.5$, $\gamma_2 = \gamma_3 = \gamma_4 = 0$	1.7312×10^9
6	(2,2), (24,2), (24,24), (2,24)	$\gamma_1 = 1.0$, $\gamma_2 = \gamma_3 = \gamma_4 = 0$	1.7312×10^9
7	(2,2), (24,2), (24,24), (2,24)	$\gamma_1 = 1.0$, $\gamma_2 = 0.5$, $\gamma_3 = \gamma_4 = 0$	1.7252×10^9
8	(2,2), (24,2), (24,24), (2,24)	$\gamma_1 = \gamma_2 = 1.0$, $\gamma_3 = \gamma_4 = 0$	1.7252×10^9

In trial solutions 1 and 2, only the first layer is open to flow, and since the producers are rate-controlled wells, we expect that the NPVs in trials 1 and 2 to be identical. However, note that also a minimum bottomhole pressure constraint of $1,000$ psi is specified for all the producers. In solution 1, since the productivity index of the only perforation in the production wells is reduced by multiplying by 0.5, the producers could not maintain the specified production rates and also satisfy the specified minimum bottomhole pressure at the later times of the simulation. Therefore, the production well controls are changed to the constant bottomhole pressure and the producers lost some oil production from the reservoir. This makes the NPV of solution 1 to be slightly smaller than the NPV of solution 2. In solutions 3 and 4, in addition to the first layer, the second layer perforation of the producers also contributes to the production from the reservoir. This results in slightly higher water production from the reservoir and therefore, the NPV in these two solutions are smaller than solution 2. Similar comments can be applied for solutions 5 to 8 except

that the NPVs of both solutions 5 and 6 are identical. In these two solutions, the production wells are closer to the injection well and the producers could maintain the specified production rate while satisfying the bottomhole pressure constraints of the wells even with reduced productivity index of the well. However, the NPVs of solutions 7 and 8 are slightly less than solutions 1 and 2. This is due to the contribution of the second layer perforation to the well productions from the reservoir which results in slightly higher water production as compared to solutions 5 and 6. The highest NPV for all the "symmetric solutions" tried is $\$1.7426 \times 10^9$ which is only 0.5% higher than the estimated optimum automatically determined with our optimization algorithm.

Case 2-Optimization of a Horizontal Production Well: The same homogeneous reservoir is again considered, but in this case, the left side of the reservoir is attached to an analytical aquifer. The aquifer is attached to gridblocks $(1:1, 13:25, 3:5)$ in the "i", "j" and "k" directions. The gridblocks attached to the aquifer are shown with a black line on the left side of the reservoir in Fig. 4.13. The horizontal production well has its axis in the "j" direction, and it is initially completed in gridblocks $(13, 12:14, 3)$, i.e., near the center of the reservoir as shown in Fig. 4.13. There are 4 optimization variables with the initial guess specified as $(x_{\mathrm{w}}, y_{\mathrm{w}}, z_{\mathrm{w}}, l_{\mathrm{w}})_{\mathrm{initial}} = (2500, 2500, 1050, 400)$ ft, i.e., the well center point is at the center of gridblock $(13, 13, 3)$ and the well extends from the center of gridblock $(13, 12, 3)$ to the center of gridblock $(13, 14, 3)$. The well control is the constant liquid production rate equal to $2,500$ STB/D. The minimum and maximum lengths, respectively, of the horizontal well are defined as 200 and 800 ft. After 56 simulation runs, the optimization algorithm converged. NPV increased from $\$1.12 \times 10^9$ at the initial guess to $\$1.85 \times 10^9$ at convergence of the optimization algorithm. The estimated optimum location of the well is $(x_{\mathrm{w}}, y_{\mathrm{w}}, z_{\mathrm{w}}, l_{\mathrm{w}})_{\mathrm{opt}} = (5000, 600, 1015, 800)$ ft, which corresponds to gridblocks $(25, 2:6, 1)$. As shown in Fig. 4.13, the producer

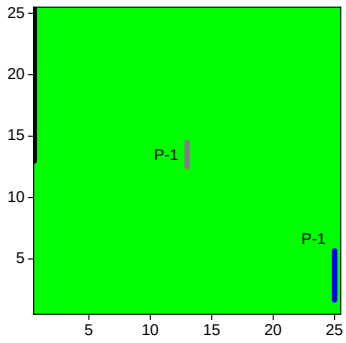

Figure 4.13: The initial and optimum locations of the horizontal producer, Synthetic homogenous reservoir, Example 2, Case 2.

was moved from its initial location in layer 3 to the opposite side of the reservoir and to the first layer. The length also was increased from 400 ft to 800 ft. From physical intuition, this is clearly a good solution.

4.4.3 Example 3. Synthetic Heterogeneous 3D Reservoir

Example 3 shows the application of the well-placement method for a 3D, two-phase (oil-water), heterogeneous reservoir. The reservoir size is $4,500 \times 2,250 \times 500$ ft with a $90 \times 45 \times 10$ gridblock system. The reservoir has heterogeneous porosity and permeability fields. The horizontal log-permeability and porosity fields of the first layer of the reservoir are shown in Figs. 4.14(a) and 4.14(b). Porosity and permeability of all reservoir layers are identical to those of layer 1. We choose layers with identical permeability and porosity fields so that we will at least have an intuitive idea of whether our optimization algorithm gives reasonable results. The vertical permeability is $k_v = 0.1k_h$. The initial reservoir pressure is $3,500$ psi. The production life of the reservoir is 2 years. In Case 1 of this example, we apply our method to optimize the locations and completions of the horizontal water injectors while the location of the vertical producers are fixed. In Case 2 of this example, the locations and completions of both vertical producers and injectors are optimized.

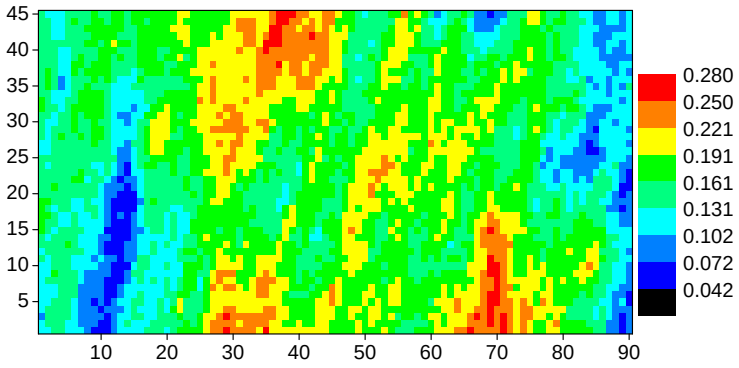

(a) Porosity

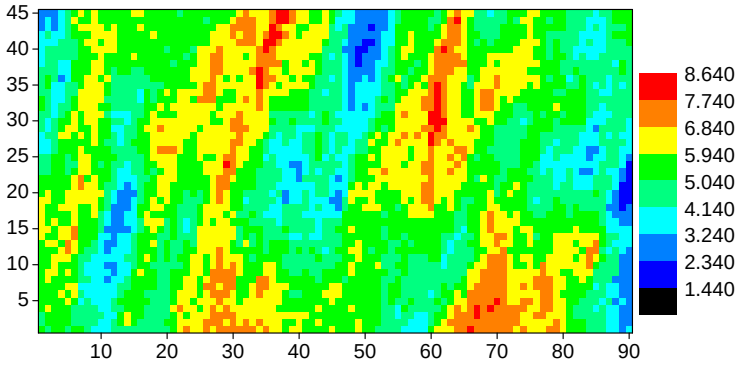

(b) Log-permeability

Figure 4.14: Horizontal log-permeability and porosity fields of layer 1 for the heterogenous reservoir, Example 3.

Case 1-Optimization of Horizontal Water Injection Wells: Six fixed vertical production wells are placed in the reservoir. All the production wells are perforated in the three top layers of the reservoir and are produced at a constant bottomhole pressure of $1,500$ psi. We consider the optimization of two horizontal injection wells where $(x_{\mathrm{w},m}, y_{\mathrm{w},m}, z_{\mathrm{w},m}, l_{\mathrm{w},m})$, $m = 1, 2$ for both injectors are the optimization variables. The axis of the injection well I-1 is in the "i" direction and the axis of injection well I-2 is in the "j" direction. The injectors are controlled with constant bottomhole pressure equal to $5,500$ psi. The horizontal injection wells are initially perforated in layer 5 in the reservoir and have lengths of 100 feet. Two different initial well locations are considered. In the first initial guess, the initial locations of the injectors

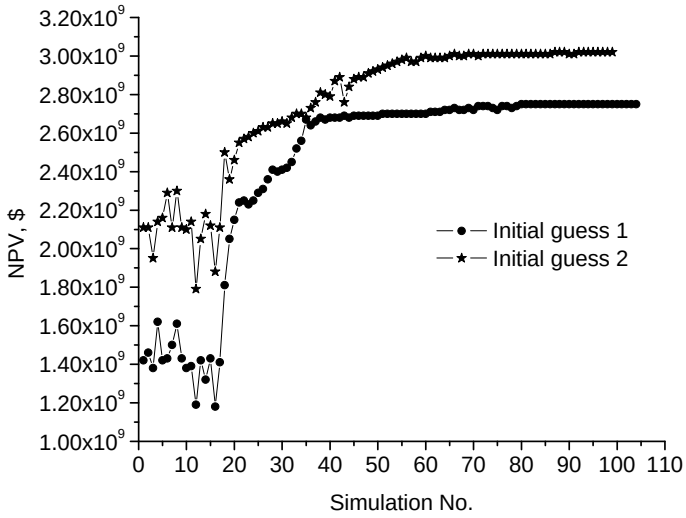

Figure 4.15: NPV plot versus number of simulation runs, Optimization of horizontal injectors, Example 3, Case 1.

form two inverted 5-spot well patterns with producers. In this case, the optimization algorithm with kh averaging (Eq. 4.14) converged after 99 reservoir simulation runs, and the NPV of the production increased from $\$2.11 \times 10^9$ initially to $\$3.00 \times 10^9$ at convergence. In the second initial guess, the injectors are initially displaced from the center of the inverted 5-spot well patterns. With the second initial guess, the optimization algorithm converged after 104 reservoir simulation runs, and the NPV increased from $\$1.42 \times 10^9$ initially to $\$2.73 \times 10^9$ at convergence. The NPV plot versus simulation runs for both initial guesses are shown in Fig. 4.15. Note that in Fig. 4.15, the first 17 simulation runs were needed to build the first quadratic model. There are 8 optimization control variables (4 optimization parameters for each well) and 17 simulation runs were needed by BOBYQA to build the first quadratic model, $(m = 2n+1)$. After the initial quadratic model is built, BOBYQA requires only one simulation run at each optimization iteration.

Fig. 4.15 shows two different initial guesses yield radically different NPV values which illustrates that the method may converge to a local optimum. The initial and final well locations for the first and second initial guesses are shown in

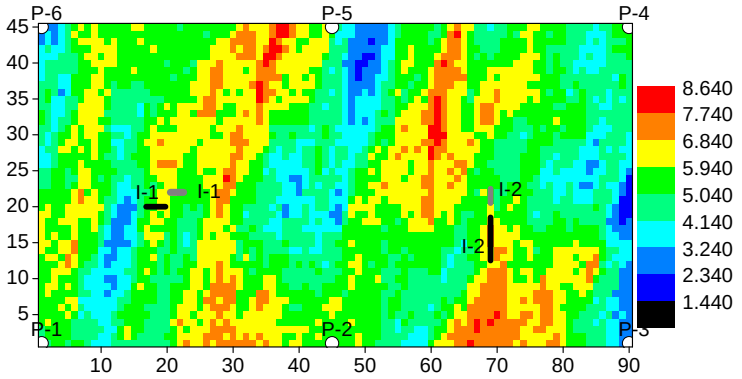

(a) initial guess 1

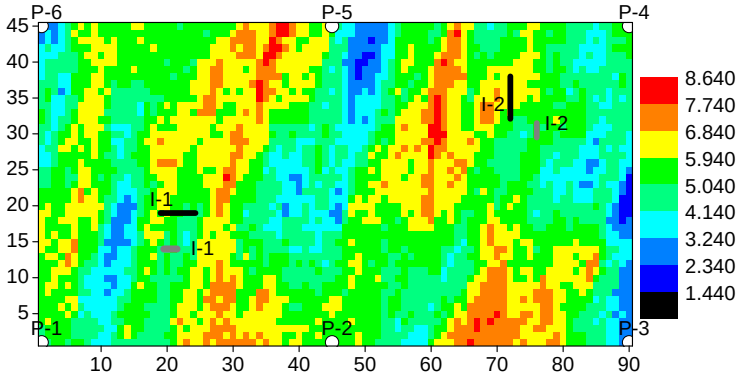

(b) initial guess 2

Figure 4.16: The initial and optimum locations of the horizontal injectors, Example 3, Case 1.

Figs. 4.16(a) and 4.16(b). The initial well trajectories are shown with gray lines, and the optimum trajectories are shown with black lines.

In the optimization run with initial guess 1, both injectors are moved to simulation layer 9 at the bottom of the reservoir. Injection well I-1 is moved to the high permeability channel at the left of its initial location, which is slightly farther away from production well P-5 and close to producer P-1. Note that there is a low permeability barrier between these two wells. The length of this well increased from 100 ft to 145 ft. Well I-2 is moved to the nearby high permeability channel and the length of the well is increased from 100 to 300 ft. In the optimization run with initial guess 2, injection well I-1 is moved to reservoir simulation layer 9 and injection

well I-2 is moved to reservoir simulation layer 10. With this initial guess, well I-1 is moved to the same location obtained with initial guess 1, but the length of the well increased from 100 ft to 270 ft. The final location of well I-2 with initial guess 2 is completely different from the location obtained with initial guess 1. With initial guess 2, the injection well I-2 is moved to the high permeability channel close to its initial location and the length of the well is increased from 100 ft to 300 ft. These results further indicate that the well-placement problem may have local maxima and that the optimization algorithm may then converge to a local maximum. However, the reader should have in mind that in practice, proposed locations and completions will be proposed by experienced reservoir engineers and using these locations and completions as initial guesses and perhaps a set of other initial guesses, the algorithm can be used to attempt to find locations and completions which give a higher NPV.

Case 2-Optimization of Vertical Injectors and Producers: In this case we optimize the location of six producers and two injectors. The optimization variables are $(x_{\mathrm{w},m}, y_{\mathrm{w},m}, z_{\mathrm{w},m}, l_{\mathrm{w},m})$, $m = 1, \ldots, 8$, where all the production and injection wells are vertical. The total number of optimization variables is 32. Similar to the previous case, both injection and production wells are bottomhole pressure-controlled wells. The bottomhole pressures of the production and injection wells, respectively, are $1,500$ and $5,500$ psi. The production wells are initially perforated at layers 1 to 3 and the injection wells are initially completed in layers 3 to 7. Optimization is performed with two different initial well locations. In the first initial guess, the initial locations of the six production wells and two injectors form two inverted 5-spot patterns. However, in the second initial guess, the injection well locations are initially displaced from the center of the inverted 5-spot well patterns. With the first initial guess, the optimization converged after 231 reservoir simulation runs, and NPV increased from $\$2.74 \times 10^9$ at the initial guess to $\$3.47 \times 10^9$ at convergence. With the second initial guess, the optimization converged after 262 reservoir simulation runs, and NPV

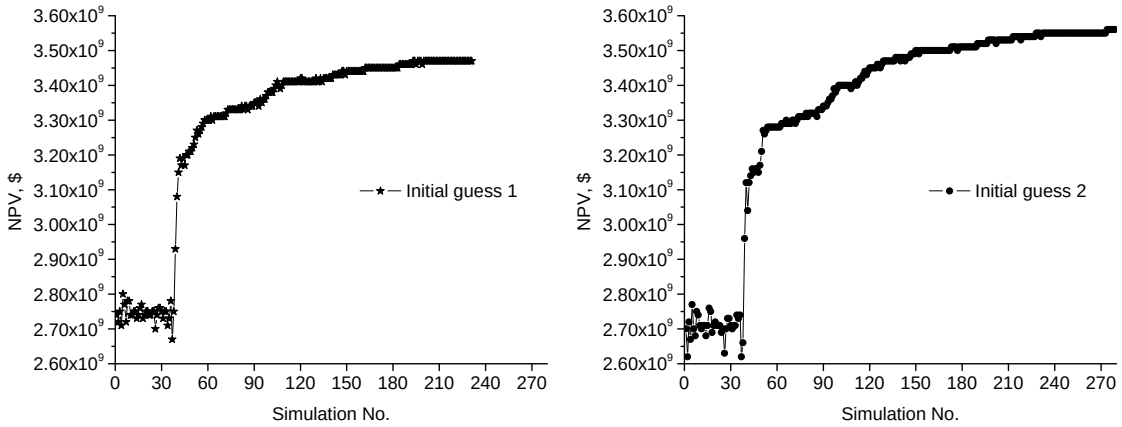

(a) initial guess 1 (b) initial guess 2

Figure 4.17: NPV plot versus number of simulation runs, Optimization of producers and injectors, Example 3, Case 2.

increased from $\$2.70 \times 10^9$ at the initial guess to $\$3.56 \times 10^9$ at convergence. NPV is plotted versus the number of reservoir simulation runs in Figs. 4.17(a) and 4.17(b) for initial guesses 1 and 2, respectively. Similar to Fig. 4.15, the first $m = n+6 = 38$ simulation runs were required to build the initial quadratic model for the BOBYQA method. Here, we chose $m = n + 6 = 38$ instead of $m = 2n + 1$ due to the fairly large number of control variables. The choice of $m = n + 6$ is also suggested by Powell [34]. Again, at the end of the optimization, we remove all the pseudo-wells except the center pseudo-well and evaluate the NPV with these center pseudo-wells. This NPV may be slightly different than the optimized NPV which is based on the presence of all pseudo-wells. Here, in this case, the evaluated NPV values with the surrounding pseudo-wells removed, are $\$3.33 \times 10^9$ and $\$3.46 \times 10^9$ for initial guesses 1 and 2, respectively.

The initial and final well parameters are summarized in Tables 4.4 and 4.5 for initial guesses 1 and 2, respectively. Initial and final locations of the injection and production wells for initial guesses 1 and 2 are shown in Figs. 4.18(a) and 4.18(b), respectively. In these figures, the production wells are shown in white and the injection wells are shown in black; the initial well locations are shown with stars and the

Table 4.4: The initial and final well parameters (x_w, y_w, z_w, l_w) of the first initial guess, Example 3, Case 3.

Well	Initial	Final
I-1	(1125.0, 1125.0, 1225.0, 250.0)	(1205.1, 1026.1, 1500.0, 144.2)
I-2	(3325.0, 1125.0, 1225.0, 250.0)	(3483.6, 1002.0, 1432.0, 308.7)
P-1	(25.0, 25.0, 1075.0, 150.0)	(98.2, 128.0, 1082.8, 240.7)
P-2	(2225.0, 25.0, 1075.0, 150.0)	(1975.3, 3.9, 1055.7, 259.2)
P-3	(4475.0, 25.0, 1075.0, 150.0)	(4326.8, 14.7, 1132.1, 248.8)
P-4	(4475.0, 2225.0, 1075.0, 150.0)	(4453.5, 2180.8, 1159.5, 231.0)
P-5	(2225.0, 2225.0, 1075.0, 150.0)	(2174.4, 2238.9, 1134.1, 251.6)
P-6	(25.0, 2225.0, 1075.0, 150.0)	(124.2, 1919.5, 1164.5, 342.5)

Table 4.5: The initial and final well parameters (x_w, y_w, z_w, l_w) of the second initial guess, Example 3, Case 3.

Well	Initial	Final
I-1	(725.0, 1325.0, 1225.0, 250.0)	(586.3, 1495.6, 1354.4, 225.5)
I-2	(3775.0, 1475.0, 1225.0, 250.0)	(3839.7, 1372.9, 1369.7, 321.7)
P-1	(25.0, 25.0, 1075.0, 150.0)	(0.0, 117.1, 1088.7, 107.3)
P-2	(2225.0, 25.0, 1075.0, 150.0)	(1922.5, 89.5, 1188.3, 451.3)
P-3	(4475.0, 25.0, 1075.0, 150.0)	(4304.3, 149.5, 1158.6, 311.8)
P-4	(4475.0, 2225.0, 1075.0, 150.0)	(4438.5, 2240.9, 1099.1, 38.7)
P-5	(2225.0, 2225.0, 1075.0, 150.0)	(2176.7, 2146.3, 1170.6, 327.2)
P-6	(25.0, 2225.0, 1075.0, 150.0)	(41.7, 2250.0, 1161.3, 254.9)

final well locations are shown with circles. The final PI multiplier for perforations at injection and production wells, respectively, are shown in Figs. 4.19 and 4.20 for initial guess 1 and in Figs. 4.21 and 4.22 for initial guess 2, respectively.

Comparing the NPV's for the initial well locations of initial guess 1 ($\$2.74 \times 10^9$) and initial guess 2 ($\$2.70 \times 10^9$) shows that for this reservoir, NPV is not very sensitive to slight changes in the injection well locations. However, comparing initial and final NPVs of both initial guesses 1 and 2 shows that for the subject reservoir, NPV is more sensitive to the well completions than to the location of the wells. This seems reasonable because the well controls are the constant bottomhole pressure, and the reservoir properties do not vary in the vertical direction; therefore, the well

rates are strongly dependent on the length of the wells.

For initial guess 1, the initial injection well locations form two inverted 5-spot patterns which is often a good configuration for water flooding. In the optimization run with initial guess 1, changes in the completions of the wells are more significant. The open perforations in both injection wells are moved to the bottom simulation layers (Figs. 4.19 and 4.21) and the total length of the perforated interval in well I-1 is reduced. The production wells were initially perforated in the top three simulation layers. Optimization increased the length of all production wells. Also, production wells P-2, P-3, P-5 and P-6 are moved to a gridblock with higher permeability. In the optimization run with initial guess 2, the length of the perforated interval in

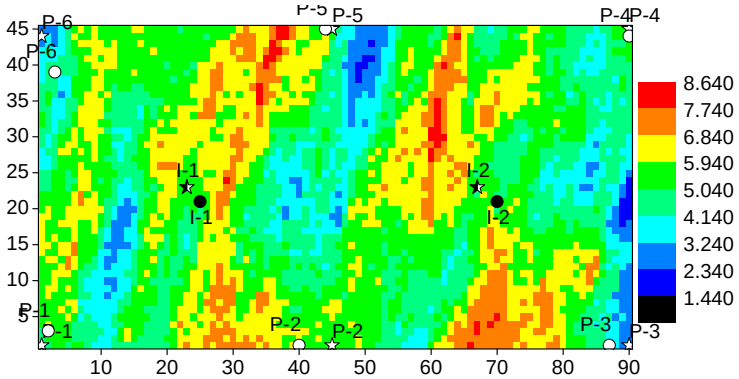

(a) initial guess 1

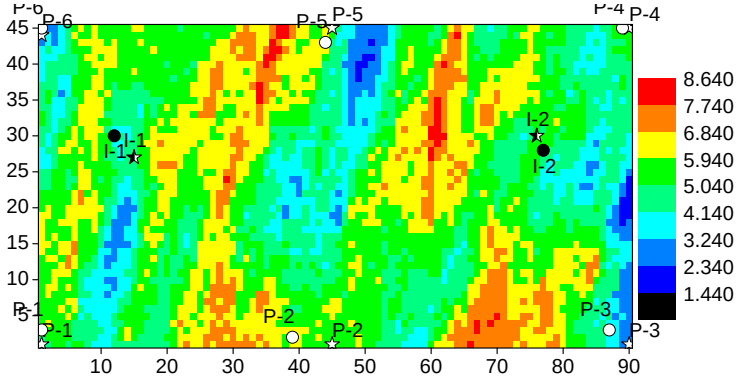

(b) initial guess 2

Figure 4.18: The initial and optimum locations of the vertical injectors and producers, Example 3, Case 2.

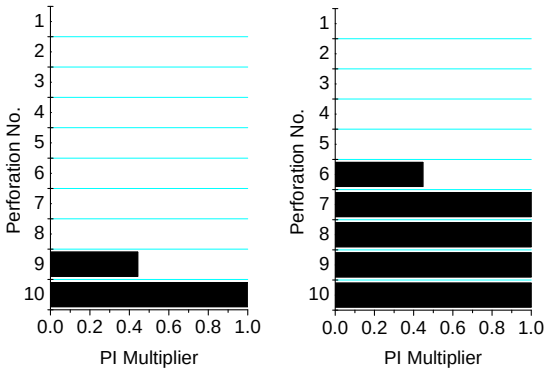

(a) well I-1 (b) well I-2

Figure 4.19: PI multipliers for perforations of the injectors, Initial guess 1, Example 3, Case 2.

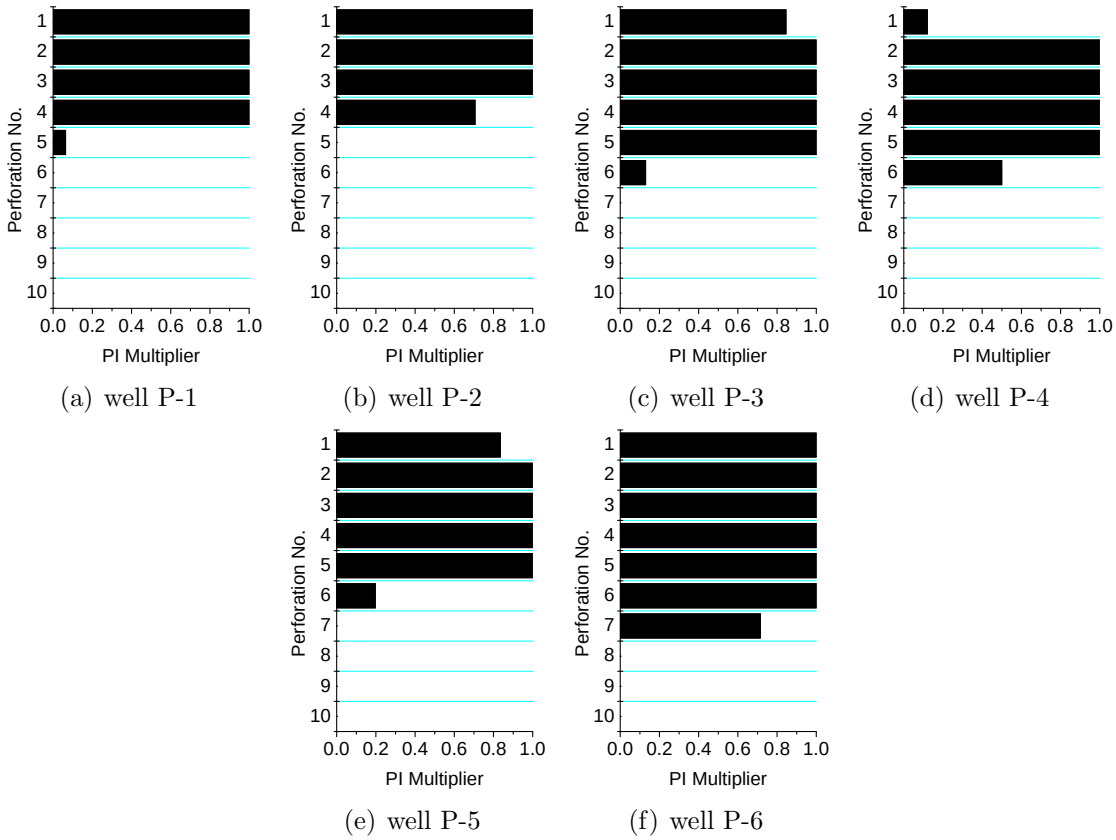

(a) well P-1 (b) well P-2 (c) well P-3 (d) well P-4

(e) well P-5 (f) well P-6

Figure 4.20: PI multipliers for perforations of the producers, Initial guess 1, Example 3, Case 2.

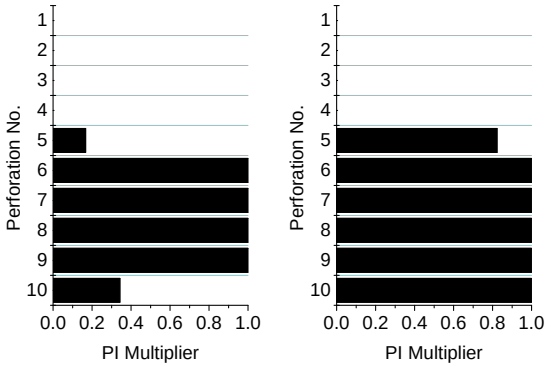

(a) well I-1 (b) well I-2

Figure 4.21: PI multipliers for perforations of the injectors, Initial guess 2, Example 3, Case 2.

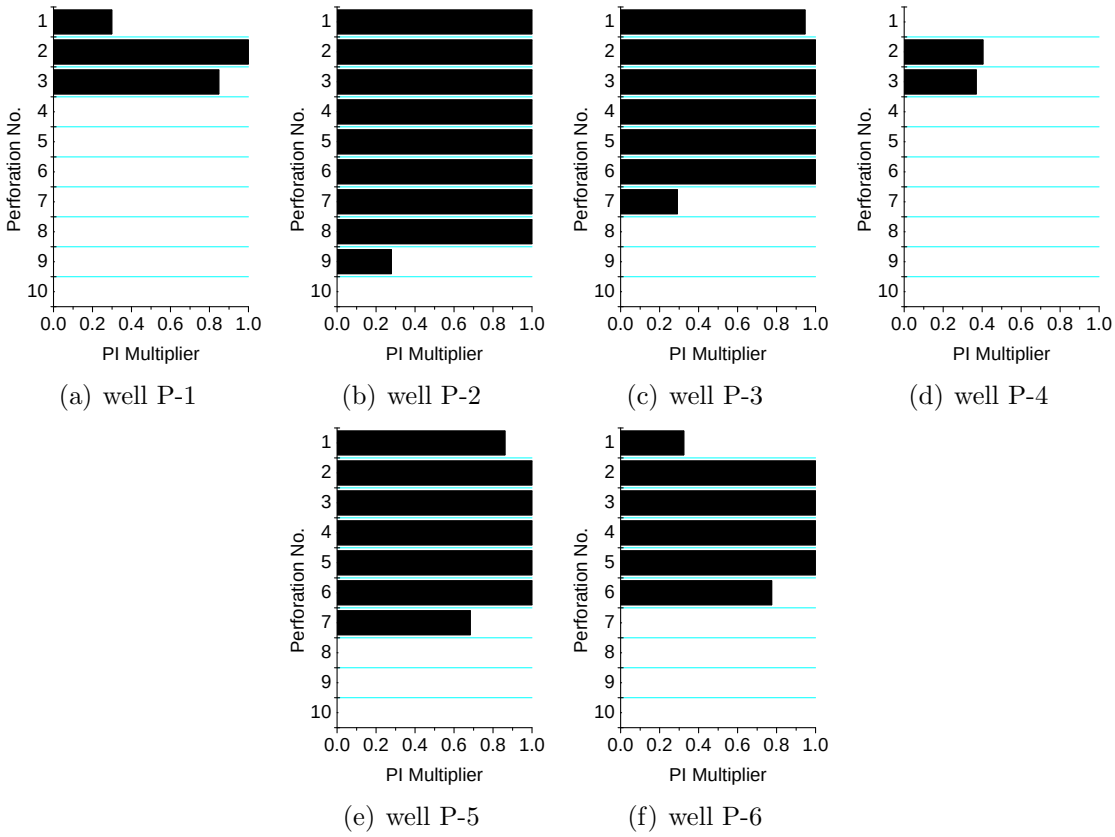

(a) well P-1 (b) well P-2 (c) well P-3 (d) well P-4

(e) well P-5 (f) well P-6

Figure 4.22: PI multipliers for perforations of the producers, Initial guess 2, Example 3, Case 2.

production wells P-2, P-3 and P-5 are increased significantly (Fig. 4.22) as they are located far away from the injection wells. However, the length of the perforated interval in production wells P-1 and P-4 are decreased because they are close to the injection wells. Similar to initial guess 1, both injection wells are completed near the bottom of the reservoir (Fig. 4.21). The final NPV for initial guess 1 with the injection wells located close to the center of inverted 5-spot well patterns is smaller than the final NPV of initial guess 2, due to the heterogeneity of the reservoir. Note that even though we started with physically reasonable initial guesses for the optimal well locations and completions, the algorithm was able to significantly increase the NPV.

4.4.4 Example 4. PUNQ Reservoir

Example 4 illustrates the application of the well-placement method for the PUNQ reservoir. This example is designed to compare the results of two approaches that we introduced for evaluating NPV when a well is moved into an inactive grid-block; see Section 4.3. The PUNQ simulation model was introduced in Example 2 of Chapter 3 and the porosity, horizontal and vertical permeability fields and the initial oil saturation distribution of the reservoir simulation model are shown in Figs. 3.6 to 3.9, respectively. In this example we set the porosity of aquifer gridblocks to 0. Therefore, the aquifer gridblocks are inactive and infeasible locations for the wells.

In this example, we consider optimizing the location of six vertical producers and three vertical injectors in the PUNQ reservoir model. Here, we only consider the optimization of the location of the wells. The optimization variables are the $(x_{\mathrm{w}}, y_{\mathrm{w}})$ coordinates of the injection and production wells and every well is perforated in all 5 simulation layers of the reservoir, i.e., $u = [x_{\mathrm{w},1}, y_{\mathrm{w},1}, \ldots, x_{\mathrm{w},N_{\mathrm{well}}}, y_{\mathrm{w},N_{\mathrm{well}}}]^T$. There are 9 wells subject to the optimization and the total number of the optimization variables is $n = 18$. We use $m = 37$ for the number of interpolation points in the BOBYQA algorithm. The production life of the reservoir is 10 years and the production and

injection wells, respectively, have specified constant bottomhole pressure of $1,500$ and $4,000$ psi, respectively. We consider two cases in this example. In the first case, the location of a well is feasible only if all the perforation gridblocks of the well are in active gridblocks. However, in the second case, the location of a well is feasible if at least one perforation gridblock of the well is in an active gridblock.

In the first case, the location of a well is feasible if all the well perforation gridblocks are active, therefore, if a well moves to a location in which any of its perforation gridblocks is an inactive gridblock, one of the two approaches explained before (Section 4.3) is used to evaluate the NPV. In the first approach, the well is automatically assigned zero rate and does not contribute to the NPV; however, in the second approach the location of the well is modified to a location in which all the perforations of the well are in active gridblocks. The well-placement optimization is done with both these approaches. The NPV corresponding to the initial locations of the wells is $\$1.82 \times 10^9$. The optimization run with the first approach (eliminating the wells with perforations in inactive gridblocks) converged after 158 simulation runs and the final NPV is $\$2.79 \times 10^9$. The evaluated NPV value with the surrounding pseudo-wells removed for this approach is $\$2.66 \times 10^9$. With the second approach (modifying the locations of the wells with perforations in inactive gridblocks), the optimization run converged after 183 simulation runs and NPV increased to $\$2.98 \times 10^9$ where the evaluated NPV value with the surrounding pseudo-wells removed is $\$2.80 \times 10^9$. The NPV plot versus the number of simulation runs for the optimization runs corresponding to both approaches are shown in Figs. 4.23(a) and 4.23(b), respectively. The first 37 simulation runs were used to build the first quadratic model in BOBYQA. As we see in Fig. 4.23(a), the approach of eliminating the well located in an infeasible location results in large changes (sharp spikes) in NPV when the well is eliminated at an iteration. This should be expected to damage the quality of the quadratic interpolation model and thus result in a smaller final NPV value. As expected, the

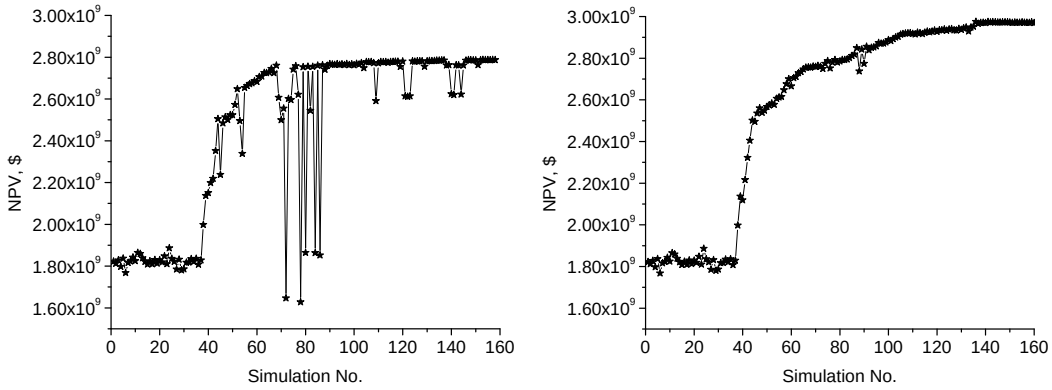

(a) Optimization run with the first approach (eliminating the well)

(b) Optimization run with the second approach (modifying the well location)

Figure 4.23: The plot of NPV versus the number of simulation runs, Example 4, Case 1.

final NPV value of the well-placement optimization with this approach ($\$2.79 \times 10^9$) is smaller than the final NPV value corresponding to the optimization run with the second approach ($\$2.98 \times 10^9$).

The initial locations of the injection and production wells and their final locations with the first and the second approaches are shown in Fig. 4.24. In this figure, the locations of the wells are shown in the plots of layer-1 horizontal log-permeability field. The injection wells are shown as black circles and the production wells are shown as white circles. The initial and final well coordinates in the PUNQ model are summarized in Table 4.6. As we see in Figs. 4.24(b) and 4.24(c), the production wells tend to separate from the injection wells. Also, the injection wells moved toward the edges of the reservoir and away from the production wells. Note that the changes in the production well locations are smaller with the first approach (Figs. 4.24(b)) compared to the second approach (Figs. 4.24(c)), which might be due to the early termination of the optimization algorithm due to the damages to the quality of the quadratic interpolation model.

In the second case, the location of a well is feasible if any of the perforations of the well is in an active gridblock. Similar to Case 1, well-placement optimization runs are performed with both approaches. In this case, none of the wells moved to a

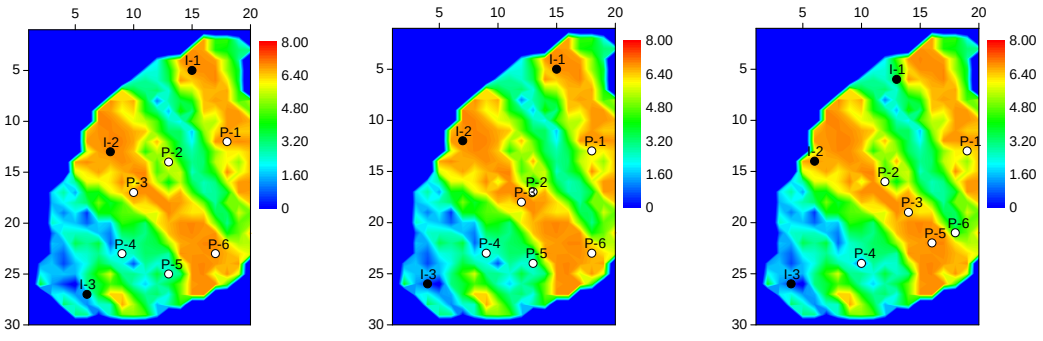

(a) Initial (b) Final, first approach (c) Final, second approach

Figure 4.24: The initial and final locations of the injection and production wells, Example 4, Case 1.

Table 4.6: The initial and final well parameters $(x_{\mathrm{w}}, y_{\mathrm{w}})$ of the injection and production wells in the PUNQ model, Example 4, Case 1.

Well	Initial	Final, first approach	Final, second approach
I-1	$(8102.7, 13593.4)$	$(7972.5, 13878.0)$	$(8102.7, 13593.4)$
I-2	$(12319.1, 8910.6)$	$(12696.9, 9744.2)$	$(12319.1, 8910.6)$
I-3	$(20563.5, 7200.0)$	$(20964.6, 8563.1)$	$(20563.5, 7200.0)$
P-1	$(12412.6, 15873.1)$	$(12106.4, 15649.7)$	$(12412.6, 15873.1)$
P-2	$(15282.5, 12857.3)$	$(13287.5, 12696.9)$	$(15282.5, 12857.3)$
P-3	$(15639.3, 12363.1)$	$(15059.1, 10925.3)$	$(15639.3, 12363.1)$
P-4	$(18448.3, 10361.5)$	$(18602.4, 10334.7)$	$(18448.3, 10361.5)$
P-5	$(19416.1, 12479.8)$	$(19783.5, 12696.9)$	$(19416.1, 12479.8)$
P-6	$(18383.2, 15464.0)$	$(18602.4, 15059.1)$	$(18383.2, 15464.0)$

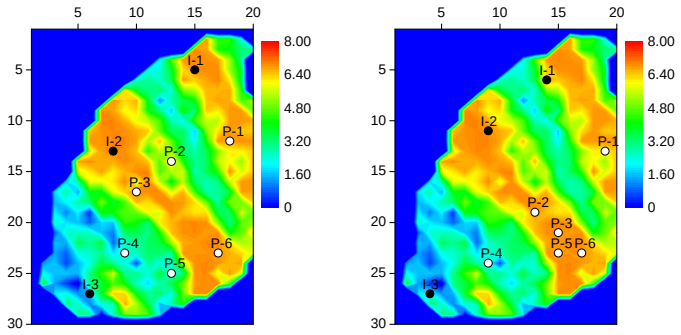

(a) Initial (b) Final

Figure 4.25: The initial and final locations of the injection and production wells, Example 4, Case 2.

location where all the gridblock perforations are inactive. Therefore, the optimization runs with both approaches gave the same results. Both optimization runs converged after 209 simulation runs and the NPV value increased from $\$1.87\times10^9$ to $\$3.04\times10^9$. The final evaluated NPV value with the surrounding pseudo-wells removed is $\$2.78\times10^9$. Note in both cases the initial well locations are the same, but the initial NPV value of the second case ($\$1.87 \times 10^9$) is larger than for the first case ($\$1.82 \times 10^9$). The reason for that is in the first case, some of the pseudo-wells corresponding to the injection well I-3 are shut-in initially as some of their perforations are in inactive gridblocks, whereas, in the second case the pseudo-well of a well is shut-in only and only if all its perforations are in inactive gridblocks. In the second case, none of the pseudo-wells of the injection well I-3 were initially shut-in and hence the initial NPVs of these two cases are different. The initial and final well locations for the second case are shown in Fig. 4.25. Note that the initial well locations are identical to the initial well locations in Case 1. The final well location parameters are summarized in Table 4.7. The plot of NPV versus the number of simulation runs is shown in Fig. 4.26. There are no sharp spikes in the NPV plot as none of the wells moved to a location where all its perforations are in inactive gridblocks.

Table 4.7: The initial and final well parameters $(x_{\mathrm{w}}, y_{\mathrm{w}})$ of the injection and production wells, Example 4, Case 2.

Well	Initial	Final
I-1	$(8419.4, 13513.2)$	$(7972.5, 13878.0)$
I-2	$(11379.0, 10087.7)$	$(12696.9, 9744.2)$
I-3	$(21000.0, 7563.9)$	$(20964.6, 8563.1)$
P-1	$(12530.7, 16200.0)$	$(12106.4, 15649.7)$
P-2	$(16112.7, 12683.0)$	$(13287.5, 12696.9)$
P-3	$(17576.5, 13962.8)$	$(15059.1, 10925.3)$
P-4	$(19015.9, 10390.9)$	$(18602.4, 10334.7)$
P-5	$(18446.8, 13656.9)$	$(19783.5, 12696.9)$
P-6	$(18351.9, 15268.6)$	$(18602.4, 15059.1)$

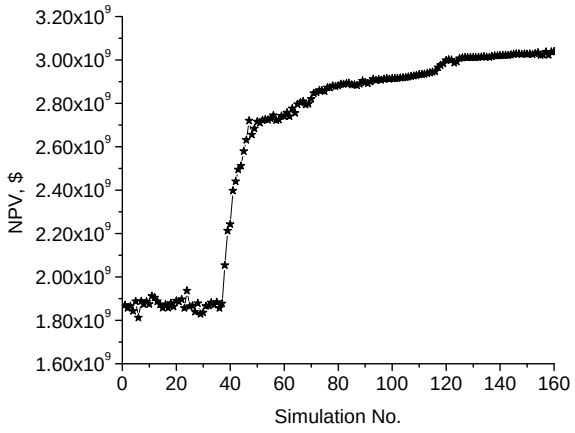

Figure 4.26: The plot of NPV versus the number of simulation runs, Example 4, Case 2.

CHAPTER 5

OPTIMIZATION OF THE WELL LOCATIONS AND TRAJECTORIES FOR DIRECTIONAL WELLS

In this chapter, we introduce a new methodology for the estimation of the location, length and trajectory of each of a set of directional wells that maximize the life-cycle net-present-value (NPV) of production from a reservoir. For efficiency in writing, we will sometimes simply refer to this problem as estimation of well trajectories. Similar to the well-placement method presented in Chapter 4, a well can be either a rate-controlled or a bottomhole pressure-controlled injection or production well, where, the well control values and the production life of the reservoir are fixed. However, it is more natural to consider pressure-controlled wells. A directional well is considered as a straight line in 3D. The well-placement problem is formulated in terms of six continuous variables which define the trajectory of a well. The trajectory parameters are the x_{w}, y_{w} and z_{w} coordinates of the center point of the well, the length of the well, l_{w}, and θ_{w} and φ_{w} which are the orientation angles of the well in the horizontal and vertical directions, respectively. A continuous NPV functional is defined by distributing the rate of the well among "gridblock perforations" which are "close" to the trajectory of the well. This NPV functional is based on the life-cycle NPV of production from the reservoir and it is a function of the six continuous well trajectory parameters, $(x_{\mathrm{w}}, y_{\mathrm{w}}, z_{\mathrm{w}}, l_{\mathrm{w}}, \theta_{\mathrm{w}}, \varphi_{\mathrm{w}})$. Similar to the well-placement method given in Chapter 4, the NPV functional is maximized using a derivative-free optimization (DFO) algorithm, BOBYQA, where we use a transformation of the control variables to improve the performance of the BOBYQA algorithm. In the following, we first introduce the optimization problem. Then we explain our method for repre-

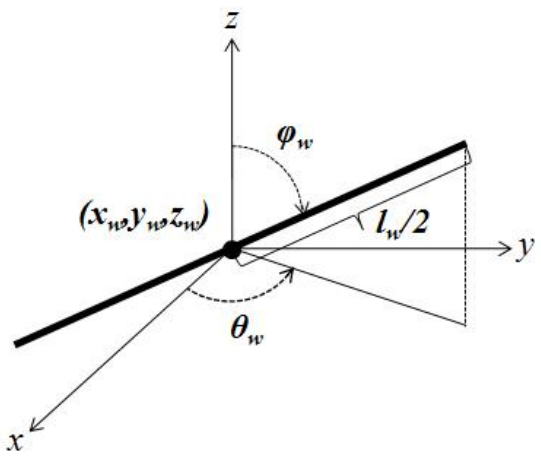

Figure 5.1: Schematic view of a directional well.

senting a directional well in the simulator. Finally, some results for the optimization of directional wells in homogeneous and heterogeneous synthetic 3D reservoir are presented.

5.1 Well-Placement Problem Definition

For the optimal well-placement problem algorithm presented in this chapter, the objective function optimized is the net-present-value (NPV) of production from the reservoir given in Eq. 2.1. The trajectory of a well inside the reservoir is represented with a straight line in the spherical coordinate system. Spherical coordinates are adopted as they allow for straightforward control of the well lengths by imposing a box constraint. The well trajectory is defined by six continuous variables $x_{\mathrm{w}}, y_{\mathrm{w}}, z_{\mathrm{w}}, l_{\mathrm{w}}, \theta_{\mathrm{w}}$ and φ_{w}, where $(x_{\mathrm{w}}, y_{\mathrm{w}}, z_{\mathrm{w}})$ are the spatial coordinates of the well center point; l_{w} is the length of the well; θ_{w} is the angle between the positive x-axis and the projection of the well trajectory onto the $x-y$ plane; φ_{w} is the angle between the well trajectory and the positive z-axis, i.e., the angle φ_{w} shows the deviation of the well trajectory from vertical. The schematic of a well and the corresponding well trajectory parameters are given in Fig. 5.1.

Here, we consider minimizing $J[u]$ when $J[u] = -\mathrm{NPV}$ and u is the vector of

variables which represent the well trajectories. The continuous optimization problem is then defined by

$$\min_{u} J[u], \tag{5.1}$$

subject to

$$u^{\text{low}} \leq u \leq u^{\text{up}}, \tag{5.2}$$

where

$$u = [x_{\text{w},1}, y_{\text{w},1}, z_{\text{w},1}, l_{\text{w},1}, \theta_{\text{w},1}, \varphi_{\text{w},1}, \ldots, x_{\text{w},N_{\text{well}}}, y_{\text{w},N_{\text{well}}}, z_{\text{w},N_{\text{well}}}, l_{\text{w},N_{\text{well}}}, \theta_{\text{w},N_{\text{well}}}, \varphi_{\text{w},N_{\text{well}}}]^T \tag{5.3}$$

is the vector of optimization variables. N_{well} is the number of wells, and $(x_{\text{w},j}, y_{\text{w},j}, z_{\text{w},j})$ and $l_{\text{w},j}$, respectively, define the location of the center point and the length of well j; $\theta_{\text{w},j}$ and $\varphi_{\text{w},j}$ are the directional angles of well j in the horizontal and vertical directions, respectively, as defined previously (Fig. 5.1). By specifying well trajectory parameters, $(x_{\text{w},j}, y_{\text{w},j}, z_{\text{w},j}, l_{\text{w},j}, \theta_{\text{w},j}, \varphi_{\text{w},j})$, we uniquely define the trajectory of well j. Eq. 5.2 defines simple bound constraints for every optimization variable. The bound constraints for the optimization variables $x_{\text{w},j}$, $y_{\text{w},j}$ and $z_{\text{w},j}$ are defined according to the reservoir boundaries because the center point of each well is required to be inside the reservoir. The upper bound for $l_{\text{w},j}$ is defined by simply setting a maximum length of the well. Because of the symmetry of the trajectory line of the well about its center point, the minimum and maximum bound values for the well trajectory parameters, $\theta_{\text{w},j}$ and $\varphi_{\text{w},j}$, are respectively 0 and 180 degrees (0 and π radians).

5.2 The Representation of a Directional Well in the Simulator

As explained in Chapter 4, in reservoir simulation models, the well models are used to model the flow between the gridblock and wellbore; see Eqs. 4.3 through 4.6. An accurate representation of a directional well inside a reservoir is still an ongoing

challenge (H. Cinco and Ramey [15], Joshi [17], Jostein Alvestad and Stava [18], Ding [12], Aavatsmark and Klausen [1] and Schlumberger [37]). In commercial simulators which use a Peaceman type well model, a well is represented by defining the perforated well gridblocks. For each perforation i of the well, the well model parameters in Eq. 4.3 (or Eq. 4.5), which consist of the length of the well inside the perforated gridblock, h_i, the radial permeability toward the well axis, k_i, and the equivalent radius, r_{o_i}, must be determined and input into the simulator. Once these well model parameters are provided, the simulator computes the transmissibility factor of the perforation by applying a form of Eq. 4.5. The Jostein Alvestad and Stava [18] and Schlumberger [37] methods utilize a Peaceman type well model for the representation of directional wells. Both these methods provide the well model parameters for Eq. 4.5.

The Schlumberger [37] method determines $k_i h_i$ in Eq. 4.5 by averaging kh for perforation i in the x, y and z directions. The average transmissibility factor for the perforation is also computed by averaging the transmissibility factors in the x, y and z directions. Then, the parameter r_{o_i} is back computed from the average value of the productivity indices in the x, y and z directions and the average $k_i h_i$ using Eq. 4.5. The detailed equations of Schlumberger [37] are given in Appendix A.1.

Jostein Alvestad and Stava [18] proposed a method to determine the well model parameters for a Peaceman type well model. In their proposed method, the well model parameters are defined as a function of the orientation angles of a directional well, θ_{w} and φ_{w}. In the Jostein Alvestad and Stava [18] method, h_i is the exact length of the part of the well inside the gridblock corresponding to perforation i. The radial permeability toward the well for perforation i, k_i is given as a weighted average of the horizontal and vertical permeabilities of the gridblock and r_{o_i} is computed by equations which involve the orientation angles of the well. The detailed equations of Jostein Alvestad and Stava [18] are given in Appendix A.2. The Jostein Alvestad

and Stava [18] definition of the radial permeability toward a directional well in an anisotropic medium is also given in Aavatsmark and Klausen [1].

A brief discussion on the performance and accuracy of both the Jostein Alvestad and Stava [18] and Schlumberger [37] methods is given in Aavatsmark and Klausen [1]. For both methods, the well is perforated only in the gridblocks penetrated by the well. An accurate consideration of the well gridblock's geometry and the intersection of the gridblock faces with the well trajectory is necessary for both these methods. For the Schlumberger [37] method, the computations regarding the intersection of the well trajectory line with gridblock faces are done in the pre-processing software named "Schedule". Since both these methods are Peaceman type well models, they do not consider the real location of the well perforation inside the simulation gridblock. The issue of the actual well location is discussed further in Section 5.5.

5.3 Distributed Representation of a Directional Well in the Simulator

In the simulation models, the reservoir is partitioned into simulation gridblocks and the source/sink terms of the flow equation (which represent the production and injection wells) are introduced by well models in the discretized flow equations. In the Peaceman type well models, the exact location of the well inside the gridblock is not considered accurately; and also, the flow from a perforation of a well is strongly dependent on the permeabilities of its perforation gridblock only. Therefore, the rate of a well, and the NPV of production from the reservoir, are not smooth functions of the well location. This can cause difficulty in any optimization algorithm and introduce spurious local minima; see the results of Zhang et al. [46] on the optimal placement of a 3D channel in a 3D reservoir, i.e., as the perforation moves from one gridblock to another gridblock, the rate and NPV will typically change discontinuously. For a well with a known trajectory, an accurate implementation of the well models of Schlumberger [37] or Jostein Alvestad and Stava [18] methods requires

the consideration of the well gridblock's geometry and the computation of intersection points of the gridblock faces with the well trajectory. These computations are usually done with pre-processing software to prepare the simulation data deck, e.g., Schedule in Eclipse. To use Schedule with a well-placement optimization algorithm would require a method to recall Schedule after every iteration of the optimization algorithm. Moreover, if we use only the perforations which correspond to the actual well location, when a perforation moves from one gridblock to another, we may experience a jump discontinuity in the rate and NPV due to a discontinuous change in the PI. As discussed below, our methodology is designed to significantly reduce, but not eliminate, such jump discontinuities.

Here, we use a derivative-free optimization method which approximates the objective function with a smooth and continuous quadratic model, and a relatively smooth objective function may increase the accuracy and efficiency of the optimization algorithm. An objective function with jump discontinuities may damage the quality of the interpolation function evaluated by the BOBYQA optimization algorithm. Therefore, in our well-placement approach, we would like to reduce the jump discontinuities of the NPV as a function of well trajectory parameters. In addition to that, our representation of a directional well in the simulator for the computation of the NPV functional does not require any pre-processing software for doing the computations regarding the intersection of the well with the faces of complex simulation gridblocks.

To define the NPV with our model, we distribute each well source/sink term among all the gridblocks "close" to the well trajectory. Therefore, the well is perforated not only in the gridblocks penetrated by the well, but is also perforated in gridblocks adjacent to the well trajectory. The rate of the original well is distributed among all these perforations such that the perforations closer to the well trajectory are given a higher portion of the rate of the well. Therefore, the effects of (1) hetero-

geneity of the reservoir permeabilities and (2) discrete locations of the wells (due to the gridding of the reservoir) on the production rates of the wells are smoothed. The distribution of the rate among the well perforations is applied by assigning a productivity index (PI) multiplier to each perforation. The procedure for determining the well perforations and distributing the rate of the well among these perforations are fully discussed in the remainder of this section.

The schematic of a directional well inside a rectangular reservoir is shown in Fig. 5.2. The outer rectangular volume shows the reservoir boundaries. The trajectory of the directional well is shown with a solid black straight line inside the reservoir. As we previously explained, the trajectory of the well j is defined by well parameters $x_{\mathrm{w},j}, y_{\mathrm{w},j}, z_{\mathrm{w},j}, l_{\mathrm{w},j}, \theta_{\mathrm{w},j}$ and $\varphi_{\mathrm{w},j}$. The green sphere shows the volume around the well which is swept by the rotation of the well with length l_{w} about its center point, $(x_{\mathrm{w}}, y_{\mathrm{w}}, z_{\mathrm{w}})$, in both orientation angles θ and φ. The inner cuboid volume refers to the volume of the rectangular box which surrounds the sphere. We initially perforate all the gridblocks which are located inside this inner rectangular volume. These gridblocks are shown in Fig. 5.2. In the following, we explain our method for determining the perforations of well j and distributing the rate of the well among its perforations. Throughout, the subscript j, which represents the well index, is dropped.

We denote the gridblocks which contain the points $(x_{\mathrm{w}} + \frac{l_{\mathrm{w}}}{2}, y_{\mathrm{w}}, z_{\mathrm{w}})$ and $(x_{\mathrm{w}} - \frac{l_{\mathrm{w}}}{2}, y_{\mathrm{w}}, z_{\mathrm{w}})$ with the gridblock indices (i_1, j_1, k_1) and (i_2, j_2, k_2), respectively. Similarly, we denote the gridblocks which contain the points $(x_{\mathrm{w}}, y_{\mathrm{w}} + \frac{l_{\mathrm{w}}}{2}, z_{\mathrm{w}})$ and $(x_{\mathrm{w}}, y_{\mathrm{w}} - \frac{l_{\mathrm{w}}}{2}, z_{\mathrm{w}})$ with the gridblock indices (i_3, j_3, k_3) and (i_4, j_4, k_4), respectively, and the gridblocks which contain the points $(x_{\mathrm{w}}, y_{\mathrm{w}}, z_{\mathrm{w}} + \frac{l_{\mathrm{w}}}{2})$ and $(x_{\mathrm{w}}, y_{\mathrm{w}}, z_{\mathrm{w}} - \frac{l_{\mathrm{w}}}{2})$ with the gridblock indices (i_5, j_5, k_5) and (i_6, j_6, k_6), respectively. The perforations of a well contains all the gridblocks with indices (i, j, k) such that (i, j, k) satisfies $i_{e1} \leq i \leq i_{e2}$,

$j_{e1} \leq j \leq j_{e2}$ and $k_{e1} \leq k \leq k_{e2}$ where,

$$\begin{aligned} i_{e1} &= \max(1, \min_{m=1}^{6}(i_m) - 1), \qquad & i_{e2} &= \min(N_x, \max_{m=1}^{6}(i_m) + 1), \\ j_{e1} &= \max(1, \min_{m=1}^{6}(j_m) - 1), \qquad & j_{e2} &= \min(N_y, \max_{m=1}^{6}(j_m) + 1), \\ k_{e1} &= \max(1, \min_{m=1}^{6}(k_m) - 1), \qquad & k_{e2} &= \min(N_z, \max_{m=1}^{6}(k_m) + 1). \end{aligned} \tag{5.4}$$

To make the NPV functional sensitive to the change in the length of the well within a gridblock, we use +1 and -1 in Eq. 5.4 to extend the box gridblock in each direction beyond gridblocks that are wholly or partially in the spherical region of Fig. 5.2. Note that depending on the length of a well and the size of the reservoir gridblocks, the number of perforated gridblocks for a well might be large. Therefore, we try to reduce the number of perforations by eliminating the perforations with negligible contribution to the flow of the well. This is done after determining the contribution of each perforation to the flow rate of the well.

For perforation i of a well, the well model parameters, k_i, h_i and r_{o_i}, should be provided to the simulator. Either the Schlumberger [37] or Jostein Alvestad and Stava [18] methods (explained in Appendices A1) may be implemented to compute

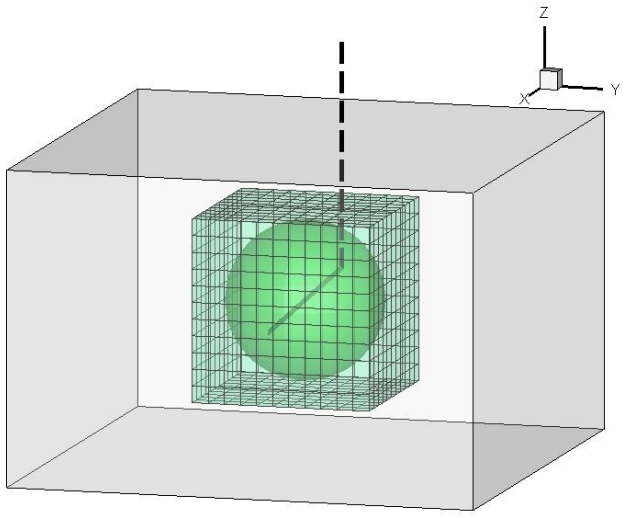

Figure 5.2: Perforated gridblocks around the well trajectory.

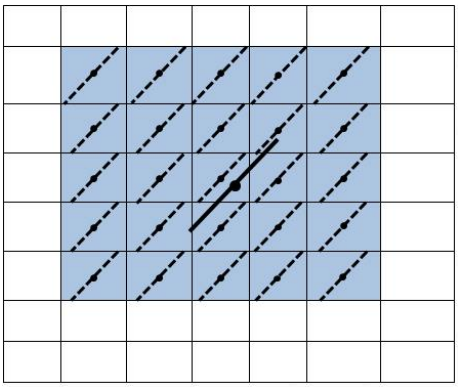

Figure 5.3: Schematic of a horizontal well in $x-y$ plane and the perforated gridblocks. The well trajectory line is shown with a solid black line. The trajectory of the perforation path in each perforated gridblock is shown with a dashed line.

the well model parameters of each perforation. Here, we focus on the Schlumberger [37] method. In order to compute the well model parameters of each perforation two assumption are made: (1) each perforated gridblock is a rectangular volume with dimensions of Δx_i, Δy_i and Δz_i and, (2) each perforated gridblock is fully penetrated in the direction of the well trajectory and the perforation path passes through the center point of the gridblock. For the purpose of illustration, consider a horizontal well in the $x - y$ plane ($\varphi_{\mathrm{w}} = 90$ degrees) as shown in Fig. 5.3.

The actual well trajectory is shown with a solid black line, but the perforations of this actual trajectory are not used directly in the simulation model. In computing the flow rates of the well in the reservoir simulator, the perforations shown as dashed lines are used. The perforated gridblocks in the current simulation layer are colored blue. The perforation trajectories in the perforated gridblocks are shown with dashed lines and as previously mentioned, it is assumed that each perforated gridblock is fully penetrated in the direction of the well trajectory and the perforation path passes through the gridblock center point, see assumptions (1) and (2) above. With these two assumptions, it is easy to compute the length of the perforation that lies within each gridblock. In Fig. 5.4, the schematic of one perforated gridblock is shown in three dimensions. Note that the coordinate axis $\tilde{x}_i - \tilde{y}_i - \tilde{z}_i$, is the local coordinate

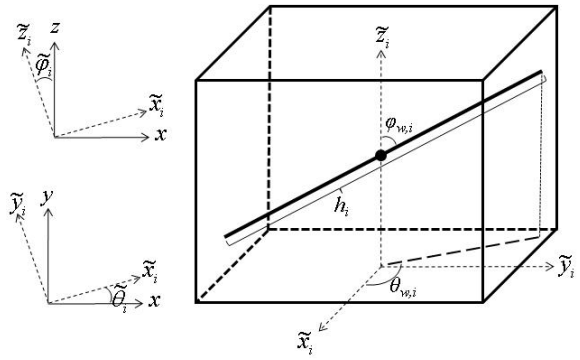

Figure 5.4: Schematic of a perforated gridblock by a 3D directional well. Note this represents one of the perforations shown as dashed lines in Fig. 5.3, not a perforation of actual well trajectory.

axis for gridblock i. The significance of the local coordinate system corresponding to each perforation gridblock, $\tilde{x}_i - \tilde{y}_i - \tilde{z}_i$, is that in the simulation model, the k_x, k_y and k_z permeabilities of a gridblock are specified in the direction of its local coordinate system, therefore, the radial permeability toward the well perforation should be computed based on the orientation angles of the perforation path with respect to the local coordinate system of the gridblock. Also, the perforation length of the well inside the gridblock depends on the orientation angles of the perforation path with respect to the local coordinate system of the gridblock. Denote $\theta_{\mathrm{w},i}$ and $\varphi_{\mathrm{w},i}$ as the orientation angles of the perforation trajectory with respect to its local coordinates system. Since the orientation angles of the well (θ_{w} and φ_{w}) are defined with respect to the global coordinate axis ($x - y - z$), we have

$$\theta_{\mathrm{w},i} = \theta_{\mathrm{w}} - \tilde{\theta}_i, \qquad \varphi_{\mathrm{w},i} = \varphi_{\mathrm{w}} - \tilde{\varphi}_i, \tag{5.5}$$

where $\tilde{\theta}_i$ is the angle between the x axis and the projection of $\tilde{x}_i$ onto the $x-y$ plane and $\tilde{\varphi}_i$ is the angle between the z axis and the projection of $\tilde{z}_i$ onto the $x-z$ plane.

Assuming the perforation gridblock i as a rectangular volume with length, width and height of Δx_i, Δy_i and Δz_i, respectively, the perforated length of the

gridblock i is denoted by h_i and is given by

$$h_i = \min(\tilde{h}_{x,i}, \tilde{h}_{y,i}, \tilde{h}_{z,i}), \tag{5.6}$$

where

$$\tilde{h}_{x,i} = \frac{\Delta x_i}{|\sin\varphi_{\mathrm{w},i}\cos\theta_{\mathrm{w},i}|}, \qquad \tilde{h}_{y,i} = \frac{\Delta y_i}{|\sin\varphi_{\mathrm{w},i}\sin\theta_{\mathrm{w},i}|}, \qquad \tilde{h}_{z,i} = \frac{\Delta z_i}{|\cos\varphi_{\mathrm{w},i}|}. \tag{5.7}$$

Note that Eqs. 5.6 and 5.7 are based on the assumptions that the gridblock is a rectangular box and the well passes through the center of the gridblock. With the information provided above for each perforation i, either the Schlumberger [37] or Jostein Alvestad and Stava [18] methods can be implemented to compute the well model parameter values of $k_i h_i$ and r_{o_i}. Note that the orientation angles of the trajectory of perforation i for computing the well model parameters are $\theta_{\mathrm{w},i}$ and $\varphi_{\mathrm{w},i}$. As previously noted, in our well-placement code, we implement the Schlumberger [37] procedure to compute the well model parameters for each perforation. The method description and its corresponding equations are given in Appendix A.1. The next step is to distribute the rate of the well among its perforations. We distribute the rate of the well among the perforations of the well so that the perforations closer to the well trajectory obtain a higher portion of the rate of the well. We use an exponentially decaying function to approximately distribute the rate of the well among its perforations, i.e., the contribution of each perforation to the rate of the well exponentially decreases as the distance of the perforation from the well trajectory increases. In order to distribute the rate of the well among its perforations, a productivity index (PI) multiplier, β_i, is assigned to each perforation PI of the well, i.e., the PI of each perforation is multiplied by β_i.

We define γ_i as the contribution of perforation i to the total rate of the well, where $\sum_i \gamma_i = 1$. The PI multiplier value of a perforation, β_i, is proportional to its

contribution to the total rate of the well, i.e., $\beta_i \propto \gamma_i$, however, the β_i's sum to a value which depends on the length of the well as explained below. If all the perforations of a well have identical productivity indices, phase mobilities and flowing drawdown/build up pressures, then the multiplier of a perforation PI exactly determines the portion of the total rate of the well assigned to that individual perforation, e.g., if $\gamma_i = \frac{\beta_i}{\sum \beta_i} = 0.15$, then 15 % of the well total flow rate would be produced from perforation i. However, since different perforations of the well have different productivity indices (PI's), different mobilities and different flowing drawdown/build up pressures, assigning a PI multiplier to a perforation only approximately specifies that γ_i times the rate of the well will flow through that perforation. Experimental results presented here show that this approximation is good enough for the purpose of our well-placement algorithm and gives a continuous NPV as a function of well trajectory parameters for the purpose of optimization. Below we show how γ_i and β_i for each perforation of the well are computed.

The trajectory parameters $x_{\mathrm{w}}, y_{\mathrm{w}}, z_{\mathrm{w}}, \theta_{\mathrm{w}}$ and φ_{w} of a well define a straight line in 3D as

$$x = x_{\mathrm{w}} + \Psi_x t, \quad y = y_{\mathrm{w}} + \Psi_y t, \quad z = z_{\mathrm{w}} + \Psi_z t. \tag{5.8}$$

where

$$\Psi_x = \sin\varphi_{\mathrm{w}} \cos\theta_{\mathrm{w}}, \qquad \Psi_y = \sin\varphi_{\mathrm{w}} \sin\theta_{\mathrm{w}}, \qquad \Psi_z = \cos\varphi_{\mathrm{w}}, \tag{5.9}$$

$(x_{\mathrm{w}}, y_{\mathrm{w}}, z_{\mathrm{w}})$ is the well center point and t is the parameter of the line. Denote the two endpoints of the well trajectory line by $(x_{\mathrm{w},e_1}, y_{\mathrm{w},e_1}, z_{\mathrm{w},e_1})$ and $(x_{\mathrm{w},e_2}, y_{\mathrm{w},e_2}, z_{\mathrm{w},e_2})$ where

$$x_{\mathrm{w},e_1} = x_{\mathrm{w}} + \Psi_x \frac{l_{\mathrm{w}}}{2}, \quad y_{\mathrm{w},e_1} = y_{\mathrm{w}} + \Psi_y \frac{l_{\mathrm{w}}}{2}, \quad z_{\mathrm{w},e_1} = z_{\mathrm{w}} + \Psi_z \frac{l_{\mathrm{w}}}{2}. \tag{5.10}$$

$$x_{\mathrm{w},e_2} = x_{\mathrm{w}} - \Psi_x \frac{l_{\mathrm{w}}}{2}, \quad y_{\mathrm{w},e_2} = y_{\mathrm{w}} - \Psi_y \frac{l_{\mathrm{w}}}{2}, \quad z_{\mathrm{w},e_2} = z_{\mathrm{w}} - \Psi_z \frac{l_{\mathrm{w}}}{2}. \tag{5.11}$$

As mentioned earlier, the contribution of the perforation i to the total rate of the well, γ_i, is a function of the distance of its gridblock center point from the well trajectory. As discussed below, we choose an exponentially decaying function to define γ_i's as a function of the distance of the perforation i gridblock center point from the well trajectory line. However, the reservoir gridblocks usually have different sizes in the x, y and z directions, e.g., the size of the gridblocks in the z direction is usually much smaller than the sizes of the gridblock in the x or y directions. Therefore, the perforation gridblocks of a well which are located in the direction of the smaller gridblock sizes (e.g., in the z direction) would have a much larger portion of the rate compared to the gridblocks located in the other directions from the well trajectory, i.e., their corresponding PI multiplier would be large. Computational experiments indicate that, this can result in a very low sensitivity of the NPV to the well trajectory parameters in the other directions (e.g., in the x or y directions). In order to define γ_i's which do not depend strongly on gridblock dimensions, we measure the distance of the gridblock from the well trajectory in a stretched coordinate system based on the average reservoir gridblock sizes in the different directions. We define a transformed coordinate system as

$$\begin{bmatrix} \hat{x} \\ \hat{y} \\ \hat{z} \end{bmatrix} = \begin{bmatrix} 1 & 0 & 0 \\ 0 & \frac{\overline{\Delta x}}{\overline{\Delta y}} & 0 \\ 0 & 0 & \frac{\overline{\Delta x}}{\overline{\Delta z}} \end{bmatrix} \begin{bmatrix} x \\ y \\ z \end{bmatrix}. \tag{5.12}$$

where $x - y - z$ is the original coordinate system and $\hat{x} - \hat{y} - \hat{z}$ is the transformed coordinate system. $\overline{\Delta x}$, $\overline{\Delta y}$ and $\overline{\Delta z}$ are the average gridblock sizes in the x, y and z directions, respectively. The transformed coordinate system is the original coordinate system stretched proportional to the average gridblock sizes in the x, y and z directions. Similarly, in the transformed coordinate system, the distances in the y and z directions are stretched proportional to the ratios $\frac{\overline{\Delta x}}{\overline{\Delta y}}$ and $\frac{\overline{\Delta x}}{\overline{\Delta y}}$, respectively,

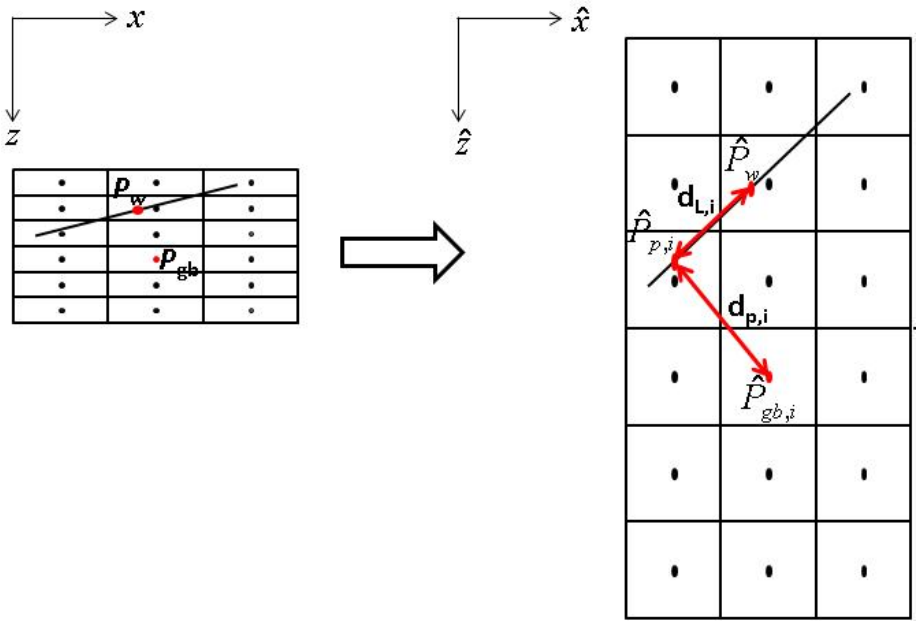

Figure 5.5: Schematic of the transformation of the coordinate system in $x-z$ plane. $\hat{P}_{\mathrm{w}}$ is the center point of the well in the transformed domain, $\hat{P}_{\mathrm{gb},i}$ is the center point of gridblock i in the transformed domain and $\hat{P}_{\mathrm{p},i}$ is the projection of $\hat{P}_{\mathrm{gb},i}$ on the well trajectory line.

i.e., $\Delta\hat{y} = \frac{\overline{\Delta x}}{\overline{\Delta y}}\Delta y$ and $\Delta\hat{z} = \frac{\overline{\Delta x}}{\overline{\Delta z}}\Delta z$.

The contribution of the perforation i to the total rate of the well, γ_i, is defined as a function of two distances $d_{\mathrm{p},i}$ and $d_{\mathrm{L},i}$. Both these distances are defined in the transformed coordinate $\hat{x}-\hat{y}-\hat{z}$. Denote the well center point in the transformed domain by $\hat{P}_{\mathrm{w}} = (\hat{x}_{\mathrm{w}}, \hat{y}_{\mathrm{w}}, \hat{z}_{\mathrm{w}})$, the center point of the perforated gridblock i in the transformed domain by $\hat{P}_{\mathrm{gb},i} = (\hat{x}_{\mathrm{gb},i}, \hat{y}_{\mathrm{gb},i}, \hat{z}_{\mathrm{gb},i})$ and the perpendicular projection of the center point of the perforated gridblock i onto the well trajectory line in the transformed domain by $\hat{P}_{\mathrm{p},i} = (\hat{x}_{\mathrm{p},i}, \hat{y}_{\mathrm{p},i}, \hat{z}_{\mathrm{p},i})$. Similarly the two endpoints of the well in the transformed domain are $\hat{P}_{\mathrm{w},e_1}$ and $\hat{P}_{\mathrm{w},e_2}$. For the purpose of illustration, the schematic of the transformation of the coordinate system in $x-z$ and $\hat{x}-\hat{y}$ planes are shown in Fig. 5.5.

Let $d_{\mathrm{p},i}$ denote the perpendicular distance of the center point of the perforation gridblock i from the well trajectory line in the transformed domain, i.e, $d_{\mathrm{p},i} = ||\hat{P}_{\mathrm{gb},i} -$

$\hat{P}_{\mathrm{p},i}||_2$, and let $d_{\mathrm{L},i}$ denote the distance from $\hat{P}_{\mathrm{p},i}$ to the well center point, $\hat{P}_{\mathrm{w}}$, in the transformed domain, i.e., $d_{\mathrm{L},i} = ||\hat{P}_{\mathrm{p},i} - \hat{P}_{\mathrm{w}}||_2$. The distances $d_{\mathrm{p},i}$ and $d_{\mathrm{L},i}$ are computed by

$$d_{\mathrm{p},i} = \sqrt{(\hat{x}_{\mathrm{gb},i} - \hat{x}_{\mathrm{p},i})^2 + (\hat{y}_{\mathrm{gb},i} - \hat{y}_{\mathrm{p},i})^2 + (\hat{z}_{\mathrm{gb},i} - \hat{z}_{\mathrm{p},i})^2}. \tag{5.13}$$

and

$$d_{\mathrm{L},i} = \sqrt{(\hat{x}_{\mathrm{p},i} - \hat{x}_{\mathrm{w}})^2 + (\hat{y}_{\mathrm{p},i} - \hat{y}_{\mathrm{w}})^2 + (\hat{z}_{\mathrm{p},i} - \hat{z}_{\mathrm{w}})^2}. \tag{5.14}$$

The contribution of perforation i of the well in the total rate of the well, γ_i, is defined as an exponential function of these two distances,

$$\gamma_i = \frac{f(d_{\mathrm{p},i})g(d_{\mathrm{L},i})}{\sum_{k=1}^{N_{\mathrm{com}}}[f(d_{\mathrm{p},i})g(d_{\mathrm{L},i})]}, \tag{5.15}$$

where N_{com} is the number of perforations of the well. The functions f and g are exponential decay functions defined as following

$$f(d_{\mathrm{p},i}) = \exp\left(-\frac{d_{\mathrm{p},i}^2}{\sigma^2}\right). \tag{5.16}$$

and

$$g(d_{\mathrm{L},i}) = \begin{cases} \exp\left(-\frac{d_{\mathrm{L},i}^2}{\sigma^2}\right) & \text{if } d_{\mathrm{L},i} > \frac{||\hat{P}_{\mathrm{p},i} - \hat{P}_{\mathrm{w},e}||_2}{2}, \\ \\ 1.0 & \text{if } d_{\mathrm{L},i} \leq \frac{||\hat{P}_{\mathrm{p},i} - \hat{P}_{\mathrm{w},e}||_2}{2}. \end{cases} \tag{5.17}$$

where

$$\sigma = \alpha\overline{\Delta x}, \tag{5.18}$$

and $\hat{P}_{\mathrm{w},e}$ is the closest endpoint of the well to the projection of the center point of gridblock i on the well trajectory line, $\hat{P}_{\mathrm{p},i}$. The parameter α determines how widely the rate is distributed among the perforations of the well. We suggest a value of α

such that $0.5 \leq \alpha \leq 1$ and for the results presented in this chapter we use $\alpha = 1$. In the following sections, we show how the value chosen for α influences the NPV functional. Since we measure the distances $d_{\mathrm{p},i}$ and $d_{\mathrm{L},i}$ in the transformed domain (where the distances in the y and z directions are stretched with reference to the $\frac{\overline{\Delta x}}{\overline{\Delta y}}$ and $\frac{\overline{\Delta x}}{\overline{\Delta z}}$, respectively), the parameter σ only depends on the average dimension of the gridblocks in the x direction, $\overline{\Delta x}$. Our choice of γ_i's is such that they sum to 1 as they are used to approximate the contribution of each perforation to the total rate of the well.

As we previously explained, all the gridblocks contained in the rectangular volume which surrounds the sphere around the well trajectory are initially considered as potential perforations. The contribution of each perforation to the total flow rate of the well is computed by applying Eq. 5.15, where the gridblocks far away from the well trajectory have much smaller contributions to the total rate of the well compared to perforated gridblocks closer to the well trajectory. In order to reduce the number of perforated gridblocks of a well, we remove the perforations which give a negligible contribution to the rate of the well. To do so, we simply filter out the perforations with a small value of γ_i. Denote $\gamma_{\max}$ as the maximum γ_i of all perforations,

$$\gamma_{\max} = \max_{1 \leq k \leq N_{\mathrm{com}}} \{\gamma_k\}. \tag{5.19}$$

Now we define $\gamma_{t,i}$ as

$$\gamma_{t,i} = \begin{cases} \gamma_i & \text{if } \gamma_i \geq \varepsilon \gamma_{\max}, \\ \\ 0 & \text{if } \gamma_i < \varepsilon \gamma_{\max}. \end{cases} \tag{5.20}$$

for $i = 1, 2, \ldots, N_{\mathrm{com}}$, where ε is a very small number and determines the threshold for removing the perforations corresponding to very small flow rates; (in our results we use $\varepsilon = 1.0 \times 10^{-6}$). The $\gamma_{t,k}$, $k = 1, 2, \ldots, \tilde{N}_{\mathrm{com}}$, correspond to the remaining

perforations where $\tilde{N}_{\text{com}}$ is the number of remaining perforations. The remaining perforations are normalized so the fractional rate contributions sum to 1.0 by defining,

$$\tilde{\gamma}_i = \frac{\gamma_{t,i}}{\sum_{k=1}^{\tilde{N}_{\text{com}}} \gamma_{t,k}}. \tag{5.21}$$

After this step, the well has $\tilde{N}_{\text{com}}$ perforated gridblocks and $\tilde{\gamma}_i$ determines the contribution of perforation i to the rate of the well. The PI multiplier of each perforation of the well, β_i is now proportional to $\tilde{\gamma}_i$. The equation for the β_i's is explained through the following illustrative example.

In Fig. 5.6, a horizontal well is shown in a grid where its axis is in the x direction and the length of the well is $2\Delta x$. Assume that the reservoir is homogenous and all the gridblocks have the same sizes in all directions. On the left hand side, the representation of the well is shown where only the two gridblocks penetrated by the well are perforated. The perforation length is $2 \times \Delta x$ and the well has two perforations, $N_{\text{c}} = 2$. On the right hand side of this figure, the distributed representation of the well is shown, where, several gridblocks are perforated ($\tilde{N}_{\text{com}} = 12$) and the perforated length of each gridblock is equal to Δx. Denote the rate of the well by q. Comparing the two representations of the well, we would like to have,

$$q = \sum_{i=1}^{N_{\text{c}}} q_i = \sum_{k=1}^{\tilde{N}_{\text{com}}} q_k, \tag{5.22}$$

where q_i is the rate of the perforation i of the well when only the penetrated gridblocks are perforated and q_k is the flow rate of the perforation k in the distributed representation of the well. Note that in our well-placement method, we represented the well by distributed perforations. Using the rates of the perforations from a well model, we have

$$\sum_{i=1}^{N_{\text{c}}} (PI)_i \lambda_i \Delta p_i = \sum_{k=1}^{\tilde{N}_{\text{com}}} (PI)_k \lambda_k \Delta p_k, \tag{5.23}$$

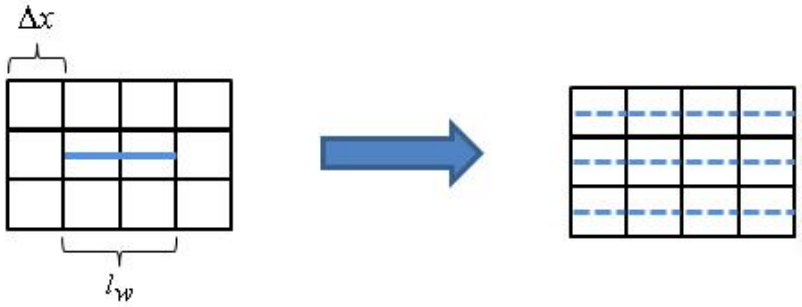

Figure 5.6: Schematic of a horizontal well by distributed perforations.

Assuming all the perforations have similar drawdown pressures and mobilities,

$$\sum_{i=1}^{N_c} (PI)_i = \sum_{k=1}^{\tilde{N}_{com}} (PI)_k, \tag{5.24}$$

Assuming that all the perforations have identical PI's, i.e., a homogenous reservoir with a uniform grid, and denoting the productivity index of each gridblock by $(PI)_{gb}$, we can write,

$$(PI)_i = (PI)_{gb}, \qquad i = 1, 2, \ldots, N_c. \tag{5.25}$$

$$(PI)_k = \beta_k (PI)_{gb}, \qquad i = 1, 2, \ldots, \tilde{N}_{com}. \tag{5.26}$$

By substituting Eqs. 5.25 and 5.26 in Eq. 5.24, it follows that

$$N_c (PI)_{gb} = (PI)_{gb} \sum_{k=1}^{\tilde{N}_{com}} \beta_k, \tag{5.27}$$

which gives

$$\sum_{k=1}^{\tilde{N}_{com}} \beta_k = N_c. \tag{5.28}$$

In general, we can write

$$\sum_{k=1}^{\tilde{N}_{com}} \beta_k = \frac{l_w}{\overline{h}}, \tag{5.29}$$

where l_{w} is the length of the well inside the reservoir and $\overline{h}$ is the average penetrated length over all the perforated gridblocks of the well.

As we previously mentioned, in order to distribute the rate of the original well among the perforations, we assign a productivity index (PI) multiplier to each perforation. Following Eq. 5.29, the PI multiplier of perforation k, β_k, is defined by

$$\beta_k = \tilde{\gamma}_k \frac{l_{\mathrm{w}}}{\overline{h}}, \tag{5.30}$$

for $k = 1, 2, \ldots, \tilde{N}_{\mathrm{com}}$. We define $\overline{h}$ as the weighted average of the penetrated lengths of the perforated gridblocks of the well, and it is given by

$$\overline{h} = \sum_{k=1}^{\tilde{N}_{\mathrm{com}}} \tilde{\gamma}_k h_k, \tag{5.31}$$

where h_k is the perforated length of the perforation of gridblock k (Eq. 4.5). Note that the $\tilde{\gamma}_k$'s are the weights for averaging the perforation lengths of the wells. The weights $\tilde{\gamma}_k$'s are adopted so that the average length of the well perforation ($\overline{h}$) is strongly dependent on the perforated length of the perforations which have a higher portion of the rate. Note that β_k's sum to $\frac{l_{\mathrm{w}}}{\overline{h}}$ which is representative of the number of gridblocks penetrated by the original well.

In this work, we use the Eclipse 100 simulator to run the simulation model and evaluate the NPV. At the initial stage of the optimization, all the simulation gridblock information, including geometrical information and the rock properties, are input to the optimization code. First, the perforated gridblocks are determined from the values of the well trajectory parameters (Eq. 5.4). Then the well model parameters including $k_k h_k$ and r_o for each perforation k are computed using the well parameters and the geometrical grid information. Each perforation of the well is assigned with a productivity index (PI) multiplier (β_k) computed from Eq. 5.30. Therefore, the well model equation in the distributed representation of the well may

simply be expressed as

$$q = \sum_{k=1}^{\tilde{N}_{\text{com}}} \beta_k (PI)_k \lambda_k \Delta p_k. \tag{5.32}$$

It is important to note that we use Eq. 5.12 only to compute the $\tilde{\gamma}_k$'s and β_k's. We still define the vector of optimization variables (Eq. 5.33 below) in terms of the original well parameters. Before we apply the optimization algorithm, however, we transform these variables again as presented in the following section.

5.4 The Optimization Algorithms

The optimal values of the set of parameters $(x_{\text{w},m}, y_{\text{w},m}, z_{\text{w},m}, l_{\text{w},m}, \theta_{\text{w},m}, \varphi_{\text{w},m})$, $m = 1, 2, \ldots, N_{\text{well}}$ are obtained by minimizing $J = -\text{NPV}$ subject to the bound constraints; see Eqs. 5.1 through 5.3. To solve the preceding optimization problem, we implement Bound Optimization BY Quadratic Approximation, BOBYQA, introduced in Chapter 2. Similar to Chapter 4, here we present a method for normalizing the optimization variables to improve the performance of BOBYQA.

As explained before, BOBYQA uses the reservoir simulator as a "black box." When optimizing the location and trajectories of directional wells, the optimization parameters are

$$u = [x_{\text{w},1}, y_{\text{w},1}, z_{\text{w},1}, l_{\text{w},1}, \theta_{\text{w},1}, \varphi_{\text{w},1}, \ldots, x_{\text{w},N_{\text{well}}}, y_{\text{w},N_{\text{well}}}, z_{\text{w},N_{\text{well}}}, l_{\text{w},N_{\text{well}}}, \theta_{\text{w},N_{\text{well}}}, \varphi_{\text{w},N_{\text{well}}}]^T \tag{5.33}$$

The total number of the optimization variables is $n = 6 \times N_{\text{well}}$. For well m, the bound values on $x_{\text{w},m}$ and $y_{\text{w},m}$ parameters are determined by the outer reservoir boundaries. The bounds on each $z_{\text{w},m}$ is the depth of the top and bottom surfaces of the reservoir at $(x_{\text{w},m}, y_{\text{w},m})$. The maximum and minimum values for the length of the well, $l_{\text{w},m}$, are specified by the user. The maximum and minimum values for the deviation angles $\theta_{\text{w},m}$ and $\varphi_{\text{w},m}$ are 0 and 180, respectively.

Similar to the discussion given in Chapter 4, BOBYQA is applied to the nor-

malized variables; where, every optimization variable is normalized and the original bounds are transformed to bounds on the normalized components of u. Hence, the parameters used in BOBYQA are all specified in the normalized domain, i.e., the values of the initial and minimum trust-region radii, ρ_{beg} and ρ_{end}, the initial point and the bound constraints are all specified in the normalized domain. The normalized components $\tilde{u_i}$, $i = 1, 2, \ldots, n$ of the normalized vector of parameters $\tilde{u}$ are defined by Eq. 4.16. For the parameter ϵ_i, based on the Powell [34] observation and as we explained in Chapter 4, we choose $\epsilon_i = 0.1$ for all optimization variables. The parameter D_i for the optimization variables $x_{\rm w}$, $y_{\rm w}$ and $z_{\rm w}$ is the average over the optimization domain of the reservoir gridblock size in a particular coordinate direction (x, y or z) appropriate for the variable u_i, i.e., D_i, for $x_{\rm w}$, $y_{\rm w}$ and $z_{\rm w}$ is respectively the average reservoir gridblock size in the x, y and z direction, respectively. The average is taken over the gridblocks inside the part of the reservoir that we consider for well-placement.

The value of D_i for the length parameter ($l_{\rm w}$) of the trajectory of the well is an arbitrary value which approximates the length of the well in a gridblock. We suggest choosing this value based on the initial direction of the well, i.e., if the well axis is initially in the x direction, choose D_i equal to the average gridblock size in the x direction. The value of D_i for the deviation angle $\varphi_{\rm w}$ is defined as the value of the change in this angle which gives a change equal to $\overline{\Delta z}$ in the depth of the two endpoints of the initial well trajectory, where $\overline{\Delta z}$ is the average gridblock size in the z-direction. For example, if the well is initially horizontal and has a length of 250 ft and $\overline{\Delta z} = 20$ ft, then a change of $\sin^{-1}(\frac{20}{250/2}) = 9.2^\circ$ degrees in the deviation angle of well displaces each endpoint of the well about 20 ft; thus we set $D_i = 9.2$ for $\varphi_{\rm w}$. Note that 250/2 is the half length of the well. Similarly, the value of D_i for the deviation angle $\theta_{\rm w}$ is defined as the value of the change in this directional angle which causes a change in the location of each endpoint of the well in the $x - y$ plane

equal to $(\overline{\Delta x}^2 + \overline{\Delta y}^2)^{1/2}$. For example, if the well is initially horizontal and has a length of 250 ft and $\overline{\Delta x} = \overline{\Delta y} = 50$ ft, then a change of $\sin^{-1}(\frac{\sqrt{50^2+50^2}}{250/2}) = 34.5^\circ$ degrees in the deviation angle of well, displaces each endpoint of the well about 70.7 ft in the $x-y$ plane; thus we set $D_i = 34.5$ for $\theta_{\rm w}$. Note if the computation of D_i for the optimization parameters $\theta_{\rm w}$ and/or $\varphi_{\rm w}$ is not possible with the given guidelines, we choose an arbitrary value for D_i for $\theta_{\rm w}$ and $\varphi_{\rm w}$ such that $0.2\tilde{\theta}^{\rm up}_{{\rm w},i} \geq 10\rho_{end}$ and/or $0.2\tilde{\varphi}^{\rm up}_{{\rm w},i} \geq 10\rho_{end}$, respectively, where $\theta^{\rm up}_{{\rm w},i} = 180$ degrees and $\varphi^{\rm up}_{{\rm w},i} = 180$ degrees. Similar to the procedure explained in Chapter 4, the value of minimum trust region radius, ρ_{end}, is specified by the user and the value of the initial trust-region, ρ_{beg}, radius is determined Eq. 4.22.

Here, we also redefine the bound constraints for $z^{\ell+1}_{{\rm w},m}$ at iteration $\ell+1$ based on the top and bottom depth of the reservoir at the $x-y$ coordinates of the well location, $(x^{\ell+1}_{{\rm w},m}, y^{\ell+1}_{{\rm w},m})$. The procedure for the denormalization of $(\tilde{x}^{\ell+1}_{{\rm w},m}, \tilde{y}^{\ell+1}_{{\rm w},m}, \tilde{z}^{\ell+1}_{{\rm w},m}, \tilde{l}^{\ell+1}_{{\rm w},m})$ to obtain the well parameters, $(x^{\ell+1}_{{\rm w},m}, y^{\ell+1}_{{\rm w},m}, z^{\ell+1}_{{\rm w},m}, l^{\ell+1}_{{\rm w},m})$ follows Eqs. 4.21 through 4.21. Bound values for optimization parameters $\theta_{{\rm w},m}$ and $\varphi_{{\rm w},m}$ do not change during optimization iterations. To find $\theta^{\ell+1}_{{\rm w},m}$ and $\varphi^{\ell+1}_{{\rm w},m}$, values of $\tilde{\theta}^{\ell+1}_{{\rm w},m}$ and $\tilde{\varphi}^{\ell+1}_{{\rm w},m}$ are denormalize by

$$\theta^{\ell+1}_{{\rm w},m} = \theta^{\rm low}_{{\rm w},m} + \frac{\tilde{\theta}^{\ell+1}_{{\rm w},m}}{\tilde{\theta}^{\rm up}_{{\rm w},m}}(\theta^{\rm up}_{{\rm w},m} - \theta^{\rm low}_{{\rm w},m}). \tag{5.34}$$

$$\varphi^{\ell+1}_{{\rm w},m} = \varphi^{\rm low}_{{\rm w},m} + \frac{\tilde{\varphi}^{\ell+1}_{{\rm w},m}}{\tilde{\varphi}^{\rm up}_{{\rm w},m}}(\varphi^{\rm up}_{{\rm w},m} - \varphi^{\rm low}_{{\rm w},m}). \tag{5.35}$$

As explained in Chapter 4, the upper and lower bounds on the $(x_{{\rm w},m}, y_{{\rm w},m})$'s are set as the boundary of the gridded area which contains the reservoir active gridblocks. Similarly we may consider two approaches for evaluating NPV when a well center point is moved into an inactive gridblock, which are, eliminating the well or modifying the location of the well center point to an active gridblock. We argued in Example 4 in Chapter 4 that, eliminating the well may damage the quality of the interpolation model.

As we know, BOBYQA is a local optimization algorithm. Even though we defined the optimization problem in a way that promotes smoothness of J, there is always a chance of converging to a local optimum which gives an unsatisfactorily low value of NPV. In Example 3 of the computational results section, the results of BOBYQA are compared with those obtained with an implementation of the Genetic Algorithm (GA). The Genetic Algorithm driver we used is based on the binary representation of the optimization variables which is usually referred to as a binary genetic algorithm (bGA) (Carroll [7], Yang et al. [43] and Carroll [8]). In bGA the range of an optimization variable (which is a real number), $u_i^{\text{up}} - u_i^{\text{low}}$, is divided into a predefined number of intervals (which is an integer number). The optimization variables of bGA algorithm are the integer numbers which represent the intervals of each optimization variable. The integer numbers are represented in binary form and GA operations (crossover and mutation) are applied in binary form. Binary representation easily handles the box bound constraints on the variables. However, the resolution of the optimization parameter value is controlled by the selected number of intervals for each optimization variable. We use bGA only for the purpose of comparing BOBYQA method with a global search method in Example 3.

5.5 NPV Functional as a Function of Well Trajectory Parameters

In this section, we discuss the defined NPV functional (given in Eq. 2.1) by our model as a function of the well trajectory parameters through a 3D synthetic reservoir example. We compare the NPV defined by our representation of the well inside the reservoir with the NPV computed by the Schlumberger [37] representation of the well inside the reservoir. Note that in our method, we also use the Schlumberger [37] method of computing the well model parameters, $k_i h_i$ and r_{o_i}, where, the well rate is distributed among gridblocks close to the trajectory of the well and the well model parameters are computed according to the procedure discussed above. (Each perforation gridblock is a rectangular volume which it is fully penetrated through

the center of the gridblock). However, in the Schlumberger [37] method, only the gridblocks penetrated by the well are perforated and the well model parameters are determined based on the geometry of each gridblock and the orientation of the well. To evaluate the NPV with the Schlumberger [37] method, the two endpoints of the well are computed from the well trajectory parameters and input to the Schedule software. Then the perforations of the well and their corresponding well model parameters are exported from the Schedule software (Schlumberger [37]). The simulator is run with these perforations and the NPV is evaluated. The NPV calculated from the runs with the Schlumberger [37] method of representing the well in the simulator is referred to as the "Schedule" method throughout.

Here, we consider both a homogeneous and a heterogenous reservoir. In both cases, the reservoir is a three-dimensional $2250 \times 2250 \times 200$ ft ($45 \times 45 \times 10$ gridblocks) simulation model. Gridblocks are 50 ft by 50 ft in the horizontal and 20 ft in the vertical direction. The depth of the reservoir's top surface is $10,000$ ft. The initial reservoir datum pressure is $3,500$ psi at a datum depth of $10,000$ ft. There are four fixed vertical water injection wells at the four corners of the reservoir. The injection wells are perforated in the two bottom layers of the reservoir (layers 9 and 10). All the injection wells are bottomhole pressure-controlled wells with the bottomhole pressure equal to $4,000$ psi. For a single production well, we investigate the sensitivity of NPV to the well trajectory parameters and compare the NPV from Schedule with the NPV from our model. For NPV computations, the oil price is fixed at 70 \$/STB; the water injection and disposal costs are 10 and 5 \$/STB, respectively, and the annual discount rate is $b = 0$. In the following, we discuss the plot of NPV with our model as a function of the production well trajectory parameters. We consider both constant-rate and constant bottomhole-pressure controls for the production well.

5.5.1 Homogeneous Reservoir

The porosity, permeability in the x direction, permeability in the y direction and the vertical permeability for the homogeneous reservoir are 0.20, 148.41 md, 74.21 md and 14.84 md, respectively. Initially, the production well is a horizontal well with its principle axis in the x direction and the well length is 250 ft with its center point in gridblock $(20, 10, 3)$, i.e., the well trajectory parameters are, $(x_{\rm w}, y_{\rm w}, z_{\rm w}, l_{\rm w}, \theta_{\rm w}, \varphi_{\rm w}) = (975, 475, 10050, 250, 0, 90)$. We consider two cases. In the first case, the production well is rate-controlled with the constant total liquid production rate equal to $2,000$ STB/D and the reservoir life is 18 years. The minimum flowing bottomhole pressure constraint of the production well is set to 200 psi, i.e, if the production well cannot maintain the specified production rate without violating the specified bottomhole pressure constraint, the well control will change to the constant bottomhole pressure of 200 psi. In the second case, the production well control is the constant bottomhole pressure of $2,000$ psi and the reservoir life is 7 years. For both the rate-controlled and bottomhole pressure-controlled wells, the reservoir life is long enough to have significant water production at the end of the reservoir life.

First, to compare the NPV from Schedule with NPV from our model, we simply change $y_{\rm w}$ keeping all other well parameters fixed. The NPV function versus $y_{\rm w}$, the y-coordinate of the center point of the well, is plotted in Fig. 5.7 for both the Schlumberger [37] method and our method of representing the well in the simulator. The black square data points show the NPV versus $y_{\rm w}$ for the case that the well perforations in the simulation model are determined by using the Schedule preprocessing software. The red, blue and green data points, respectively, correspond to our method of representing the well in simulator with the parameters $\alpha = 1.0$, $\alpha = 0.75$ and $\alpha = 0.5$, respectively; see Eqs. 5.16-5.18. For both methods, NPV is evaluated at $y_{\rm w} = 475$, 487.5, 499, 501, 525 and 549 ft, where $y_{\rm w} = 500$ ft corresponds to the boundary between two rows of gridblocks and $y_{\rm w} = 475$ and 525 ft correspond

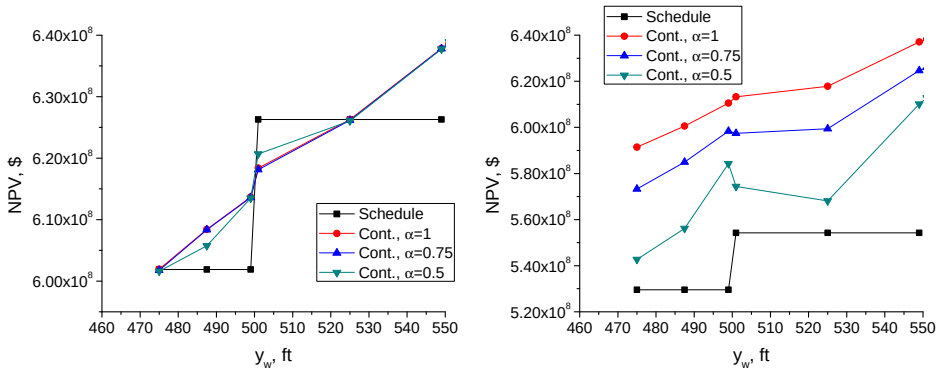

(a) rate-controlled well (b) bottomhole pressure-controlled well

Figure 5.7: NPV as a function of $y_{w,j}$, Homogeneous reservoir.

to the y-coordinate of the gridblock center points in these two rows of gridblocks. As it is shown in Fig. 5.7, the y_w location of a horizontal well aligned in the x direction inside a gridblock is immaterial in the Schedule method. For all three values of $y_w = 475$, 487.5 and 499 ft, the production well is completed in gridblocks (18:22,10,3). Once the well is moved across the boundary of the gridblock ($y_w = 500$ ft), there is a jump in NPV. For $y_w = 501$, 525 and 549 ft, the production well is completed in gridblocks (18:22,11,3). On the other hand, our method of representing the well is sensitive to the location of the well inside a gridblock because the well rate is distributed among the neighboring rows of gridblocks in addition to the gridblocks penetrated by the well. The contribution of each perforation rate to the total rate of the well, γ_i, for $\alpha = 1.0$ are shown for $y_w = 475$, 487.5 and 499 ft in Figs. 5.8, 5.9 and 5.10, respectively. In each figure, only the γ_i's for the perforations in simulation layers 2, 3 and 4 are shown.

The horizontal and vertical ordinates in Figs. 5.8 through 5.10 are respectively the i and j indices of the perforated gridblocks. As we see in Figs. 5.8 to 5.10, once the well moves in the y direction even within the same gridblock, the γ_i's of the perforations change, e.g., compare Figs. 5.8(a), 5.9(a) and 5.10(a). The values of the productivity index multipliers, β_i's, (not shown here) are proportional to the values

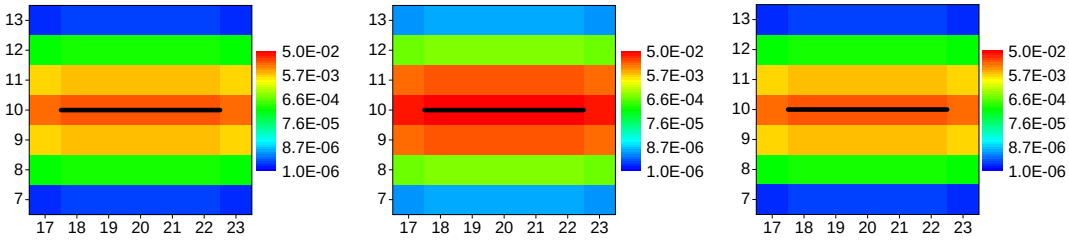

(a) simulation layer 2 (b) simulation layer 3 (c) simulation layer 4

Figure 5.8: The values of γ_i for each perforation of the well for $y_w = 475$ ft, Homogeneous reservoir. The x and y-ordinates correspond to the i and j indices of the perforated gridblocks, respectively.

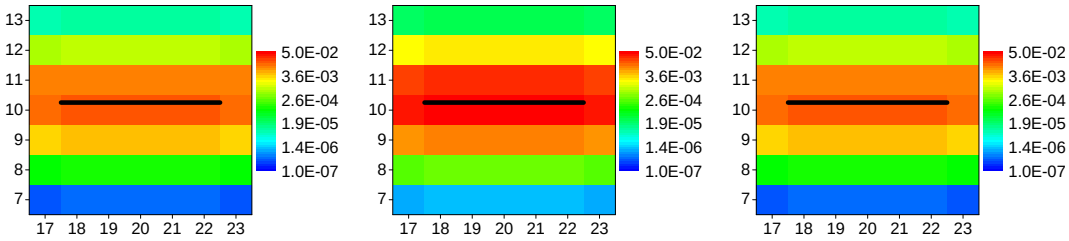

(a) simulation layer 2 (b) simulation layer 3 (c) simulation layer 4

Figure 5.9: The values of γ_i for each perforation of the well for $y_w = 487$ ft, Homogeneous reservoir. The x and y-ordinates correspond to the i and j indices of the perforated gridblocks, respectively.

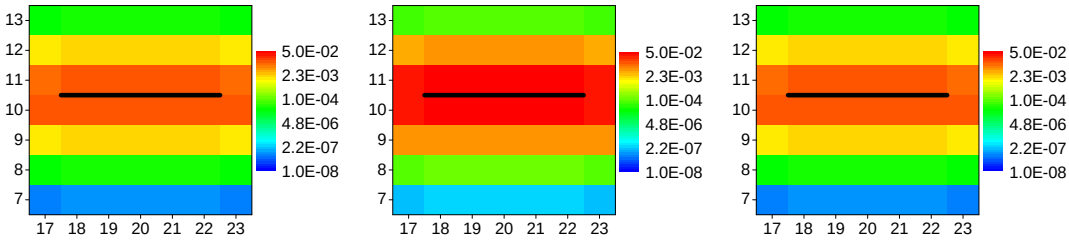

(a) simulation layer 2 (b) simulation layer 3 (c) simulation layer 4

Figure 5.10: The values of γ_i for each perforation of the well for $y_w = 499$ ft, Homogeneous reservoir. The x and y-ordinates correspond to the i and j indices of the perforated gridblocks, respectively.

of γ_i's but their values add up to $\frac{l_w}{h} = \frac{250}{50} = 5$. Note that, as we previously explained, the perforations with a negligible portion of the rate will be eliminated in order to decrease the number of perforated gridblocks. Therefore, all the perforations shown in Figs. 5.8 through 5.10 may not be present when running the simulator to evaluate the NPV.

In our method we perforate the surrounding gridblocks of the well trajectory as well as the gridblocks actually penetrated by the well. The representation of the well with distributed perforations is approximate because (i) different perforations may have different well indices (due to the difference in permeabilities and size of the perforation gridblocks), (ii) different perforations have different phase mobilities due to the difference in their pressures and saturations, and (iii) different well perforations have different flowing drawdown pressures (the difference between the well bottomhole pressure and the perforation gridblock pressure). Even though the perforations of a well may have different drawdown pressures, phase mobilities and productivity indices, for a rate-controlled well, the total production rate of the well is constant. Therefore, when the rate-controlled well is located at the center of a gridblock, the NPV value from our method and the one from the Schedule method are very close, see $y_w = 475$ ft and $y_w = 525$ ft in Fig. 5.7(a). As the well moves within the gridblock and in the y direction, the rate fractions of the total production rate corresponding to the oil and water phases change, which results in a change in NPV as a function of y_w. For a bottomhole pressure-controlled well, the summation of the rates of the distributed perforations is not equal to the rate of the well which has the perforations only at the penetrated gridblocks. Note that the productivity index multipliers of the perforations sum to the right value of $\frac{l_w}{h}$, however, assuming that the PI's of the perforations are additive requires the assumptions of identical drawdown pressure, phase mobility and productivity indices for all perforations. These conditions do not generally hold. In the case under consideration, the reservoir is homogeneous so all

the perforations have identical productivity indices because gridblock perforations have identical permeabilities and the gridblock dimensions are uniform. However, due to the distributed perforations and the variation in the flowing drawdown pressure and possibly phase mobilities of the perforations, the NPV from our method is not identical with the NPV from Schedule, i.e., in the constant bottomhole pressure case, our approximation over estimates NPV comparing to the Schedule method (see Fig. 5.7(b) for bottomhole pressure-controlled well). The most important thing that the reader should observe regarding Figs. 5.7(a) and 5.7(b) is that for the two $\alpha = 1$ cases, the NPV computed from our method is an increasing continuous function of y_{w}, so that given the choice of whether y_{w} should be in the gridblock corresponding to $y_{\mathrm{w}} = 475$ ft or $y_{\mathrm{w}} = 525$ ft, our optimization procedure would put the well in the gridblock with the y-coordinate of its center point corresponding to $y_{\mathrm{w}} = 525$ ft, i.e., our optimal choice of y_{w} would be consistent with the choice based on the NPV computing using the Schedule pre-processing software.

For smaller values of α ($\alpha = 0.75$ and 0.5), fewer surrounding gridblocks will be perforated and the β_is of the perforations which are further away from the well trajectory are smaller. Thus, as α decreases, our NPV approximation in the bottomhole pressure control case becomes closer to the NPV from Schedule (at $y_{\mathrm{w}} = 475$ ft and $y_{\mathrm{w}} = 525$ ft) but becomes noisy. For smaller values of α, the difference in the flowing drawdown pressures of different perforations are larger, because of the variations in the PI multipliers of the perforations. In the case presented here, when the horizontal well produced at a fixed bottomhole-pressure moves across a boundary between two gridblocks ($y_{\mathrm{w}} = 500$ ft), the rate of the well is larger than for a well close to the center of either of those gridblocks ($y_{\mathrm{w}} = 475$ ft or $y_{\mathrm{w}} = 525$ ft). This makes our approximation inaccurate when the location of the well is close to the boundary between two gridblocks (see Fig. 5.7(b)). To better explain this situation, assume that a well with distributed perforations has only three perforations in three

adjacent rows of gridblocks. If the actual well location is close to the center point of the perforation gridblock in the middle row, the PI multiplier corresponding to that perforation would be much larger than the ones for the other perforations (exponential function behavior). The perforations with small β_i's would have negligible rates and the perforation with a large β_i would have a large rate but the drawdown pressure for the perforation with large β_i is such that the total rate of the perforations would be close to the rate that the well would have if the well had only a single perforation in the gridblock close to its location. However, if the location of the well is close to the boundary of the two gridblocks, both perforations have significant PI multipliers and drawdown pressures would be large for both perforations, so that, both perforations would have a significant flow rate and the total rate of the well would be larger than the rate that the well would have if it were perforated in only one gridblock. This is because the rate of a perforation of a bottomhole pressure-controlled well is not a linear function of the productivity index multiplier of that perforation. The preceding discussion is valid only for a well with constant bottomhole pressure control. This behavior can be observed in Fig. 5.7(b) at $y_{\mathrm{w}} = 500$ ft for $\alpha = 0.5$ (and to a much smaller degree for $\alpha = 0.75$). In Figs. 5.11(a) and 5.11(b), the cumulative oil production, the cumulative water production and the cumulative liquid production for the bottomhole pressure-controlled production well are shown as a function of y_{w} for $\alpha = 1.0$ and $\alpha = 0.5$, respectively. Fig. 5.11(a) pertains to the case where $\alpha = 1.0$. As its shown in this figure, the cumulative oil production increases and the cumulative water production decreases as the well moves in the y direction and away from the nearby injection wells. Although the cumulative production from the well increases as the well moves across the boundary, however, the increase in the cumulative production is not significant. Therefore, for $\alpha = 1.0$ the NPV increases as a function of y_{w}; see Fig. 5.7(b) for $\alpha = 1.0$. Fig. 5.11(b) pertains to the case where $\alpha = 0.5$. As explained before, for $\alpha = 0.5$ the cumulative liquid

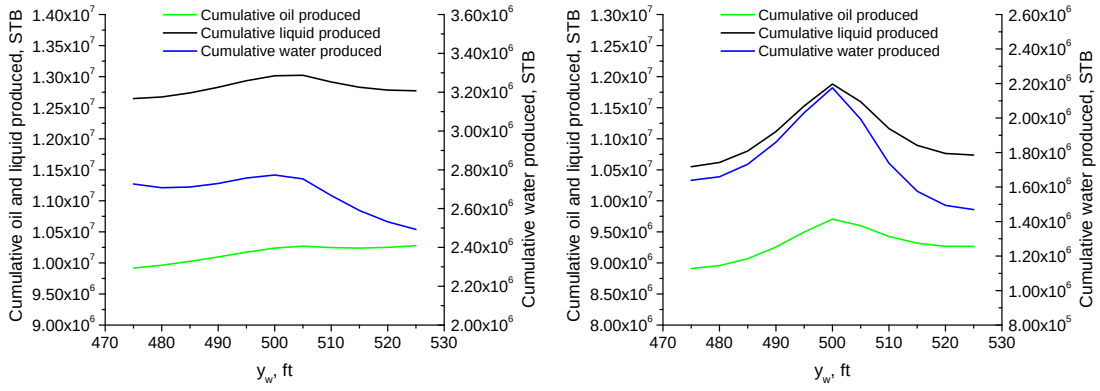

(a) $\alpha = 1.0$ (b) $\alpha = 0.5$

Figure 5.11: Cumulative oil production, cumulative water production and cumulative liquid production as a function of y_{w} for the bottomhole pressure-controlled well, Homogeneous reservoir.

production from the well significantly increases when the well crosses the boundary between two rows of gridblocks at $y_{\mathrm{w}} = 500$ ft. Therefore, for $\alpha = 0.5$, NPV is a noisy function of y_{w}; see Fig. 5.7(b) for $\alpha = 0.5$.

If the well control is a constant production rate and the well center point is at a gridblock center, our NPV approximation would be very close to the Schedule NPV as the total rate of the well is constant regardless of the values of β_is for the perforations of a well. However, the NPV with our model changes continuously as the rate of each perforation changes when the location of the well changes; see Fig. 5.7(a).

Plots of the NPV as a function of horizontal orientation angle, θ_{w}, and vertical orientation angle, φ_{w}, for the production well controlled with the specified constant bottomhole pressure and the specified liquid production rate are given in Figs. 5.12 and 5.13, respectively. In these two figures, the well trajectory parameters, except the orientation angles, have the fixed values given by of $(x_{\mathrm{w}}, y_{\mathrm{w}}, z_{\mathrm{w}}, l_{\mathrm{w}}) = (975, 475, 1050, 250)$. In Fig. 5.12(a) and 5.13(a), φ_{w} is fixed at 90 degrees (the well is horizontal) and θ_{w} changes from 0 to 180 degrees while all other well parameters remain fixed. In Figs. 5.12(b) and 5.13(b), θ_{w} is fixed at 0 degrees (the well

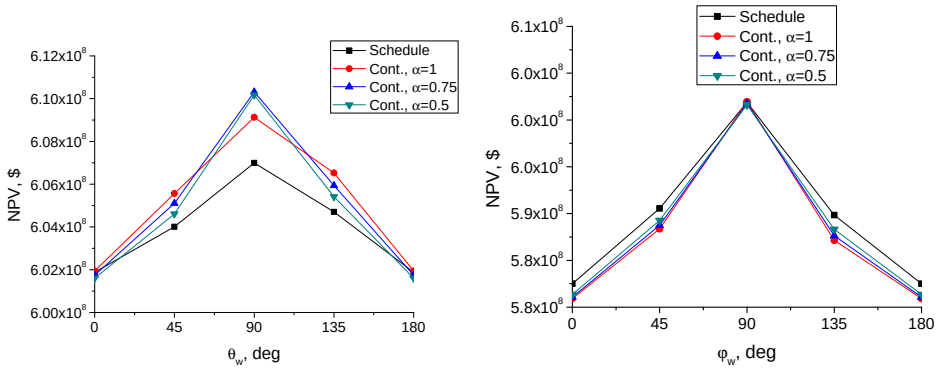

(a) NPV vs. θ_{w} (b) NPV vs. φ_{w}

Figure 5.12: NPV as a function of θ_{w} and φ_{w}, Rate-controlled well, Homogeneous reservoir.

in aligned in the x direction) and φ_{w} changes from 0 to 180 degrees while all other well parameters remain fixed. Similar to the plots of NPV versus y_{w}, the NPV plots computed by running the simulator using our approximate representation of the well inside the reservoir and the NPV plots which are computed when the well perforations are determined with Schedule, are in a better agreement for the rate-controlled well. For the bottomhole pressure-controlled well, the NPV plots with our method of representing the well inside the reservoir are more approximate, however, note that the change of NPV with respect to the change of the orientation angles follow the same trend in both Schedule and our method. Because of this, optimization results obtained based on our well model should be consistent with Schedule. Based on our experimentation, which includes the results shown in Figs. 5.7, 5.12 and 5.13, we suggest using $\alpha = 1$.

5.5.2 Heterogenous Reservoir

The problem considered here is very similar to the one just presented for the homogenous reservoir except, here, the reservoir is heterogenous. However, all the comparisons and the plots presented in this section are similar to the ones for the homogenous reservoir discussed previously. The log-permeability field of the heterogenous reservoir in the x direction and the porosity field of the reservoir for

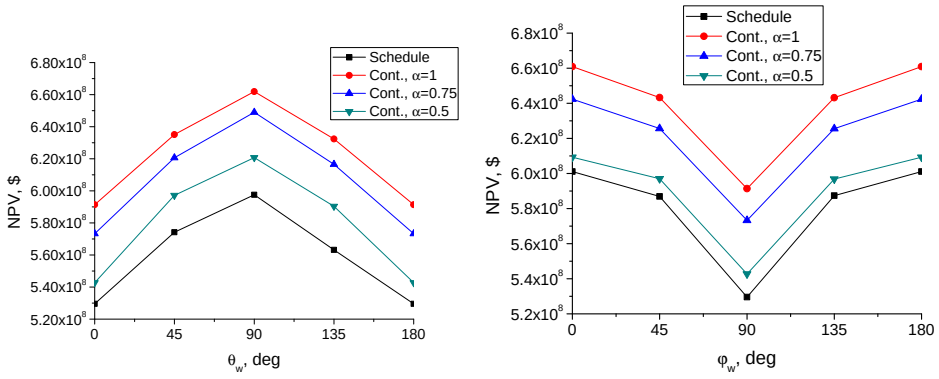

(a) NPV vs. θ_{w} (b) NPV vs. φ_{w}

Figure 5.13: NPV as a function of θ_{w} and φ_{w}, Bottomhole pressure-controlled well, Homogeneous reservoir.

simulation layers 1 to 10 are shown in Figs. 5.14 and 5.15, respectively. The permeability in the y and z directions are 0.5 and 0.1 times the corresponding gridblock permeability in the x direction, i.e, $k_y = 0.5k_x$ and $k_z = 0.1k_x$. As in the homogenous case, there are four vertical water injection wells completed in the bottom two layers near the four corners of the reservoir. These injection wells operate at a constant bottomhole pressure equal to 4000 psi.

We consider a horizontal production well in the x direction with its center point located in gridblock $(20, 10, 3)$ and length equal to 250 ft, i.e., the well trajectory parameters are, $(x_{\mathrm{w}}, y_{\mathrm{w}}, z_{\mathrm{w}}, l_{\mathrm{w}}, \theta_{\mathrm{w}}, \varphi_{\mathrm{w}}) = (975, 475, 10050, 250, 0, 90)$. Well controls with a constant liquid production rate of $2,000$ STB/Day and with a constant bottomhole pressure of $2,000$ psi are both considered. The NPV plots with respect to y_{w}, θ_{w} and φ_{w}, respectively, are shown in Figs. 5.16 to 5.18 for the rate-controlled and the bottomhole pressure-controlled wells. In Fig. 5.16, $y_{\mathrm{w}} = 500$ and 550 ft correspond to the boundaries between adjacent rows of gridblocks and $y_{\mathrm{w}} = 475$ and 525 ft correspond to the y-coordinate of the gridblock center points in two adjacent rows of gridblocks. The NPV obtained with our method is a closer approximation of the NPV from Schedule for the rate-controlled well than for the bottomhole pressure-controlled well. For a heterogenous reservoir, in addition to

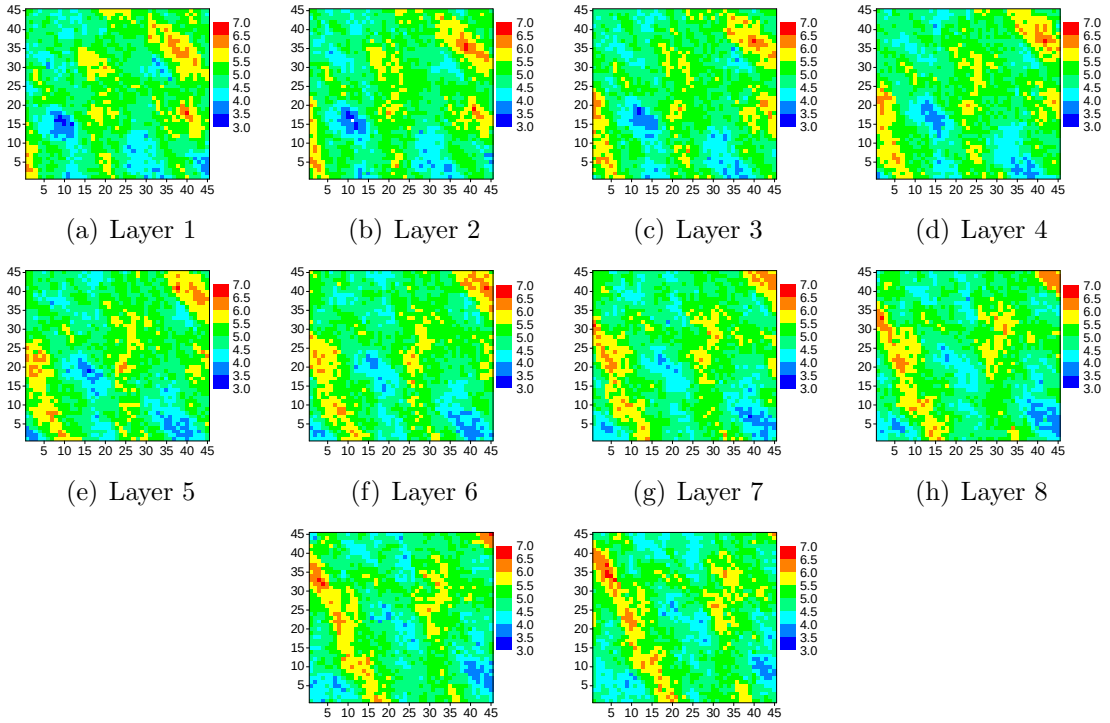

(a) Layer 1 (b) Layer 2 (c) Layer 3 (d) Layer 4

(e) Layer 5 (f) Layer 6 (g) Layer 7 (h) Layer 8

(i) Layer 9 (j) Layer 10

Figure 5.14: Log-permeability field of the reservoir in the x direction, Heterogenous Reservoir.

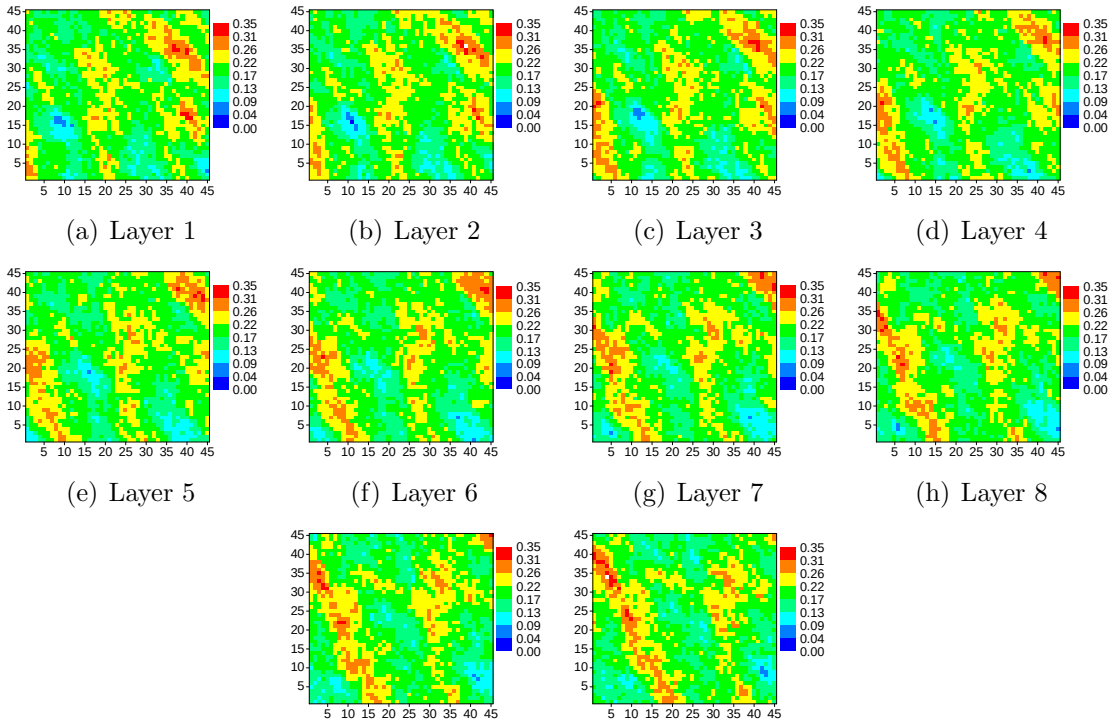

(a) Layer 1 (b) Layer 2 (c) Layer 3 (d) Layer 4

(e) Layer 5 (f) Layer 6 (g) Layer 7 (h) Layer 8

(i) Layer 9 (j) Layer 10

Figure 5.15: Porosity field of the reservoir, Heterogenous Reservoir.

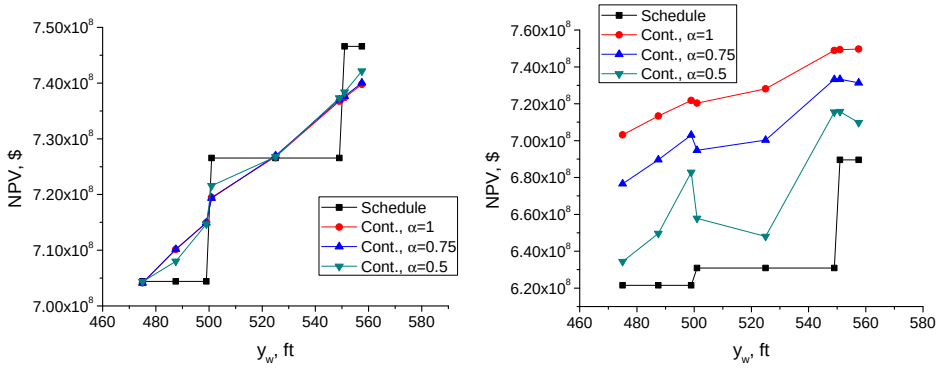

(a) rate-controlled well (b) bottomhole pressure-controlled well

Figure 5.16: NPV as a function of y_{w}, Heterogeneous reservoir.

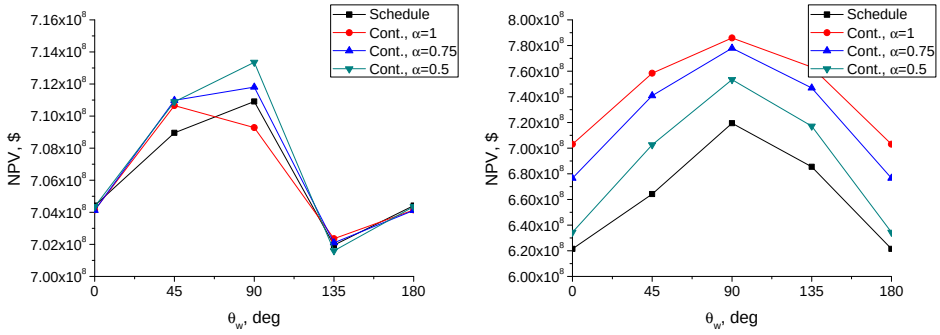

(a) rate-controlled well (b) bottomhole pressure-controlled well

Figure 5.17: NPV as a function of θ_{w}, Heterogeneous reservoir.

the difference in the mobilities and drawdown pressures of the perforations, the productivity indices of the perforations are also different due to the difference in the permeability of their gridblocks. Therefore, the NPV is more approximate. As in the homogenous case, the NPV is noisy for smaller values of α when a bottomhole pressure-controlled well crosses the boundary between two gridblocks.

The results of Figs. 5.16 through 5.18 show that, the NPV from our well model with $\alpha = 1$ displays the same trend as the NPV using the well rates computed using the Schedule pre-processing software, except in case Fig. 5.17(a) for a rate-controlled well. In this case, based on our model, NPV is optimized with $\theta_{\mathrm{w}} \approx 45$ degrees whereas $\theta_{\mathrm{w}} \approx 90$ corresponds to the optimal angle according to the Schedule results. Note, however, the difference between the two corresponding NPV's is negligible.

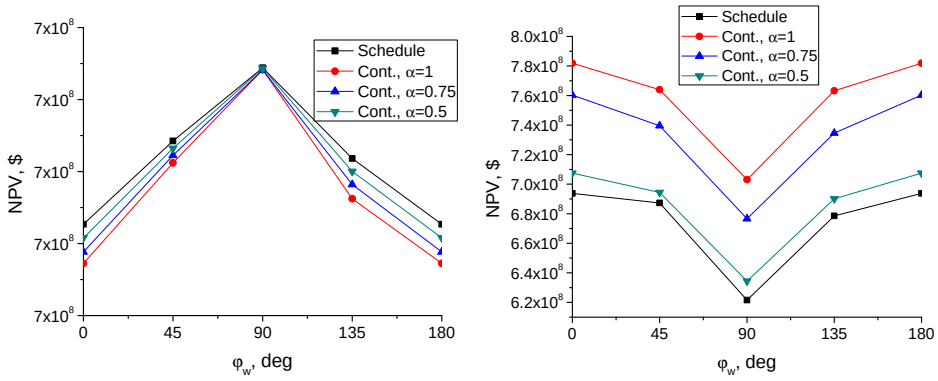

(a) rate-controlled well (b) bottomhole pressure-controlled well

Figure 5.18: NPV as a function of φ_w, Heterogeneous reservoir.

For this example $\alpha = 0.75$ appears to yield optimum parameter estimates from our method that are more consistent with the results from Schedule. Nevertheless, we still recommend $\alpha = 1$ while recognizing some experimentation may be required to obtain the best value of α.

5.6 Optimization Results

In this section, we present the results generated from our algorithm for a set of example problems. In Example 1, we determine the optimum location of a production well for the synthetic homogeneous and heterogeneous reservoirs discussed in the previous section. In Example 2, we consider a homogenous and heterogeneous layered reservoir and we apply our algorithm to optimize the trajectory of a production well. The significance of this example is that the NPV in this example is very sensitive to the vertical orientation angle of the well. Example 3 is a 3D anticline reservoir with a strong edge-water drive. In this example, we consider optimization of the trajectories of two production wells. We also present a comparison between the performances of BOBYQA and GA for our well-placement algorithm. In Example 4, we consider optimizing the locations of producers and water injection wells for the PUNQ-S3 3D three-phase reservoir model. In all examples, the objective is to maximize the NPV by optimizing the trajectories of the production wells. The first three examples

are two-phase oil-water reservoirs and PUNQ is a three-phase reservoir model. In all examples presented in this section, the oil price is fixed at 70 \$/STB; the water injection and disposal costs are 10 and 5 \$/STB, respectively and the annual discount rate is $b = 0$. In the PUNQ example, we do not consider any revenue or cost for the produced gas from the reservoir.

5.6.1 Example 1. Optimization of a Single Production Well in a 3D Reservoir

In this example, we consider both homogeneous and heterogenous reservoirs described in the previous section. Here, we optimize the trajectory of the production well for each reservoir model. We consider the constant-rate and constant bottomhole-pressure controls for the production well.

Case 1- Homogeneous Reservoir: We consider the optimization of the location, length and trajectory angles of a production well. We consider both bottomhole pressure-controlled and rate-controlled wells. The homogeneous reservoir is the one described in Sub-Section 5.5.1. Recall that there are water injection wells completed in the bottom two layers in each corner of the reservoir. For both types of well controls, we start with two different initial sets of well parameters. For the first initial guess, the well is a horizontal well with its principle axis in the x direction and with the length of 250 ft and its center point is located in gridblock $(20, 10, 3)$, i.e., $(x_{\mathrm{w}}, y_{\mathrm{w}}, z_{\mathrm{w}}, l_{\mathrm{w}}, \theta_{\mathrm{w}}, \varphi_{\mathrm{w}}) = (975, 475, 10050, 250, 0, 90)$. For the second initial guess, the well is horizontal and aligned in the y direction where its center point is located in gridblock $(25, 35, 3)$ and has a length of 250 ft, i.e., the well trajectory parameters, $(x_{\mathrm{w}}, y_{\mathrm{w}}, z_{\mathrm{w}}, l_{\mathrm{w}}, \theta_{\mathrm{w}}, \varphi_{\mathrm{w}}) = (1225, 1725, 10050, 250, 90, 90)$. The maximum length for the production well is 500 ft. The summary of the optimization runs for both initial guesses are shown in Table 5.1.

The values of NPV in the first and fourth rows of results in Table 5.1 correspond to the evaluated NPV when the well perforations are determined with the

Table 5.1: The summary of the optimization runs for both initial guesses, Homogeneous reservoir, Example 1, Case 1.

	Rate-controlled well		BHP controlled well	
	Init. Guess 1	Init. Guess 2	Init. Guess 1	Init. Guess 2
Initial NPV, Schedule	$\$6.02 \times 10^8$	$\$6.33 \times 10^8$	$\$5.30 \times 10^8$	$\$6.27 \times 10^8$
Initial NPV	$\$6.02 \times 10^8$	$\$6.36 \times 10^8$	$\$5.91 \times 10^8$	$\$6.91 \times 10^8$
Final NPV	$\$8.35 \times 10^8$	$\$8.36 \times 10^8$	$\$9.04 \times 10^8$	$\$9.05 \times 10^8$
Final NPV, Schedule	$\$8.35 \times 10^8$	$\$8.31 \times 10^8$	$\$8.98 \times 10^8$	$\$8.97 \times 10^8$
No. of Sim. runs	49	60	79	62

Schedule software with the initial and final well trajectory parameters, respectively. The values of NPV in the second and third rows of results correspond to the initial and final NPV values of the optimization runs which uses our representation of the well in the simulator. The Schedule results in row 4 of data as well as corresponding results for other example were obtained by inputting the optimal well trajectory estimated by our procedure into Schedule and then running the simulator. Note that the NPV values obtained with our well model are close to those obtained using the Schedule software. Also note that the estimated optimal NPV values obtained from the two initial guesses differ by less than 0.5%.

The initial and final well parameters are listed in Table 5.2. The schematic of the reservoir and the initial and final locations of the production well for both initial guesses are shown in Figs. 5.19(a) and 5.19(b) for the rate-controlled and bottomhole pressure-controlled wells, respectively. In Fig. 5.19, the two initial guesses are shown with two different colors where the initial locations are shown in a dashed line and the final well locations are shown in solid lines. The production rate from the reservoir is constant for a rate-controlled well. For both initial guesses of the rate-controlled production well, the final trajectories of the well are horizontal and the well is moved to the top layer of the reservoir. This is expected as the thickness of the reservoir is much smaller than the dimensions of the reservoir in the x and y directions, and the water injection wells are perforated at the bottom of the reservoir. Also, the well

Table 5.2: The initial and final well trajectory parameters $(x_w, y_w, z_w, l_w, \theta_w, \varphi_w)$ for the production well, Homogeneous reservoir, Example 1, Case 1.

Rate-controlled well, Init. Guess 1	Initial well param.	$(975, 475, 10050, 250, 0, 90)$
	Final well param.	$(1134.3, 1125.4, 10000.4, 198.5, 0.0, 90.5)$
Rate-controlled well, Init. Guess 2	Initial well param.	$(1225, 1725, 10050, 250, 90, 90)$
	Final well param.	$(1125.5, 1128.8, 10000.0, 319.3, 95.7, 90.1)$
BHP-controlled well, Init. Guess 1	Initial well param.	$(975, 475, 10050, 250, 0, 90)$
	Final well param.	$(1123.4, 1070.5, 10021.2, 377.1, 113.8, 90.4)$
BHP-controlled well, Init. Guess 2	Initial well param.	$(1225, 1725, 10050, 250, 90, 90)$
	Final well param.	$(1135.1, 1145.3, 10015.8, 391.0, 67.5, 89.5)$

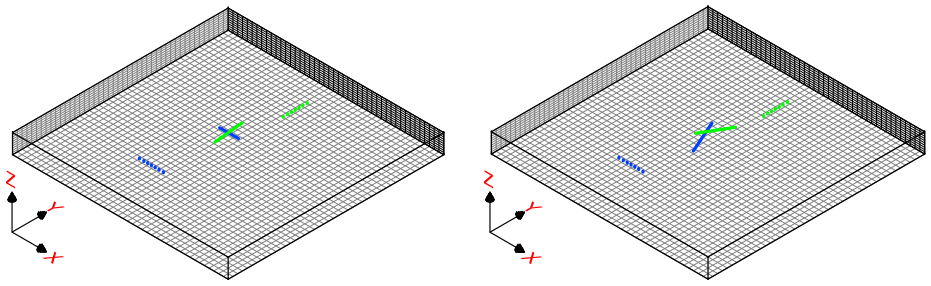

(a) rate-controlled well (b) BHP controlled well

Figure 5.19: The initial and final well locations, Homogeneous reservoir, Example 1, Case 1. The initial locations are shown in dashed lines and the final well locations are shown in solid lines. The well locations corresponding to initial guesses 1 and 2 are shown in blue and green colors, respectively.

is moved to the center of the reservoir which is also expected as the four vertical injection wells are at the corners of the reservoir. The horizontal orientation angles of the well obtained for the two initial guesses are $\theta = 0$ and 96 degrees, respectively, i.e., the values of θ did not change significantly from its initial value during the iterations of the optimization algorithm.

The final trajectories of the bottomhole pressure-controlled production wells are horizontal, at the center of the reservoir and in the top simulation layer. Again this is reasonable considering the location and perforations of the fixed injection wells. For a BHP-controlled well, the production rate from a perforation of a well depends on the productivity index of the perforation which is a function of the length

of the well inside the perforation gridblock (h_i) and the radial permeability of the perforation gridblock toward the well (k_i), see Eqs. 4.4 and 4.5. The orientation angles of the well in both horizontal and vertical directions determines both the length of the well in a gridblock and the radial permeability toward the well. We recall that although the reservoir is homogeneous, the permeability in the z and y directions are respectively 0.1 and 0.5 times the permeability in the x direction. The final trajectories of both initial guesses are approximately aligned in the y direction. This is reasonable as it gives a high value of the radial permeability toward the well, $k_i \approx \sqrt{k_x k_z}$, and also tends to delay water breakthrough and maximize sweep efficiency as the vertical water injection wells are at the corners of the reservoir. For the final trajectories obtained with initial guesses 1 and 2, $k_i h_i$ of a perforation of the well is larger than the one for a well aligned in the y direction which gives a larger production rate from the reservoir. The final trajectory obtained with initial guesses 1 and 2 have $k_i h_i$ equal to 2458 and 2446 md.ft, respectively, which both are larger than the one for a perforation of a well oriented in the y direction ($\sqrt{k_x k_z}\Delta y = 2347$ md.ft).

Here, we compare our final NPVs for the two initial guesses with the NPV's for 6 well trajectory trials with the $(x_{\mathrm{w}}, y_{\mathrm{w}})$ coordinates of the well locations at the exact center of the reservoir. Four trials are for the cases where the well is aligned in the x or y direction and has the length of 250 or 500 ft. In the other two trials, all well trajectory parameters except the horizontal orientation angle (θ_{w}) correspond to the optimum solution with the second initial guess. For the horizontal orientation angle values in these two trials, we use $\theta_{\mathrm{w}} = 0$ and 90 degrees, respectively. The summary of the well trajectory parameters and the NPVs are listed in Table 5.3. Our final NPVs of the optimization runs with both initial guesses are larger than four well trajectory trials. Two trials gave just slightly higher (0.3 percent) or similar NPV values compared to our final NPV values. Thus, it appears our method obtained a

Table 5.3: Comparison of our optimum NPV with the NPV for some trials of the well trajectory, Homogeneous reservoir, Example 1, Case 1.

Trial	Well trajectory parameters	NPV
1	$(1125, 1125, 10010, 250, 0, 90)$	$\$8.75 \times 10^8$
2	$(1125, 1125, 10010, 250, 90, 90)$	$\$8.94 \times 10^8$
3	$(1125, 1125, 10010, 500, 0, 90)$	$\$9.08 \times 10^8$
4	$(1125, 1125, 10010, 500, 90, 90)$	$\$9.03 \times 10^8$
5	$(1135.1, 1145.3, 10015.8, 391.0, 0, 89.5)$	$\$9.03 \times 10^8$
6	$(1135.1, 1145.3, 10015.8, 391.0, 90, 89.5)$	$\$9.05 \times 10^8$
Our final solution with initial guess 1	$(1123.4, 1070.5, 10021.2, 377.1, 113.8, 90.4)$	$\$9.04 \times 10^8$
Our final solution with initial guess 2	$(1135.1, 1145.3, 10015.8, 391.0, 67.5, 89.5)$	$\$9.05 \times 10^8$

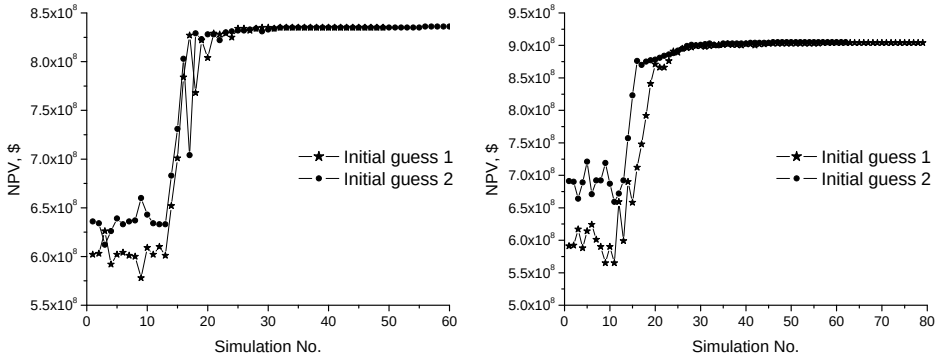

(a) rate-controlled well (b) BHP controlled well

Figure 5.20: NPV versus the optimization iteration number, Homogeneous reservoir, Example 1, Case 1.

good estimate of the optimum NPV.

The plot of NPV versus the iteration number is shown in Fig. 5.20 for the rate-controlled and bottomhole pressure-controlled wells. As we explained in Chapter 2, BOBYQA needs $n + 2 \leq m \leq [(n + 1)(n + 2)]/2$ simulation runs to build the first quadratic approximation of the objective function. There are 6 optimization variables and we choose $m = 2n + 1 = 13$ for the size of initial interpolation set for BOBYQA. In Fig. 5.20, the first 13 simulation runs are used to build the initial quadratic model. In all cases, fewer than 80 reservoir simulation runs were used to obtain the optimal estimates of well location, length and trajectory angles.

Table 5.4: The summary of the optimization runs for both initial guesses, Heterogenous reservoir, Example 1, Case 1.

	Rate-controlled well		BHP controlled well	
	Init. Guess 1	Init. Guess 2	Init. Guess 1	Init. Guess 2
Initial NPV, Schedule	$\$7.04 \times 10^8$	$\$4.90 \times 10^8$	$\$6.22 \times 10^8$	$\$4.93 \times 10^8$
Initial NPV	$\$7.04 \times 10^8$	$\$4.88 \times 10^8$	$\$7.04 \times 10^8$	$\$5.47 \times 10^8$
Final NPV	$\$8.18 \times 10^8$	$\$8.29 \times 10^8$	$\$8.91 \times 10^8$	$\$8.84 \times 10^8$
Final NPV, Schedule	$\$8.16 \times 10^8$	$\$8.27 \times 10^8$	$\$8.85 \times 10^8$	$\$8.71 \times 10^8$
No. of Sim. runs	48	70	55	69

Case 2- Heterogenous Reservoir: This case is the same as Example 1, Case 1, except that the reservoir geology is heterogenous. The heterogeneous reservoir is the one described in Sub-Section 5.5.2. Similar to Example 1, Case 1, we try to optimize the location of the producer with two different initial guesses for the set of six well parameters. Again we consider both a rate-controlled production well and a constant bottomhole pressure-controlled well. Recall that there are water injection wells completed in the bottom two layers in each corner of the reservoir. The summary of the optimization runs for both initial guesses are shown in Table 5.4. Note the NPV values from Schedule are fairly close to the NPV values from the well model we use in the optimization algorithm.

The initial well trajectory parameters and also the final well trajectory parameters after the optimization for both initial guesses 1 and 2 are listed in Table 5.4. The values of NPV in the first and fourth rows of results in Table 5.4 correspond to the evaluated NPV when the well perforations are determined by the Schedule method. The values of NPV in the second and third rows of results correspond to the initial guesses and final NPV values after optimization.

The results for the two initial guesses (Tables 5.4 and 5.5) are sufficiently different so that, it is clear that BOBYQA converged to a local optimum, however, the optimum NPVs for both initial guesses are fairly close even though there is considerable variation in the values of the estimated optimal well parameters, see

Table 5.5: The initial and final well trajectory parameters $(x_w, y_w, z_w, l_w, \theta_w, \varphi_w)$ for the production well, Heterogenous reservoir, Example 1, Case 2.

Rate-controlled well, Init. Guess 1	Initial well param.	$(975, 475, 10050, 250, 0, 90)$
	Final well param.	$(695.4, 934.4, 10000.4, 307.4, 0.0, 90.2)$
Rate-controlled well, Init. Guess 2	Initial well param.	$(1225, 1725, 10050, 250, 90, 90)$
	Final well param.	$(696.5, 915.2, 10011.3, 500.0, 132.6, 89.3)$
BHP-controlled well, Init. Guess 1	Initial well param.	$(975, 475, 10050, 250, 0, 90)$
	Final well param.	$(791.5, 926.7, 10026.4, 396.7, 141.1, 93.2)$
BHP-controlled well, Init. Guess 2	Initial well param.	$(1225, 1725, 10050, 250, 90, 90)$
	Final well param.	$(896.1, 919.2, 10013.7, 240.9, 88.7, 83.5)$

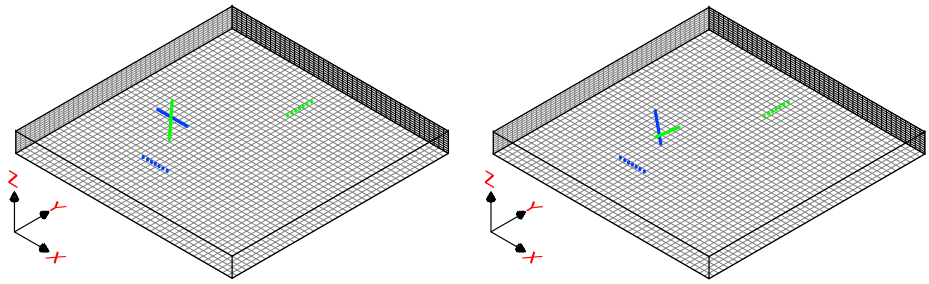

(a) rate-controlled well (b) BHP controlled well

Figure 5.21: The initial and final well locations, Heterogenous reservoirs, Example 1, Case 2. The initial locations are shown in dashed lines and the final well locations are shown in solid lines. The well locations corresponding to initial guesses 1 and 2 are shown in blue and green colors, respectively.

the values of θ_w and l_w in particular in Table 5.5. The schematic of the reservoir and the initial and final locations of the production well for both initial guesses are shown in Figs. 5.21(a) and 5.21(b) for rate-controlled and bottomhole pressure-controlled wells, respectively. In Figs. 5.21(a) and 5.21(b), the results for the two initial guesses are shown with two different colors where the initial locations are shown by a dashed line and the final well locations are shown as solid lines. Similar to the homogenous reservoir, the final trajectory of the well is very close to horizontal ($\varphi_w = 90$ degrees) and the well is moved to the top of the reservoir to delay water production. However, the location of the well is not at the center of the reservoir anymore.

Plots of NPV versus the iteration number are shown in Fig. 5.22 for the

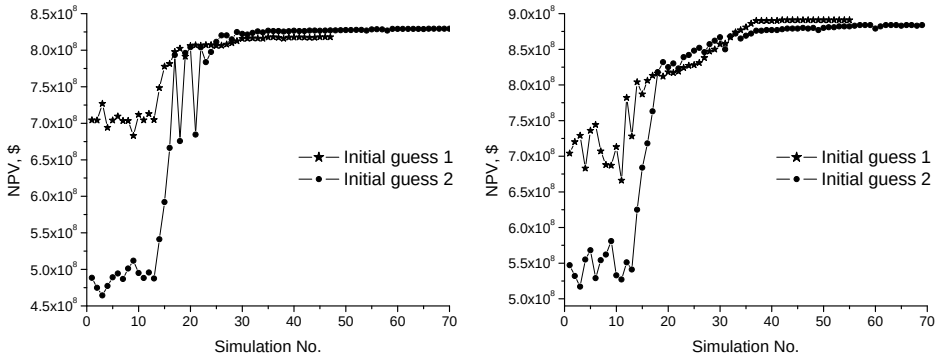

(a) rate-controlled well (b) BHP controlled well

Figure 5.22: NPV versus the optimization iteration number, Heterogenous reservoir, Example 1, Case 1.

rate-controlled and bottomhole pressure-controlled wells.

5.6.2 Example 2. Single Production Well in a Layered Reservoir

In this example, we consider the optimization of the trajectory of a production well in a layered reservoir. The reservoir simulation model is a three-dimensional model with $45 \times 45 \times 20$ gridblocks ($2250 \times 2250 \times 220$ ft). The gridblocks are uniform with $\Delta x = \Delta y = 50$ ft. The simulation model has 10 reservoir layers of good quality sand which alternates with 10 shale layers which are essentially impermeable. Each sandstone layer is 20 ft thick and each shale layer is 2 ft thick. Simulation layers 1, 3, 5, 7, 9, 11, 13, 15, 17 and 19 are sandstone layers and other layers are shale layers. The depth of the reservoir top surface is $10,000$ ft. The initial reservoir datum pressure is $3,500$ psi at datum depth of $10,000$ ft. The porosity and permeability of the shale layers are 0.001 and 0.0001 md, respectively. Therefore, the simulation layers are effectively isolated vertically.

Similar to Example 1, we consider both a homogenous case and a heterogenous case. We consider the optimization of the location, length and trajectory of a production well for two production scenarios for the reservoir. In the first scenario, the production from the reservoir is due to the depletion of the reservoir (no water injection) and the production period of the reservoir is 1 year. In the sec-

ond scenario, there are four fixed vertical water injection wells at the four corners of the reservoir and the production time period of the reservoir is 3 years. All the injectors are perforated in layers 1 to 20 and operate at the constant bottomhole pressure of $4,000$ psi. In both scenarios, the production well operates at the specified bottomhole pressure of 2,000 psi. Similar to the previous example, we consider two different initial guesses for the well parameters, $(x_{\rm w}, y_{\rm w}, z_{\rm w}, l_{\rm w}, \theta_{\rm w}, \varphi_{\rm w})$. In the optimization runs with initial guess 1, the production well is initially considered to be a horizontal well in layer 5 (third reservoir layer) and the well axis is in the x direction and has a length of 300 ft. The well trajectory parameters for the initial guess 1 are $(x_{\rm w}, y_{\rm w}, z_{\rm w}, l_{\rm w}, \theta_{\rm w}, \varphi_{\rm w}) = (475.0, 475.0, 10054.0, 300.0, 0.0, 90.0)$. In the optimization runs with the second initial guess, the well is initially inclined and has a length of 200 ft. The set of well parameters for the initial guess 2 is $(x_{\rm w}, y_{\rm w}, z_{\rm w}, l_{\rm w}, \theta_{\rm w}, \varphi_{\rm w}) = (1475.0, 1725.0, 10054.0, 200.0, 90.0, 30.0)$. The maximum length for the production well is 500 ft in all optimization runs.

Case 1- Homogeneous Reservoir Layers: In this case, the reservoir layers of the simulation model are homogenous. The porosity and permeability of the simulation layers corresponding to the reservoir layers are 0.2 and 148.41 md, respectively. The reservoir simulation layers are isotropic, i.e., $k_x = k_y = k_z$. As mentioned above, we apply our well-placement optimization algorithm to two different initial guesses. The summary of the optimization runs for both scenarios (no water injection and with water injection) are shown in Table 5.6. Two observations are important. First, the estimated optimal NPV values based on our well model are virtually identical for both initial guesses. Secondly, even though the NPV values from our model and Schedule evaluated at the initial guesses are not the same, the NPV values from Schedule and our model evaluated at the estimated optimal values are not so different. The difference between our NPV value and the one from the Schedule method at the initial guesses is due to the fact that the reservoir layers are completely

Table 5.6: The summary of the optimization runs for both scenarios, Homogeneous reservoir layers, Example 2, Case 1.

		Depletion (No water injection)	With water injection
Initial Guess 1	Initial NPV, Schedule	$\$3.81 \times 10^7$	$\$7.03 \times 10^7$
	Initial NPV	$\$3.21 \times 10^7$	$\$1.18 \times 10^8$
	Final NPV	$\$1.20 \times 10^8$	$\$8.71 \times 10^8$
	Final NPV, Schedule	$\$1.24 \times 10^8$	$\$8.63 \times 10^8$
	No. of Sim. runs	150	58
Initial Guess 2	Initial NPV, Schedule	$\$9.59 \times 10^7$	$\$3.99 \times 10^8$
	Initial NPV	$\$8.58 \times 10^7$	$\$4.62 \times 10^8$
	Final NPV	$\$1.20 \times 10^8$	$\$8.70 \times 10^8$
	Final NPV, Schedule	$\$1.24 \times 10^8$	$\$8.41 \times 10^8$
	No. of Sim. runs	127	96

isolated by the shale layers. With the Schedule method, the well is perforated only at the gridblocks which are penetrated by the well. At the initial guesses and with the Schedule method, most reservoir layers do not contribute in the production from the reservoir as they are not penetrated by the well and also the reservoir layers are isolated by the shale layers. With our method, more simulation layers of the reservoir are perforated, hence, more layers contribute to the production from the reservoir. Therefore, at the initial guesses, the production from the reservoir and also the NPV from our method is much larger than the one from the Schedule method. At the final locations, all reservoir layers are penetrated by the production well and therefore, the NPV from both methods are close.

The initial and estimated optimal well locations and trajectories with initial guesses 1 and 2 are shown in Fig. 5.23(a) and Fig. 5.23(b), respectively. In these figures, the well trajectory based on the initial guess for the vector of parameters is shown with a red line and the optimal well trajectories for the first production scenario (depletion) and the second production scenario (water injection) are shown with a green line and a blue line, respectively. The initial and final well trajectory parameters corresponding to the optimization runs with the two initial guesses are

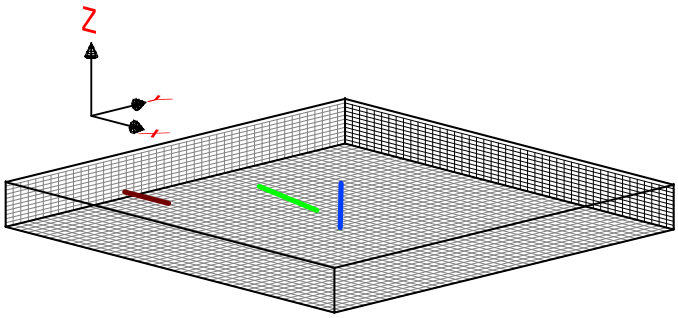

(a) Initial guess 1

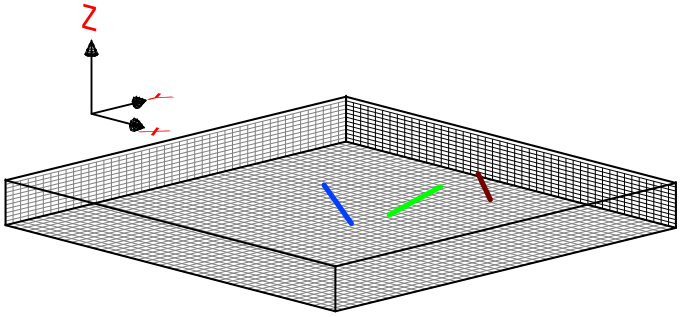

(b) Initial guess 2

Figure 5.23: The initial and final well locations and trajectories, Homogeneous reservoir layers, Example 2, Case 1. The initial well trajectory is shown with a red line and the estimated optimal well trajectories for the first production scenario (depletion) and the second production scenario (water injection) are shown with a green line and a blue line, respectively.

listed in Table 5.7. Note that in Fig. 5.23, only the part of the well trajectory inside the reservoir is plotted, however, in Table 5.7, the full length of the well (including the part of the well which may locate outside the reservoir) is listed.

We first consider the primary depletion scenario. Although the estimated well parameters obtained for the two initial guesses are not similar, the estimated optimal NPV's from the two initial guesses are identical. Since the sandstone layers are separated by shale layers, simple reservoir physics dictates the optimal inclination angle, φ_w, should be such that the well penetrates all reservoir layers and our algorithm achieves this results in both cases which is essentially apparent from the results of Table 5.7. The well vertical inclination angle is changed from 90 degrees to 65.2 degrees in the optimization run with initial guess 1 and from 30 degrees to

Table 5.7: The initial and final well trajectory parameters corresponding to the optimization runs with the two initial guesses, Homogeneous reservoir layers, Example 2, Case 1.

		Well trajectory parameters
Initial Guess 1	Initial	$(475, 475, 10054, 300, 0, 90)$
	Final - No water injection	$(855.4, 1039.4, 10107.6, 500.0, 100.7, 65.2)$
	Final - With water injection	$(1125.5, 1131.3, 10085.9, 477.3, 0.0, 178.3)$
Initial Guess 2	Initial	$(1475, 1725, 10054, 200, 90, 30)$
	Final - No water injection	$(1354.6, 1398.3, 10098.4, 419.5, 179.7, 59.9)$
	Final - With water injection	$(1141.1, 1083.5, 10093.4, 264.2, 67.7, 34.6)$

59.9 in the optimization run with initial guess 2 and the length of the well increased during optimization runs with both initial guesses so that the final trajectory of the well penetrates all reservoir layers. Also, the well is moved toward the center of the reservoir, however, the final location of the well's center point is not exactly at the center of the reservoir which is $(x, y, z) = (1125, 1125, 10110)$ ft, as the NPV is not very sensitive to the spatial location of the well in the x and y directions for the one year reservoir life specified for this problem. This is obvious because although in the final well locations of the optimization runs with the two initial guesses the well center point locations are different, but the final NPVs are identical.

In the second scenario (water injection scenario), the well is moved to the center of the reservoir during the optimization run for both initial guesses, as this location is the farthest distance from all the injection wells and the specified reservoir life is longer in this case. The final trajectory of the well for the optimization run with the first initial guess is vertical and penetrates all reservoir layers. For the optimization run with the second initial guess, the inclination angle is 34 degrees but the well still penetrates all reservoir layers. Note that a vertical or close to vertical final trajectory of the well gives a perfect water flood of all reservoir layers with

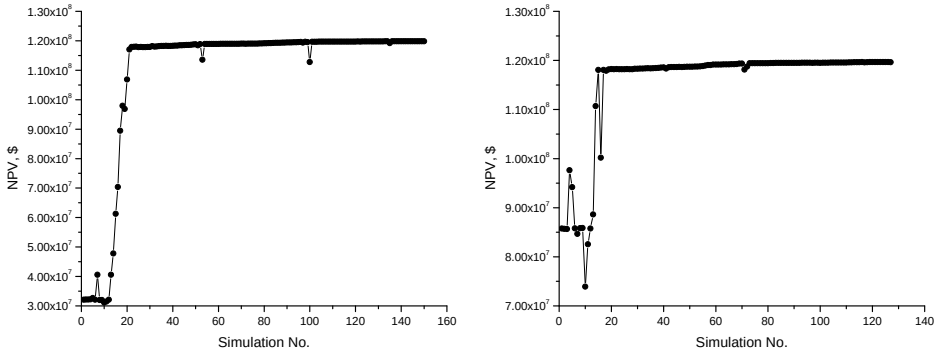

(a) Initial guess 1 (b) Initial guess 2

Figure 5.24: The plot of NPV versus the reservoir simulation runs for the no water injection scenario, Homogeneous reservoir layers, Example 2, Case 1.

minimal water production. The estimated NPV obtained with the first initial guess ($\$8.63 \times 10^8$) is slightly greater than the estimated optimal NPV with the second initial guess ($\$8.41 \times 10^8$). For the purpose of comparison, we evaluate the NPV of a possible trial solution by the Schedule method for a fully penetrating vertical production well at the center of the reservoir. The NPV for this trial solution is $\$8.63 \times 10^8$ which is identical to our estimated NPV with initial guess 1; see Table 5.6.

The NPV versus the reservoir simulation runs for the first production scenario (depletion) and the second production scenario (water injection) are shown in Figs. 5.24 and 5.25, respectively. Figs. 5.24(a) and Figs. 5.25(a) correspond to the optimization runs with the first initial guess and Figs. 5.24(b) and Figs. 5.25(b) correspond to the optimization runs with the second initial guess. One interesting feature found from a detailed examination of the iterations shown in Figs. 5.24(a) and 5.24(b) is that the early iterations in these plots correspond to the iterations where the change in the well trajectory is mostly in the vertical orientation angle of the well. The later iterations in these figures correspond to iterations where the changes in the trajectory of the well are mostly in the location of its center point in the $x - y$ plane. As we see, we obtain only small improvements in NPV at later iterations which indicates that the NPV is less sensitive to the location of the well than to the vertical inclination angle of the well trajectory.

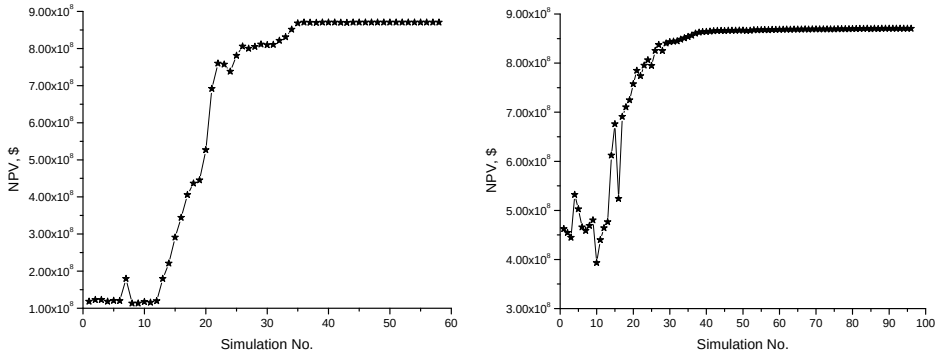

(a) Initial guess 1 (b) Initial guess 2

Figure 5.25: The plot of NPV versus the reservoir simulation runs for the production scenario with water injection, Homogeneous reservoir layers, Example 2, Case 1.

Case 2- Heterogeneous Reservoir Layers: In this case, the sandstone reservoir layers of the simulation model have heterogenous porosity and permeability fields. We use the same k_x and porosity fields shown in Figs. 5.14 and 5.15 for the reservoir layers and assume that the reservoir layers are isotropic, i.e., $k_x = k_y = k_z$. The summary of the optimization runs for both production scenarios for the reservoir with heterogenous layers are shown in Table 5.8. The results are consistent with those obtained in the homogenous reservoir layer case and are self explanatory.

The initial and final well locations and trajectories of the optimization runs

Table 5.8: The summary of the optimization runs for both scenarios, Heterogeneous reservoir layers, Example 2, Case 2.

		Depletion (No water injection)	With water injection
Initial Guess 1	Initial NPV, Schedule	$\$3.81 \times 10^7$	$\$7.03 \times 10^7$
	Initial NPV	$\$3.12 \times 10^7$	$\$1.18 \times 10^8$
	Final NPV	$\$1.18 \times 10^8$	$\$8.48 \times 10^8$
	Final NPV, Schedule	$\$1.20 \times 10^8$	$\$8.26 \times 10^8$
	No. of Sim. runs	67	82
Initial Guess 2	Initial NPV, Schedule	$\$9.60 \times 10^7$	$\$3.67 \times 10^8$
	Initial NPV	$\$8.65 \times 10^7$	$\$4.29 \times 10^8$
	Final NPV	$\$1.18 \times 10^8$	$\$8.37 \times 10^8$
	Final NPV, Schedule	$\$1.19 \times 10^8$	$\$8.07 \times 10^8$
	No. of Sim. runs	33	86

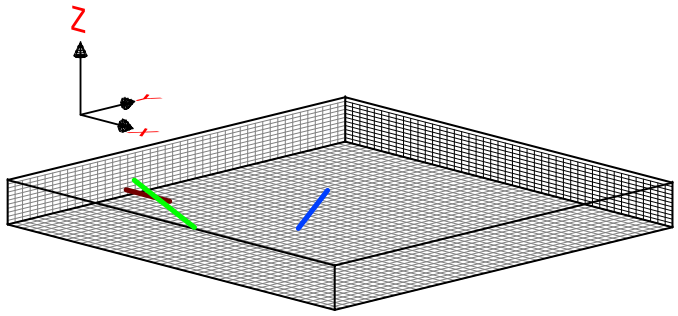

(a) Initial guess 1

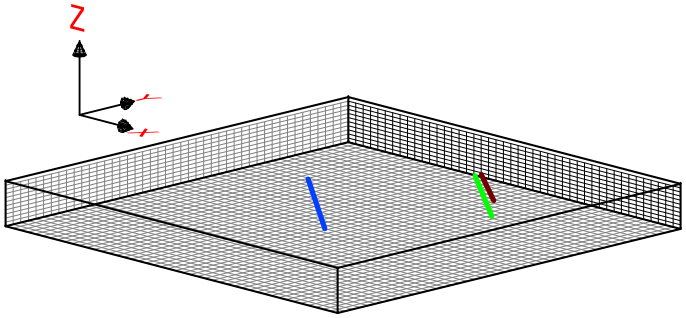

(b) Initial guess 2

Figure 5.26: The initial and final well locations and trajectories, Heterogeneous reservoir layers, Example 2, Case 2. The initial well trajectory is shown with a red line and the estimated optimal well trajectories for the first production scenario (depletion) and the second production scenario (water injection) are shown with a green line and a blue line, respectively.

with initial guesses 1 and 2 are shown in Fig. 5.26(a) and Fig. 5.26(b), respectively. The initial well trajectories are shown with a red line and the final well trajectories for the first production scenario (depletion) and the second production scenario (water injection) are shown with a green line and a blue line, respectively. The initial and final well trajectory parameters corresponding to the optimization runs with the two initial guesses are listed in Table 5.9. Note that in Fig. 5.26, only the part of the well trajectory inside the reservoir is plotted, however, in Table 5.9, the full length of the well (including the part of the well which may locate outside the reservoir) is listed.

We first consider the primary depletion scenario. The estimated location of the well is close to its initial location for both initial guesses. Yet even though

Table 5.9: The initial and final well trajectory parameters corresponding to the optimization runs with the two initial guesses, Heterogeneous reservoir layers, Example 2, Case 2.

		Well trajectory parameters
Initial Guess 1	Initial	$(475, 475, 10054, 300, 0, 90)$
	Final - No water injection	$(528.5, 508.0, 10096.5, 335.7, 35.4, 53.0)$
	Final - With water injection	$(1181.8, 960.5, 10029.4, 489.6, 4.2, 139.6)$
Initial Guess 2	Initial	$(1475, 1725, 10054, 200, 90, 30)$
	Final - No water injection	$(1465.3, 1715.0, 10105.6, 263.8, 92.4, 27.8)$
	Final - With water injection	$(1074.0, 1051.7, 10212.6, 498.9, 0.0, 27.3)$

the estimated optimal locations in Figs. 5.26(a) and 5.26(b) are quite different, the estimated optimal NPV value is $\$1.18 \times 10^8$ for both initial guesses; see Table 5.8. Similar to the explanation given for the homogenous reservoir layer case, we expect that the optimal inclination angle, φ_{w}, be such that the well penetrates all reservoir layers. Our algorithm achieves this results in both cases; see Table 5.9. For example, with initial guess 1, $\varphi_{\mathrm{w}} = 90$ degrees, i.e., the well is horizontal which is clearly not optimal but the estimated optimal value of this inclination angle is $\varphi_{\mathrm{w}} = 53$ degrees so with the estimated length $l_{\mathrm{w}} = 335.7$ ft, the estimated optimal well penetrates all reservoir layers. The fact that the well is not moved towards the center of the reservoir during optimization is a consequence of the heterogenous permeability field of the reservoir.

Next we consider the results for the scenario where there are four completely-perforating vertical water injection wells at the four corners of the reservoir. Unlike the primary depletion case, the well location is changed radically by applying the optimization algorithm. Specifically the final well location for both initial guesses is fairly near the center of the reservoir (Figs. 5.26(a) and 5.26(b)) which is the expected results as this makes the well roughly equidistant from the injectors. Recall that the

permeability and porosity fields are heterogenous, so there is no reason to expect that the optimal location is exactly at the center. We evaluate the NPV of a possible trial solution by the Schedule method, for a vertical production well at the center of the reservoir which penetrates all reservoir layers. The NPV for this trial solution is $\$7.96 \times 10^8$ which is smaller than our estimated NPV with both initial guesses (8.26×10^8 for initial guess 1 and 8.07×10^8 for initial guess 2). Moreover, although the two initial guesses yield significantly different estimates of the optimal values of some well parameters (Table 5.9), the estimated optimal NPV value for the two initial guesses are quite close (8.48×10^8 for initial guess 1 and 8.37×10^8 for initial guess 2); see Table 5.8. Finally, we note that the results of Table 5.9 include that the estimated optimal production well penetrates all layers as expected.

For completeness, the plots of NPV versus the simulation run index are shown in Figs. 5.27 and 5.28. Figs. 5.27(a) and Figs. 5.28(a) correspond to the optimization runs with the first initial guess and Figs. 5.27(b) and Figs. 5.28(b) correspond to the optimization runs with the second initial guess.

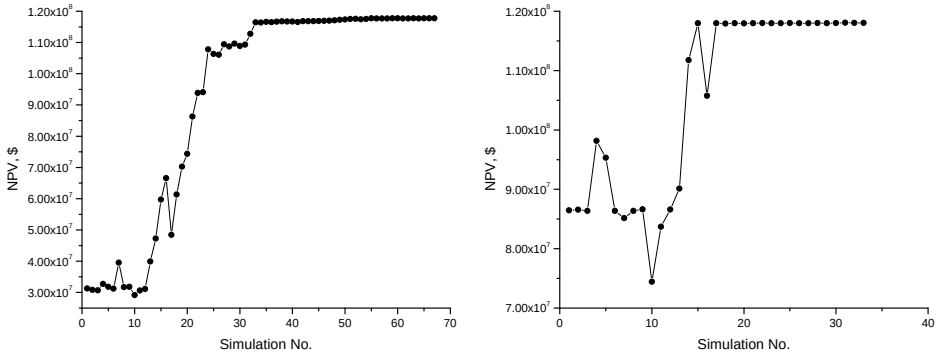

(a) Initial guess 1 (b) Initial guess 2

Figure 5.27: The plot of NPV versus the reservoir simulation runs for the no water injection scenario, Heterogeneous reservoir layers, Example 2, Case 2.

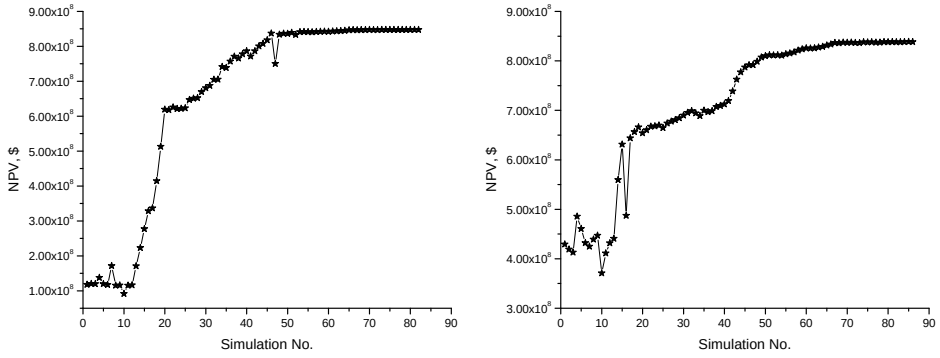

(a) Initial guess 1 (b) Initial guess 2

Figure 5.28: The plot of NPV versus the reservoir simulation runs for the production scenario with water injection, Heterogeneous reservoir layers, Example 2, Case 2.

5.6.3 Example 3. Optimization of the Trajectory of Multiple Production Wells in an Anticline Reservoir with Aquifer

In this example, we consider an anticline reservoir. The reservoir model is a three-dimensional $2000 \times 6500 \times 500$ ft ($40 \times 130 \times 10$ gridblocks) simulation model. Gridblock sizes are 50 ft in both horizontal and vertical directions. The initial reservoir datum pressure is $3,500$ psi at the datum depth of $5,000$ ft and the depth of the water oil contact is $5,300$ ft. The schematic of the reservoir, the depths of the reservoir top surface, bottom surface and the depth of the water-oil contact are shown in Fig. 5.29. The reservoir has heterogeneous permeability and porosity fields. The horizontal log-permeability and porosity fields of the first simulation layer of the reservoir are given in Fig. 5.30. Porosity and permeability of all reservoir layers are identical to layer 1. The vertical permeability is $k_v = 0.1k_h$.

We consider two cases. In the first case, there is a strong aquifer connected to the north edge as well as a strong aquifer connected to the south edge of the reservoir. In the second case, only the aquifer connected to the south edge of the reservoir is active. In this example, the aquifers are numerical aquifers, i.e., the pore volumes of the gridblocks below the water-oil contact are multiplied by a large number. In both cases, we try to optimize the location, length and trajectory of two production wells in the reservoir. In both cases, the reservoir life is 5 years and both production

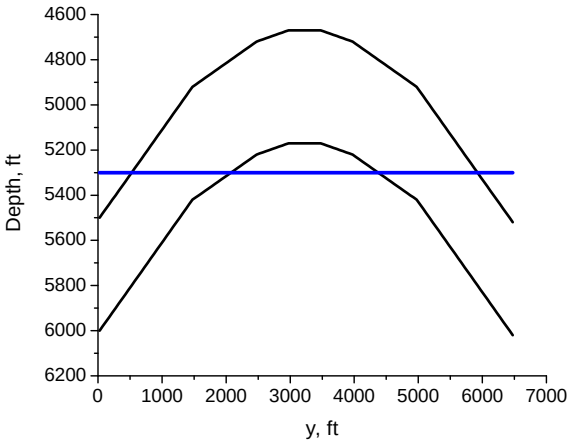

Figure 5.29: The schematic of the structure of the reservoir, Example 2.

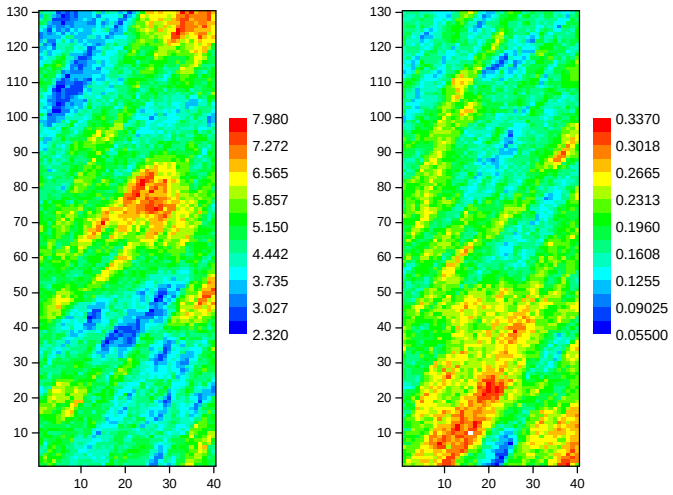

(a) log-permeability field (b) porosity field

Figure 5.30: The horizontal log-permeability and porosity fields of the first simulation layer of the reservoir, Example 2.

wells operate on constant specified bottomhole pressure of $1,500$ psi. The maximum length for the production wells in both cases is 500 ft.

Similar to the previous examples, we use BOBYQA to solve the optimization problem with two different initial guesses. However for this example, we also compare results obtained with BOBYQA with those obtained from an implementation of the GA. The genetic algorithm implementation that we use is based on the binary representation of the optimization variables. We choose 64, 128, 32, 32, 16 and 16

for the number of intervals for the optimization parameters x_w y_w, z_w, l_w, θ_w and φ_w, respectively. These values are chosen based on the number of reservoir gridblocks in the domain of each optimization parameters for x_w y_w, z_w and l_w parameters. Choosing 16 for the number of intervals for the deviation angle parameters implies that the resolution of these parameters are $180/16 = 11.2$ degrees. The number of the optimization variables are $6 \times 2 = 12$. For the GA, we choose 20 and 50 for the population size and the number of generations, respectively. Note that for the fairly small number of optimization variables (n=12), running GA with the population size of 20 for 50 generations is a conservative and costly choice of these parameters.

As recommended in the GA code (Carroll [8]), we use the options of elitism to be invoked (best individual replicated into the next generation). We also use the uniform crossover option with two children per pair of parents. A range of values for the GA parameters are addressed in the literature. Here we try two sets of values for the crossover probability (p_c) and mutation probability (p_m). The two choices for GA parameters are shown in Table 5.10. In set 1, we choose the crossover and mutation probability values of 0.5 and 0.1, respectively. GA with set 1 parameters tends to investigate the search domain more randomly (large value of p_m) looking for a global optimum. With this setting, there is a lower risk of being trapped in a local optimum but convergence usually takes longer. In parameter set 2, we choose the crossover and mutation probability values of $p_c = 0.7$ and $p_m = 0.05$, respectively. The GA run with this set of parameters tends to generate less random solutions and is more likely to improve the solutions of previous generations to reach convergence faster, but may be less likely to find a global optimum.

Case 1- Aquifers at both North and South Edges of the Reservoir are Active: The pore volume of the aquifer gridblocks (the gridblocks which are located below the water-oil contact) at both the north and south edges of the reservoir are multiplied by 300 to make the aquifers active and strong. Two production wells are subject

Table 5.10: The choices for GA parameters, Example 3.

	Parameter set 1	Parameter set 2
No. of generations	50	50
Population size	20	20
Crossover probability, p_c	0.5	0.7
Mutation probability, p_m	0.1	0.05

to the optimization. Similar to the previous examples, we run our well-placement optimization algorithm with two different initial guesses for the well trajectory parameters. The optimization using BOBYQA converged after 114 and 96 simulation runs for the optimization runs with the first and second initial guesses. The NPV increased from $\$3.20\times10^9$ to $\$3.83\times10^9$ for the optimization run with the first initial guess, and from $\$3.37\times10^9$ to $\$3.79\times10^9$ for the optimization run with the second initial guess, respectively.

A summary of the BOBYQA results with both initial guesses and the GA runs with both sets of parameters are shown in Table 5.11. The initial and final well trajectory parameters for both production wells are summarized in Table 5.12 and 5.13 for the BOBYQA and GA runs, respectively. Note that although the final NPVs of GA and BOBYQA are close, the final trajectories are not very similar. Here, we used GA as a global search optimizer to investigate the performance of BOBYQA for solving the optimization problem. In general, we can say BOBYQA obtains a close estimate of the optimum NPV obtained with the GA but BOBYQA obtained this optimum with far fewer reservoir simulator runs than were required by the GA. It is important to note that the main contribution of our work is our procedure for modeling wells and for determining optimization parameters; any optimization algorithm can be used. Note, however, that the final solution obtained with BOBYQA depends on the initial guess, which suggests that using several initial guesses may be a good strategy for applying our well-placement methodology. Note, based on the results of Table 5.11, we could estimate optimum parameters with BOBYQA for sev-

Table 5.11: The summary of BOBYQA and GA runs, Example 3, Case 1.

	BOBYQA		GA	
	Init. guess 1	Init. guess 2	Param. set 1	Param. set 2
Initial NPV, Schedule	$\$2.93 \times 10^9$	$\$3.16 \times 10^9$	-	-
Initial NPV	$\$3.20 \times 10^9$	$\$3.37 \times 10^9$	-	-
Final NPV	$\$3.83 \times 10^9$	$\$3.79 \times 10^9$	$\$3.84 \times 10^9$	$\$3.86 \times 10^9$
Final NPV, Schedule	$\$3.82 \times 10^9$	$\$3.74 \times 10^9$	$\$3.80 \times 10^9$	$\$3.84 \times 10^9$
No. of Sim. runs	114	96	1000	1000

Table 5.12: The initial and final well trajectory parameters $(x_{\mathrm{w}}, y_{\mathrm{w}}, z_{\mathrm{w}}, l_{\mathrm{w}}, \theta_{\mathrm{w}}, \varphi_{\mathrm{w}})$ for both production wells in BOBYQA optimization runs, Example 3, Case 1.

			Well parameters
Initial Guess 1	Prd-1	Initial	$(475.0, 2775.0, 4915.0, 150.0, 45.0, 45.0)$
		Final	$(934.8, 2952.5, 4831.8, 367.7, 59.2, 0.0)$
	Prd-2	Initial	$(1475.0, 3225.0, 4895.0, 150.0, 45.0, 45.0)$
		Final	$(1493.7, 3267.6, 4733.4, 283.5, 40.1, 4.7)$
Initial Guess 2	Prd-1	Initial	$(975.0, 2475.0, 4945.0, 150.0, 45.0, 45.0)$
		Final	$(1109.9, 2659.8, 4822.2, 500.0, 52.0, 32.6)$
	Prd-2	Initial	$(975.0, 3475.0, 4895.0, 150.0, 45.0, 45.0)$
		Final	$(941.4, 3361.5, 4806.9, 321.5, 88.6, 4.8)$

eral different initial guesses faster than applying the GA once. Moreover, the choice of parameters to reach convergence to a global optimum as efficiently as possible can be challenging with the GA optimization algorithm.

The schematic of the reservoir and the initial and final well locations of BOBYQA optimization runs with the initial guesses 1 and 2 are shown in Figs. 5.31(a) and 5.31(b). The initial well trajectories are shown with dots and the final well trajectories are shown in lines. Each production well is shown with a different color. We see in both figures that the well locations are modified, also the length of both wells are increased significantly. Moreover, the final trajectories of both wells are very close to vertical except for well P-1 for the run with the second initial guess, which has an inclination angle of 32.6 degrees from the vertical. The best locations of the production wells with the GA optimization runs with the parameter sets 1

Table 5.13: The well trajectory parameters $(x_w, y_w, z_w, l_w, \theta_w, \varphi_w)$ corresponding to the estimate of optimal solutions for both production wells of GA optimization runs, Example 3, Case 1.

		Estimate of optimal well parameters
Parameter set 1	Prd-1	$(1523.8, 3161.4, 4815.2, 306.8, 180.0, 0.0)$
	Prd-2	$(634.9, 3267.7, 4750.7, 355.1, 180.0, 12.0)$
Parameter set 2	Prd-1	$(603.2, 3338.6, 4799.0, 483.9, 108.0, 156.0)$
	Prd-2	$(1333.3, 3409.5, 4702.3, 483.9, 96.0, 120.0)$

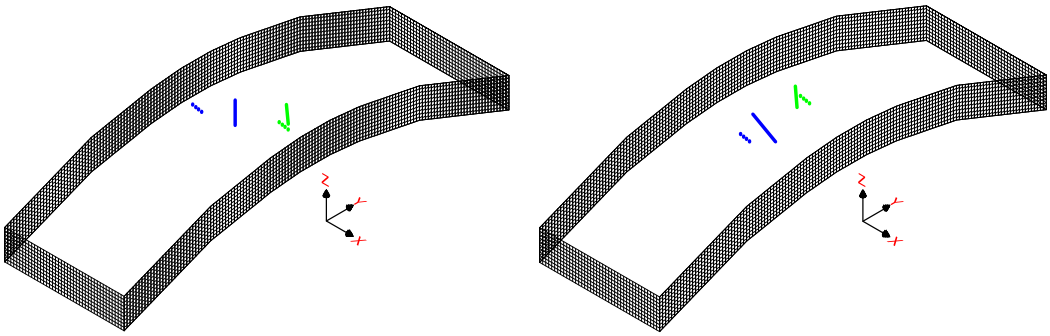

(a) Initial guess 1 (b) Initial guess 2

Figure 5.31: The schematic of the structure of the reservoir and the initial and final well locations and trajectories of BOBYQA optimization runs, Example 3, Case 1. The initial well trajectories are shown with dots and the final well trajectories are shown in lines. Production well P-1 is shown in blue and production well P-2 is shown in green.

and 2 are shown in Figs. 5.32(a) and 5.32(b), respectively. As can also be seen by comparing the results of Figs. 5.31 and 5.32 and the results of Tables 5.12 and 5.13, the estimated optimal wells from GA and BOBYQA are quite different even though both algorithms yield a similar estimation of the optimal NPV (Table 5.11).

The plot of NPV versus the number of simulation runs is given in Figs. 5.33(a) and 5.33(b) for the BOBYQA optimization with initial guesses 1 and 2, respectively. The first 25 simulation runs in Figs. 5.33(a) and 5.33(b) correspond to the simulation runs required to build the initial interpolation set in the BOBYQA optimization algorithm (we use $m = 2n + 1 = 25$ for the number of initial interpolation points). The NPV plots for the optimization runs with GA with parameter sets 1 and 2 are

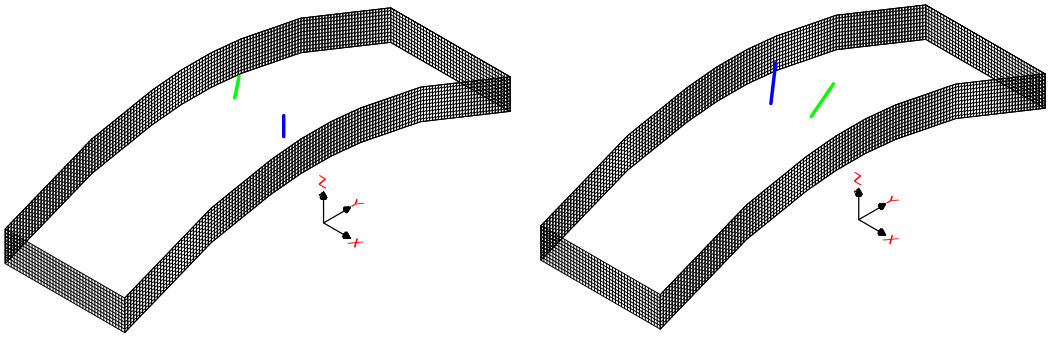

(a) Parameter set 1 (b) Parameter set 2

Figure 5.32: The well locations and trajectories corresponding to the estimates of optimal solutions with GA optimization runs, Example 3, Case 1.

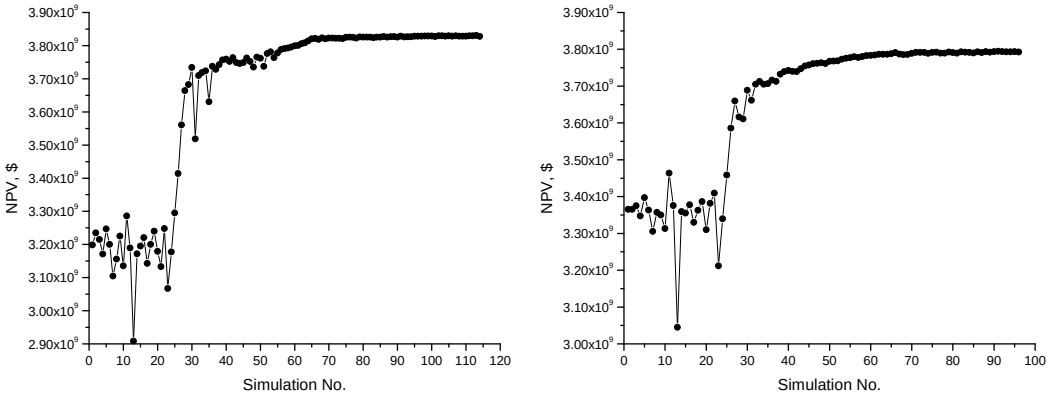

(a) Initial Guess 1 (b) Initial Guess 2

Figure 5.33: The plot of NPV versus the number of simulation runs for the optimization runs using BOBYQA, Example 3, Case 1.

shown in Figs. 5.34(a) and 5.34(b), respectively. The best NPV from GA with $1,000$ simulation runs are $\$3.84 \times 10^9$ and $\$3.86 \times 10^9$ for GA runs with the parameter sets 1 and 2, respectively. In Figs. 5.34(a) and 5.34(b), the black dots show the NPV of individuals at all generations. The blue line shows the plot of average NPV of the generations and the red line shows the maximum NPV of each generation.

Case 2- Only the South Edge Aquifer is Active: In this case, the pore volume of the aquifer gridblocks in the south edge of the reservoir (the gridblocks at south edge of the reservoir which are located below the water-oil contact) are multiplied by 300 to make the aquifer strong and active in the south edge of the reservoir.

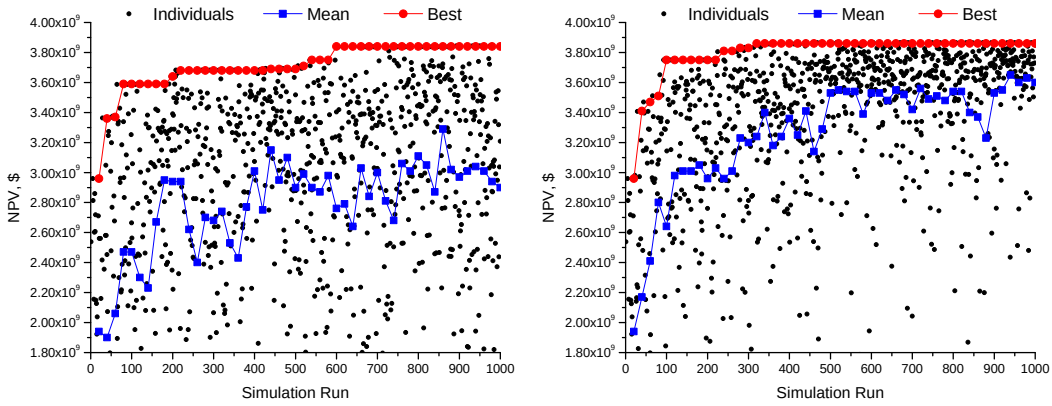

(a) Parameter set 1

(b) Parameter set 2

Figure 5.34: The plot of NPV versus the number of simulation runs for the optimization runs using GA, Example 3, Case 1. The black dots show the NPV of individuals at all generations. The blue line shows the plot of average NPV of the generations and the red line shows the maximum NPV of each generation.

The pore volume of the aquifer gridblocks in the north edge of the reservoir are multiplied by 1 (remained unchanged). Similar to Case 1, two production wells are considered for the optimization and we use two different initial guesses for the trajectory parameters of the wells. Note that the initial guesses are different than the ones chosen for Case 1. As we mentioned before both production wells operate on specified bottomhole pressure of 1,500 psi and the reservoir life is 5 years. With initial guess 1, the optimization converged after 181 simulation runs and NPV increased from $\$2.09 \times 10^9$ to $\$2.75 \times 10^9$ during the optimization process. The optimization with initial guess 2 converged after 77 simulation runs and NPV increased from $\$2.14 \times 10^9$ to $\$2.71 \times 10^9$. Note that the values of estimated NPV for the two initial guesses are very close. A summary of the BOBYQA and GA results are shown in Table 5.14. Note that the four estimates of the optimal NPV are very close but BOBYQA used far fewer simulation runs than were used by GA.

The initial and final well locations of the BOBYQA optimization runs with both initial guesses are shown in Figs. 5.35(a) and 5.35(b) with the initial well trajectories shown with dots and the final well trajectories shown as lines. Each production well is shown with a different color. The final trajectories of the wells are almost

Table 5.14: The summary of BOBYQA and GA runs, Example 3, Case 2.

	BOBYQA		GA	
	Init. guess 1	Init. guess 2	Param. set 1	Param. set 2
Initial NPV, Schedule	$\$1.81 \times 10^9$	$\$1.82 \times 10^9$	-	-
Initial NPV	$\$2.09 \times 10^9$	$\$2.14 \times 10^9$	-	-
Final NPV	$\$2.75 \times 10^9$	$\$2.71 \times 10^9$	$\$2.75 \times 10^9$	$\$2.75 \times 10^9$
Final NPV, Schedule	$\$2.74 \times 10^9$	$\$2.71 \times 10^9$	$\$2.74 \times 10^9$	$\$2.74 \times 10^9$
No. of Sim. runs	181	77	1000	1000

Table 5.15: The initial and final well trajectory parameters $(x_{\mathrm{w}}, y_{\mathrm{w}}, z_{\mathrm{w}}, l_{\mathrm{w}}, \theta_{\mathrm{w}}, \varphi_{\mathrm{w}})$ for both production wells in BOBYQA optimization runs, Example 3, Case 2.

			Well parameters
Initial Guess 1	Prd-1	Initial	$(475.0, 2975.0, 4895.0, 150.0, 45.0, 45.0)$
		Final	$(966.1, 3373.0, 4810.5, 342.4, 105.8, 9.5)$
	Prd-2	Initial	$(1475.0, 2975.0, 4895.0, 150.0, 45.0, 45.0)$
		Final	$(1256.9, 3717.5, 4807.4, 312.6, 83.5, 27.4)$
Initial Guess 2	Prd-1	Initial	$(475.0, 4475.0, 5045.0, 150.0, 45.0, 45.0)$
		Final	$(623.2, 4698.3, 5069.7, 198.0, 64.8, 8.2)$
	Prd-2	Initial	$(1475.0, 4475.0, 5045.0, 150.0, 45.0, 45.0)$
		Final	$(1247.1, 4190.3, 5000.4, 279.1, 56.4, 1.7)$

vertical, except for well P-2 with the first initial guess, where we obtained $\varphi_{\mathrm{w}} = 27.4$ degrees; see Table 5.15. Note that for both initial guesses, the optimal well locations are closer to the north edge of the reservoir than the south edge, which is as expected because the only active aquifer is at the south edge. Despite this, for initial guess 2, well P-2 in green in Fig. 5.35(b) was moved towards the south during the optimization process. The best locations of the production wells with GA optimization runs with the parameter sets 1 and 2 are shown in Figs. 5.36(a) and 5.36(b), respectively. The initial and final well trajectory parameters for both production wells are summarized in Table 5.15 for BOBYQA and in 5.16 for the GA runs, respectively. For parameter set 2, the GA places the two producers close together (Fig. 5.34) but orientation angles, θ_{w} and φ_{w}, for the two producers are quite different; see Table 5.16.

Table 5.16: The well trajectory parameters $(x_w, y_w, z_w, l_w, \theta_w, \varphi_w)$ corresponding to the estimate of optimal solutions for both production wells of GA optimization runs, Example 3, Case 2.

		Estimate of optimal well parameters
Parameter set 1	Prd-1	$(1142.9, 4047.2, 4923.6, 162.0, 156.0, 0.0)$
	Prd-2	$(1015.9, 3692.9, 4835.2, 435.6, 12.0, 144.0)$
Parameter set 2	Prd-1	$(1142.9, 3976.4, 4832.9, 451.7, 120.0, 12.0)$
	Prd-2	$(1142.9, 3763.8, 4796.8, 467.8, 12.0, 144.0)$

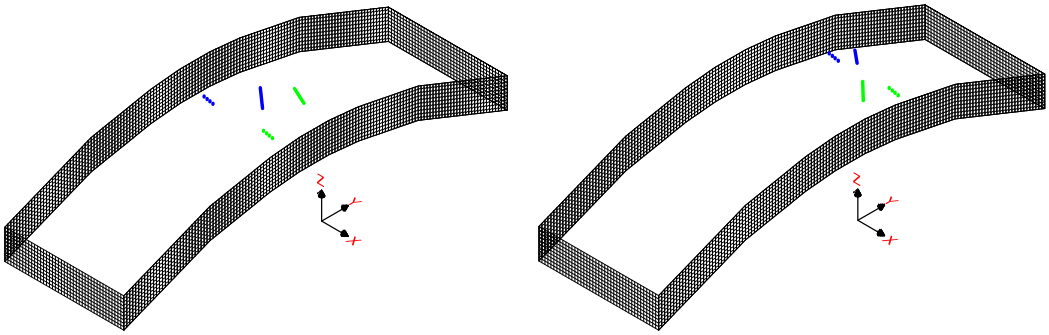

(a) Initial guess 1 (b) Initial guess 2

Figure 5.35: The schematic of the structure of the reservoir and the initial and final well locations and trajectories of BOBYQA optimization runs, Example 3, Case 2. The initial well trajectories are shown with dots and the final well trajectories are shown in lines. Production well P-1 is shown in blue and production well P-2 is shown in green.

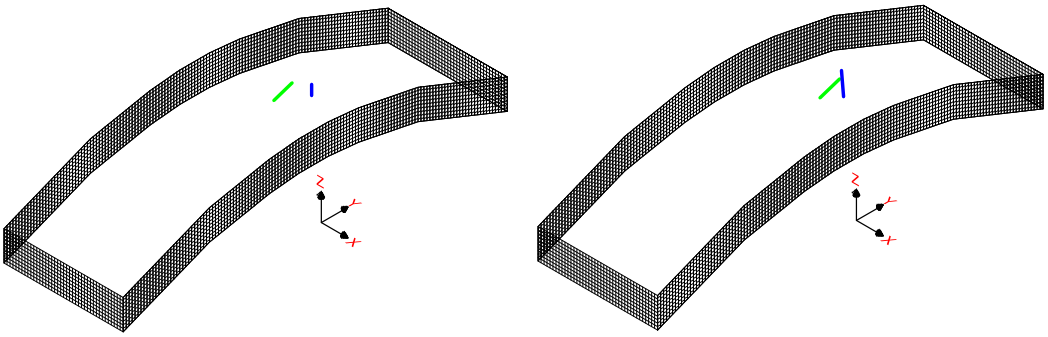

(a) Parameter set 1 (b) Parameter set 2

Figure 5.36: The well locations and trajectories corresponding to the estimates of optimal solutions with GA optimization runs, Example 3, Case 2.

The plot of NPV versus the number of simulation runs is given in Figs. 5.37(a) and. 5.37(b) for the BOBYQA runs with the first and the second initial guesses. The first 25 simulation runs correspond to the simulation runs required to build the initial interpolation set in the BOBYQA optimization algorithm. The NPV plots for the optimization runs of GA with parameter sets 1 and 2 are shown in Figs. 5.38(a) and 5.38(b), respectively, where the best NPV from GA runs after $1,000$ simulation runs is $\$2.75 \times 10^9$. In Figs. 5.38(a) and 5.38(b), the black dots show the NPV of individuals at all generations. The blue line shows the plot of average NPV of the generations and the red line shows the maximum NPV of each generation.

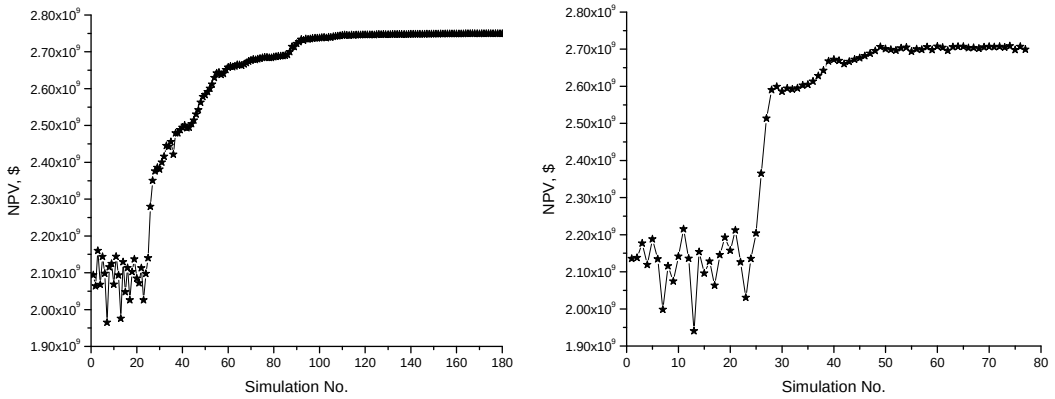

(a) Initial Guess 1 (b) Initial Guess 2

Figure 5.37: The plot of NPV versus the number of simulation runs for the optimization runs using BOBYQA, Example 3, Case 2.

5.6.4 Example 4. The Optimization of the Trajectory of Production and Injection Wells in the PUNQ Simulation Model

In this example we consider the optimization of the locations and trajectories of the production and injection wells in the PUNQ reservoir. The PUNQ model has analytical aquifers attached to the north, west and south edges of the reservoir. Since the PUNQ simulation model gridblock sizes in the x and y directions are large, we refine the simulation grid in these directions. Each gridblock of the original PUNQ simulation model is refined to 9 gridblocks by decreasing both Δx and Δy by a

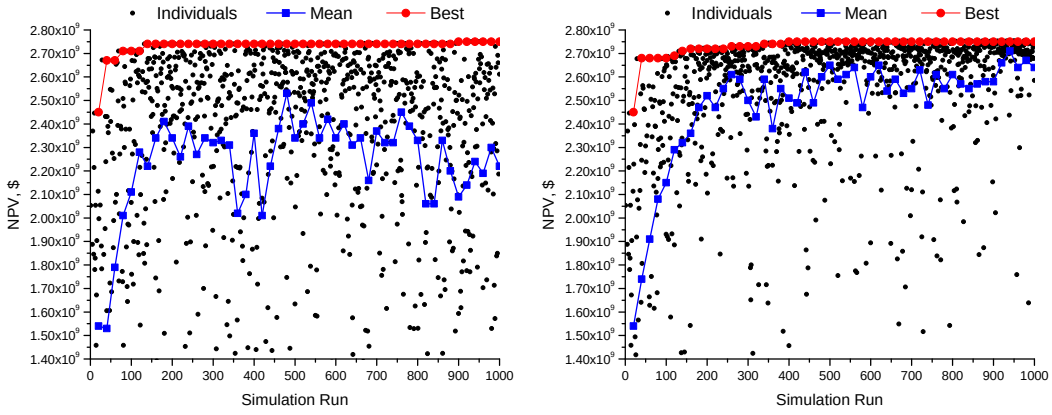

(a) Parameter set 1 (b) Parameter set 2

Figure 5.38: The plot of NPV versus the number of simulation runs for the optimization runs using GA, Example 3, Case 2. The black dots show the NPV of individuals at all generations. The blue line shows the plot of average NPV of the generations and the red line shows the maximum NPV of each generation.

factor of three. The horizontal permeability, vertical permeability and porosity fields of 5 reservoir layers are shown in Figs. 5.39 to 5.41. We present two cases in this example. In Case 1, we optimize the trajectories of the six production wells in the PUNQ reservoir. In Case 2, we remove the analytical aquifers of the reservoir and we optimize the trajectories of six production wells and three water injection wells in the reservoir.

Case 1. Optimization of the Trajectory of Six Production Wells: We wish to optimize the locations and trajectories of six production wells. The production wells are bottomhole pressure-controlled with the specified bottomhole pressure equal to 1,500 psi at all producers. The production period of the reservoir is 20 years. We

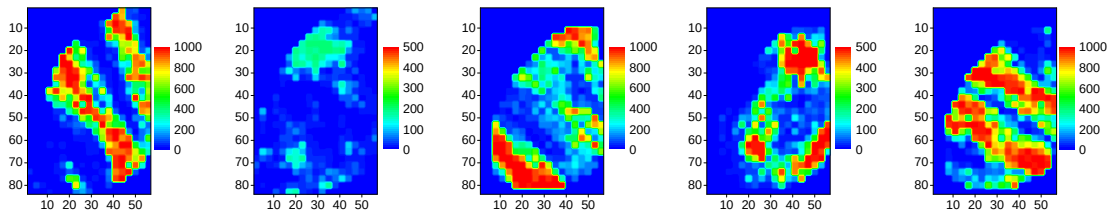

(a) Layer 1 (b) Layer 2 (c) Layer 3 (d) Layer 4 (e) Layer 5

Figure 5.39: The horizontal permeability field of the PUNQ reservoir, Example 4.

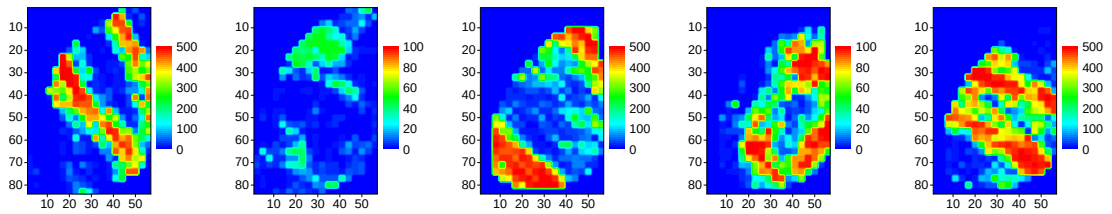

(a) Layer 1 (b) Layer 2 (c) Layer 3 (d) Layer 4 (e) Layer 5

Figure 5.40: The vertical permeability field of the PUNQ reservoir, Example 4.

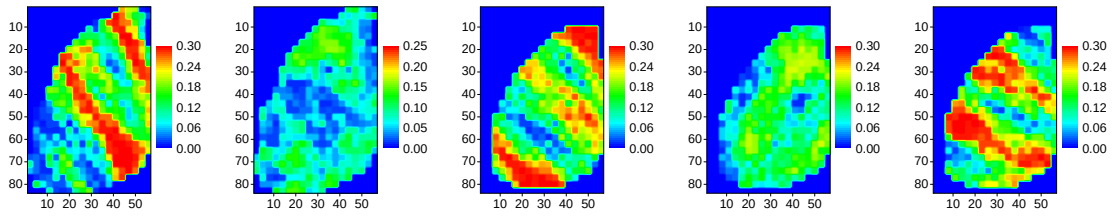

(a) Layer 1 (b) Layer 2 (c) Layer 3 (d) Layer 4 (e) Layer 5

Figure 5.41: The porosity field of the PUNQ reservoir, Example 4.

consider two initial guesses of the initial well trajectory parameters. In initial guess 1, we set the initial well center points of the six producers at the original PUNQ production well locations. In the second initial guess, we use completely arbitrary locations for the well center points. In both initial guesses, the initial orientation angles of the wells are chosen fairly arbitrarily but close to horizontal. Each well has 6 parameters and therefore, there are $n = 36$ optimization variables. BOBYQA needs $n + 2 \leq m \leq [(n + 1)(n + 2)]/2$ simulation runs to build the first quadratic approximation of the objective function. Here in this example, we try choices of $m = n + 2$ and $m = 2n + 1$. The results of the optimization runs for both initial guesses are summarized in Table 5.17, with the plot of NPV versus the number of reservoir simulation runs for both trials are shown in Fig. 5.42. From the results of Fig. 5.42 and Table 5.17, we see that the estimate of the optimal NPV depends more strongly on the initial guesses where $m = 2n + 1$. We have no explanation for this behavior and at this point do not know if this is a general result or only applies to this example. The most important result is that in all cases, we obtained a significant improvement in NPV by optimization.

Table 5.17: The summary of optimization runs for optimizing production wells in the PUNQ model, Example 4, Case 1.

	Initial guess 1		Initial guess 2	
	$m = n + 2$	$m = 2n + 1$	$m = n + 2$	$m = 2n + 1$
Initial NPV, Schedule	$\$3.05 \times 10^9$	$\$3.05 \times 10^9$	$\$2.64 \times 10^9$	$\$2.64 \times 10^9$
Initial NPV	$\$3.07 \times 10^9$	$\$3.07 \times 10^9$	$\$2.67 \times 10^9$	$\$2.67 \times 10^9$
Final NPV	$\$3.71 \times 10^9$	$\$3.78 \times 10^9$	$\$3.62 \times 10^9$	$\$3.44 \times 10^9$
Final NPV, Schedule	$\$3.54 \times 10^9$	$\$3.63 \times 10^9$	$\$3.50 \times 10^9$	$\$3.30 \times 10^9$
No. of Sim. runs	157	327	172	314

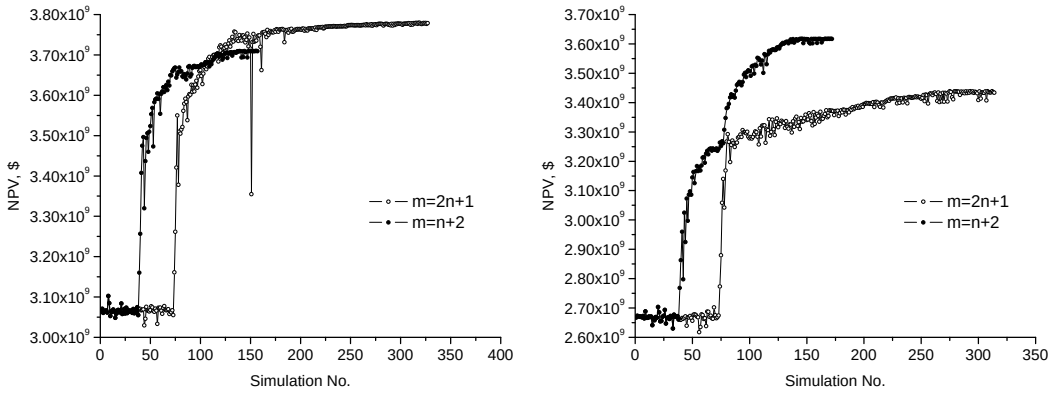

(a) Trial 1 (PUNQ initial locations) (b) Trial 2

Figure 5.42: The plot of NPV versus the number of simulation runs, Optimizing production wells in the PUNQ model, Example 4, Case 1.

The initial and final well trajectory parameters of the six production wells of the optimization runs with initial guesses 1 and 2 are listed in Tables 5.18 and 5.19, respectively. The initial and final well trajectories projected onto the top surface of the reservoir are shown in Figs. 5.43 and 5.44. The well trajectories are shown with black lines.

The perforations corresponding to the initial and final trajectories of the wells on the horizontal permeability fields of the 5 simulation layers of the reservoir are shown in Figs. 5.45 through 5.47 for the optimization runs with the first initial guess. The perforated layers corresponding to the initial and final trajectories of the production wells are summarized in Tables 5.20 through 5.22. Similar plots and tables for the optimization runs with the second initial guess are shown in Figs. 5.48.

Table 5.18: The initial and final trajectory parameters $(x_{\mathrm{w}}, y_{\mathrm{w}}, z_{\mathrm{w}}, l_{\mathrm{w}}, \theta_{\mathrm{w}}, \varphi_{\mathrm{w}})$ of the production wells for initial guess 1, Example 4, Case 1.

Initial	P-1	$(5610.2, 3838.6, 7763.8, 250.0, 0.0, 80.0)$
	P-2	$(5019.7, 6791.3, 7772.5, 250.0, 45.0, 80.0)$
	P-3	$(9744.1, 10334.7, 7799.3, 250.0, 90.0, 80.0)$
	P-4	$(6200.8, 2657.5, 7798.6, 250.0, 0.0, 80.0)$
	P-5	$(8563.0, 9744.1, 7793.5, 250.0, 90.0, 80.0)$
	P-6	$(9744.1, 3838.6, 7810.4, 250.0, 45.0, 80.0)$
Final, $m = n + 2$	P-1	$(5851.4, 3470.7, 7798.0, 333.2, 32.9, 78.0)$
	P-2	$(7404.6, 6743.7, 7687.4, 303.9, 19.5, 90.2)$
	P-3	$(10019.1, 9307.6, 7766.6, 320.0, 137.0, 88.7)$
	P-4	$(6507.7, 3822.2, 7720.0, 170.4, 38.7, 76.7)$
	P-5	$(9022.7, 9735.4, 7758.3, 360.9, 163.8, 89.1)$
	P-6	$(9870.9, 4295.2, 7787.6, 339.3, 81.0, 87.0)$
Final, $m = 2n + 1$	P-1	$(6008.8, 3573.3, 7749.9, 268.0, 0.0, 65.8)$
	P-2	$(7266.6, 7381.2, 7712.6, 291.2, 27.6, 81.6)$
	P-3	$(10191.6, 10074.4, 7772.5, 189.9, 99.6, 88.8)$
	P-4	$(6489.1, 2899.8, 7763.6, 229.7, 45.8, 83.7)$
	P-5	$(8537.2, 9379.3, 7722.0, 291.9, 141.1, 86.3)$
	P-6	$(9717.1, 4329.9, 7802.0, 277.4, 12.4, 90.1)$

Table 5.19: The initial and final well trajectory parameters $(x_{\mathrm{w}}, y_{\mathrm{w}}, z_{\mathrm{w}}, l_{\mathrm{w}}, \theta_{\mathrm{w}}, \varphi_{\mathrm{w}})$ of the production wells for initial guess 2, Example 4, Case 1.

Initial	P-1	$(9153.5, 3248.0, 7781.1, 250.0, 45.0, 80.0)$
	P-2	$(6200.8, 2657.5, 7798.6, 250.0, 0.0, 80.0)$
	P-3	$(3838.6, 4429.1, 7774.2, 250.0, 90.0, 80.0)$
	P-4	$(5019.7, 7972.4, 7782.2, 250.0, 45.0, 80.0)$
	P-5	$(6791.3, 10334.7, 7810.2, 250.0, 45.0, 80.0)$
	P-6	$(9153.5, 12106.3, 7811.9, 250.0, 90.0, 80.0)$
Final, $m = n + 2$	P-1	$(9947.0, 3738.0, 7831.3, 409.2, 2.2, 87.5)$
	P-2	$(5784.1, 3041.6, 7809.6, 258.7, 73.0, 72.6)$
	P-3	$(4038.9, 4094.7, 7744.0, 17.5, 46.8, 81.8)$
	P-4	$(6374.0, 7883.1, 7720.6, 148.7, 69.1, 89.3)$
	P-5	$(7936.1, 9203.9, 7757.0, 22.5, 69.6, 84.0)$
	P-6	$(9393.0, 10738.1, 7752.8, 236.0, 73.8, 79.6)$
Final, $m = 2n + 1$	P-1	$(9109.9, 3542.5, 7776.5, 341.2, 48.5, 99.3)$
	P-2	$(6179.0, 2785.7, 7789.9, 256.9, 2.7, 79.0)$
	P-3	$(3764.4, 4365.9, 7739.8, 176.6, 102.2, 82.0)$
	P-4	$(5707.2, 8058.7, 7767.6, 260.7, 43.1, 87.9)$
	P-5	$(7166.6, 10029.1, 7759.7, 192.9, 76.1, 87.2)$
	P-6	$(9346.3, 10393.3, 7842.2, 305.9, 35.0, 9.7)$

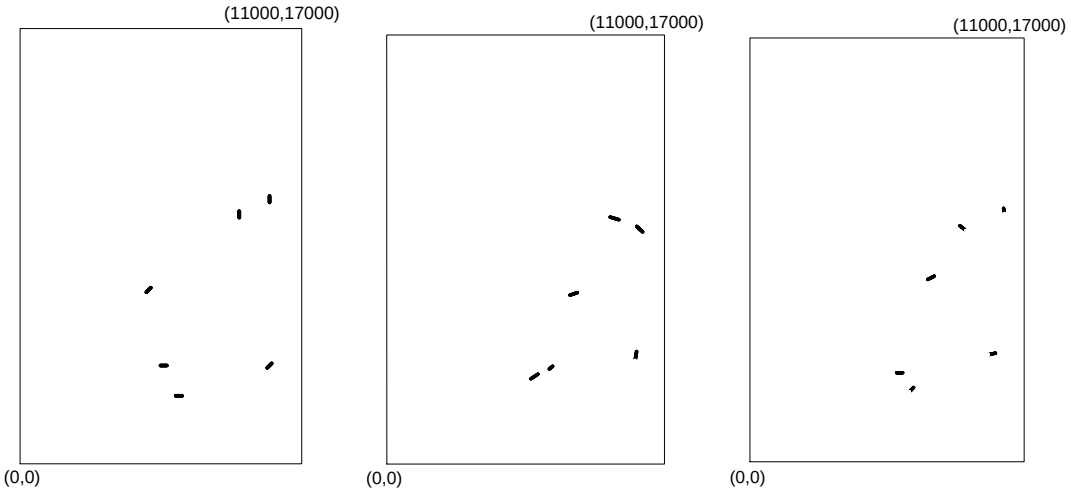

(a) Initial (b) Final, $m = n + 2$ (c) Final, $m = 2n + 1$

Figure 5.43: The initial and final well trajectories of the producers projected onto the top reservoir surface for the first initial guess, Example 4, Case 1. The well trajectories are shown with black lines.

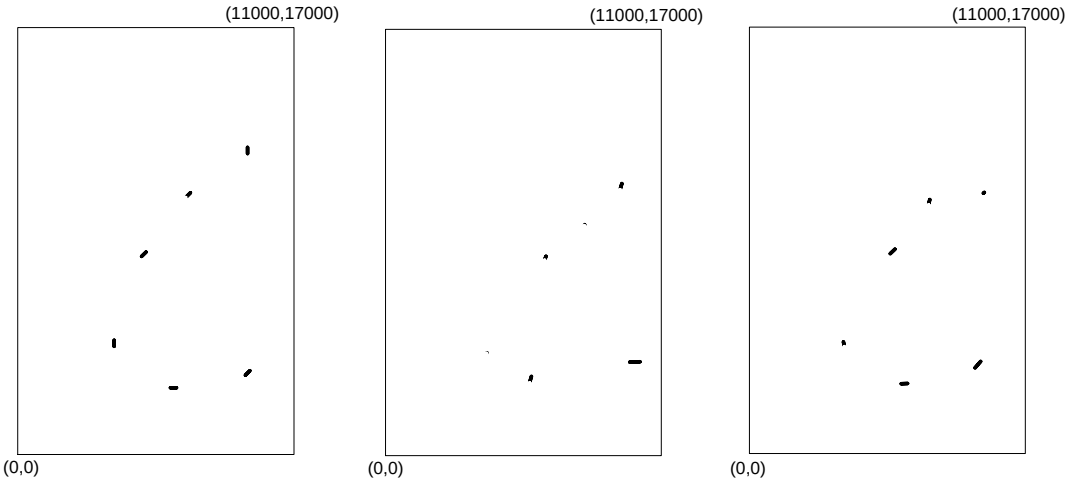

(a) Initial (b) Final, $m = n + 2$ (c) Final, $m = 2n + 1$

Figure 5.44: The initial and final well trajectories of the producers projected onto the top reservoir surface for the second initial guess, Example 4, Case 1. The well trajectories are shown with black lines.

through 5.50 and Tables 5.23 through 5.25.

As we mentioned above, aquifers are connected to the edges on the north, west and south sides of the reservoir, but, the main contribution of the water influx into the reservoir is from the aquifer connected to the west side of the reservoir. The direction of the water influx is mainly from the north-west, which is the direction of

permeability channels of the reservoir; see Figs. 5.39 and 5.40. For the optimization run with the first initial guess, we see from Fig. 5.43 that the wells are moved toward the inside and away from the west side of the reservoir to reduce the amount of produced water. From Fig. 5.45 we see that initially most of the perforations of the wells are in the bottom layers of the reservoir. However, in the final well trajectories (Figs. 5.46 and 5.47), we see that the perforations of the wells are in the top layers of the reservoir to reduce the amount of water production from the reservoir. Similar results are obtained for initial guess 2; see Fig. 5.44 and Figs. 5.48 through 5.50.

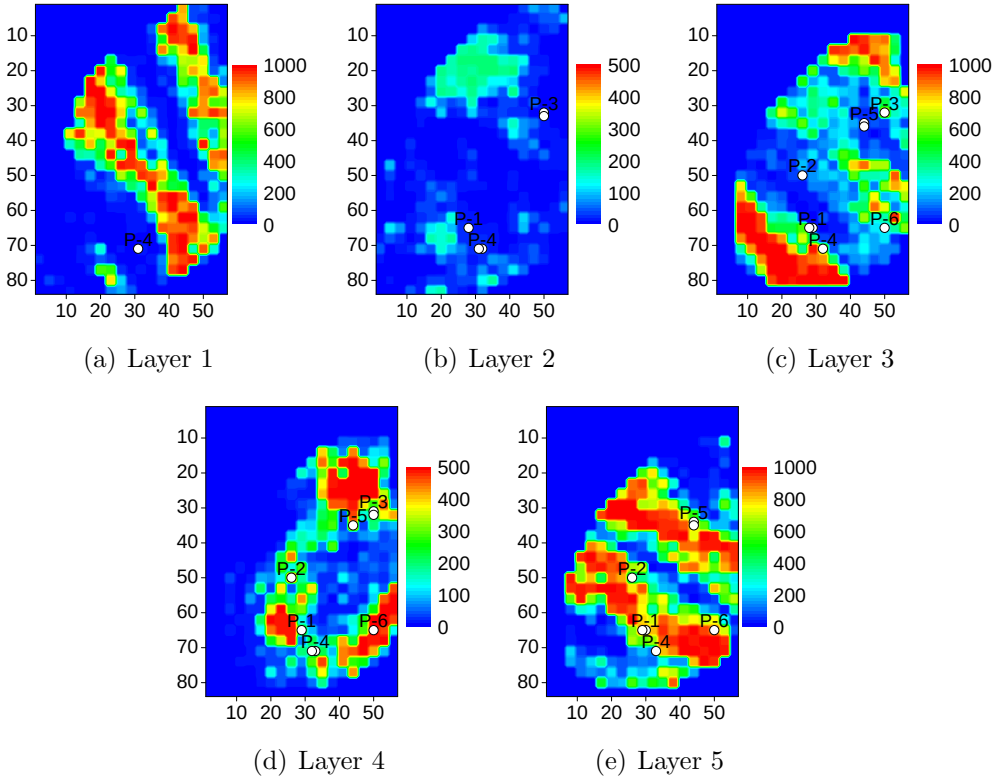

(a) Layer 1 (b) Layer 2 (c) Layer 3

(d) Layer 4 (e) Layer 5

Figure 5.45: The perforations shown as white circles corresponding to the initial trajectory of the production wells on the horizontal permeability fields of the 5 simulation layers, Initial guess 1, Example 4, Case 1.

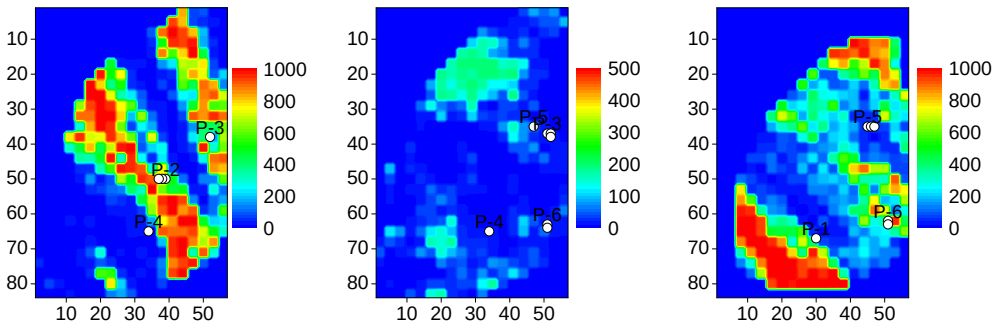

(a) Layer 1

(b) Layer 2

(c) Layer 3

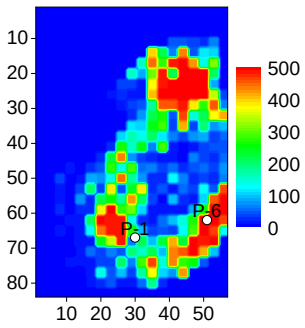

(d) Layer 4

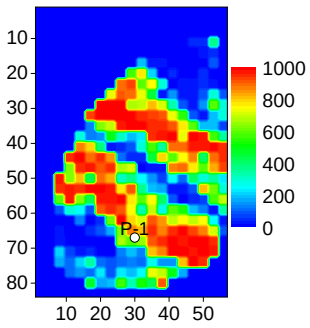

(e) Layer 5

Figure 5.46: The perforations shown as white circles corresponding to the final trajectory of the production wells on the horizontal permeability fields of the 5 simulation layers, Initial guess 1 with $m = n + 2$, Example 4, Case 1.

Table 5.20: The perforated layers corresponding to the initial trajectory of the production wells in the PUNQ model, Initial guess 1, Example 4, Case 1.

	P-1	P-2	P-3	P-4	P-5	P-6
Perforated layers	2, 3, 4, 5	3, 4, 5	2, 3, 4	1, 2, 3, 4, 5	3, 4, 5	3, 4, 5

Table 5.21: The perforated layers corresponding to the final trajectory of the production wells in the PUNQ model, Initial guess 1 with $m = n + 2$, Example 4, Case 1.

	P-1	P-2	P-3	P-4	P-5	P-6
Perforated layers	3, 4, 5	1	1, 2	1, 2	2, 3	2, 3, 4

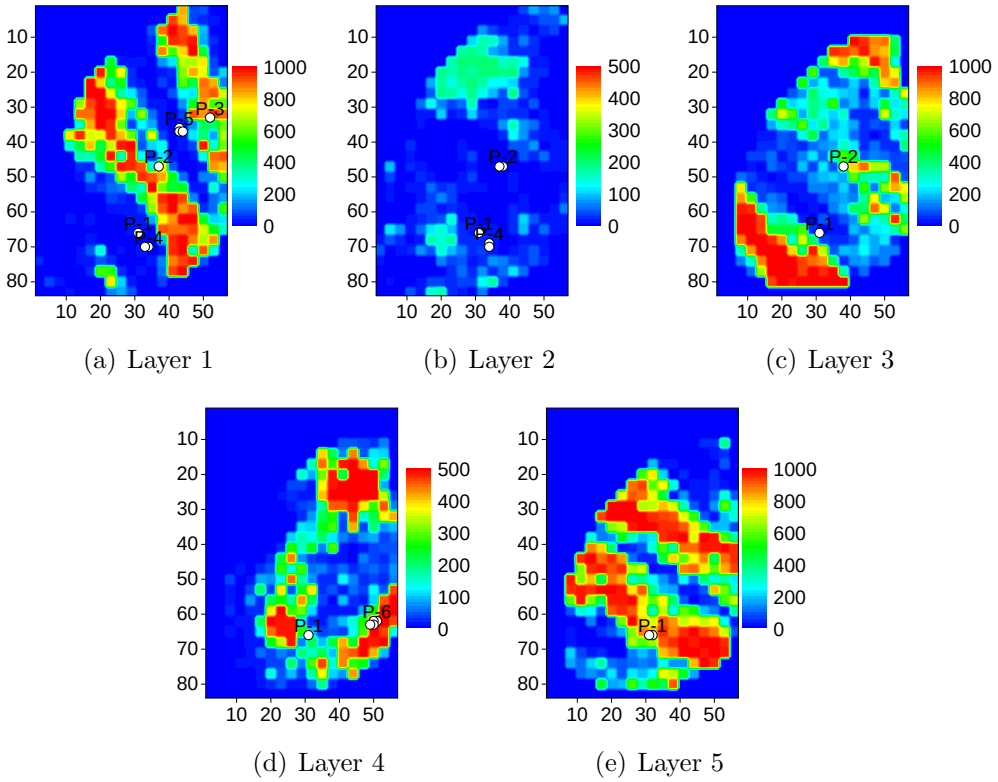

(a) Layer 1 (b) Layer 2 (c) Layer 3

(d) Layer 4 (e) Layer 5

Figure 5.47: The perforations shown as white circles corresponding to the final trajectory of the production wells on the horizontal permeability fields of the 5 simulation layers, Initial guess 1 with $m = 2n + 1$, Example 4, Case 1.

Table 5.22: The perforated layers corresponding to the final trajectory of the production wells in the PUNQ model, Initial guess 1 with $m = 2n + 1$, Example 4, Case 1.

	P-1	P-2	P-3	P-4	P-5	P-6
Perforated layers	1, 2, 3, 4, 5	1, 2, 3	1	1, 2	1	4

Table 5.23: The perforated layers corresponding to the initial trajectory of the production wells in the PUNQ model, Initial guess 2, Example 4, Case 1.

	P-1	P-2	P-3	P-4	P-5	P-6
Perforated layers	2, 3, 4	1, 2, 3, 4, 5	1, 2, 3, 4, 5	2, 3, 4, 5	2, 3, 4	2, 3, 4

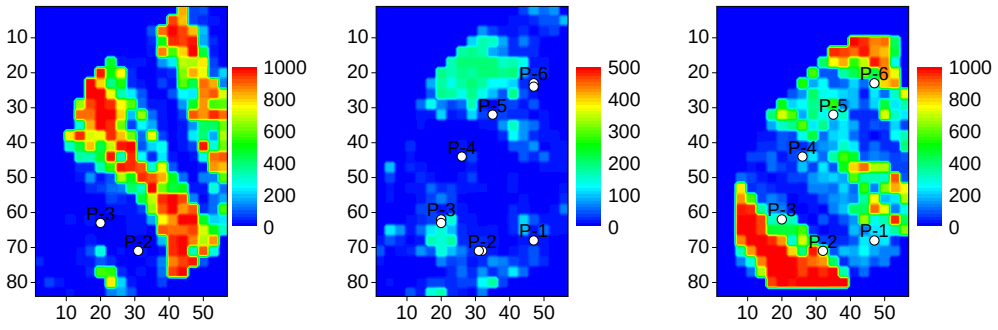

(a) Layer 1 (b) Layer 2 (c) Layer 3

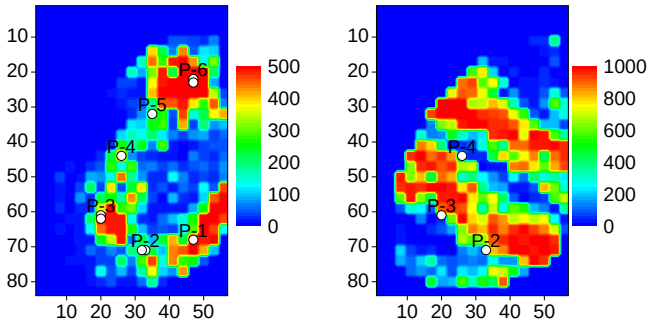

(d) Layer 4 (e) Layer 5

Figure 5.48: The perforations shown as white circles corresponding to the initial trajectory of the production wells on the horizontal permeability fields of the 5 simulation layers, Initial guess 2, Example 4, Case 1.

Table 5.24: The perforated layers corresponding to the final trajectory of the production wells in the PUNQ model, Initial guess 2 with $m = n + 2$, Example 4, Case 1.

	P-1	P-2	P-3	P-4	P-5	P-6
Perforated layers	5	2, 3, 4, 5	1	1	2	1, 2

Table 5.25: The perforated layers corresponding to the final trajectory of the production wells in the PUNQ model, Initial guess 2 with $m = 2n + 1$, Example 4, Case 1.

	P-1	P-2	P-3	P-4	P-5	P-6
Perforated layers	1, 2, 3, 4, 5	1, 2, 3, 4, 5	1	2, 3	1	1, 2, 3, 4, 5

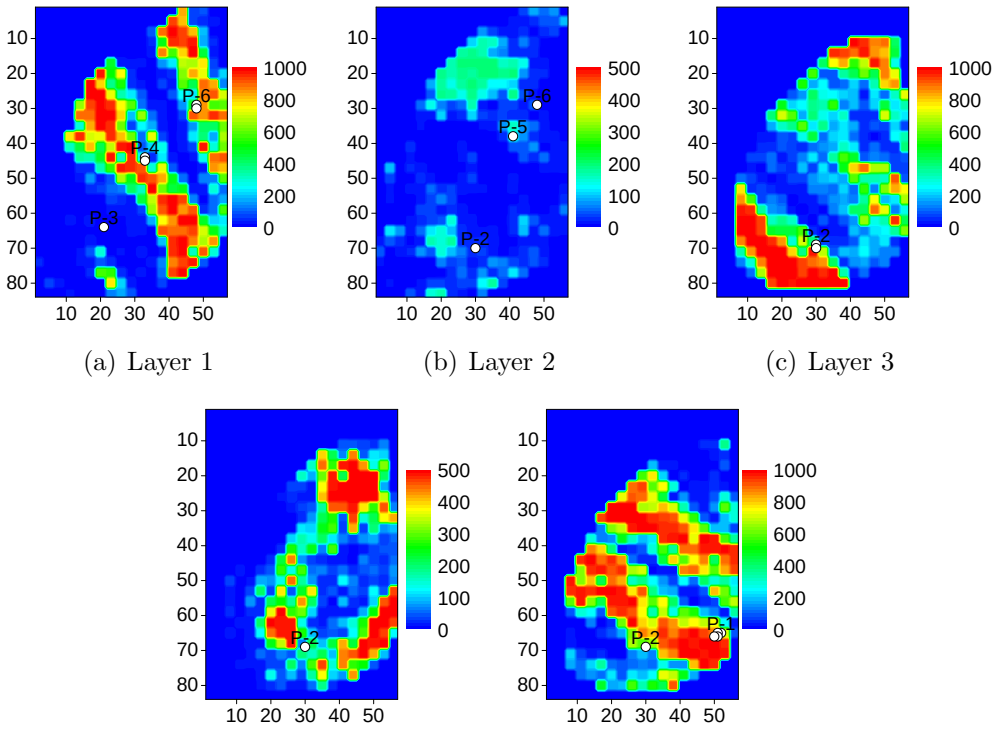

(a) Layer 1 (b) Layer 2 (c) Layer 3

(d) Layer 4 (e) Layer 5

Figure 5.49: The perforations shown as white circles corresponding to the final trajectory of the production wells on the horizontal permeability fields of the 5 simulation layers, Initial guess 2 with $m = n + 2$, Example 4, Case 1.

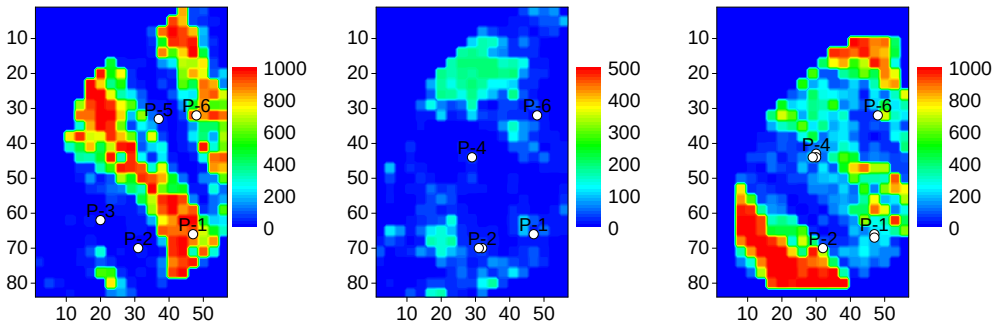

(a) Layer 1 (b) Layer 2 (c) Layer 3

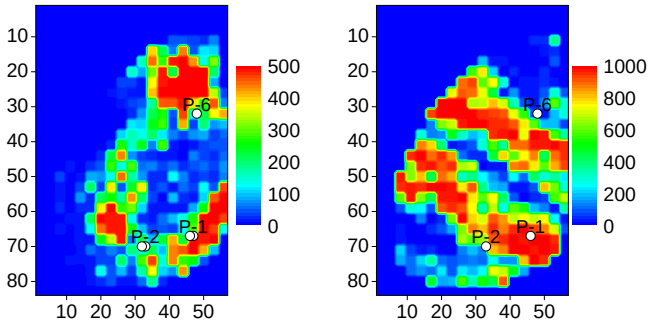

(d) Layer 4 (e) Layer 5

Figure 5.50: The perforations shown as white circles corresponding to the final trajectory of the production wells on the horizontal permeability fields of the 5 simulation layers, Initial guess 2 with $m = 2n + 1$, Example 4, Case 1.

Case 2. Optimization of the Trajectory of Six Producers and Three Injectors: We wish to optimize the location of six production wells and three injection wells in the PUNQ model where the reservoir aquifers are eliminated. The production wells are bottomhole pressure-controlled with the specified bottomhole pressure equal to 1,500 psi at all producers. The injection wells are bottomhole pressure-controlled wells with the specified bottomhole pressure equal to 4,000 psi at all injectors. The production period of the reservoir is 10 years. Similar to Case 1 of this example, we consider two initial guesses for the well trajectory parameters. In initial guess 1, we set the initial well center points of the six producers at the PUNQ production well locations and the initial well center points of the injectors are chosen arbitrarily. In the second initial guess, we use completely arbitrary locations for the well center points of the injection and production wells. In both initial guesses, the initial orientation angles of the wells are chosen fairly arbitrarily but close to horizontal, i.e., the orientation angle φ_{w} is close to 90 degrees. Each well has 6 parameters and therefore, there are $n = 9 \times 6 = 54$ optimization variables. We use $m = n + 2$ for the number of interpolation points in the BOBYQA algorithm. The results of the optimization runs for both initial guesses are summarized in Table 5.26, and the plot of NPV versus the number of reservoir simulation runs for both initial guesses is shown in Fig. 5.51. Note that there is a relatively large difference between the NPV from our model and the one from the Schedule method. As we discussed in Section 5.5, our model overestimates the rate of a bottomhole pressure-controlled well. In this case, all the production and injection wells are bottomhole pressure-controlled wells, and therefore, this difference is more significant. However, note that the changes in the NPV of our model and the one from the Schedule method are consistent.

The initial and final well trajectory parameters of six production and three injection wells corresponding to the optimization runs with initial guesses 1 and 2

Table 5.26: The summary of optimization runs for the PUNQ model, Example 4, Case 2.

	Initial guess 1	Initial guess 2
Initial NPV, Schedule	$\$1.57 \times 10^9$	$\$1.84 \times 10^9$
Initial NPV	$\$1.13 \times 10^9$	$\$1.38 \times 10^9$
Final NPV	$\$3.03 \times 10^9$	$\$3.10 \times 10^9$
Final NPV, Schedule	$\$2.80 \times 10^9$	$\$2.86 \times 10^9$
No. of Sim. runs	272	279

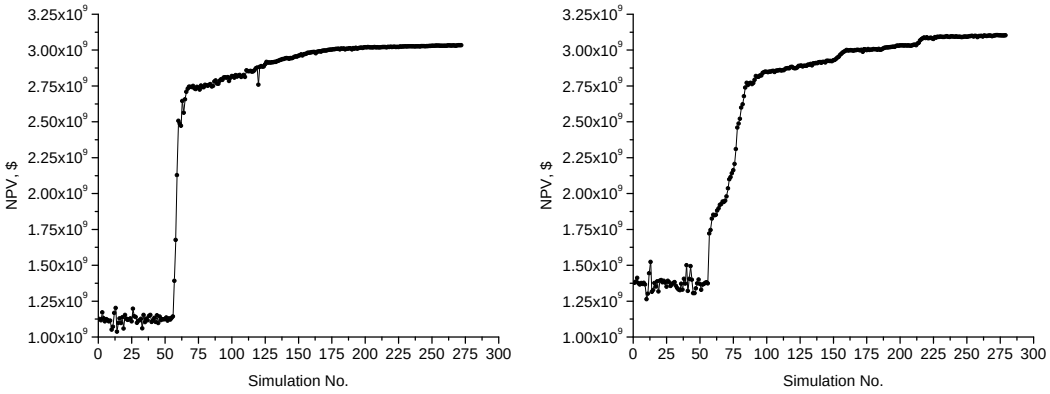

(a) Initial guess 1 (PUNQ initial locations for producers)

(b) Initial guess 2

Figure 5.51: The plot of NPV versus the number of simulation runs, Example 4, Case 2.

are listed in Tables 5.27 and 5.28, respectively. The initial and final well trajectories projected onto the top surface of the reservoir are shown in Figs. 5.52 and 5.53. The well trajectories of the production wells are shown with black lines and the well trajectory of the injection wells are shown with red lines.

Similar to the results for Case 1, the perforations corresponding to the initial and final trajectories of the wells on the horizontal permeability fields of the 5 simulation layers of the reservoir are shown in Figs. 5.54 and 5.55 for the optimization run with the first initial guess. The perforated layers corresponding to the initial and final trajectories of the production wells are summarized in Tables 5.29 and 5.30. Similar plots and tables for the optimization run with the second initial guess are shown in Figs. 5.56 and 5.57 and in Tables 5.31 and 5.32. In Figs. 5.54 through 5.57,

Table 5.27: The initial and final trajectory parameters $(x_{\mathrm{w}}, y_{\mathrm{w}}, z_{\mathrm{w}}, l_{\mathrm{w}}, \theta_{\mathrm{w}}, \varphi_{\mathrm{w}})$ of the production and injection wells for initial guess 1, Example 4, Case 2.

Initial	I-1	(8563.0, 13878.0, 7841.5, 200.0, 0.0, 80.0)
	I-2	(2263.8, 6791.3, 7847.2, 200.0, 45.0, 80.0)
	I-3	(3248.0, 2657.5, 7822.2, 200.0, 0.0, 80.0)
	P-1	(5610.2, 3838.6, 7763.8, 250.0, 0.0, 80.0)
	P-2	(5019.7, 6791.3, 7772.5, 250.0, 45.0, 80.0)
	P-3	(9744.1, 10334.7, 7799.3, 250.0, 90.0, 80.0)
	P-4	(6200.8, 2657.5, 7798.6, 250.0, 0.0, 80.0)
	P-5	(8563.0, 9744.1, 7793.5, 250.0, 90.0, 80.0)
	P-6	(9744.1, 3838.6, 7810.4, 250.0, 45.0, 80.0)
Final	I-1	(7913.7, 14812.9, 7852.1, 193.6, 66.7, 81.4)
	I-2	(2095.2, 6796.7, 7852.8, 71.9, 160.0, 53.1)
	I-3	(1573.4, 2144.3, 7898.2, 251.3, 43.8, 61.9)
	P-1	(6599.2, 3849.3, 7751.2, 294.1, 78.1, 71.6)
	P-2	(6600.8, 7695.4, 7739.0, 213.7, 40.6, 73.0)
	P-3	(9745.9, 9871.2, 7843.5, 164.6, 142.1, 75.9)
	P-4	(6748.4, 2989.9, 7765.4, 334.7, 54.2, 86.6)
	P-5	(9484.9, 9082.0, 7815.8, 281.4, 132.2, 77.4)
	P-6	(9893.4, 4805.2, 7786.3, 461.2, 71.1, 90.6)

Table 5.28: The initial and final well trajectory parameters $(x_{\mathrm{w}}, y_{\mathrm{w}}, z_{\mathrm{w}}, l_{\mathrm{w}}, \theta_{\mathrm{w}}, \varphi_{\mathrm{w}})$ of the production wells for initial guess 2, Example 4, Case 2.

Initial	I-1	(8563.0, 13878.0, 7841.5, 200.0, 0.0, 80.0)
	I-2	(2263.8, 6791.3, 7847.2, 200.0, 45.0, 80.0)
	I-3	(3248.0, 2657.5, 7822.2, 200.0, 0.0, 80.0)
	P-1	(9153.5, 3838.6, 7777.9, 250.0, 45.0, 80.0)
	P-2	(6791.3, 2657.5, 7797.2, 250.0, 0.0, 80.0)
	P-3	(3838.6, 4429.1, 7774.2, 250.0, 90.0, 80.0)
	P-4	(5019.7, 8563.0, 7794.9, 250.0, 45.0, 80.0)
	P-5	(7381.9, 10334.7, 7806.4, 250.0, 45.0, 80.0)
	P-6	(9744.1, 9547.2, 7786.5, 250.0, 90.0, 80.0)
Final	I-1	(8370.8, 14500.7, 7856.1, 195.0, 0.2, 79.2)
	I-2	(2295.4, 6702.4, 7827.1, 233.7, 177.4, 65.1)
	I-3	(2259.1, 2148.4, 7863.5, 95.1, 47.9, 62.4)
	P-1	(9547.8, 4487.5, 7776.8, 324.7, 13.2, 77.1)
	P-2	(7029.2, 2876.5, 7780.3, 225.6, 23.8, 75.2)
	P-3	(3582.6, 3971.6, 7747.3, 24.6, 61.8, 65.5)
	P-4	(5932.5, 8477.6, 7784.5, 66.5, 143.1, 89.2)
	P-5	(7820.5, 9660.3, 7748.9, 117.8, 76.7, 91.3)
	P-6	(9786.3, 8860.5, 7754.5, 267.7, 85.2, 81.9)

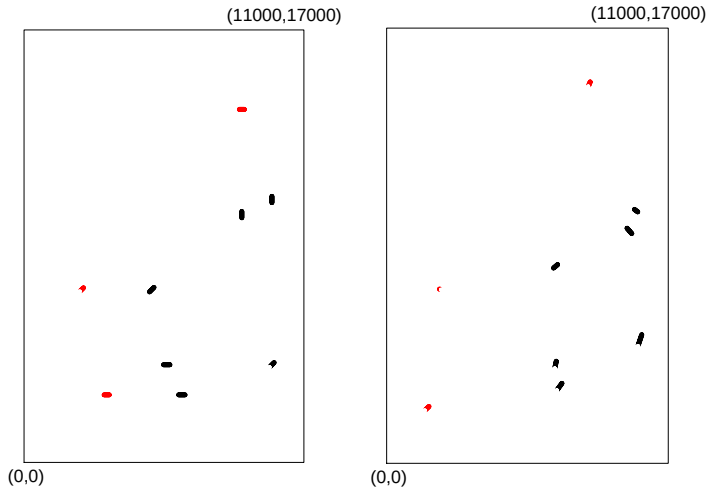

(a) Initial (b) Final

Figure 5.52: The initial and final well trajectories of the producers and the injectors projected onto the top reservoir surface for the first initial guess, Example 4, Case 2. The well trajectories of the production wells are shown with black lines and the well trajectory of the injection wells are shown with red lines.

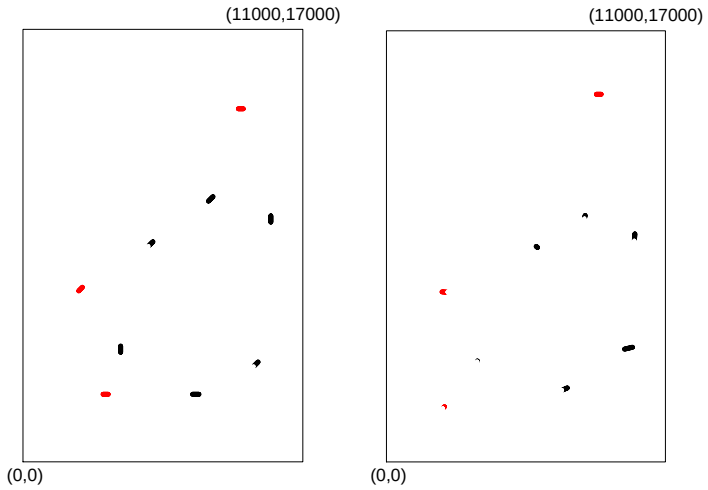

(a) Initial (b) Final

Figure 5.53: The initial and final well trajectories of the producers and the injectors projected onto the top reservoir surface for the second initial guess, Example 4, Case 2. The well trajectories of the production wells are shown with black lines and the well trajectory of the injection wells are shown with red lines.

the perforations corresponding to the production wells are shown with white circles and the perforations corresponding to the injection wells are shown with black circles.

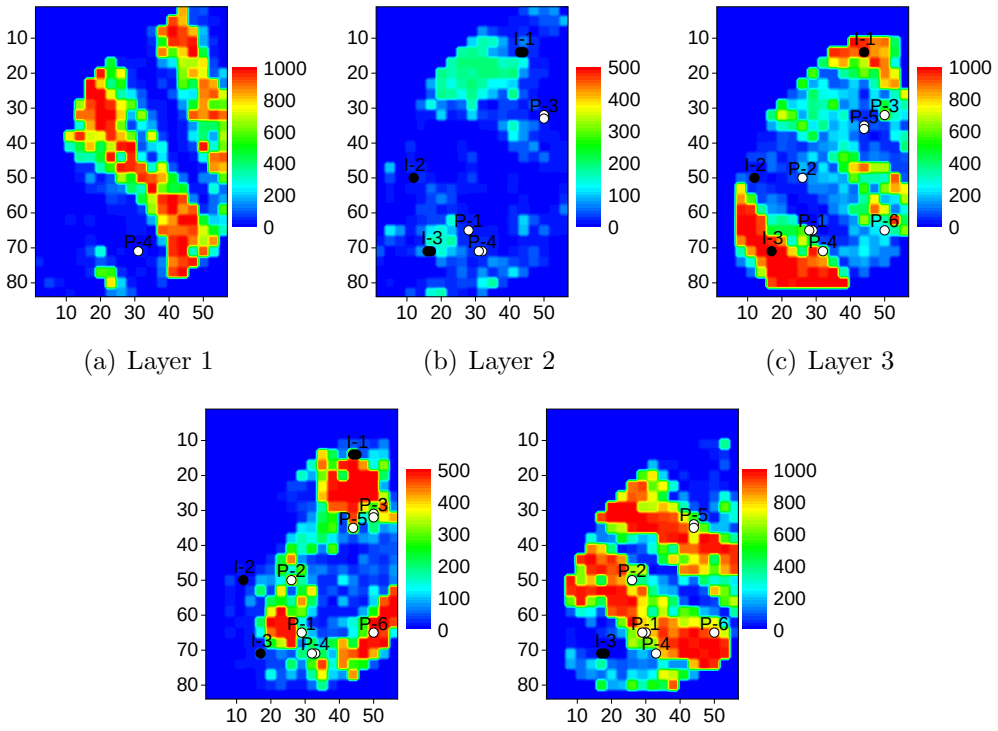

(a) Layer 1 (b) Layer 2 (c) Layer 3

(d) Layer 4 (e) Layer 5

Figure 5.54: The perforations corresponding to the initial trajectory of the production and injection wells on the horizontal permeability fields of the 5 simulation layers, Initial guess 1, Example 4, Case 2. The perforations corresponding to the production wells are shown with white circles and the perforations corresponding to the injection wells are shown with black circles.

Table 5.29: The perforated layers corresponding to the initial trajectories of the production and injection wells in the PUNQ model, Initial guess 1, Example 4, Case 2.

Producers	Perforated layers	Injectors	Perforated layers
P-1	2, 3, 4, 5	I-1	2, 3, 4
P-2	3, 4, 5	I-2	2, 3, 4
P-3	2, 3, 4	I-3	2, 3, 4, 5
P-4	1, 2, 3, 4, 5	-	-
P-5	3, 4, 5	-	-
P-6	3, 4, 5	-	-

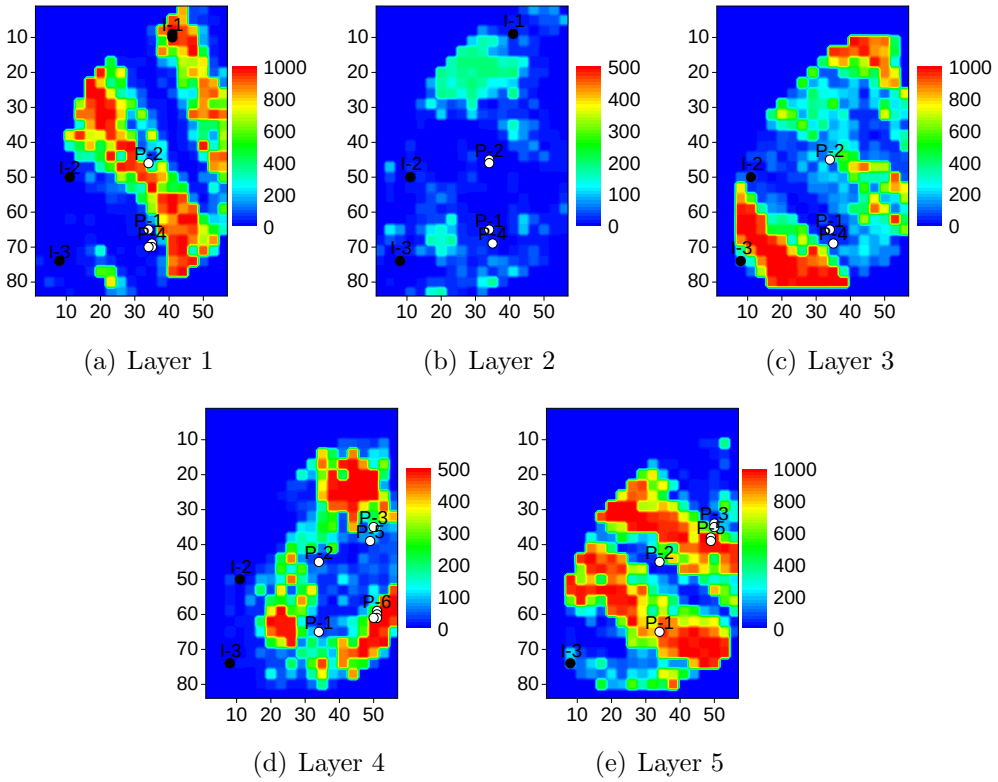

(a) Layer 1 (b) Layer 2 (c) Layer 3

(d) Layer 4 (e) Layer 5

Figure 5.55: The perforations corresponding to the final trajectory of the production and injection wells on the horizontal permeability fields of the 5 simulation layers, Initial guess 1, Example 4, Case 2. The perforations corresponding to the production wells are shown with white circles and the perforations corresponding to the injection wells are shown with black circles.

Table 5.30: The perforated layers corresponding to the final trajectories of the production and injection wells in the PUNQ model, Initial guess 1, Example 4, Case 2.

Producers	Perforated layers	Injectors	Perforated layers
P-1	1, 2, 3, 4, 5	I-1	1, 2
P-2	1, 2, 3, 4, 5	I-2	1, 2, 3, 4
P-3	4, 5	I-3	1, 2, 3, 4, 5
P-4	1, 2, 3	-	-
P-5	4, 5	-	-
P-6	4	-	-

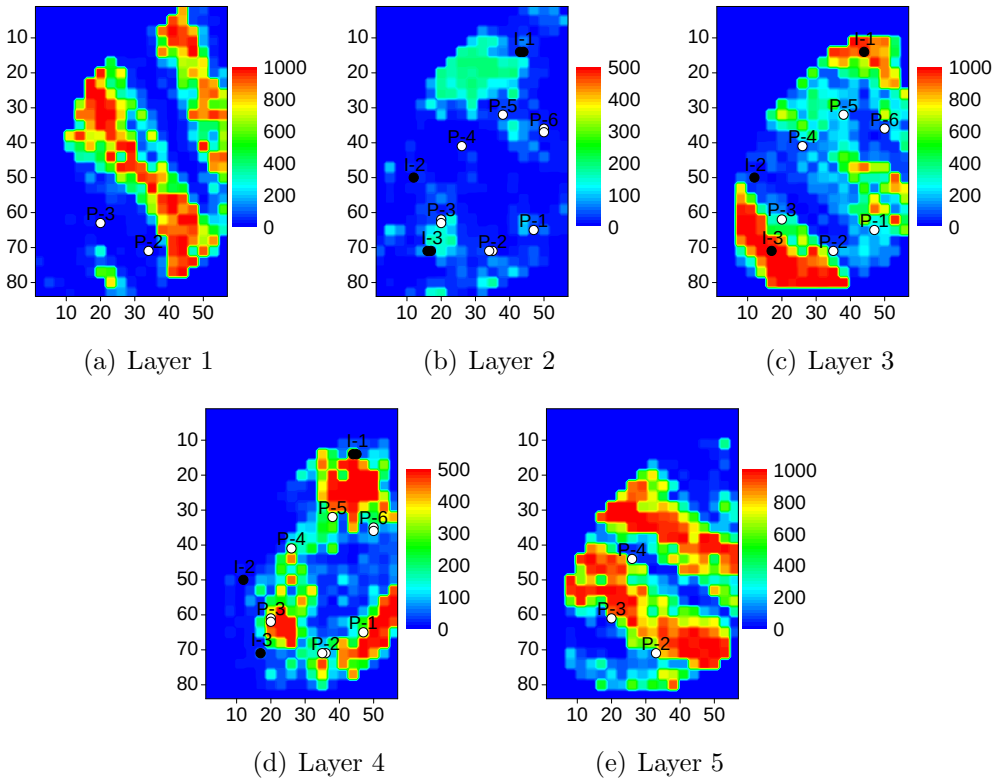

(a) Layer 1 (b) Layer 2 (c) Layer 3

(d) Layer 4 (e) Layer 5

Figure 5.56: The perforations corresponding to the initial trajectory of the production and injection wells on the horizontal permeability fields of the 5 simulation layers, Initial guess 2, Example 4, Case 2. The perforations corresponding to the production wells are shown with white circles and the perforations corresponding to the injection wells are shown with black circles.

Table 5.31: The perforated layers corresponding to the initial trajectories of the production and injection wells in the PUNQ model, Initial guess 2, Example 4, Case 2.

Producers	Perforated layers	Injectors	Perforated layers
P-1	2, 3	I-1	2, 3, 4
P-2	1, 2, 3, 4, 5	I-2	2, 3, 4
P-3	1, 2, 3, 4, 5	I-3	2, 3, 4, 5
P-4	2, 3, 4, 5	-	-
P-5	2, 3, 4	-	-
P-6	2, 3, 4	-	-

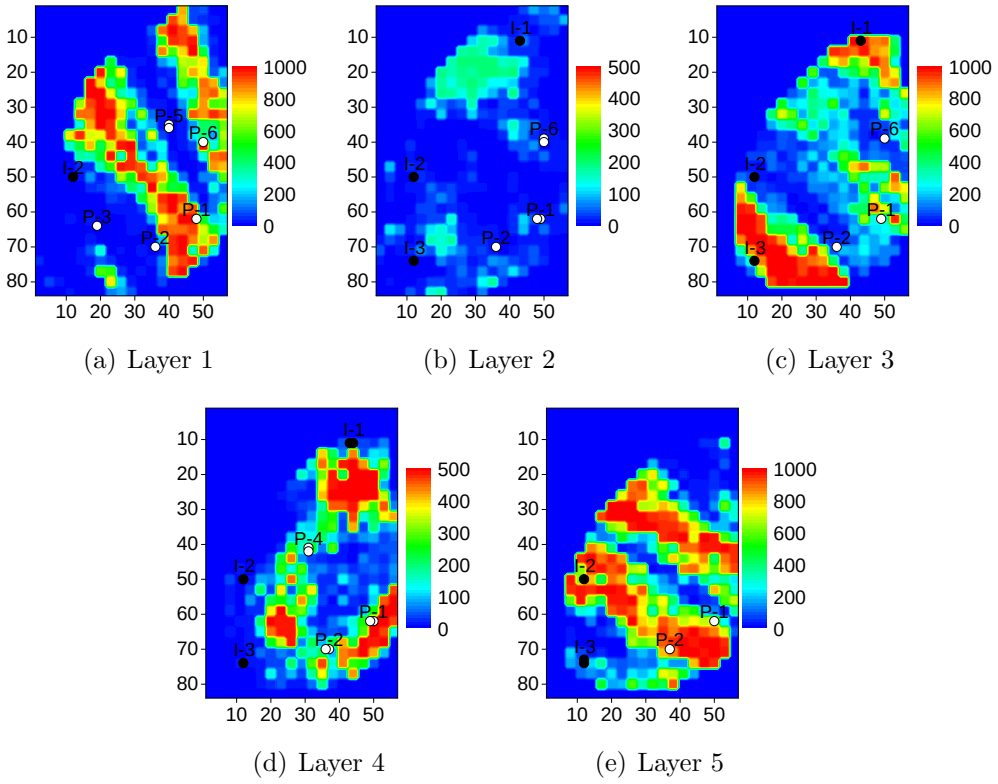

(a) Layer 1 (b) Layer 2 (c) Layer 3

(d) Layer 4 (e) Layer 5

Figure 5.57: The perforations corresponding to the final trajectory of the production and injection wells on the horizontal permeability fields of the 5 simulation layers, Initial guess 2, Example 4, Case 2. The perforations corresponding to the production wells are shown with white circles and the perforations corresponding to the injection wells are shown with black circles.

Table 5.32: The perforated layers corresponding to the final trajectories of the production and injection wells in the PUNQ model, Initial guess 2, Example 4, Case 2.

Producers	Perforated layers	Injectors	Perforated layers
P-1	1, 2, 3, 4, 5	I-1	2, 3, 4
P-2	1, 2, 3, 4, 5	I-2	1, 2, 3, 4, 5
P-3	1	I-3	2, 3, 4, 5
P-4	4	-	-
P-5	1	-	-
P-6	1, 2, 3	-	-

Similar to the results presented in the previous examples, the final well trajectories of the wells strongly depend on the initial guesses for the well trajectories. However, the final NPVs for both initial guesses are close, event hough the well trajectories are very different. With initial guess 1, the production and injection wells are moved away from each other, i.e, the injection wells are moved toward the reservoir edges in the north and west sides of the reservoir; see Fig. 5.52. The production wells are moved toward the opposite direction of the injection wells towards the east of the reservoir. With initial guess 2, the injection wells also tend to separate from the production wells, however, the changes in the well locations are smaller than the changes obtained with initial guess 1.

The plots for the field cumulative oil production, field cumulative water production and field cumulative water injection with the initial and estimated optimal well trajectories corresponding to the optimization runs with initial guesses 1 and 2 are shown in Figs. 5.58 and 5.59, respectively. In Figs. 5.58 and 5.59, the production data corresponding to the simulation run with the initial well trajectories are shown with dots and the plot of production data corresponding to the simulation run with optimized well trajectories of the wells are shown with line. Note that there is a break in the y-ordinate of the Figs. 5.58(b), 5.58(c) and 5.59(b). With initial guess 1, after optimizing the location and trajectories of the wells, we produce almost the same amount of oil (slightly less than the amount of oil produced with the initial trajectories of the well), however, the amount of produced water and also the amount of injected water is significantly reduced, which leads to a significant increase in NPV. With the optimization of the well trajectories with initial guess 2, the amount of produced oil from the reservoir is increased and the amount of injected water and also the amount of produced water is decreased. From these results we clearly see that the optimization of well trajectories significantly reduced water cycling in the water flooding process of the reservoir.

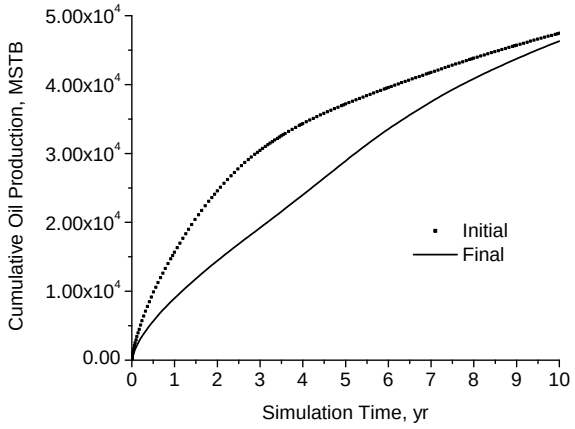

(a) Cumulative Oil Production

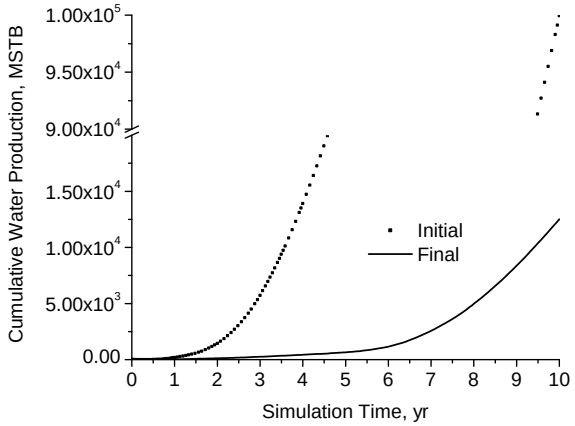

(b) Cumulative Water Production

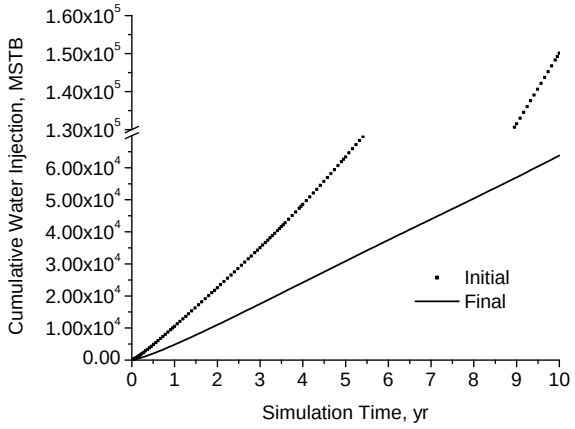

(c) Cumulative Water Injection

Figure 5.58: The production and injection data corresponding to the simulation runs with the initial and final trajectories of the wells, Initial guess 1, Example 4, Case 2.

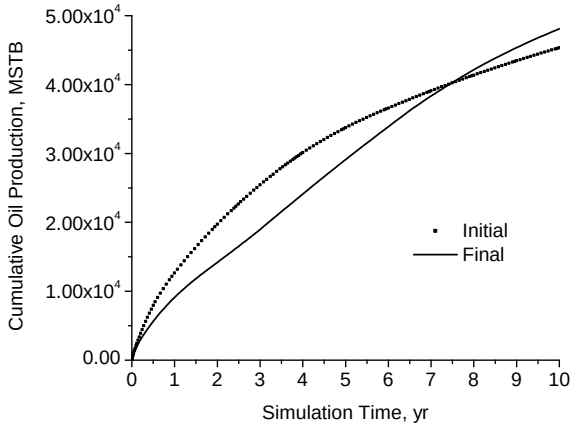

(a) Cumulative Oil Production

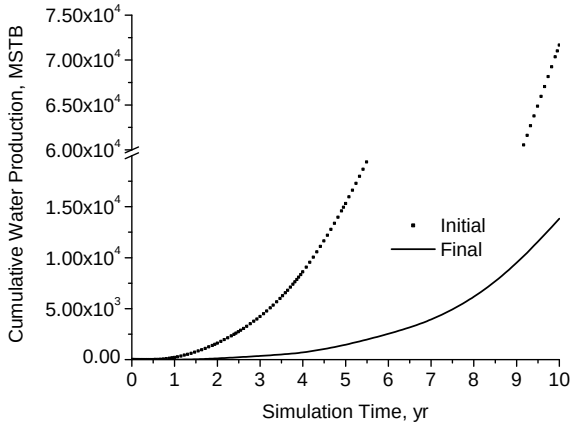

(b) Cumulative Water Production

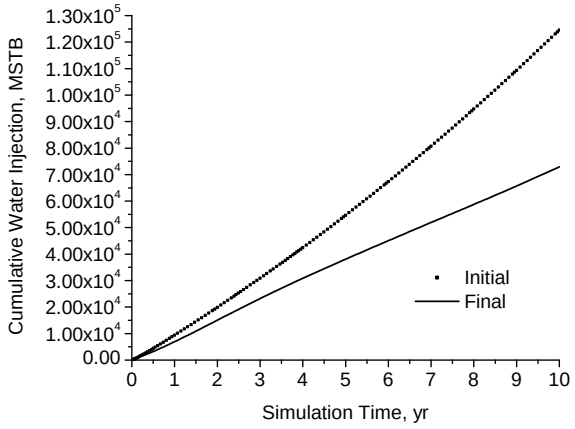

(c) Cumulative Water Injection

Figure 5.59: The production and injection data corresponding to the simulation runs with the initial and final trajectories of the wells, Initial guess 2, Example 4, Case 2.

CHAPTER 6

CONCLUSIONS

The general optimal well-placement problem is difficult because it requires simultaneously optimizing the number of wells, the well trajectories and the well schedule and controls to maximize a NPV functional subject to the field operational and economic constraints. Moreover, the optimal solution depends on the specified economics and the production life of the reservoir.

In Chapter 3, a well-placement algorithm is introduced to simultaneously optimize the number of wells, the well locations and the well rates of rate-controlled vertical injection and production wells. The optimal solution found depends on the total field injection and production rates that are specified; thus, we have developed and illustrated the applicability of a two-stage algorithm for estimating an optimal solution to the problem. The first stage (initialization step) estimates optimal field injection and production rates that are appropriate for the given reservoir life specified and thus essentially eliminates the dependance of the solution on the reservoir life specified. The algorithm also incorporates a procedure to honor a minimum bottomhole pressure specified at producers and a specified maximum injection well pressure. It also has a built in procedure to escape from a local maximum so other local maxima can be identified. The following specific conclusions are warranted.

- The initialization step, allows one to determine reasonable total production/injection rates and improves the robustness of the well-placement algorithm.

- Using the initialization step to determine total injection/production rates to define equality constraints in the well-placement optimization algorithm results

in a higher value of the modified NPV function, J, than is obtained by applying the well-placement algorithm without the initialization step.

- The method we have used to ensure that nonlinear constraints represented by bounds on bottomhole pressures are satisfied results in a robust optimization procedure and avoids the need to implement an adjoint method to compute the gradient of these nonlinear constraints, thus enabling the use of Eclipse 300 in our algorithm for the solution of the optimal well-placement problem.

- The optimized well locations are a sub-set of the initial locations of the wells and depend on the choice of the initial locations for the wells. However, in the examples presented in this dissertation, we showed that with reasonable initial sets of well locations, which cover all the reservoir area, the optimized NPV's are fairly close. It is worth mentioning that a similar approach conceptually can be adopted for the well-placement of more general trajectories for 3D rate-controlled wells. However, one should include all the possible trajectories of the wells (vertical, horizontal, directional with different orientation angles) distributed over the area of the reservoir in the initial set of well locations. This makes the application of the method prohibitively complex and computationally expensive and will generally yield a sub-optimal solution.

- The objective function of the well-placement optimization problem may have several local optima. With the algorithm presented here, one can obtain a set of local maximum points where the best maximum represents the estimated optimal solution of the problem.

- It is shown through examples that the application of Handels et al. [16] method to simply move the wells from the final locations obtained using the rates obtained from the two-stage algorithm derived in this work sometimes, but not always, results in a small additional increase in the modified NPV function.

In Chapter 4, a derivative-free well-placement optimization procedure is developed. The optimization procedure simultaneously optimizes the well locations and lengths (completions) of any combination of horizontal and vertical wells operating at specified rates or bottomhole pressures. Similarly, in Chapter 5, a method is presented for optimal placement of directional wells operating at specified rates or bottomhole pressures. For the well-placement methods of Chapters 4 and 5, the focus is on optimizing the locations and trajectories of the wells while the well controls and the production life of the reservoir are specified. For the methods presented in Chapters 4 and 5, the following conclusions are warranted.

- The well-placement problem can be defined in terms of continuous variables which represent the location, length and trajectory of each of the wells.

- The NPV can be defined as a relatively smooth function of the continuous well trajectory parameters. With this formulation, the BOBYQA algorithm can be applied to obtain a complete algorithm for the optimal well-placement which is easy to implement, computationally feasible and does not require an adjoint code for gradient calculations.

- The method developed can be applied to either rate-controlled or pressure-controlled wells. Note that since BOBYQA uses the reservoir simulator as a "black box", the economic and field operating constraints (e.g., maximum water cut constraint for the production wells) can be introduced in the reservoir simulator as reactive constraints.

- As is discussed through examples, the objective function of the well-placement problem might be noisy and may have several local maxima. Similar to gradient-based methods, the proposed well-placement method may converge to local optimal solutions, and, therefore the final results depend on the initial well locations, which should be selected based on best engineering practice.

- The proposed methods were successfully applied for the optimization of vertical, horizontal and directional well locations, lengths and trajectories in 3D synthetic and PUNQ reservoirs.

BIBLIOGRAPHY

[1] I. Aavatsmark and R.A. Klausen. Well index in reservoir simulation for slanted and slightly curved wells in 3d grids. *SPE Journal*, 8(1):41–48, 2003.

[2] W. Bangerth, H. Klie, M.F. Wheeler, P.L. Stoffa, and M.K. Sen. On optimization algorithm for the reservoir oil well placement problem. *Computational Geosciences*, 10:303–319, 2006.

[3] B.L. Beckner and X. Song. Field development planning using simulated annealing - optimal economic well scheduling and placement. In *Proceedings of the 1995 SPE Annual Technical Conference and Exhibition, 22-25 October 1995, Dallas, Texas*, 1995.

[4] A.C. Bittencourt and R.N. Horne. Reservoir development and design optimization. In *Proceedings of the 1997 SPE Annual Technical Conference and Exhibition, 5-8 October 1997, San Antonio, Texas*, 1997.

[5] Zyed Bouzarkouna, Didier Ding, and Anne Auger. Well placement optimization with the covariance matrix adaptation evolution strategy and meta-models. *Computational Geosciences*, 16:75–92, 2012. ISSN 1420-0597. URL `http://dx.doi.org/10.1007/s10596-011-9254-2`. 10.1007/s10596-011-9254-2.

[6] D.R. Brouwer and J.D. Jansen. Dynamic optimization of water flooding with smart wells using optimial control theory. *SPE Journal*, 9(4):391–402, 2004.

[7] D. L. Carroll. Chemical laser modeling with genetic algorithms. *AIAA J.*, 34 (2):338–346, 1996.

[8] David L. Carroll. Fortran genetic algorithm (GA) driver. `http://cuaerospace.com/carroll/ga.html`, 1999. [Online; accessed 2011].

[9] A. Centilmen, T. Ertekin, and A.S. Grader. Applications of neural networks in multiwell field development. In *Proceedings of the 1999 SPE Annual Technical Conference and Exhibition, 3-6 October 1999, Houston, Texas*, 1999.

[10] C. Chen. *Adjoint-Gradient-Based Production Optimization With The Augmented Lagrangian Method*. PhD. thesis, University of Tulsa, Tulsa, Oklahoma, USA, 2011.

[11] A.R. Conn, N.I.M. Gould, and P.L. Toint. *Trust-region methods*. MPS-SIAM series on optimization. Society for Industrial and Applied Mathematics, 2000. ISBN 9780898714609.

[12] Y. Ding. A generalized 3d well model for reservoir simulation. *SPE Journal*, 4 (1):437–450, 1996.

[13] Alexandre A. Emerick, E. Silva, B. Messer, L. Almeida, D. Szwarcman, M. Pacheco, and M.Vellasco. Well placement optimization using a genetic algorithm with nonlinear constraints. In *Proceedings of the SPE Reservoir Simulation Symposium*, number SPE 118808, 2009.

[14] Orhan Gunduz and Mustafa M. Aral. A dirac-delta function notation for source/sink terms in groundwater flow. *Journal of Hydrologic Engineering*, 10 (5):420–427, 2005.

[15] F.G. Miller H. Cinco and H.J. Ramey. Unsteady-state pressure distribution created by a directionally drilled well. *Journal of Petroleum Technology*, 27(11): 1392–1400, 1975.

[16] M. Handels, M. J. Zandvliet, D. R. Brouwer, and J. D. Jansen. Adjoint-based

well-placement optimization under production constraints. In *Proceedings of the SPE Reservoir Simulation Symposium*, number SPE 105797, 2007.

[17] S.D. Joshi. Augmentation of well productivity with slant and horizontal wells. *Journal of Petroleum Technology*, 40(6):729–739, 1988.

[18] Kjell Christoffersen Jostein Alvestad, Kent Holing and Ole Stava. Interactive modelling of multiphase inflow performance of horizontal and highly deviated wells. In *Proceedings of the 1994 SPE Europian Petroleum Computer Conference held in Aberdeen, U.K., 15-17 March 1994*, 1994.

[19] J. F. B. M. Kraaijevanger, P. J. P. Egberts, J. R. Valstar, and H. W. Buurman. Optimal waterflood design using the adjoint method. In *Proceedings of the SPE Reservoir Simulation Symposium*, number SPE 105764, page 15, 2007.

[20] J.W. Lee, C. Park, J.M. Kang, and C.K. Jeong. Horizontal well design incorportaed with interwell interference, drilling location, and trajectory for the recovery optimization, SPE-125539. In *Proceedings of the SPE/EAGE Reservoir Characterization and Simulation Conference, 19-21 October 2009, Abu Dhabi, UAE*, 2009.

[21] Gaoming Li and Albert C. Reynolds. Uncertainty quantification of reservoir performance predictions using a modification of spsa algorithm. *Computational Geosciences*, 15(3):451–462, 2010.

[22] Ruijian Li, A. C. Reynolds, and D. S. Oliver. History matching of three-phase flow production data. *SPE Journal*, 8(4):328–340, 2003.

[23] Jorge Nocedal and Stephen J. Wright. *Numerical Optimization*. Springer, New York, 1999.

[24] Jorge Nocedal and Stephen J. Wright. *Numerical Optimization*. Springer, New York, 2006.

[25] Karl P. Norrena and Clayton V. Deutsch. Automatic determination of well placement subject to geostatistical and economic constraints. In *Proceedings of the 2002 SPE International Thermal Operations and Heavy Oil Symposium and International Horizontal Well Technology Conference, 4-7 November 2002, Calgary, Alberta, Canada*, 2002.

[26] Jrme Onwunalu and Louis Durlofsky. Application of a particle swarm optimization algorithm for determining optimum well location and type. *Computational Geosciences*, 14:183–198, 2010. ISSN 1420-0597. URL `http://dx.doi.org/10.1007/s10596-009-9142-1`. 10.1007/s10596-009-9142-1.

[27] Umut Ozdogan and Roland N. Horne. Optimization of well placement under time-dependent uncertainty. *SPE Reservoir Evaluation & Engineering*, 9(2): 135–145, 2006.

[28] D. W. Peaceman. Interpretation of well block pressures in numerical reservoir simulation. *SPE Journal*, 18(6):183–194, 1978.

[29] D. W. Peaceman. Interpretation of well-block pressures in numerical reservoir simulation with non-square grid blocks and anisotropic permeability. *SPE Journal*, 23(6):531–543, 1983.

[30] D. W. Peaceman. Representation of a horizontal well in numerical reservoir simulation. *SPE Advanced Technology Series*, 1(1):7–16, 1993.

[31] M. J.D. Powell. Uonyqa: unconstrained optimization by qudratic approximation. *Math programming*, 92:555–582, 2002.

[32] M. J.D. Powell. Least frobenius norm updating of quadratic models that satisfy interpolation conditions. *Math programming*, 100:183–215, 2004.

[33] M. J.D. Powell. *The NEWUOA software for unconstrained optimization without*

*derivatives **in** large-scale nonlinear optimization, eds G. Di Phillo and M. Roma.* Springer, 2006.

[34] M.J.D. Powell. The BOBYQA algorithm for bound constrained optimization without derivatives. Technical Report DAMTP 2009/NA06, Unversity of Cambridge, 2009.

[35] P. Sarma, L.J. Durlofsky, and K. Aziz. Implementation of adjoint solution for optimal control of smart wells. In *Proceedings of the SPE Reservoir Simulation Symposium*, number SPE 92864, 2005.

[36] Pallav Sarma and Wen H. Chen. Efficient well placement optimization with gradient-based algorithm and adjoint models, SPE, 112257. In *Proceedings of the 2008 SPE Intelligent Energy Conference and Exhibition*, 2008.

[37] Schlumberger. *Schedule User Guide.* Schlumberger, 2008.

[38] Schlumberger. *Eclipse Technical Description.* Schlumberger, 2008.

[39] Y. Shuai, Christopher D. White, Hongchao Zhang, and Ting Sun. Using multiscale regularization to obtain realistic optimal control strategies. In *Proceedings of the SPE Reservoir Simulation Symposium*, number SPE 142043, 2011.

[40] S. Vlemmix, G.J.P. Joosten, D.R. Brouwer, and J.D. Jansen. Adjoint-based well trajectory optimization in a thin oil rim, SPE-121891. In *Proceedings of the SPE EUROPEC/EAGE Annual Conference an Exhibition, 8-11 June 2009, Amsterdam, The Netherlands*, 2009.

[41] Chunhong Wang, Gaoming Li, and A. C. Reynolds. Optimal well placement for production optimization. In *Proceedings of the SPE Eastern Reginal Meeting*, number SPE 111154, 2007.

[42] Zhan Wu, A. C. Reynolds, and D. S. Oliver. Conditioning geostatistical models to two-phase production data. *SPE Journal*, 3(2):142–155, 1999.

[43] G. Yang, L.E. Reinstein, S. Pai, Z. Xu, and D.L. Carroll. A new genetic algorithm technique in optimization of permanent 125-i prostate implants. *Medical Physics*, 25(12):2308–2315, 1998.

[44] Burak Yeten, Louis J. Durlofsky, , and Khalid Aziz. Optimization of nonconventional well type, location and trajectory. In *Proceedings of the 2002 SPE Annual Technical Conference and Exhibition, 29 September-2 October 2002, San Antonio, Texas*, 2002.

[45] M.J. Zandvliet. *Model-based Lifecycle Optimization of Well Locations and Production Settings in Petroleum Reservoirs*. Ph.D. thesis, Delft University of Technology, Netherlands, 2008.

[46] Fengjun Zhang, A. C. Reynolds, and D. S. Oliver. The impact of upscaling errors on conditioning a stochastic channel to pressure data. *SPE Journal*, 8(1): 13–21, 2003.

[47] Kai Zhang, Gaoming Li, A. C. Reynolds, Liming Zhang, and Jun Yao. Optimal well placement using and adjoint gradient. *Journal of Petroleum Science and Engineering*, 73:220–226, 2010.

[48] H. Zhao, C. Chen, S. Do, G. Li, and A. Reynolds. Maximization of a dynamic quadratic interpolation model for production optimization. In *Proccedings of the SPE Reservoir Simulation Symposium, The Woodlands, Texas, USA, 21-23 February*, number SPE 141317, 2011.

APPENDIX A

TRANSMISSIBILITY FACTOR OF A PERFORATION OF A DIRECTIONAL WELL

A.1 Schlumberger [37] Method

The transmissibility factor of each perforation of a well is computed by Eq. 4.4 given the values of r_{o_i} and $k_i h_i$. Let $\tilde{x}_i - \tilde{y}_i - \tilde{z}_i$, represent the local coordinate system for gridblock i where $\tilde{e}_{x,i}$, $\tilde{e}_{y,i}$ and $\tilde{e}_{z,i}$ are the unit vectors in the $\tilde{x}_i$, $\tilde{y}_i$ and $\tilde{z}_i$ directions, respectively. Denoting the axis (centerline) of the well located within gridblock i by the vector $\vec{H}_i$, we have

$$\vec{H}_i = h_{x,i}\tilde{e}_{x,i} + h_{y,i}\tilde{e}_{y,i} + h_{z,i}\tilde{e}_{z,i} \tag{A.1}$$

where $h_{x,i}$, $h_{y,i}$ and $h_{z,i}$ are the components of the segment length of the well in the direction of coordinate axis $\tilde{x}_i$, $\tilde{y}_i$ and $\tilde{z}_i$, respectively. Note $||\vec{H}_i||_2$ is the length of the well. To determine $\vec{H}_i$, we have to determine the two endpoints at which the well intersects the boundary of the gridblock.

In the Schlumberger [37] method, $k_i h_i$ for perforation i is determined by the equation:

$$k_i h_i = \sqrt{(\sqrt{k_{y,i}k_{z,i}}h_{x,i})^2 + (\sqrt{k_{x,i}k_{z,i}}h_{y,i})^2 + (\sqrt{k_{x,i}k_{y,i}}h_{z,i})^2}, \tag{A.2}$$

where $k_{x,i}$, $k_{y,i}$ and $k_{z,i}$, respectively, are the permeability of gridblock i in the $\tilde{x}_i$, $\tilde{y}_i$ and $\tilde{z}_i$ directions, respectively. Similarly, $h_{x,i}$, $h_{y,i}$ and $h_{z,i}$ are the segment length of the well located in gridblock i and in the $\tilde{x}_i$, $\tilde{y}_i$ and $\tilde{z}_i$ directions, respectively.

To compute r_{o_i} for a perforation, the Schlumberger [37] method first determines the transmissibility factor of a perforation as a weighted average of the transmissibility factors in the $\tilde{x}_i$, $\tilde{y}_i$ and $\tilde{z}_i$ directions. Then, the value for r_{o_i} is back calculated from the computed average transmissibility factor of the perforation using Eq. A.7, where the value of $k_i h_i$ is given by Eq. A.2. The transmissibility factors in $\tilde{x}_i$, $\tilde{y}_i$ and $\tilde{z}_i$ directions are computed based on Peaceman equation. For example, the transmissibility factor in the $\tilde{x}_i$ direction is computed by the following equations.

$$T_{x,i} = \frac{2\pi\alpha\sqrt{k_{y,i}k_{z,i}}h_{x,i}}{\ln\frac{r_{o_{x,i}}}{r_w}}, \tag{A.3}$$

where α is a unit conversion factor with $\alpha = 1.127 \times 10^{-3}$ in the field units used here and

$$r_{o_{x,i}} = 0.28 \left(\frac{\left[\left(\frac{k_{y,i}}{k_{z,i}}\right)^{1/2} \Delta z_i^2 + \left(\frac{k_{z,i}}{k_{y,i}}\right)^{1/2} \Delta y_i^2 \right]^{1/2}}{\left[\left(\frac{k_{y,i}}{k_{z,i}}\right)^{1/4} + \left(\frac{k_{z,i}}{k_{y,i}}\right)^{1/4} \right]} \right). \tag{A.4}$$

The transmissibility factors in the $\tilde{y}_i$ and $\tilde{z}_i$ directions, $PI_{y,i}$ and $PI_{z,i}$, have similar definitions. Then the average transmissibility factor of the perforation is computed by

$$\overline{T_i} = \sqrt{T_{x,i}^2 + T_{y,i}^2 + T_{z,i}^2} \tag{A.5}$$

Finally r_{o_i} is back calculated from the average transmissibility factor using the value of $k_i h_i$ computed by Eq. A.2 by solving

$$\overline{T_i} = \frac{2\pi\alpha k_i h_i}{\ln\frac{r_{o_i}}{r_w}}, \tag{A.6}$$

for r_{o_i} to obtain

$$r_{o_i} = e^{\left(\frac{2\pi\alpha k_i h_i}{\overline{T_i}}\right)} \times r_w. \tag{A.7}$$

A.2 Jostein Alvestad and Stava [18] Method

Similarly, denote the local coordinate axis of the gridblock i by $\tilde{x}_i - \tilde{y}_i - \tilde{z}_i$. In the Jostein Alvestad and Stava [18] method, $k_i h_i$ of perforation i is computed by

$$k_i h_i = \left(\Psi_x^2 k_{y,i} k_{z,i} + \Psi_y^2 k_{x,i} k_{z,i} + \Psi_z^2 k_{x,i} k_{y,i}\right)^{1/2} h_i, \tag{A.8}$$

where

$$\Psi_x = \sin\varphi_{\mathrm{w}} \cos\theta_{\mathrm{w}}, \qquad \Psi_y = \sin\varphi_{\mathrm{w}} \sin\theta_{\mathrm{w}}, \qquad \Psi_x = \cos\varphi_{\mathrm{w}}. \tag{A.9}$$

are the weights defined as a function of the orientation angles of the well trajectory line measured with respect to the local coordinate system of the gridblock; h_i is the length of the part of the well inside the gridblock corresponding to the perforation i and $k_{x,i}$, $k_{y,i}$ and $k_{z,i}$ are the permeabilities of the gridblock corresponding to the perforation i in the $\tilde{x}_i$, $\tilde{y}_i$ and $\tilde{z}_i$ directions, respectively. Note that to determine h_i, we have to determine the two endpoints at which the well intersects the boundary of the gridblock. In the Jostein Alvestad and Stava [18] method, the equivalent radius for each perforation i ,r_{o_i}, is computed by the following set of equations,

$$r_{o_i} = G \frac{\left(\Delta L_{1,i}^2 + \Delta L_{2,i}^2\right)^{1/2}}{\frac{1}{2}\left(A_{1,i}^{1/2} + A_{2,i}^{1/2}\right)}, \tag{A.10}$$

where

$$\Delta L_{1,i}^2 = \left(\frac{k_{y,i}}{k_{z,i}}\right)^{1/2} \Delta z_i^2 \Psi_x^2 + \left(\frac{k_{z,i}}{k_{x,i}}\right)^{1/2} \Delta x_i^2 \Psi_y^2 + \left(\frac{k_{x,i}}{k_{y,i}}\right)^{1/2} \Delta y_i^2 \Psi_z^2. \tag{A.11}$$

$$\Delta L_{2,i}^2 = \left(\frac{k_{z,i}}{k_{y,i}}\right)^{1/2} \Delta y_i^2 \Psi_x^2 + \left(\frac{k_{x,i}}{k_{z,i}}\right)^{1/2} \Delta z_i^2 \Psi_y^2 + \left(\frac{k_{y,i}}{k_{x,i}}\right)^{1/2} \Delta x_i^2 \Psi_z^2. \tag{A.12}$$

$$A_{1,i} = \left(\frac{k_{y,i}}{k_{z,i}}\right)^{1/2} \Psi_x^2 + \left(\frac{k_{z,i}}{k_{x,i}}\right)^{1/2} \Psi_y^2 + \left(\frac{k_{x,i}}{k_{y,i}}\right)^{1/2} \Psi_z^2. \tag{A.13}$$

and

$$A_{2,i} = \left(\frac{k_{z,i}}{k_{y,i}}\right)^{1/2} \Psi_x^2 + \left(\frac{k_{x,i}}{k_{z,i}}\right)^{1/2} \Psi_y^2 + \left(\frac{k_{y,i}}{k_{x,i}}\right)^{1/2} \Psi_z^2. \tag{A.14}$$

with $G = 0.1404$.